

Cyclostratigraphic concepts and methods for correlation and characterisation of low net-to-gross alluvial stratigraphy

Baars, T.F.

DOI

[10.4233/uuid:68eb31aa-dbee-4727-9f6a-a6e91ad8ea7a](https://doi.org/10.4233/uuid:68eb31aa-dbee-4727-9f6a-a6e91ad8ea7a)

Publication date

2023

Document Version

Final published version

Citation (APA)

Baars, T. F. (2023). *Cyclostratigraphic concepts and methods for correlation and characterisation of low net-to-gross alluvial stratigraphy*. [Dissertation (TU Delft), Delft University of Technology]. <https://doi.org/10.4233/uuid:68eb31aa-dbee-4727-9f6a-a6e91ad8ea7a>

Important note

To cite this publication, please use the final published version (if applicable). Please check the document version above.

Copyright

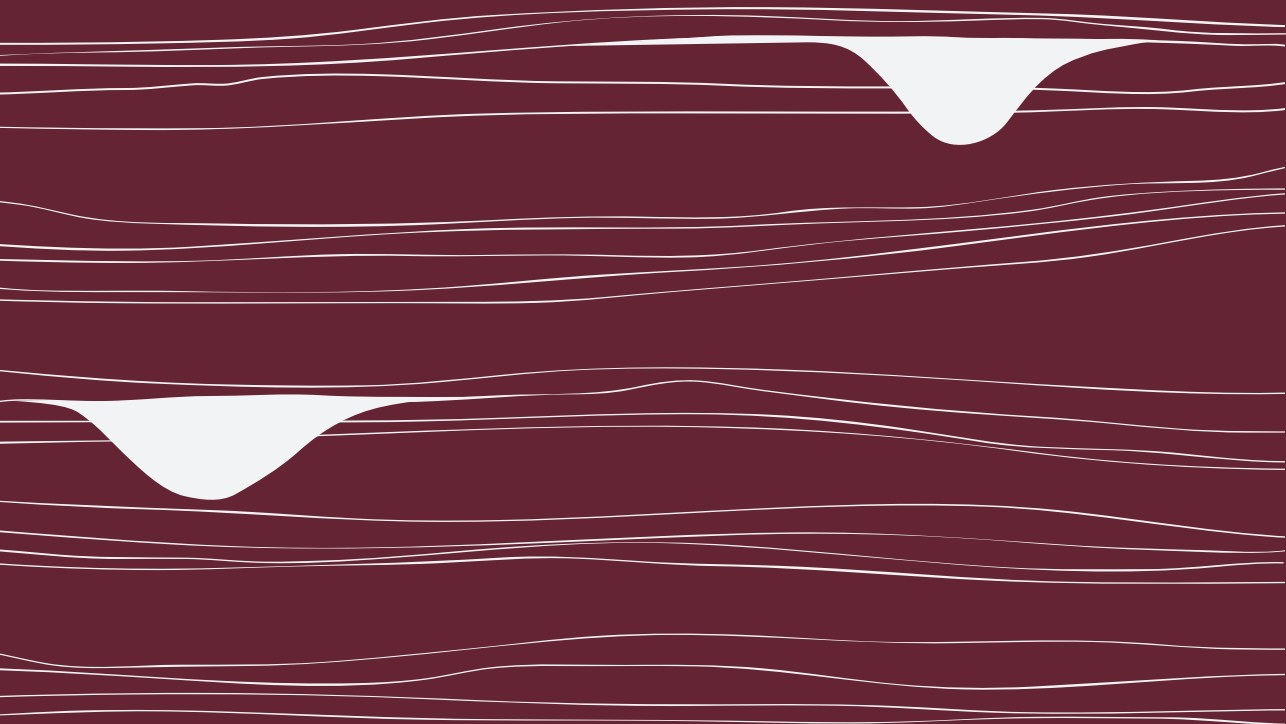
Other than for strictly personal use, it is not permitted to download, forward or distribute the text or part of it, without the consent of the author(s) and/or copyright holder(s), unless the work is under an open content license such as Creative Commons.

Takedown policy

Please contact us and provide details if you believe this document breaches copyrights. We will remove access to the work immediately and investigate your claim.

Cyclostratigraphic concepts and methods for correlation and characterisation of low net-to-gross alluvial stratigraphy

Timothy Florian Baars



Cyclostratigraphic concepts and methods for correlation and characterisation of low net-to-gross alluvial stratigraphy

Dissertation

For the purpose of obtaining the degree of doctor at Delft University of Technology
by the authority of the Rector Magnificus prof.dr.ir. T.H.J.J. van der Hagen,
chair of the Board for Doctorates,
to be defended publicly on
Friday 13 October 2023 at 12:30 o'clock

by

Timothy Florian BAARS
Master of Science in Earth Sciences
Born in Hoevelaken, the Netherlands

This dissertation has been approved by the promotors.

Composition of the doctoral committee:

Rector Magnificus
Prof. dr. A.W. Martinius
Dr. H.A. Abels

Chairperson
Delft University of Technology, promotor
Delft University of Technology, copromotor

Independent members:

Prof. dr. S. Geiger
Em. prof. dr. I. Cojan
Dr. J.E.A. Storms
Dr. M. Ghinassi
Drs. C.R. Geel
Prof. dr. P.J. Vardon

Delft University of Technology
École des Mines de Paris
Delft University of Technology
University of Padova
TNO Earth, Environmental and Life Sciences
Delft University of Technology, reserve member

This study was supported by Topsector Energie (Grant Number TKI2018-03-GE) with financial aid from Equinor ASA and Wintershall Noordzee B.V.



Keywords: Alluvial architecture, Bighorn Basin, Floodplain fines, Orbital forcing, Predictive stratigraphic models

The author can be reached through e-mail: t.f.baars@gmail.com

Printed by: ProefschriftMaken || www.proefschriftmaken.nl

Copyright © Timothy Florian Baars, p/a Department of Geoscience & Engineering, Delft University of Technology, 2023

All rights reserved. No parts of this publication may be reproduced in any form, by print or photo print, microfilm or other means, without written permission by the author.

Rivers know this: There is no hurry. We shall get there some day.

A.A. Milne

Contents

Summary		viii
Chapter 1:	Introduction	2
Chapter 2:	The Bighorn Basin, Wyoming, USA, as an outcrop example	12
Chapter 3:	Lateral and vertical characteristics of floodplain aggradation cycles in the lower Eocene Willwood Formation, Bighorn Basin, Wyoming, USA	23
Chapter 4:	Sandstone body character and river planform styles of the lower Eocene Willwood Formation, Bighorn Basin, Wyoming, USA	41
Chapter 5:	Stratigraphic relation between river channels and channel sandstone bodies with floodplain sedimentary environments and stratigraphy in the Willwood Formation of the Bighorn Basin, Wyoming, USA	67
Chapter 6:	Long-term alluvial changes driven by orbital eccentricity in the lower Eocene Bighorn Basin, Wyoming	89
Chapter 7:	A cyclostratigraphic framework of the Upper Carboniferous Westoe and Cleaver formations in the southern North Sea Basin as a methodology for stratigraphic reservoir characterisation	101
Chapter 8:	Implementation of cyclostratigraphic concepts and methodology in the Upper Triassic Lunde Formation to improve stratigraphic reservoir characterisation	129

Chapter 9:	A cyclostratigraphic reservoir correlation and characterisation methodology	169
Chapter 10:	Synthesis	175
Author Contributions		186
Supplementary material		188
Literature		200
Acknowledgements		222
Curriculum Vitae		224
Samenvatting		226

Summary

Alluvial deposits in the subsurface are essential for geo-energy production and storage in many regions worldwide. Accurate correlation and characterisation of alluvial stratigraphy requires an understanding of how river channels were spatially deposited and which geomorphological processes acted upon them. This is especially true for low net-to-gross alluvial stratigraphy, which has a relatively low reservoir sandstone content and high non-reservoir floodplain deposits. Here, channel sandstones are often isolated from each other, and display poor three-dimensional connectivity with each other. Due to this, both correlation and characterisation in low net-to-gross alluvial systems is challenging.

Regional continuous surfaces, such as palaeosols or coal seams, could help correlate such deposits as they show a large lateral extent of up to tens of kilometres. The formation of palaeosols or coal seams is commonly controlled by factors that operate independent of the fluvial system at a basin-wide scale, so-called allogenic factors. One of the main allogenic forcings in fluvial systems on the upstream end of the system (the source area) is climate variability which occurs at a range of temporal scales. This climate control is often cyclic in nature. In those cases where the signal is preserved, there can be a strong vertical repetitive spacing between palaeosols or coal seams, making them helpful in predicting alluvial architecture. By identifying and correlating these regionally continuous surfaces, it may be possible to improve stratigraphic correlation and characterisation of sandstone distribution in low net-to-gross fluvial stratigraphy.

This thesis investigates the potential of orbital forced cyclic climate control on fluvial systems and its application to reservoir characterisation and subsurface correlation. To do so, six studies are presented. Four of these studies are focused on an outcrop analogue case in the Bighorn Basin, Wyoming, USA, where well-exposed floodplain red beds of the early Eocene are studied. These red beds form a rhythmic alternation with pale brown colour beds and are hypothesised to be precession-paced orbital forced. The findings of these studies are subsequently applied in two subsurface case studies in the North Sea.

Chapter 3 uses a three-dimensional digital outcrop model to study the lateral and vertical variability of floodplain cycles in the Bighorn Basin. Most alternations are consistently traceable throughout the model; however, there is significant lateral and vertical thickness variability. A strong relationship exists between thickness variability and average palaeoflow in the lateral direction, where variability in thickness is larger perpendicular to the palaeoflow than alongside the palaeoflow direction. This variability is interpreted to result from morphological elements oriented in palaeoflow directions causing more consistency of sedimentary features. In the vertical direction, there are significant thickness variations among successive sedimentary alternations; thinner cycles follow thicker-than-average floodplain cycles. This variability is argued to be caused by internal palaeotopographic differences and is believed to be counterbalanced by compensational stacking behaviour.

Chapter 4 investigates the sandstone bodies of the Bighorn Basin. A total of four channel lithofacies associations are recognised, which are interpreted to be deposits of four river planform styles: crevasse channel, trunk channel, braided-like channel, and sinuous-like channel, respectively, with the latter two styles being dominant. The alternating presence of sinuous and braided river styles offers insights for a new reconstruction of a palaeogeographic model for the Bighorn Basin. In the schematised model, several transverse systems confluence with an axial system roughly following the basin axis in line with previous reconstructions.

Chapter 5 combines the observations of the previous two chapters and investigates the relationship between the floodplain cyclicity and channelised sandstone bodies. Sandstone bodies are documented to have a preferred vertical position at the base of floodplain cycles and a thickness relationship between the two is found. Based on the observations, two depositional models are discussed for the floodplain cycles. A model driven by channel aggradation, superlevation and avulsion, and a model driven by fluvial activity and inactivity phases. Both models indicate that the detection of floodplain cyclicity can point to sandstone body cyclicity and impact the vertical distribution of sandstone bodies.

Chapter 6 documents large-scale (100-200 m) changes in alluvial stratigraphy. Based on a floodplain stratigraphic framework, two distinct intervals are documented. A sinuous dominated interval with strongly pronounced palaeosol colours and a braided interval with less well-pronounced palaeosol colours. Based on a stable carbon isotope record, the stratigraphy is correlated to the marine realm. This allowed a correlation between the defined intervals with long-eccentricity. Braided fluvial architecture dominated during periods of eccentricity minima, whereas sinuous fluvial architecture was dominant during periods of eccentricity maxima. This correlation suggests that the link between orbital eccentricity climate forcing, and river planform styles and floodplain character can provide an instrument for future alluvial stratigraphic analyses and that similar patterns can be found in the subsurface.

Chapter 7, the first subsurface case study, investigates the Upper Carboniferous Westoe and Cleaver formations in the southern North Sea. Coarsening-upwards sequences, also known as cyclothems, are used to correlate wells on a high resolution and over large distances. Cyclothems show varying thicknesses and lithological characters, and different types are defined. This variability is interpreted as internal fluvial dynamics. Two well correlations are made—one manual correlation and one semi-automated, based on the automatic detection of cyclothems. The manual approach is deemed more accurate for the correlation of individual wells. Averaged stratigraphic trends of the correlations are compared, and similar results in sandstone content are found with two intervals where sandstone content levels increase. These intervals are linked to long-eccentricity control via base-level fluctuation and may guide exploration in the otherwise low net-to-gross setting.

Chapter 8, the second subsurface case study, investigates the Upper Triassic Lunde Formation in the northern North Sea. Stable alternations of high and weak-to-moderate pedogenesis were found in the floodplain record and were used to correlate wells over a 1-5 km distance. Additional wells over greater distances were added using a generated stable carbon record isotope for tie-points. The resulting floodplain-based stratigraphic zonation was compared to the existing reservoir zonation, and refinements were suggested. Averaged stratigraphic trends show variability in sandstone content levels, and combined with isotope excursion spacing, this matches expected relationships of orbital forcing. However, due to absent dating, no conclusions can be made.

All the findings on alluvial stratigraphy and implications for subsurface reservoir characterisation are summarised in seven main conclusions, and a general methodology for a cyclostratigraphic approach to reservoir correlation and characterisation is presented. Ultimately, this thesis shows that cyclic patterns in the low net-to-gross systems can be documented in the floodplain deposits and that implementing cyclostratigraphic concepts for alluvial correlation and characterisation can complement and improve existing models.



1

Introduction

1.1 How to characterise the subsurface

How does one view the subsurface? How do we get access? What tools can and should we use? What will the images tell us? Characterising the subsurface has been a longstanding effort of geologists, and over the years, they have made impressive strides in their ability to visualise and predict what lies below. For example, measurements and cores from boreholes offer a one-dimensional peek into the subsurface, providing an intricate and detailed view (e.g. Vaughan et al., 1999; Müller et al., 2004, Archer et al., 2020), while seismic surveys provide a broader but less detailed glimpse into the depths (e.g. Maynard et al., 2006; Mahon and Wallace, 2022). Despite the advancements, characterising the subsurface remains challenging. The complexity of predicting the subsurface arises from the many, and often interrelated variables at play, from rock formations to fluid movement, making it a veritable puzzle for geologists to solve.

This challenge is only magnified in alluvial systems where the character of rock properties is constantly shifting and changing due to the relatively unpredictable behaviour of rivers (Wainman and McCabe., 2020). Nevertheless, such subsurface characterisation and prediction are important for our energy supply and utilisation of natural resources. River channel sandstone deposits formed in alluvial systems form a common target for hydrocarbon energy resources but also play an important role in a more sustainable future as they can serve as geothermal targets or be used for storing carbon dioxide and/or hydrogen.

As we can never fully view the subsurface, the key lies in reducing uncertainty in the prediction of rock properties. This prediction can, for example, be done via conceptual and numerical models (e.g. Martinius et al., 2014; Nystuen et al., 2014; Noorbergen et al., 2018; Le Cottonnec et al., 2020; Wang et al., 2020; de Hoop and Voskov, 2021). Input for such models is commonly taken from outcrop analogues and combined with measurements taken from the subsurface. From this knowledge, scenarios can be developed and tested to reduce uncertainty further. This PhD thesis studies a less common point of view to reducing uncertainty and building scenarios for characterising alluvial reservoirs, that of the control of regular-paced climate variability on rock property distributions

Climate changes can significantly impact depositional environments, as evidenced by the changes we increasingly see today (Cazenave et al., 2004). Similarly, in the past, climate change caused alterations now present in the rock record and, thus, variability in reservoir rock units (e.g. Cecil et al., 2003; Kasse et al., 2003; Giblin and Davies, 2012; Sharma et al., 2023). Part of this climate variability is paced on a quasi-periodic time scale. Such pacing has a good potential to be predictive and could be utilised to provide better constraints on reservoir build-up. Storage of this climate signal in the rock record is commonly not optimal in fluvial sandstones because the signal is often cryptic or not preserved. To the contrary, the 'less' interesting, non-permeable, and often overlooked river floodplain deposits better store such climate signals.

1.2 Low net-to-gross alluvial reservoir performance

In this thesis, low net-to-gross alluvial stratigraphy is examined. In such stratigraphy, river floodplain deposits are in abundance. The concept of net-to-gross defines the fraction of a reservoir occupied by conducting media with high permeability and porosity. How well a reservoir performs depends mainly on the connectivity between these conducting media (Larue and Hovadik, 2006). Often, "low" net-to-gross alluvial reservoirs are defined as reservoirs with 30% or less sandstone. This number is derived from a random distribution of the conducting media in a three-dimensional cube. If the

conducting medium, sandstone in the case of a fluvial reservoir, is assumed to be randomly distributed, approximately 30% sandstone content is needed to achieve conductivity between sandstone elements (Percolation theory; King, 1990; Larue and Hovadik, 2006; King and Masihi, 2009)

This 30% forms a reasonable estimate for random connectivity in three dimensions. However, the actual connectivity and performance in low net-to-gross alluvial reservoirs highly depends on the reservoir's architecture. This architecture can be defined as the spatial distribution, geometry, and proportions of different types of fluvial deposits in the alluvial succession (Leeder, 1978; Allen 1978; Gouw, 2007). Therefore, factors such as channel width and thickness ratios, channel sinuosity, channel stacking patterns, and the influence and distribution of floodplain fines form important features in assessing the performance of low net-to-gross alluvial reservoirs.

1.2.1 Alluvial stratigraphic correlation

To accurately characterise the stratigraphic variability of these parameters and the overall alluvial architecture, the correlation of wells is needed. However, due to poor three-dimensional connectivity and isolated spatial occurrence of sandstones in low net-to-gross alluvial stratigraphy (Fig. 1.1a) (e.g. Dalrymple et al., 2001; Villamizar et al., 2015; van Toorenburg et al., 2016; Varela et al., 2021), the correlation of sandstones between wells based on well log and core data challenging (Fig. 1.1bandc). Furthermore, the channel sandstone bodies are often thin (<10 m) and hard to identify on seismic data, and established marine biostratigraphic correlation methods cannot be used due to large distances to the shoreline or a low vertical stratigraphic resolution. Magnetostratigraphic, radiometric dating, and chemostratigraphy are sometimes used for correlation, but they often do not provide the required resolution or are challenging to integrate. Therefore, there is a need for stratigraphic correlation concepts that consider the fluvial deposits themselves to characterise alluvial architecture (e.g. O'Mara and Turner, 1995; Donselaar et al., 2011; Ojik et al., 2011).

A potential solution is the recognition of regionally continuous surfaces or marker horizons in wells and logs based on a particular set of rock characteristics (e.g. O'Mara and Turner, 1995; Bridge and Tye, 2000, Shepard, 2009). The erosional surfaces at the base of channel complexes are frequently used marker horizons. However, the lateral continuity of such surfaces is often limited, certainly with respect to average well distances (Wainman and McCabe, 2020). In low net-to-gross reservoirs, the lateral continuity is typically hundreds of meters to kilometre scale depending on the orientation of the section (strike or parallel) (Allen et al., 1974; Pranter et al., 2009). On the contrary, the floodplain intervals affected by long periods of non-deposition on the floodplain of a fluvial system, such as coal seams or strongly developed palaeosols, commonly show large lateral extent of up to tens of kilometres (Allen, 1974; Kraus et al., 2002; van der Meulen et al., 2020; Opluštil et al., 2022). However, these often thin intervals' lateral continuity and vertical spacing can be difficult to assess based on sparse well data, even more so when long continuous cores are absent. Also, determining which palaeosol or coal seam in one well correlates with a similar one in another well can be challenging.

The formation of regionally continuous palaeosol intervals or coal seams is commonly controlled by factors that operate independent of the fluvial system at a basin-wide scale, so-called allogenic factors (Abels et al., 2013; Jirásek et al., 2018, Noorbergen et al., 2018). One of the main allogenic forcings in fluvial systems on the upstream end of the system (the source area) is climate variability which occurs at a range of temporal scales. This climate control is often cyclic in nature, and in those cases where the signal is preserved, there can be a strong vertical repetitive spacing between regionally

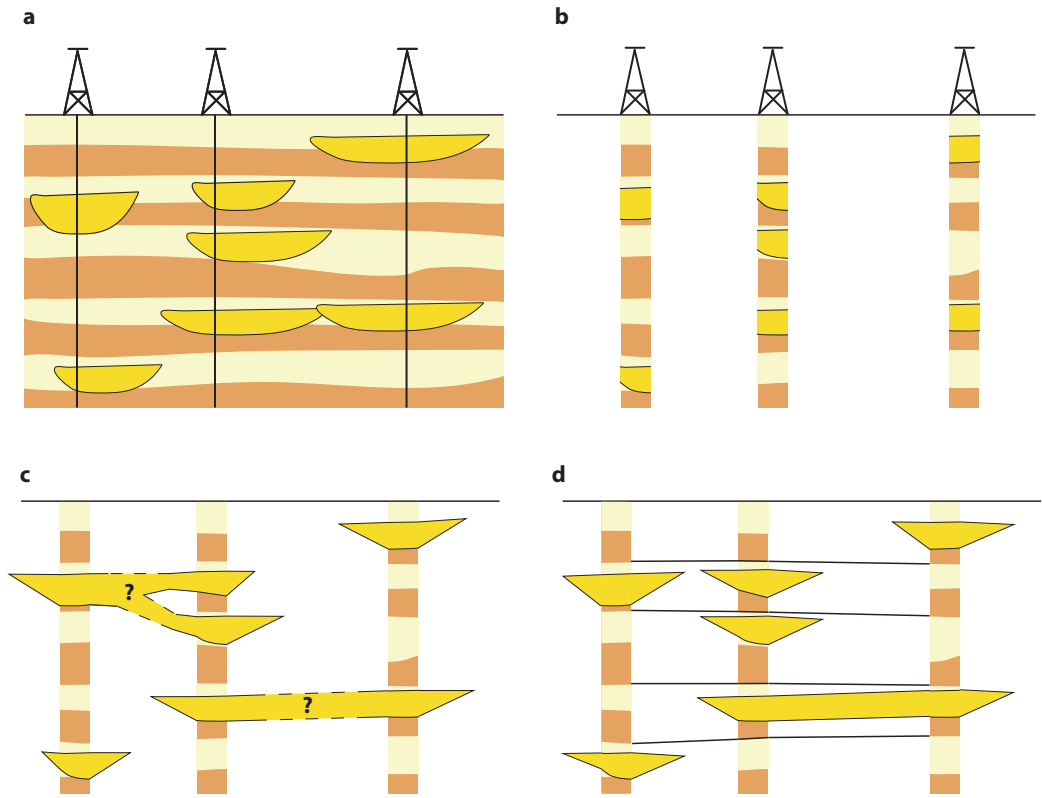


FIGURE 1.1 a) An illustration of a hypothetical alluvial reservoir in the subsurface and b) How well data would display the reservoir. c) Based on only the well data, the correlation of reservoir sandstones results in multiple potential solutions. d) Based on chronostratigraphic concepts, such as regional surface markers, the number of potential solutions can be constrained, and the reservoir can be better assessed.

continuous palaeosol intervals or coal seams, making them (potentially) useful for prediction of alluvial architecture. By identifying and correlating these regionally continuous surfaces, it may thus be possible to improve stratigraphic correlation and better characterise sandstone stratigraphy in low net-to-gross fluvial reservoirs (Fig. 1.1d).

1.3 Controls on fluvial stratigraphy

Beerhower (1964) proposes an end-member model in which internal, so-called autogenic, or external, so-called allogenic, controls produce fluvial stratigraphic patterns and since then numerous research has been done on the impact of both components (e.g. Cecil et al., 1993; Stouthamer and Berendsen, 2007; Gibling et al., 2010; Hajek and Straub, 2017; Foreman and Straub, 2017; Wang et al., 2020). Autogenic controls are processes that are intrinsic to the sedimentary system, for example, the migration of a point-bar in a meandering river, an avulsion in the river pathway, or the switching of a lobe in a delta (Gibling et al., 2010; Jones and Hajek, 2007). Such processes occur relatively fast

1977). These changes are caused by the gravitational pull of the sun, moon, planets, and other masses in our solar system, and they can significantly affect the Earth's climate by altering the amount of solar energy or insolation reaching the top of Earth's atmosphere. The dominant variations of the Earth's orbital parameters are known as Milankovitch cycles and are summed by three movements: precession (operating at 21 kyr), obliquity (40 kyr), and eccentricity (100 and 400 kyr), each with a quasi-stable period (Berger, 1988; Laskar et al., 2004). Precession refers to the change in the direction of the Earth's rotational axis in proximity to the nodes of the eccentric orbit around the sun, obliquity refers to changes in the angle of the Earth's axis of rotation, and eccentricity refers to changes in the eccentricity of the Earth's orbit around the sun (Fig. 1.3).

Changes in the precession can generate insolation differences of up to 20% depending on season and latitude (Loutre et al., 2004) and can invoke significant changes in the climate. These changes occur via a series of non-linear system processes, such as changes in clouds, vegetation, weathering patterns, and discharge variability (Hilgen et al., 2015). Modelling studies, such as Bosmans et al. (2012), have shown that shifts in low- and mid-latitude monsoonal systems from land to ocean and vice versa can lead to notable variations in precipitation patterns due to precession-induced variation in insolation. In the geological record, such changes translate into cyclic patterns of, for example, landscape changes between mudflats and lakes (Abels et al., 2009). Such changes are also expected to have a significant imprint in the fluvial domain because sediment load, discharge variability and vegetation changes all affect the fluvial system (e.g. Schumm, 1985; Mohrig et al., 2000; Church, 2006; Tal and Paola, 2010)

1.5 Orbital forcing in fluvial records

Olsen (1990) is one of the first studies suggesting the imprint of orbital forcing on fluvial deposits. In the Upper Devonian Kap Graah Group in Greenland, Olsen (1990) correlated cyclic changes in channel slope and size to discharge variability controlled by precession and eccentricity. Since then, numerous studies have reported observations and interpretations of orbital forcing imprints. For instance, Valero et al. (2017) identified changes in channel density in the Almazán Basin in Spain, while Smith et al. (2014) observed an alternation of alluvial and lacustrine modes within the Green River Formation in Wyoming, USA, which correlated with an eccentricity pacing. Noorbergen et al. (2020) showed that stratigraphic patterns in coal-dominated fluvial systems of the Fort Union Formation in the lower Paleocene were also driven by eccentricity-related climate cycles, resulting in major coal seams alternating with channel sandstone bodies. Similarly, coal-bearing fluvial cycles were documented in the Upper Silesian Basin in the Czech Republic, the Pannonian Basin in Hungary, and the Donets Basin in Ukraine (Nádor et al., 2007; Davidov et al., 2010; Jirásek et al., 2018; Opluštil et al., 2022). In the Karoo Basin in South Africa, Lanci et al. (2022) found various cycles in lithological element variations linked to eccentricity, obliquity, and precession, hypothesised to result from changes in hydrological regimes and in the Escanilla Formation in the south-Pyrenean foreland basin, Sharma et al. (2023) documented changes in alluvial style by discharge variability linked to an eccentricity pacing. Lastly, Abdul Aziz (2008) and Abels et al. (2013) reported on the frequency of distinct red palaeosols in the Bighorn Basin in Wyoming, USA, which were likely paced at the precession scale.

While the cyclic patterns documented in these studies may align with the frequency ratios of orbital cycles, it is important to note that autogenic forcing can cause similar patterns or at least may have a similarly strong imprint. Laboratory-controlled experiments have shown that avulsion and

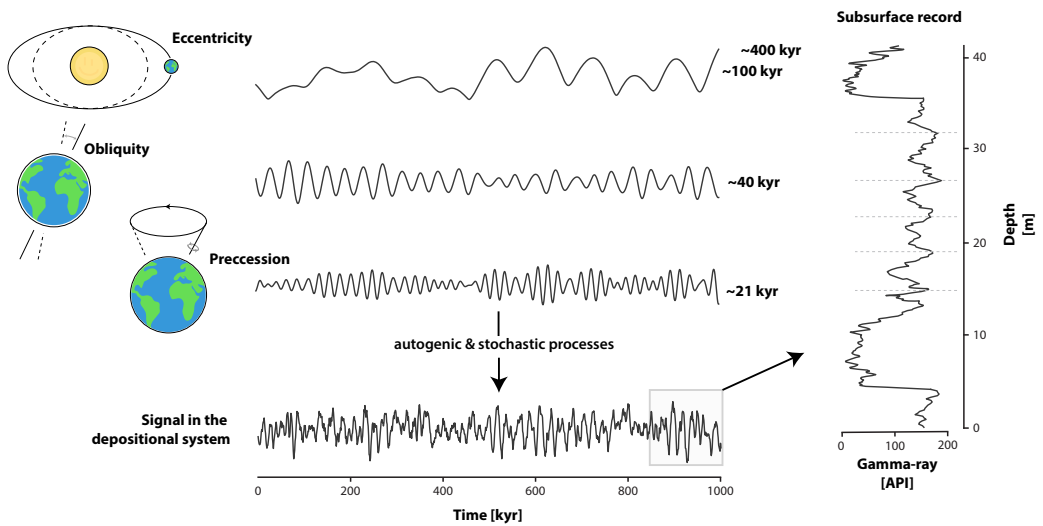


FIGURE 1.3 An overview of the orbital cycles and how they can imprint the geological record. Eccentricity with a periodicity of 100 and 400 kyr represents the fluctuation of the earth’s orbit around the sun. Obliquity with a periodicity of 40 kyr represents the tilt of the earth’s axis. Precession with 21 kyr periodicity represents the change in the orientation of its rotational axis. As these three motions cause the amount of insolation falling on the earth, the signal in a depositional basin is ‘contaminated’ or distorted by a series of non-linear system processes such as changes in vegetation, weathering patterns and discharge variability. In the geological record, this signal is stored by and combined with local processes and gaps in the record. Based on Cyclostratigraphy Intercomparison Project (2023).

lateral migration of channels can build stratigraphy with similar patterns through the compensational stacking of channel bodies (Hajek and Straub, 2017). These authors showed that lateral variation in accommodation space was caused by cyclic movement of channel belts across the basin. Nonetheless, observation of cyclic character of palaeosol successions or coal seams in fluvial successions, with suggestions of orbital forcing or not, indicates that regionally continuous surfaces could have a repetitive character and value for subsurface characterisation.

1.5.1 Floodplain fines

Fluvial sediments can be broadly classified into two types: coarse-grained channel deposits and fine-grained floodplain sediments. Channel deposits are created by the progradation of large-scale bar forms and periodic channel abandonment, accumulating channel-bar, and channel-fill sediments (Aslan, 2013). In contrast, overbank deposits are formed in flood-basin environments due to overbank flooding and avulsion. These sediments are finer-grained than channel deposits and can be found further away from the river’s main channel.

While there have been numerous studies focused on sandstone bodies for reservoir characterisation (e.g. Jordan and Pryor, 1992; Bridge and Tye, 2000; Törnqvist and Bridge, 2002; Jensen and Pedersen, 2010; Sahoo et al., 2020), there have been fewer studies focused on overbank deposits and

their potential for use for well correlation (e.g. Varela et al., 2012, 2021). Overbank deposits can be valuable for understanding changes in the depositional environment over time, as they capture not only depositional episodes but also periods of non-deposition and soil development. By documenting changes in vegetation, climate, and other indirect proxies (Kraus, 2002), floodplain deposits offer a unique perspective on the depositional environment. This makes them an interesting target of study, as they contain most of the sediment archive in low net-to-gross systems and have the potential to provide valuable insights into the evolution of fluvial systems in general.

1.6 Hypothesis

This thesis investigates the potential of orbital forced climate control on fluvial systems and the application to reservoir characterisation and subsurface correlation. As argued above, this approach has the potential to further improve our understanding of the subsurface. One of the challenges is to determine how this improved understanding can be integrated into already existing subsurface workflows and methods. Therefore, this thesis aims to answer the following question:

Can cyclic patterns in low net-to-gross alluvial strata be identified and understood, and can they be used to improve well correlations and decrease subsurface uncertainties related to reservoir architecture and sandstone connectivity?

1.7 Thesis approach

This thesis presents a total of six studies of fluvial systems: four analogue outcrop studies and two subsurface implementation studies. These studies span an age range from the Upper Carboniferous to the Early Eocene and investigate both semi-arid and humid basins. The following sections provide a short overview of these studies, allowing the reader to better navigate through this thesis.

1.7.1 The Bighorn Basin

The Willwood Formation in the early Eocene Bighorn Basin (Wyoming, USA) forms an excellent outcrop analogue for subsurface low net-to-gross fluvial systems, and **Chapter 2** discusses this alongside the basin setting, climate, sediments, and the study area. Floodplain fines of the Willwood Formation show a stable cyclic lithology arrangement alternating between red to purple palaeosols and yellow to brown heterolithic deposits (Kraus, 1987; Abdul Aziz et al., 2008; Abels et al., 2013). However, all analyses performed until now are on one-dimensional sections or concerned with the correlation of several sections at relatively short distances. For this thesis, a detailed, spatially expanded analysis has been carried out to fully evaluate the potential of the floodplain cycles for correlation, and to document the variability in lateral and vertical domains. In **Chapter 3**, forty-four of these floodplain cycles are analysed in a georeferenced digital outcrop model, followed by a detailed statistical analysis of stratigraphy.

Following the evaluation of the floodplain succession, the channel sandstone bodies are analysed in **Chapter 4**. This analysis is done using outcrop observations and a digital outcrop model. Facies and facies associations are characterised, and one hundred eight sandstone bodies are identified and grouped into different facies associations. Based on these associations, interpretations regarding fluvial style are made, and a reconstruction of the palaeogeography of the Bighorn Basin during the early Eocene times is presented.

1.7.2 Stratigraphic models

With both floodplain and channel deposits characterised, Chapters 5 and 6 document the relationship between both. In **Chapter 5**, channel sandstone bodies are related to their adjacent floodplain deposits by investigating the outcropping channel margins and their relationship with the laterally adjacent floodplain deposits. The model for allogenic forcing of the floodplain cycles, as proposed by Abels et al. (2013) is evaluated.

Chapter 6 analyses larger-scale stratigraphic trends (100-200 m). To achieve this, the floodplain stratigraphic framework constructed in Chapter 3 has been populated with identified channel sandstone bodies described in Chapter 4. The different fluvial styles are analysed in stratigraphy, and two hyperthermal events are used as time constrain to compare changes in fluvial style to pace orbital forced cyclicity.

1.7.3 Application to the subsurface

After a review of the autogenic and allogenic controls operating on the Willwood Formation, the findings and methods are applied to two selected subsurface case studies.

In **Chapter 7**, the subsurface case study on the Upper Carboniferous Westoe and Cleaver Formations in the Southern North Sea Basin is reported. This succession has been studied because of the abundantly occurring coal seams in the stratigraphy. These coal seams served as reliable regional correlation markers for decades. Sedimentary repetitions, also known as cyclothems, were identified in nineteen wells over a large area of approximately 100 km long by 30 km wide. Combined with biostratigraphic data, two correlation panels are constructed perpendicular to the average palaeoflow direction. The correlation was done twice: once based on manual correlation and once based on a semi-automatic correlation method. Subsequently, the resulting stratigraphies were analysed, and depositional models were evaluated.

The Late Triassic Lunde Formation of the Southern North Sea forms the second subsurface case study and is reported in **Chapter 8**. The formation is known for its distinct and abundant red palaeosol deposits. A detailed analysis of the floodplain has been conducted. This analysis was followed by the analysis of lithological repetitions in the floodplain fines; the results of this analysis were subsequently used to construct a correlation framework between wells. Because there is an absence of dating and good chronostratigraphic control, multiple high-resolution stable isotope records were obtained to serve as tie points for correlation. The resulting stratigraphic correlation has been compared to the existing reservoir zonation, and depositional models were evaluated.

1.7.4 A cyclostratigraphic approach to correlation and characterization

The two last chapters assesses the application and potential impact of the study results. In **Chapter 9**, a generalised workflow for the application of floodplain-based reservoir correlation and characterisation is proposed. The requirements necessary to apply the proposed analytical workflow and the steps which need to be followed are discussed. In **Chapter 10**, a synthesis is presented. Here the study's main results are discussed, as are their implications for reservoir correlation and characterisation, while also looking at possibilities for further study in alluvial strata and application to the subsurface.



2

The Bighorn Basin, Wyoming, USA, as
an outcrop example

2.1 The Bighorn Basin

The Willwood Formation of the Bighorn Basin in northwestern Wyoming is globally renowned for its striking red and purple palaeosol beds and extensive fossil record. It boasts a remarkable collection of mammal and vertebrate fauna from the Palaeocene and early Eocene periods, attracting researchers since the early 1880s. Numerous studies have reconstructed the palaeoenvironmental setting, floodplain sedimentation, palaeoclimate, and tectonic control of the basin, making it one of the best-studied continental alluvial outcrops worldwide. Moreover, the Bighorn Basin is one of the few terrestrial records of the early Eocene hyperthermal events. These hyperthermal events are associated with significant carbon cycle perturbations and global warming changes leading to environmental shifts. These events have been meticulously mapped, and their environmental impact has been studied. The signature negative carbon isotope excursions provide excellent correlation control over the entire basin, and the resulting lilac-purple-coloured palaeosols allow for precise correlation over vast lateral distances.

Due to its semi-arid climate, the basin's geological structures are exposed with excellent visibility (Fig. 2.1). The basin's lateral, kilometre-scale, continuously traceable, and well-exposed outcrops, along with the extensive research already conducted, make it an ideal outcrop analogue for mapping out alluvial stratigraphy, architecture, and unravelling the controlling mechanisms of deposition.

The upcoming chapters (3 up to and including 6) will focus on the Willwood Formation of the Bighorn Basin, which serves as an outcrop analogue for low net-to-gross alluvial stratigraphy. The studied site is a low net-to-gross reservoir analogue, with net-to-gross levels of approximately 16% (SD: 6). This represents channel sandstone bodies but excludes crevasse splays and levee deposits. The current chapter will discuss several recurring topics, such as basin setting, palaeoclimate, sedimentology, and the standard analysis methods employed in the upcoming chapters.



2.2 Basin setting

2.2.1 Structural setting

The Bighorn Basin is a Laramide intermontane basin located in northwestern Wyoming in the Western Interior of the United States. It is approximately 200 km long and 80 km wide (Fig. 2.2; Kraus and Middleton, 1987) and is bounded by the Beartooth Mountains to the west, the Absaroka range to the southwest, the Bighorn Mountains to the east, and the Pryor Mountains to the northeast (Foose et al., 1961; Lillegraven and Ostresh, 1988). During the mid to late Paleocene (Gingerich, 1983), overthrust-faulting caused the Beartooth Mountains to form the western margin of the Bighorn Basin. This margin is believed to be relatively steep, with approximately 7 km of structural relief (Wise, 2000).

Similarly, on the eastern margin, overthrusting caused the Bighorn Mountains to have a long, shallowly dipping slope on the Bighorn Basin side and a steep thrust scarp on the west-located Powder River Basin side (Hoy and Ridgway, 1997; Yonkee and Weil, 2015). The southern part of the Bighorn Basin was relatively low, likely forming a gentle rise separating the Bighorn Basin from the Powder River Basin in the south (Wing and Bown, 1985). In the northeast, extending to the Bighorn Mountains, the Pryor Mountains are considered asymmetric anticlines that experienced overthrusting in later stages (Blackstone, 1940).

Uplift around the basin's southern margin formed the southern Bighorn and the Owl Creek Mountains, which thrust southward in the early to mid-Eocene (Wing and Bown, 1985). Generally,

FIGURE 2.1 An overview of the Willwood Formation in the McCullough Peaks area of the Bighorn Basin. The vast extent of the outcrop and the low vegetation cover make it an ideal outcrop analogue for mapping out alluvial stratigraphy and architecture and unravelling the controlling mechanisms of deposition.



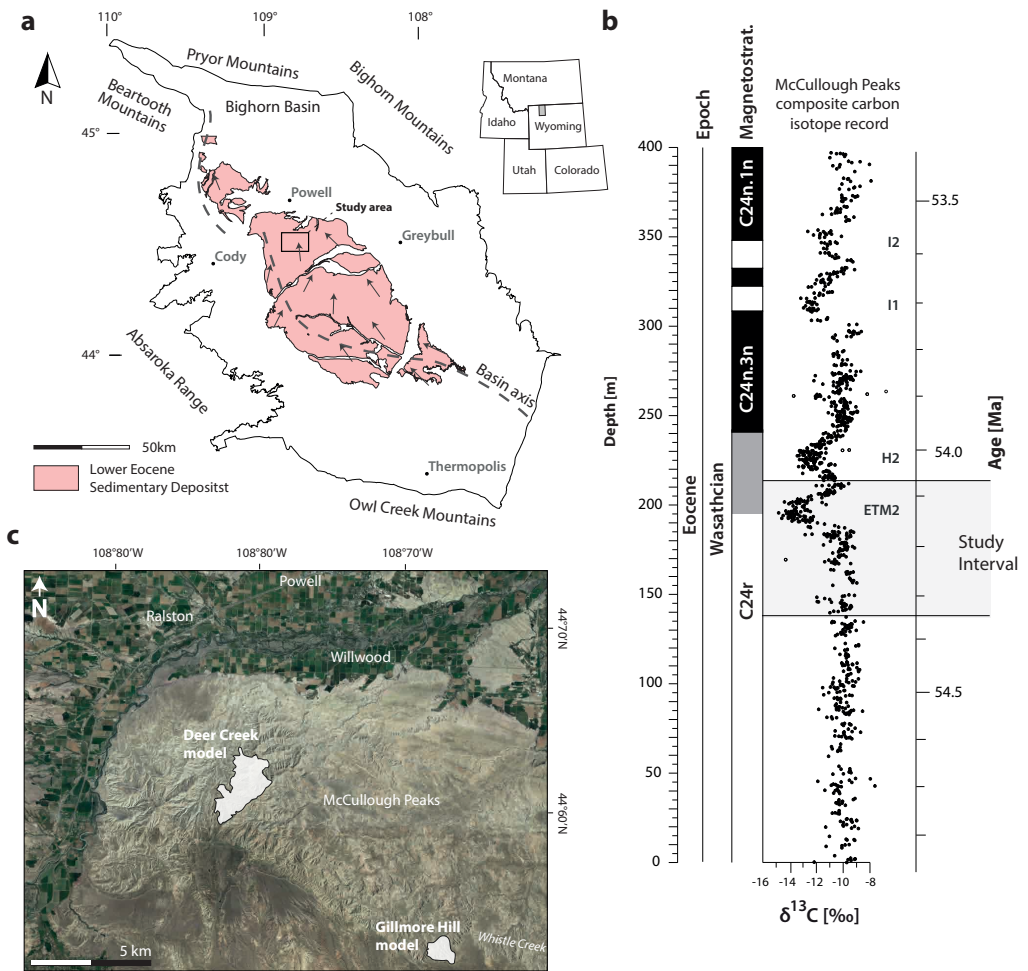


FIGURE 2.2 The Bighorn Basin, Wyoming, United States, and the location of the study areas. a) The outline of Bighorn Basin with Eocene deposits highlighted (modified from USGS survey, 2010). The basin axis follows Finn et al. (2010), and the arrows represent palaeocurrent data from Neasham & Vondra (1972). Note that the Washakie Range present during the Eocene is now covered by the Absaroka Mountains (Yonkee & Weil, 2015) and the Pryor Mountains present during the Eocene are now not distinguishable from the Bighorn Mountains (Blackstone, 1940). b) A Stratigraphic overview of the study interval with depth, age, magenotstratigraphy (Clyde et al., 1994; Abels et al., 2012), the $\delta^{13}\text{C}$ bulk composite record based on pedogenic carbonate in the Deer Creek area (Abels et al., 2016) with the indication of two hyperthermal events, Eocene Thermal Maximum 2 (ETM2, also known as H1) and Hyperthermal 2 (H2) and the highlighted rectangle indicating the study interval. The age is based on the geological timescale of Gradstein et al. (2010). c) The McCullough Peaks area in the north of the Bighorn Basin, with both study areas highlighted in white. Satellite imagery from Google Earth Pro (version 7.3.6.; Eye altitude 40 km).

major reverse thrusts verged to the south in the Owl Creek Mountains (Gries, 1983), resulting in a gentle northern slope of the Owl Creek Mountains during the early Eocene.

Present-day, the Absaroka Mountains form the western margin of the Bighorn Basin. This range was formed by volcanic activity and was not emplaced until near the end of the Willwood Formation deposition (Smedes and Prostka, 1972; Sundell, 1990). It is believed that in the early Eocene, the western boundary of the basin was the Washakie Range, which was located farther west compared to the present-day western border with a steep front towards the east (van Houten, 1944; Kraus, 1983, 1985; Sundell, 1990; Lillegraven, 2009).

2.2.2 Sediment provenance and drainage

Neasham and Vondra (1972) suggested most Willwood sandstone units to be subarkose, with a mainly western source. In contrast, Kraus and Middleton (1987) indicated that most sandstone bodies in their study area (the Clarks Fork Basin in front of the Beartooth Range and more northward than the study area of this thesis) are litharenites, with the primary source area in the Beartooth Mountains. Likely multiple provenances are sourcing the Bighorn Basin, but they commonly originate from its western side. Extensive discussion on this has been presented by Owen et al. (2019), where the authors summarised several different source areas to the west that have been proposed in the literature, including the Cody Arch by van Houten (1944) and Sundell (1990) and the Washakie Range by Lillegraven (2009) and Kraus (1985).

As mentioned, the overprinting of the Washakie Range makes it difficult to constrain the characteristics of the fluvial system fed by this source. However, faults in the Washakie range likely influenced the development of the Willwood sedimentary sequences (Yonkee and Weil, 2015). According to Owen et al. (2019), when the Willwood system was active, it was characterised as a distributive fluvial system with conglomeratic input from the Washakie Range. Kraus (1984) reported early Eocene fanglomerates forming an alluvial fan system sourcing from this range. Based on their detrital zircon geochronology of quartzite clasts, Malone et al. (2017) and Syzdek et al. (2019) provided additional hypotheses for the provenance of fluvial systems to the west closer to the Sevier thrust belt (see the Willwood conglomerates at Meeteetse in Figure 2 of Malone et al., 2017). According to work by DeCelles et al. (1991), the Beartooth fluvial systems comprise several ephemeral coarse-grained alluvial fans and braid-plain deposits, although these are Paleocene in age and thus older than the studied stratigraphic interval in this thesis.

There might also be a sizeable contribution of sediment from the Bighorn Mountains to the easternmost basin fill. Still, comparatively less sediment would influence the study area, given several progressive unconformities in between and the relatively gentle gradient. Westerly palaeocurrents are rarely documented in the eastern and south-eastern parts of the basin (Owen et al., 2019), suggesting that the east side of the basin might have contributed little to the basin fill. The Pryor Mountains are not considered a vital sediment source (Wilson, 1936; Seeland, 1998; Owen et al., 2019).

The dominant palaeoflow direction is interpreted to be north-northwest to north-northeast during the late Paleocene and early Eocene (Neasham and Vondra, 1972; Kraus, 1980; Kraus and Middleton, 1987; Seeland, 1998; Foreman, 2014; Owen et al., 2017, 2019; Wang et al., 2021a), thus approximately paralleling the trend of the basin axis (Kraus and Middleton, 1987; Finn et al., 2010) flowing out of the basin between the Beartooth and Pryor Mountains. Furthermore, there was likely a “Pryor Gap” between the Pryor Mountains and the Bighorn Mountains (see Figure 2 in Blackstone, 1940), which

could have served as an exit for the fluvial system during the deposition of the Willwood Formation (Dickinson et al., 1988; Owen et al., 2019).

2.3 Early Eocene climate

The global early Eocene is interpreted to be in a hothouse state, with a worldwide average temperature $\sim 12^{\circ}\text{C}$ higher than the current global average (Westerhold et al., 2020; Scotese et al., 2021). The early Eocene Bighorn Basin is suggested to have been in a warm-temperate to a subtropical environment with seasonal precipitation (Van Houten, 1948). The basin landscape may resemble modern-day savannahs, with broad open areas interspersed with forest-bordering streams (Neasham, 1967). In the meantime, it is alternatively suggested to be like canopy-structure woodlands by Secord et al. (2008). In the northwest of the basin, lacustrine deposits are reported in front of the Pryor Mountains (Yuretich et al., 1984), while swampy to lacustrine deposits are indicated to be present in front of the Bighorn Mountains (Wing and Bown, 1985; Davies-Vollum and Wing, 1998).

Two significant climatic events occurred in the study interval as two hyperthermal events were recorded. The Eocene Thermal Maximum 2 (ETM2, also known as H1) is associated with the Elmo clay layer in the deep marine realm. The event is associated with the second largest hyperthermal document in the early Paleogene marine record and corresponds to significant high-latitude temperature changes (Sluijs et al., 2009). The ETM2 event is followed by a smaller event, the H2 hypothermal, around 100 thousand years later. Both hyperthermal events are marked by a significant negative carbon isotope excursion of 2-3 ‰ $\delta^{13}\text{C}$ (Fig. 2.2; Abels et al., 2012, 2016; D'ambrossia et al., 2017).

2.4 Willwood Formation sediments

The lower Eocene Willwood Formation consists of a series of alluvial deposits that are currently exposed in the central part of the basin roughly along the north-northwest-south-southeast extending basin axis (Fig. 2.2). It is mainly composed of sandstones, siltstones, and claystones, parts of which have undergone intensive pedogenic modification (Kraus and Davies-Vollum, 2004). Extensive studies have been carried out, with a focus on palaeosols (Kraus, 1999, 2002), processes of river avulsion (Neasham and Vondra, 1972; Kraus and Gwinn, 1997; Kraus and Davies-Vollum, 2004) and fluvial sedimentology (Kraus and Middleton, 1987; Willis and Behrensmeyer, 1995; Kraus and Gwinn, 1997; Kraus, 2001; Owen et al., 2017, 2019). The Basin subsidence during the Paleocene and Eocene was suggested to be continuous (Foreman, 2014), with a long-term average rate approximating 329 m/Myr (Abel et al., 2013).

2.4.1 Channel sandstone bodies

Channel sandstone bodies are classified into two main categories, sheet- and ribbon-type sandstone bodies and are spatiotemporally dispersed unevenly across the basin (Van Houten, 1944; Kraus, 1985, 2001; Kraus and Middleton, 1987; Kraus and Gwinn, 1997). In terms of their origin, ribbon-type sandstone bodies are interpreted to represent a distributary fluvial network linked to the process of avulsion (Kraus, 1985, 2001; Kraus and Middleton, 1987; Kraus and Gwinn, 1997), while sheet-type sandstone bodies are interpreted as the product of the possibly present axial river system (Kraus and Middleton, 1987; Seeland, 1998; Foreman, 2014). More recently, Owen et al. (2017) subdivided the sheet geometry into five types: massive channel body geometry, semi-amalgamated channel body

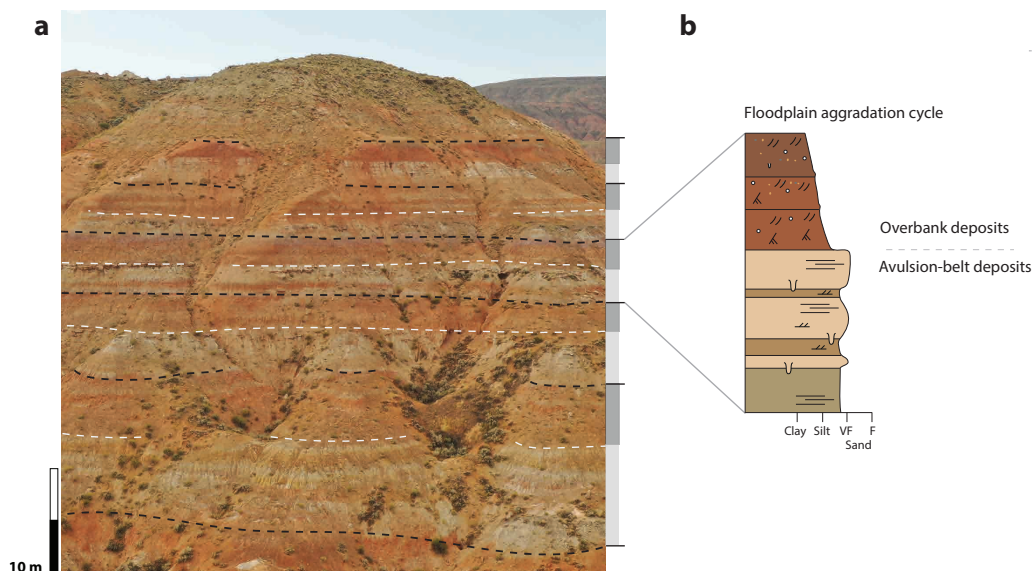


FIGURE 2.3 a) an outcrop section in the Deer Creek area of the McCullough Peaks area showing the floodplain fines of the Willwood Formation where an alternation of well-developed palaeosol and weak to moderately developed soils and heterolithic deposits can be observed representing floodplain sedimentary repetitions. The black and white stipple lines trace the tops of the two facies with the well-developed palaeosols and heterolithic avulsion-belt deposits, respectively (Kraus, 1987). b) A schematic lithological log of a single floodplain sedimentary aggradation cycle with both deposits.

geometry, internally amalgamated channel body geometry, offset stacked channel body geometry, and isolated channel body geometry. Owen et al. (2019) linked the complex nature of the Bighorn Basin infill to the component depositional systems with a relatively wide axial system and several transverse distributive fluvial systems by systematically analysing the downstream trends of channel percentage and geometry as well as grain size. River planforms that contribute to the fluvial deposits in the Bighorn Basin are thought to mainly include sinuous rivers and braided rivers (e.g. Van Houten, 1944; Bown and Kraus, 1983, 1987; Kraus, 1987, 2001; DeCelles et al., 1991; Willis and Behrensmeier, 1995; Kraus and Wells, 1999; Davies-Vollum and Kraus, 2001; Kraus and Davies-Vollum, 2004; Foreman, 2014; Owen et al., 2017, 2019).

2.4.2 Overbank deposits

Most sediment of the Willwood Formation has been deposited on the floodplains of the river systems. Here two kinds of deposits are recognised, claystones with moderately to strongly developed palaeosols and heterolithic deposits ranging from claystone up to sandy siltstone (Kraus and Gwinn, 1997; Abels et al., 2013). The heterolithic deposits are interpreted as avulsion belt deposits formed as the basin's channel relocated to different positions on the floodplain (e.g. Kraus and Aslan, 1993; Kraus, 1996; Kraus and Gwinn, 1997). The claystones with moderately to strongly developed palaeosols are interpreted as true-overbank intervals (Kraus, 1987; Kraus and Aslan, 1993; Clyde and Christensen,

2003), and their colours range from purple and purple-red to yellow-brown. They are classified as vertic palaeosols and have a cumulative character with overprinting older palaeosol profiles with younger profiles resulting in complex horizons with different stages of pedogenesis (Abels et al., 2013).

2.4.3 Floodplain aggradation cycles

The floodplain of the Willwood Formation exhibits a regular alternation between heterolithic and true-overbank deposits, occurring at a scale of 4 to 10 m with an average of 7 m and extends laterally for at least 5 km (Fig. 2.3; Kraus, 1987; Kraus and Aslan, 1993; Clyde and Christensen, 2003; Abdul Aziz et al., 2008; Abels et al., 2013). This alternation of well-developed palaeosol with weak to moderate pedogenic alternation was initially termed a “simple pedofacies cycle” by Kraus (1987) and has been related to the autogenic behaviour of river systems. Lateral channel movement via avulsion causes periods of high and low aggradation, resulting in strong and weak overbank pedogenic development.

Using integrated stratigraphic age constraints, Abels et al. (2013) estimate the period of the alternation to be around 21.6 kyr, which falls within the range of the astronomical precession cycle during the early Eocene. This periodicity suggests that allogenic forcing could drive the alternation, as astronomical-forced climate change could lead to basin-wide changing conditions. Abels et al. (2013) propose a model where an avulsion phase led to laterally extensive heterolithic deposits. Here, a new river course levels out the superelevation of the channel over the adjacent floodplain. Afterwards, a new river steadily aggrades starting from the avulsion-belt deposits, slowly creating superelevation, while true overbank deposits can develop strong soil profiles. Triggered by an external force, such as by precession-driven climate change every 21 kyr, the next avulsion phase occurs (Fig. 2.3b).

However, numerical modelling by Hajek et al. (2010, 2012) and Hajek and Straub (2017) suggest that similar time scales can result from autogenic avulsion alone, resulting in the same alternating patterns on the floodplain. Therefore, while the alternation of the floodplain deposits is interpreted as the result of allogenic and autogenic processes, further research is needed to understand the underlying mechanisms fully.

In this thesis, the term “floodplain aggradation cycles” describes the alternations. However, the use of the word “cycle” and cyclostratigraphy remains a topic of debate within the geological community. In the Willwood Formation, sedimentary alternations on the floodplain are documented to repeat regularly in facies and thickness. While the term “cycle” describes these alternations, it should be noted that this does not necessarily imply that they are solely the result of allogenic forcing. The alternations could be the result of autogenic forcing, allogenic forcing, or a combination of both allogenic and autogenic factors.

2.5 Study Area

In this study, two locations in the northwestern Bighorn Basin were studied. Both sites are in the McCullough Peaks. The Deer Creek area is situated near the basin axis (Kraus and Middleton, 1987) and comprises an area of relatively large exposures. The study interval here represents about 300 m of alluvial stratigraphy in which the Eocene Thermal Maximum 2 (ETM2) and subsequent H2 events occur (Abels et al., 2016). The Gillmore Hill area is situated ca. 17 km to the southern side of the basin axis (Fig. 2.2). Here, the ETM2 interval also has been documented (Abels et al., 2012; D’Ambrosia et al., 2017), indicating the same time of deposition for both sites.

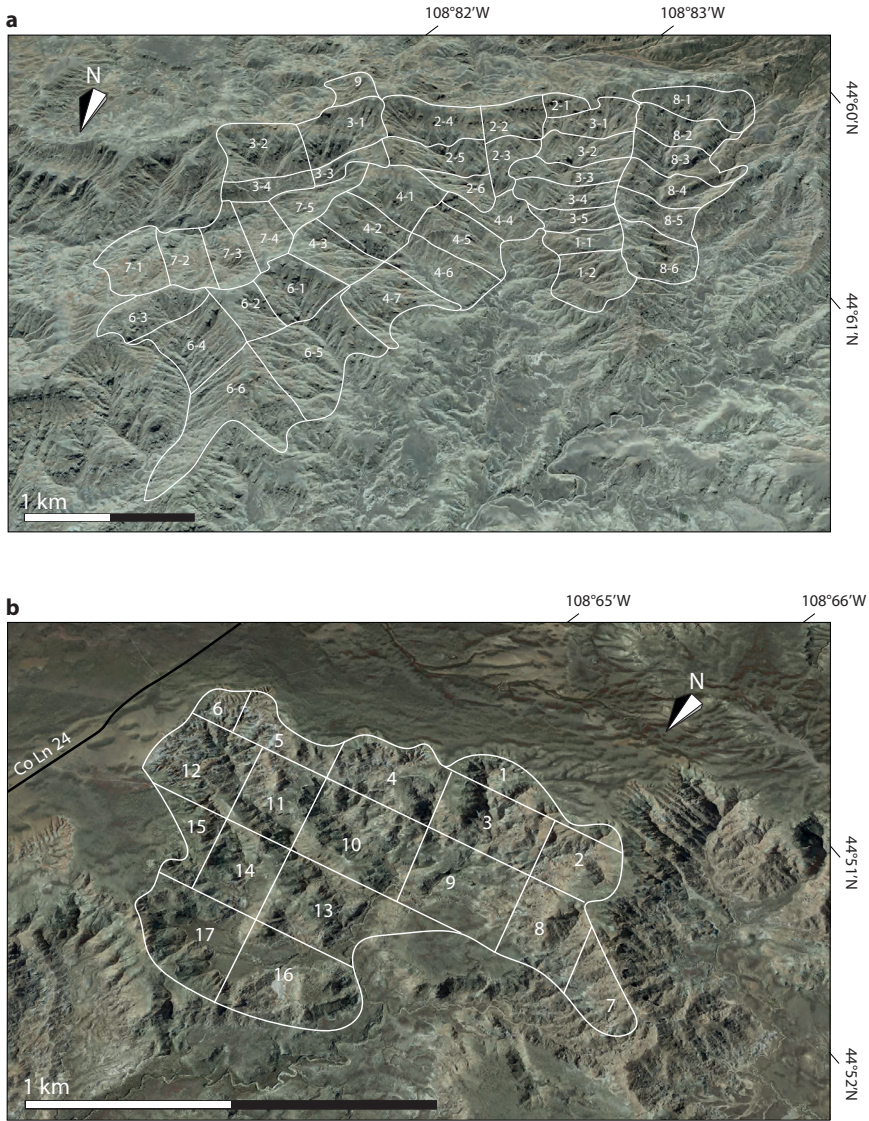


FIGURE 2.4 An overview of the digital outcrop models used in this thesis. a) The Deer Creek digital outcrop model outline with individual tilled models shown by number. b) The Gillmore Hill digital outcrop model outline with individual tilled models shown by number. Satellite imagery from Google Earth Pro (version 7.3.6.; Eye altitude 10 and 6 km respectively).

This hypothermal resulted in distinctive thick purple palaeosol with vast lateral extent in both sites. A total of 8 purple soils have been defined as occurring during the ETM2 and the H2 carbon isotope excursion intervals in the Deer Creek area. (Abels et al., 2012).

2.6 UAV-based photogrammetry

For both studied sites, a digital outcrop model was constructed. These models allow large-scale mapping of the alluvial strata, tracing floodplain aggradation cycles, and document channel sandstone's lateral effect on the floodplain. To do so, multirotor unmanned aerial vehicles (UAV; DJI Phantom 4 Pro and DJI Mavic 2 Pro) were used. A 20-megapixel camera mounted on the UAV automatically took photographs every three seconds. The UAV was manually flown parallel to the outcrop surface at a speed of 5-10 m/s to provide a 60% horizontal overlap between successive photos.

The Deer Creek model includes 21144 photos taken on thirty-four flights (Fig. 2.4a), covering a total area of ~10 km². Fifty-seven ground control points (GCPs) were placed and surveyed using an Emlid Reach GNSS receiver, which from now on is referred to as the rover. The Gillmore Hill digital outcrop model (Fig. 2.4b) covers an area of ~2.5 km² and 100 m of stratigraphy, including 7746 photographs and consists of forty-nine GCPs.

Accuracy of GCPs was improved by using the Post-Processed Kinematic (PPK) positioning technique which compares the rover-recorded GCP position to a second Emlid Reach GNSS receiver that acted as a stationary local base station. Both the rover and base station recorded raw GNSS measurements, which were then processed using the open-source GNSS post-processing package RTKLIB (version 2.4.2). The position of the base station was calibrated by collecting several hours of data and running the PPK solution against the nearest public Continuous Operating Reference Station (CORS) based in Fishtail, Montana (P722). The GCP positions were then determined with centimetre accuracy relative to the local base station.

Agisoft PhotoScan (Version 1.6.3, July 2020; current Metashape) was used to build the three-dimensional digital models using the structure from the motion multi-view stereo (SfM-MVS) photogrammetric method. A triangulated digital surface mesh was created, and the photos were draped onto the surface as the texture. Due to the large size of the area mapped, the complete photogrammetric image set was split into multiple smaller model sections. A tiled model was generated for each section, allowing the entire three-dimensional outcrop model to be imported into LIME (version 2.2.2; Buckley et al., 2019) for visualisation and interpretation.



3

Lateral and vertical characteristics of floodplain aggradation cycles in the lower Eocene Willwood Formation, Bighorn Basin, Wyoming, USA

Abstract

Sedimentation on river floodplains is a complex process that involves overbank flooding, crevasse splaying, and river avulsion deposits. The resulting floodplain stratigraphy often exhibits sedimentary alternations of fine clastic overbank deposits on which soils developed and heterolithic, coarser clastic crevasse splay and avulsion-belt deposits. These floodplain aggradation cycles have been linked to lateral migration and avulsion of channels by internal dynamics, external factors, or a combination of both. To better understand floodplain aggradation cycles' spatial and vertical variability, a detailed mapping is conducted using a three-dimensional digital outcrop model targeting the lower Eocene Willwood Formation in the Deer Creek area of the McCullough Peaks, situated in the basin axis of northern Bighorn Basin. Forty-four floodplain aggradation cycles are identified in 300 m of stratigraphy with an average thickness of 6.8 m and a standard deviation of 2.0 m in compacted stratigraphy. Most sedimentary alternations are consistently traceable throughout the model, indicating their spatial consistency. At the same time, rapid lateral thickness changes are observed in individual floodplain aggradation cycles, which can be up to 4 m over a distance of 400 m. Variogram analysis of both field and numerical model results demonstrates that the thickness of a floodplain aggradation cycle at one locality is significantly related to that at another locality over a longer distance in the palaeoflow direction and perpendicular to the palaeoflow direction. This is interpreted as a result of morphological elements oriented in palaeoflow directions shaping more consistency of sedimentary features in palaeoflow directions. Strong compensational stacking occurs at 2-3 floodplain aggradation cycles at a scale of around 14-21 m. Full compensational stacking seems to occur at larger scales of over 40 m. It is suggested that the spatial and vertical thickness variability of the floodplain aggradation cycles and their compensational stacking behaviour are primarily driven by autogenic processes. External climate forcing may have interacted with these autogenic processes, producing the laterally-persistent and vertically-repetitive floodplain aggradation cycles in the Willwood Formation of the Bighorn Basin, Wyoming.

Chapter 3 has been submitted to the Geological Society of America Bulletin: Wang, Y., Baars, T.F., Storms, J.E.A., Martinius, A.W., Gingerich, P.D., Chmielewska, M., Buckley, S.J., Abels, H.A, 2023, Lateral and vertical characteristics of floodplain aggradation cycles in the lower Eocene Willwood Formation, Bighorn Basin, Wyoming, USA. Author contributions can be found on page 187.

3.1 Introduction

Alluvial stratigraphy is primarily shaped by channel migration and avulsion and the long-term creation of accommodation for sediment accumulation (J. Allen, 1978; P. Allen, 2008; Ashworth et al., 2004; Hajek and Wolinsky, 2012). Analysis of alluvial stratigraphy is commonly performed by examining the distribution and configuration of channel sandstone bodies and accompanying floodplain sediment (J. Allen, 1978; Bridge and Leeder, 1979). River avulsion is a significant process in channelised depositional systems, occurring when a riverbed is superelevated above the surrounding floodplain by a threshold value or when a triggering event, such as a flood, compels a river to cross a stability threshold (Jerolmack and Mohrig, 2007; Jones and Schumm, 1999; Karszenberg and Bridge, 2008; Mohrig et al., 2000; Slingerland and Smith, 2004). There are two types of avulsions: local and regional. Local avulsions affect the fluvial systems within a particular area, while regional avulsions affect the larger fluvial landscape (Slingerland and Smith, 2004). While local and regional avulsions can be fully autogenic, their frequency and magnitude of occurrence are also subject to the influence of external forces such as climate, tectonics, and base level (Kraus and Aslan, 1993; Slingerland and Smith, 2004; Atchley et al., 2004; Cleveland et al., 2007; Simpson and Castelltort, 2012; Abels et al., 2013; Burgess et al., 2016a, 2016b; Chadwick et al., 2020; Wang, 2021).

Palaeosol-bearing alluvial stratigraphy is frequently characterised by meter-scale fining-upward sedimentary alternations composed of two primary components (Kraus, 1987; Atchley et al., 2004; Cleveland et al., 2007; Abels et al., 2013). The lower component comprises heterolithic, bedded, silt-to-sandy deposits that display minimal evidence of pedogenesis. These heterolithics have been linked to crevasse splay and avulsion-belt deposits (Kraus and Aslan, 1993). The upper component is dominated by more homogeneous, fine siliciclastic sediments that exhibit stronger signs of pedogenesis and contain recognisable palaeosols. These fine deposits have been associated with true overbank deposition on relatively distal floodplains (Kraus and Aslan, 1993). Such floodplain aggradation cycles have been identified in various locations, including the Devonian of East Greenland (Olsen, 1990), the Cretaceous-Paleogene of West Texas (Atchley et al., 2004), the Triassic of New Mexico (Cleveland et al., 2007), the Eocene of northern Wyoming (Kraus, 1987; Abels et al., 2013), the Middle Permian of the Karoo Basin in South Africa (Lanci et al., 2022), and the Paleozoic of the Upper Silesian Basin (Opluštil et al., 2022).

The origin of floodplain aggradation cycles has been attributed to various factors, with autogenic channel migration and avulsion being a commonly proposed mechanism (Kraus and Aslan, 1993; Clyde and Christensen, 2003). Alternatively, some researchers indicated these could be linked to changes in base-level or climatic factors (Kraus and Aslan, 1993; Atchley et al., 2004; Cleveland et al., 2007). The repetitive character of the floodplain aggradation cycles, their vertical consistency and lateral persistence, and the coincidence of their period in time with the 21 kyr precession cycle have made some researchers relate the floodplain aggradation cycles in the Willwood Formation in the Bighorn Basin, Wyoming, to variations in climatic conditions driven by the astronomical precession cycle (Kraus and Aslan, 1993; Abdul Aziz et al., 2008; Abels et al., 2013, 2016; van der Meulen et al. 2020). Abels et al. (2013) elaborated a model consisting of an overbank phase during which channel belts were relatively stable in position and gradually aggrading and an avulsion phase during which regional avulsions levelled channel belt superelevations (For more information about the Willwood Formation and the geological setting, see Chapter 2).

Previous studies have examined the characteristics and age of these floodplain aggradation cycles in one-dimensional (1D) stratigraphic sections, as described by Abdul Aziz et al. (2008) and Abels et al. (2013). More recent studies have included age control and the correlation of coeval floodplain aggradation cycles across parallel sections at a kilometre scale (Abels et al., 2016; Westerhold et al., 2018; van der Meulen et al., 2020). However, these studies have not investigated individual floodplain aggradation cycles' lateral and vertical variability in continuous outcrops. While regional climate forcing is expected to create regionally consistent/comparable stratigraphy, local processes such as channel migration, splaying, and avulsion could cause lateral and vertical variations.

To address these knowledge gaps, a study is conducted tracing the floodplain aggradation cycles in the Willwood Formation of the Deer Creek area of the McCullough Peaks in the northern Bighorn Basin, Wyoming (see Chapter 2: Fig. 2.2). The traceability of floodplain aggradation cycles over a large area is demonstrated using a UAV-based digital outcrop model, and their characteristics in the quantified lateral and vertical thickness variability and their compensational stacking behaviour are analysed.

3.2 Methodology

3.2.1 Identification of boundaries between floodplain aggradation cycles

Floodplain aggradation cycles were traced in a digital outcrop model (Fig. 3.1, for more information about the digital outcrop model, see Chapter 2). When tracing floodplain aggradation cycle boundaries, the transition from fine siliciclastics with strong palaeosols (usually red-to-purple in colour) to more sandy deposits with weak or no palaeosols (usually pale brown, yellowish, or orange) were deemed the most reliable indicator of boundary placement throughout the digital outcrop model. This indicator differs from the approach taken by Abels et al. (2013), who typically located boundaries at the top of the strongest soil development index (SDI) values, often corresponding to the reddest soil on freshly exposed rock surfaces. However, in the used models, weathering has made it challenging to identify the strongest SDI values, so it was opted for a more consistent and reproducible approach across all floodplain aggradation cycles and three interpreters: tracing the red-to-yellow transitions that are most clear and leave less room for uncertainty. This approach in floodplain aggradation cycle boundary identification helps reduce interpretive bias and ensures greater applicability and consistency in the interpretations.

3.2.2 Variogram analysis

The variogram is a mathematical function that quantifies the dissimilarity between pairs of data points as a function of the separation distance or lag distance (h) (Pyrzcz and Deutsch, 2003). Typically, the variogram values increase with lag distances, indicating increasing dissimilarity between the data points. A variogram can be calculated as follows (Pyrzcz and Deutsch, 2003):

$$y(h) = \frac{1}{2N(h)} \sum_{a=1}^{N(h)} (z(\mu_a) - z(\mu_a + h))^2$$

where $y(h)$ is a measure of dissimilarity between two data points over lag distance h , and the dissimilarity here refers to the difference of floodplain aggradation cycle thickness in this chapter; $N(h)$ is the number of data point pairs; μ_a is a data point at location a in 2-D space; $\mu_a + h$ is a data point

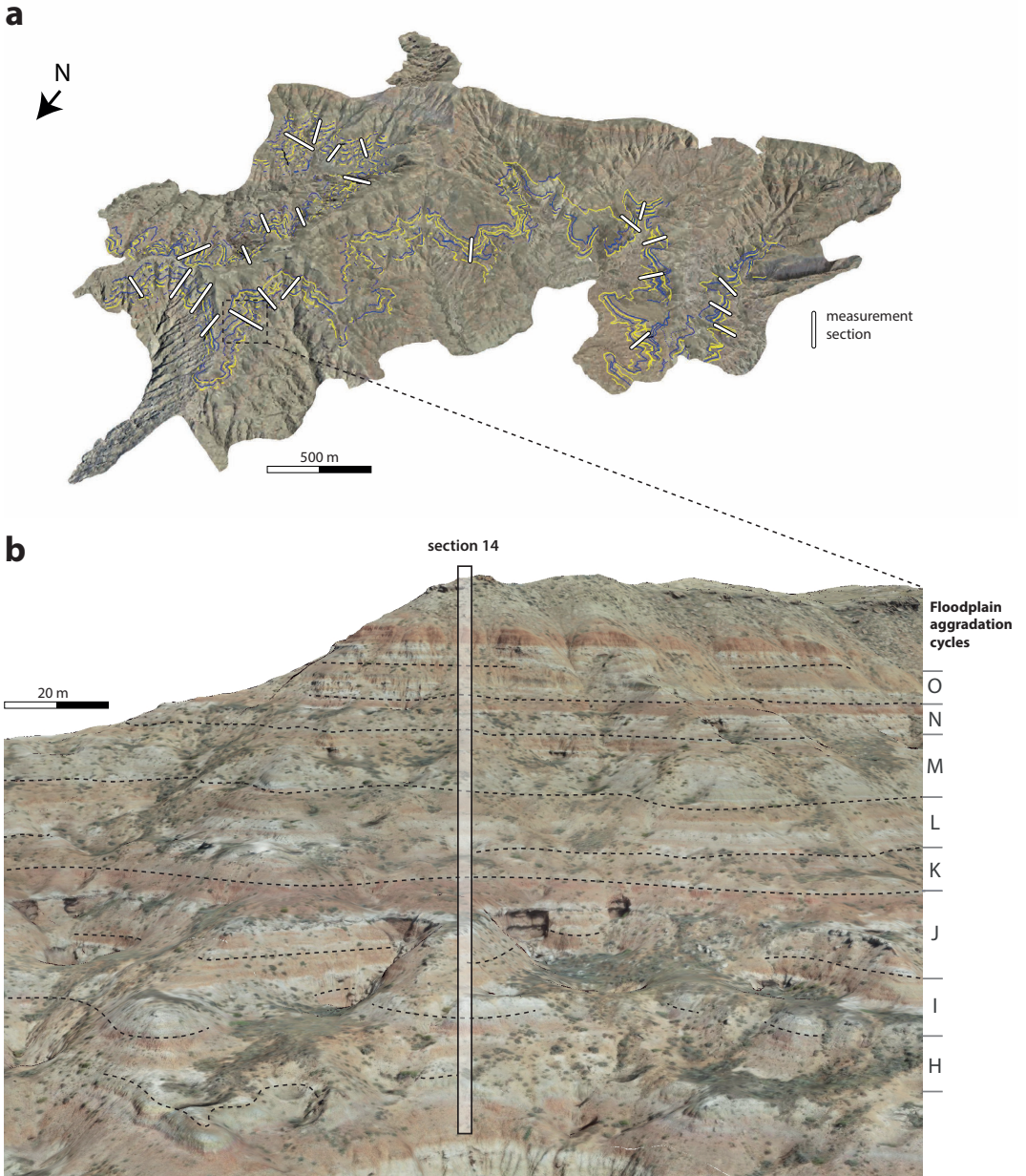


FIGURE 3.1 Tracing floodplain aggradation cycles using photogrammetric models and individual UAV and camera photos. a) The interpreted 3D photogrammetric model in the McCullough Peaks area provides an overview, depicting traced boundaries for seven successive floodplain aggradation cycles. b) A zoomed-in outcrop section in the 3D model shows how floodplain aggradation cycle boundaries (blue and yellow lines) are traced and how a digital section (S14) is constructed.

separated from (μ_a) by the distance h ; $z(\mu_a)$ is the numerical value at the data point μ_a , and $z(\mu_a + h)$ is the numerical value at the location $\mu_a + h$.

Floodplain aggradation cycle thicknesses were measured on outcrop surfaces in the model every 20 m when possible. The measured floodplain aggradation cycle thicknesses were analysed as a 2-D directional variogram (supplementary data Ch3S3) using Python codes developed by Pycrz (2020). Variograms were calculated in six directions with equal azimuth zones of 30°, 60°, 90°, 120°, 150°, and 180° based on the observed statistical anisotropy in the variogram map. The lag distance was set to 100 m and the lag tolerance to 50 m. A search strategy with a wide azimuth tolerance of 30° and a large bandwidth of 2 km reduces the nugget effect near the origin (Zhang et al., 2005). In a directional variogram, a range is identified when the sill ($\gamma(h) = 1$) is reached (supplementary data Ch3S3). Within the range, the floodplain aggradation cycle thickness at one locality is stochastically related to that at another, which is referred to as the spatial continuity of the floodplain aggradation cycle thickness.

To help understand the relationship between variogram features and sedimentary processes, a numerical stratigraphy model developed by Wang et al. (2021) was analysed for their Scenario A40. In this scenario, cyclic changes in water discharge and sediment supply with a wavelength of 10 kyr and an amplitude of 40% produced four cycles that broadly match the floodplain aggradation cycles in the Willwood Formation.

3.2.3 Compensational stacking analysis

Compensational stacking is a phenomenon in which a depositional system preferentially fills topographic lows and avoids deposition on topographic highs until they subside to become lows (Straub et al., 2009; Straub and Pyles, 2012). Two metrics were used to analyse compensational stacking: the coefficient of variation (CV) and the compensational stacking index (σ_{ss}).

Coefficient of variation

The coefficient of variation (CV) is defined as the ratio of the standard deviation over the mean of a data series (herein, the measured series of floodplain aggradation cycle thickness), and thus a smaller CV indicates less variability. Successive depositional units (floodplain aggradation cycles) were combined as assemblages, and the CV was calculated for each assemblage to test for compensational stacking. For example, floodplain aggradation cycles 1 and 2 can be combined as an assemblage, and the thickness of the assemblage is rescaled by dividing it by the regional mean thickness. This rescaling allows for the comparison of thickness variation among different assemblages. An example of how the CV was calculated for a stratigraphic interval with three floodplain aggradation cycles is provided in Supplementary data Ch3S1. This chapter defines an assemblage as fully compensated when the CV value stops decreasing and stabilising.

Compensational stacking index

The standard deviation of sedimentation/subsidence (σ_{ss}) (Wang et al., 2011) can be used to characterise the compensational timescale:

$$\sigma_{ss}(T) = \left\{ \int_0^L \left[\frac{r(T;x)}{r(x)} - 1 \right]^2 dL \right\}^{1/2}$$

Where $r(T;x)$ is the average deposition rate at a horizontal coordinate of x during a time interval of T , L is the cross-basin length, and $r(x)$ is the local long-term sedimentation rate.

Theoretically, σ_{ss} is expected to decrease as T increases, following a power-law trend (Equation 3, Straub et al., 2009; Wang et al., 2011):

$$\sigma_{ss} = a' T^{-k}$$

Where a' is a coefficient, and k is termed the compensation index. By reorganising Equation 3, we can get:

$$\log(\sigma_{ss}) = \log(a') - k * \log(T)$$

Therefore, the slope is $-k$, and the intersection is $\log(a')$ for the relationship between $\log(T)$ and $\log(\sigma_{ss})$.

Straub and Wang (2013) provide an intuitive illustration of the compensational timescale (T_c), which can be used to differentiate between stratigraphy that is partially influenced by autogenic forcing and stratigraphy that is solely influenced by allogenic forcing (see Fig. 3.2 in Straub and Wang, 2013). Figure 3 of Wang et al. (2011) shows that T_c is characterised by a value of $k = 1$, indicating that the stratigraphic stacking is purely compensational beyond this timescale (Straub et al., 2009). A practical workflow to identify the compensational timescale is presented in Supplementary Data Ch3S2.

3.3 Results

3.3.1 Tracing of floodplain aggradation cycles

This chapter identifies forty-four floodplain aggradation cycles over a ~300-m stratigraphic interval (Fig. 3.1a). The stratigraphy containing these forty-four floodplain aggradation cycles starts seven floodplain aggradation cycles below the base of the Deer Creek Amphitheater section (DCA) of Abels et al. (2013). It ends at or above the top of the Upper Deer Creek section (UDC) of Abels et al. (2012) and the Creek Star Hill section (CSH) of Abels et al. (2016). The lower ten floodplain aggradation cycles and the upper eleven floodplain aggradation cycles have limited lateral extents within the digital outcrop model. In contrast, most other floodplain aggradation cycles can be traced up to 4 km in the northeast-southwest direction and ~2.5 km in the southeast-northwest direction. A composite section that includes all forty-four floodplain aggradation cycles is constructed by combining available trenched sections (DCA, CSH, and UDC sections; see Abels et al., 2012, 2016). The labelling system of Abels et al. (2013) and Abels et al. (2012) is extended rather than introducing a new one (Fig. 3.2) to maintain consistency with previous labelling systems. The floodplain aggradation cycles P1 to P3 correspond to ETM2, while floodplain aggradation cycles P5 to P8 correspond to H2 (Abels et al., 2012, 2016).

Among the forty-four floodplain aggradation cycles, seven successive floodplain aggradation cycles with the largest exposure area were traced continuously in the lateral extent throughout the model (Fig. 3.1b), following regionally persistent boundaries, the reasoning of which has been described in the Methodology section. The boundaries between these alternations in this study are, on average, 0.6 m higher than those defined by Abels et al. (2013) in their composite trenches (Fig. 3.3). Despite this difference, the boundaries defined in this chapter are still effective at separating the overbank phase of the lower floodplain aggradation cycle from the avulsion phase of the upper floodplain aggradation cycle. However, certain local factors can complicate the lateral tracing of floodplain aggradation cycle boundaries, such as channel sandstone bodies, soil horizon splitting or merging, debris and

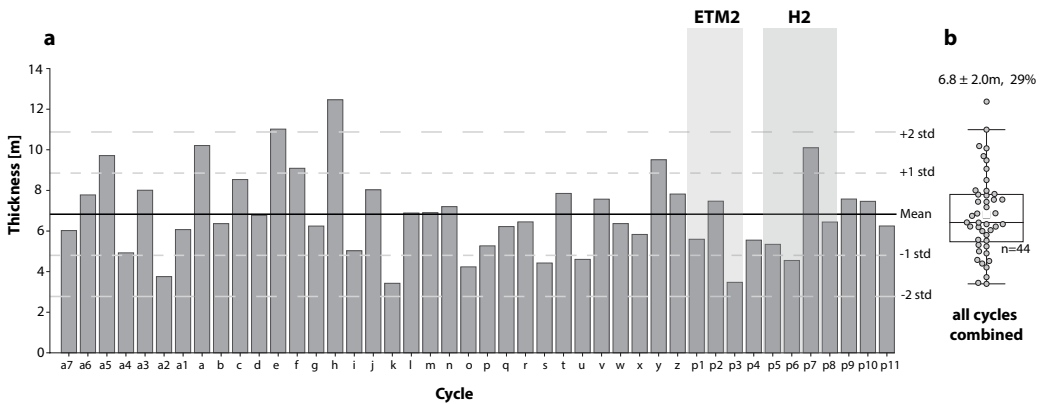


FIGURE 3.2 Thicknesses of forty-four floodplain aggradation cycles in the composite stratigraphy. A) The bar diagram depicts the thickness variability and labelling of the floodplain aggradation cycles. b) The boxplot shows the mean (6.8 m), standard deviation (2.0 m), and coefficient of variation (CV; standard deviation/mean; 29%) of the forty-four floodplain aggradation cycle thicknesses. The box boundaries represent lower and upper quartiles, lines extending from boxes indicate the 1st to 2nd and 3rd to 4th quartile ranges, lines and squares within boxes indicate median and mean values and points outside boxes represent outliers.

vegetation covering outcrops, and low resolution in digital outcrop models. In some cases, it is found that boundaries had clear red/purple to yellow transitions at different stratigraphic levels, with offsets of a few decimetres to 1 or 2 m. It was attempted to maintain consistency by placing the overbank to avulsion phase transition at the stronger of the two transitions and tracing it laterally across the model. In a few cases, this means that laterally the transition had to shift from one soil to another preceding or successive soil at less than 2 m stratigraphic distance.

3.3.2 Quantifying the lateral thickness variability of floodplain aggradation cycles

Seven extensively-outcropped floodplain aggradation cycles in the middle of the studied stratigraphy were traced over the whole panel to analyse individual alternations thickness variability and spatial correlation. These floodplain aggradation cycles are labelled H to N. The regional-averaged thicknesses of the individual floodplain aggradation cycles vary between 3.7 m (alternation K) and 9.7 m (alternation L), with a coefficient of variation (CV) ranging between 17% to 28%. The average thickness of all seven floodplain aggradation cycles is 7.3 m with a standard deviation of 2.6 m (Fig. 3.4).

A total of twenty-two digital sections, such as section 14 shown in Figure 1b, were created in the digital outcrop model, with the top of floodplain aggradation cycle N flattened to form a horizontal reference level (Fig. 3.5). These sections show that the thicknesses of these floodplain aggradation cycles vary rapidly in the lateral direction, with a maximum of 4 m over a distance of 400 m.

Variograms for the seven floodplain aggradation cycles are calculated to investigate the spatial correlation of floodplain aggradation cycle thicknesses. The correlatable distance is, on average, 1.3 km in the long-range direction and 0.6 km in the short-range direction (Fig. 3.6a and supplementary data Table Ch3S4). The variogram ellipse's aspect ratio (i.e., long-range/short-range) ranges from

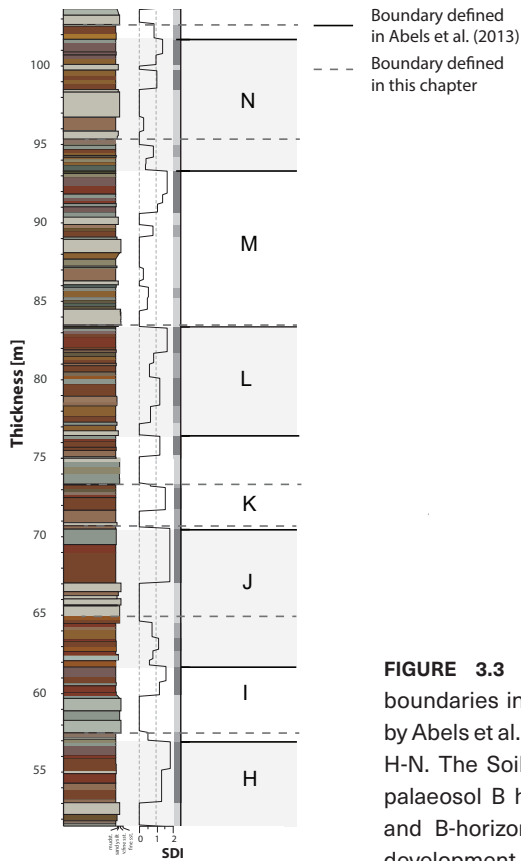


FIGURE 3.3 Comparison of floodplain aggradation cycle boundaries in this Chapter (dashed line) and cycle boundaries by Abels et al. (2013) (solid line) for floodplain aggradation cycles H-N. The Soil Development Index (SDI) curve is a function of palaeosol B horizon thickness, horizon development intensity, and B-horizon rubification (an estimate for the level of soil development. For an explanation of the method, see Chapter 5).

1.4 to 5.3, with an average of 2.2 (supplementary data Table Ch3S4). The long-range azimuth ranges between 310° and 080°, averaging 001° (Fig. 3.6b and Table supplementary data Ch3S4), which is consistent with the average palaeoflow direction measured in the dune-scale cross-beddings in the field ($004^\circ \pm 24^\circ$; Fig. 3.6c; Wang et al., 2022; Chapter 4). Unlike the classic 1D variograms that exhibit monotonically-increasing patterns, repetitive and non-repetitive, non-monotonic patterns in variograms along specific azimuth directions are observed (along azimuth 35° non-monotonic repetitive, and azimuth 125°, non-monotonic non-repetitive, for example, in Fig. 3.7).

A similar analysis was applied to the thickness distribution of cycle three in the numerical model data scenario A40 from Wang et al. (2021; Fig. 3.8). The centre of the basin was used to avoid the influence of upstream or downstream factors (Fig. 3.8c). The variogram analysis of the modelled data indicates an extended range of 22 km in the palaeoflow direction and a short range of 6 km perpendicular to palaeoflow direction (Fig. 3.8d). Increasing correlations with increasing lag distances were observed in the modelled data, with strong correlation (low variogram values) occurring at distances above 10 km (azimuth 030°, Fig. 3.8d), which may relate to the sizes of major channel belts.

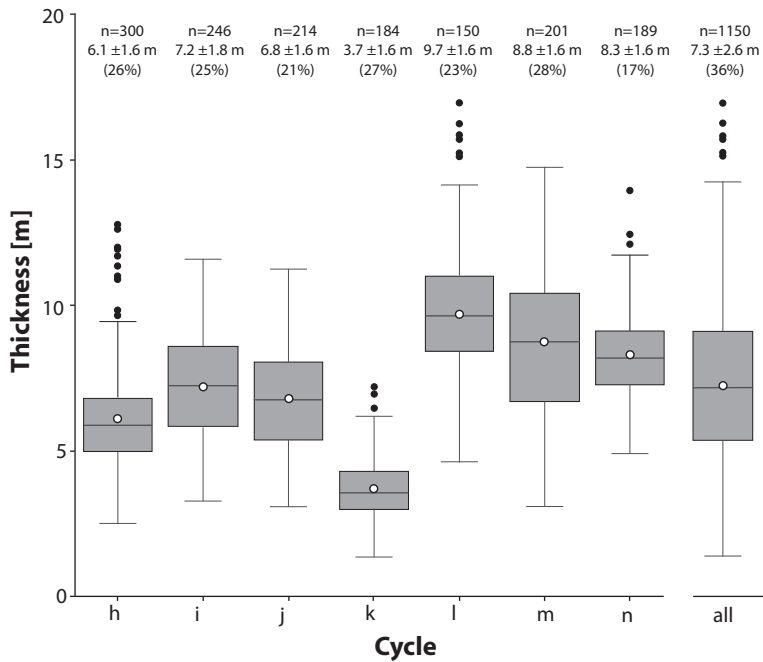


FIGURE 3.4 Box plots illustrating the thickness variability of floodplain aggradation cycles H-N. The right boxplot is based on 1150 measurements equally contributed by the seven floodplain aggradation cycles by randomly selecting 150 measurements from each floodplain aggradation cycle. See Figure 3 for an explanation of the components of the boxplot. Note that the number combination of “a ± b (c)” above each boxplot represents “regional average ± standard deviation (CV).”

3.3.3 Quantifying the vertical thickness variability of floodplain aggradation cycles

The thickness of floodplain aggradation cycles varies locally and can display significant vertical variability. Thicker floodplain aggradation cycles often rest on top of thinner ones and vice versa. For example, in S18 (Fig. 3.5), we observe a thick floodplain aggradation cycle (L) overlaid by a thinner one (M). Similarly, the 1D cross-section consisting of forty-four floodplain aggradation cycles (Fig. 3.2) displays significant vertical variability in floodplain aggradation cycle thicknesses, with an average of 6.8 m and a standard deviation of 2.0 m. Compensational stacking, in which successive floodplain aggradation cycles offset the thickness variations of one another, can reduce the thickness variability of a stratigraphic assemblage containing several floodplain aggradation cycles.

The coefficient of variation (CV) of seven floodplain aggradation cycles in the digital sections was calculated and is shown in Figure 9. It is found that assemblages containing two or more successive floodplain aggradation cycles have a much smaller CV (14%) than those with just one floodplain aggradation cycle (23%). Assemblages containing six or more successive floodplain aggradation cycles have a CV of only 6%, indicating total compensation. Calculating the compensational stacking index shows the scale-dependent decay of σ_{ss} (Fig. 3.9), indicating more substantial compensation over a longer time (Straub et al., 2009; Wang et al., 2011; Straub and Wang, 2013). The strength of compensation, as quantified by κ , has a lower magnitude of 0.53 within the determined compensational timescale (T_c),

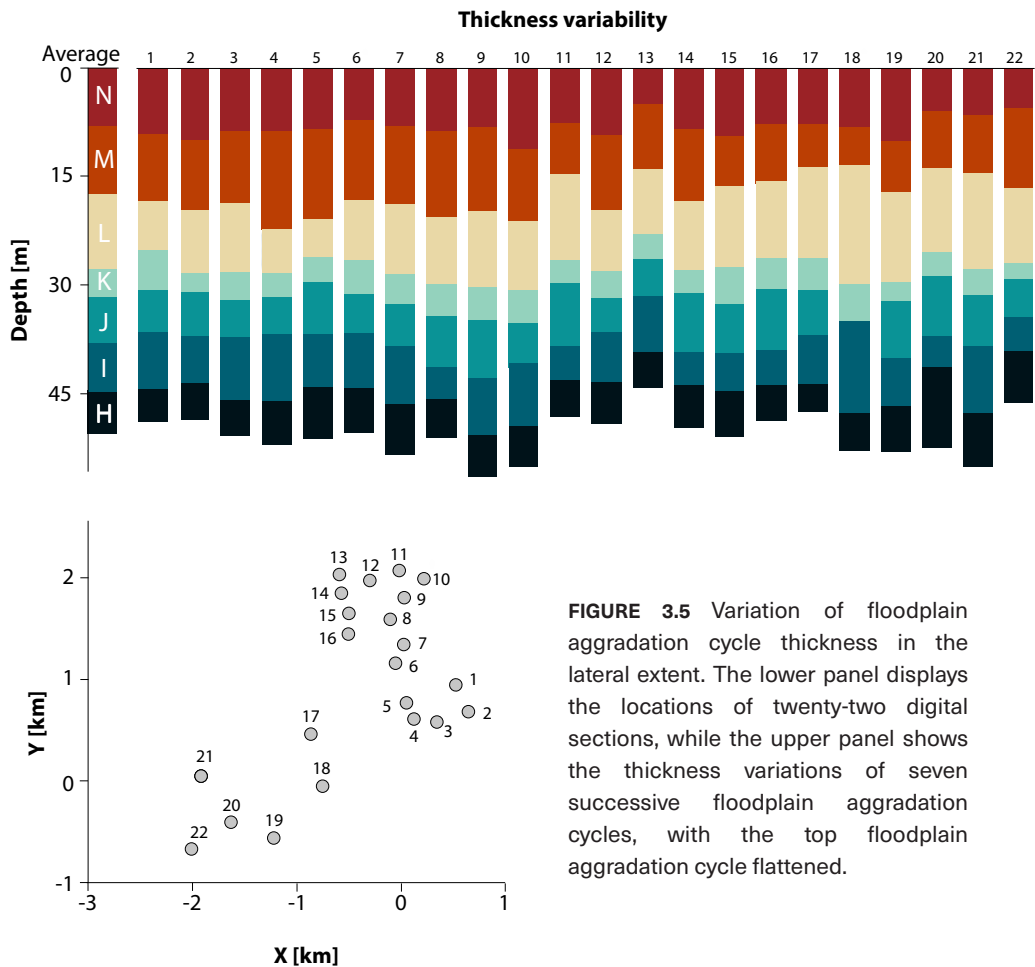


FIGURE 3.5 Variation of floodplain aggradation cycle thickness in the lateral extent. The lower panel displays the locations of twenty-two digital sections, while the upper panel shows the thickness variations of seven successive floodplain aggradation cycles, with the top floodplain aggradation cycle flattened.

which is about twelve floodplain aggradation cycles, indicating random to compensational filling ($k = 0.5-0.75$) that is mainly driven by autogenic forcing (Straub and Wang, 2013). When the stratigraphic assemblage contains more than twelve floodplain aggradation cycles, k approaches 1, indicating total compensation. In this case, the long-term sedimentation rate closely approaches the basin subsidence rate.

3.4 Discussion

3.4.1 Interpreting the lateral thickness variability of floodplain aggradation cycles

The lateral thickness variability of individual floodplain aggradation cycles traced in the continuous outcrops of the Willwood Formation is large. One individual floodplain aggradation cycle may be up to four times thicker at one location than that at another (Fig. 3.4). As matrix sediment colours change from red to pale (Fig. 3.1), the tracing is argued to be confident as here, the transitions from high to low pedogenic intensity are well visible. Thickness measurement inaccuracy may be arguable at 1-2 m scales as occasionally lateral tracing may jump one individual soil profile up or down. However,

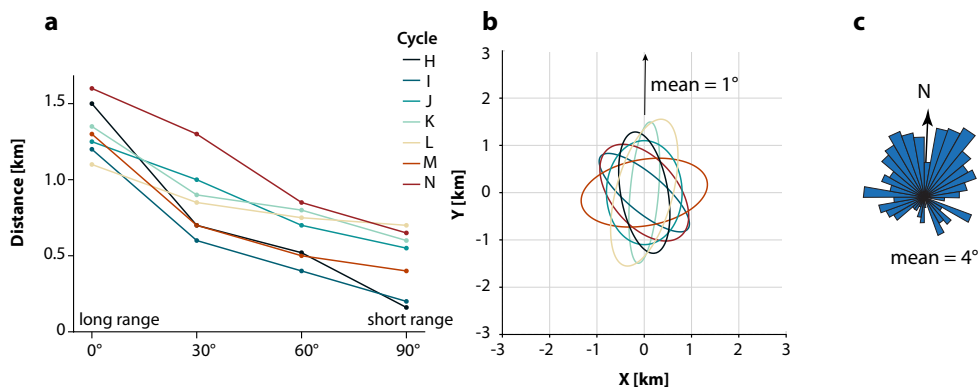


FIGURE 3.6 a) Variation of ranges with azimuth, with long-range azimuth 000° and the short-range azimuth 090°. b) Oriented variogram ellipses with long and short ranges as long and short axes. c) Field-measured palaeoflow directions in the dune-scale cross-stratifications (Chapter 4).

this does not significantly alter the regional mapping results. The current chapter did not include a dynamic backstripping exercise (e.g., Célérier, 1988) with active sedimentation for decompacting the stratigraphic series, which would require resources beyond the scope of this chapter. Therefore, all presented results are based on compacted stratigraphy.

The observed large lateral thickness variability of individual floodplain aggradation cycles could be attributed to several factors. First, differential consolidation and compaction between different lithologies in the compacted stratigraphy may have played a role during and after deposition. Sand-rich deposits such as crevasse splay deposits are more resistant to consolidation and later compaction. The data shows thicker-than-average floodplain aggradation cycles at local sections are often sand-rich. This chapter can not determine how much the thickness variability relates to early consolidation, later compaction, or the other processes influencing lateral thickness variability.

The second driver of thickness variability relates to variable aggradation rates within different morphological elements of the Willwood Formation fluvial systems. Aggradation rates decrease away from channel belts, followed by crevasse splays and levees, and are the lowest on the distal floodplains (Mackey and Bridge, 1995; Kraus et al., 1999; Mohrig et al., 2000; Törnqvist and Bridge, 2002; Hajek and Straub, 2017). Rapid sedimentation near the channel belt is accompanied by slow sedimentation on distal floodplains where only suspended load may arrive during peak floods. This spatial change in aggradation rate may all occur in the same phase of the floodplain aggradation cycles causing lateral thickness variability within the individual sedimentary alternation. Lower degrees of consolidation and compaction of coarser-grained material even strengthen the morphodynamical effect of higher aggradation rates near the channel belts, as these sediments are also the coarsest. Both processes work in the same direction.

Meanwhile, it is observed that the thicknesses of floodplain aggradation cycles are more consistent in the palaeoflow direction, both in field and numerical data (Fig. 8.6 to 8.8). This consistency could relate to the morphological segmentation of the Willwood Formation floodplains by channel belts that are dominantly oriented in the downstream direction. The Bighorn Basin had transverse river systems from the basin margins and axial river systems flowing north over the basin axis (Owen et al., 2019; Wang et al., 2022). The study area is located over the basin axis, and it seems unlikely that

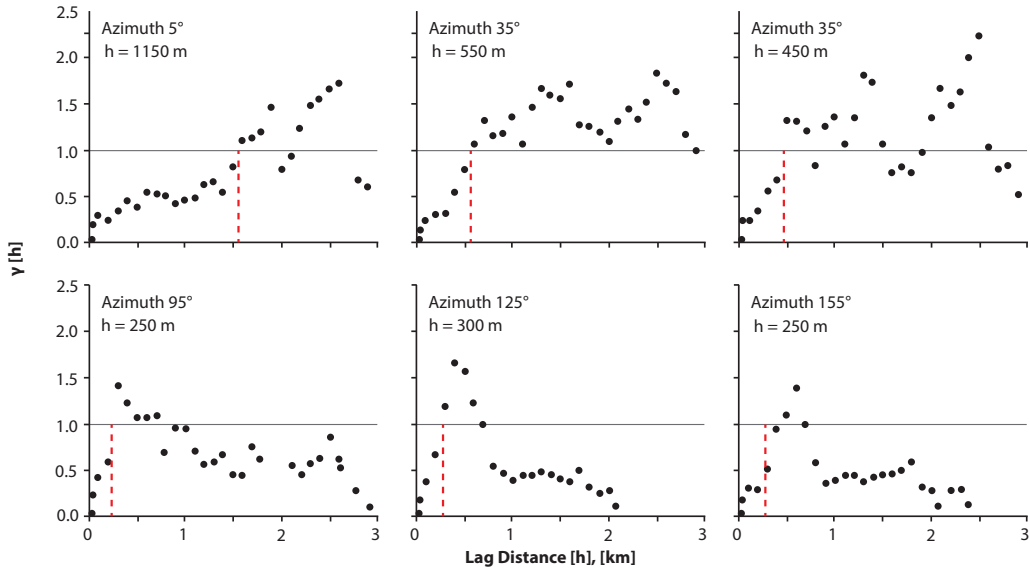


FIGURE 3.7 One-dimensional directional variograms for floodplain aggradation cycle H with different azimuths. Red circles and lines indicate the ranges along different azimuths. Information on how to read variograms has been explained in the Methodology section.

transverse and axial river systems interacted at this location, although this scenario can not be entirely excluded. The consistency scale would be lower if differently oriented river systems governed the area. In the numerical model data, consistency is on the order of 5-15 km, much longer than that in the field data, where consistency is between 1-2 km (Fig. 3.7 and 3.8). However, it is challenging to draw definitive conclusions from this difference because the dimensional values in the numerical model cannot be scaled to any field situation.

Nevertheless, the critical influence of palaeoflow is seen in both numerical and field data. For a single fluvial landscape, the properties of floodplain deposits may change quite significantly within 1 to 2 km (Mohrig et al., 2000). However, our field data relates to changing properties of complete floodplain aggradation cycles that last around 21 kyr (Abels et al., 2013, 2016; van der Meulen et al., 2020). So, the floodplain aggradation cycles studied here result from a long history of successive fluvial landscapes, each with its local morphodynamic changes of moving channel belts and local crevasse splays and avulsions. To that extent, one could argue that the observed downstream consistency of the floodplain aggradation cycles at 1-2 km scales still shows consistency of fluvial landscapes at time scales of thousands of years.

Overall, it is argued that the large lateral thickness variability of individual meter-scale floodplain aggradation cycles results from a combination of factors. These are differential early-stage consolidation and late-stage compaction and the different aggradation rates related to the morphologic elements within the fluvial systems that governed the area. These controls are primarily autogenic (Hajek and Straub, 2017) and may have been strengthened or diminished by external changes.

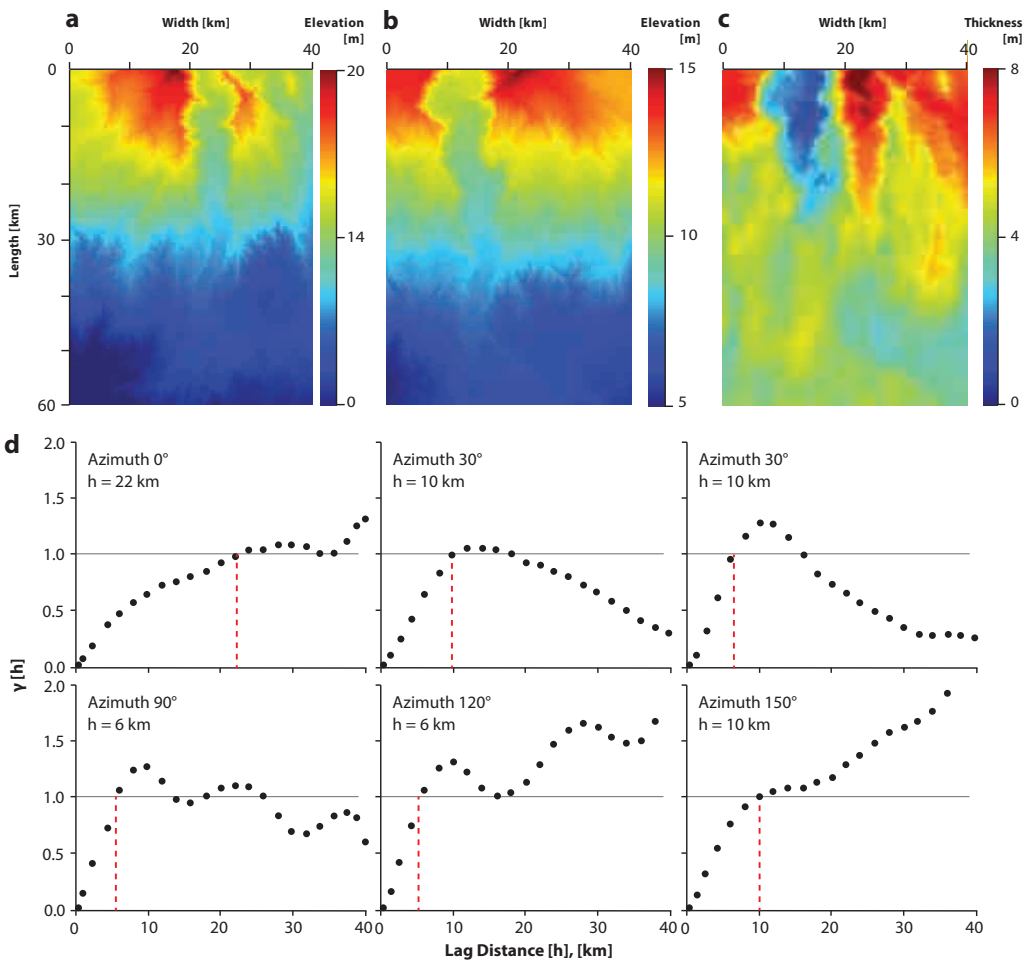


FIGURE 3.8 Geostatistical analysis using the Scenario A40 data from Wang et al. (2021). a) The elevation map of the base of cycle 3. b) The elevation map of the top of cycle 3. c) The thickness map of cycle 3. d) Directional variograms using the data constrained in the red rectangular of panel C.

3.4.2 Interpreting the vertical thickness variability of floodplain aggradation cycles

Vertically, floodplain aggradation cycles with thicknesses below the average are often followed by alternations that are thicker than the average (Fig. 2 and 4). The coefficient to variation of the thickness variability of individual floodplain aggradation cycles goes down from 23% to 14%, from one alternation to the sum of two alternations, and further down to 10% for the sum of three alternations (Fig. 3.9). This suggests that much of the vertical thickness variability in the landscape is counterbalanced by variable deposition over two to three successive floodplain aggradation cycles. However, it is also possible that differential compaction may play a role. In the data, locally thicker floodplain aggradation cycles are more often coarse-grained and are expected to compact less. If a locally thick floodplain aggradation cycle represents a relatively high location on the floodplains, it is expected to receive a suspended load in the next floodplain aggradation cycle dominantly. This

results in a locally thin floodplain aggradation cycle consolidating and compacting even more than the preceding coarse-grained, thicker floodplain aggradation cycle. In this way, differential compaction strengthens the reduction of the coefficient of variation of floodplain aggradation cycle thicknesses over two to three alternations. However, it can not be determined if the relative importance of differential compaction and topographic infilling is in these results. Syn-sedimentary or early-stage consolidation can create increased topographic differences on a landscape that was initially flatter. Distal floodplain fines may consolidate more than proximal sands, increasing the gradient between the channel belts and the distal floodplains (Törnqvist et al., 2008).

Total compensation of floodplain aggradation cycle thicknesses seems to require the stacking of six to twelve floodplain aggradation cycles in the study data (Fig. 3.9), which would amount to 120 to 240 kyr if these floodplain aggradation cycles occur at precession scale like previous studies suggest (Kraus and Aslan, 1993; Abels et al., 2013, 2016). This calculated T_c is much longer than the 10-67 kyr estimated by Straub et al. (2020) based on the maximum channel-belt sandstone body thickness and long-term sedimentation rates in the Bighorn Basin. This discrepancy is expected because the method used by Straub et al. (2020) is more applicable when there is no external forcing. As shown by the modelling results of Wang et al. (2021), T_c is prolonged from 2.0 kyr in a fully autogenic scenario by 2.5 times to 5.1 kyr in two scenarios with allogenic forcing (see their Fig. 3.4). This is because the river behaviour can be influenced by the allogenic forcing, such as forced incision during a specific period, which may prevent compensational stacking from occurring. Moreover, data resolution may also play a role. If sedimentary beds lower than floodplain aggradation cycles in the hierarchy are used, the estimated T_c might also be lower. However, age constraints would not be able at that scale using field data. Furthermore, using multiple long 1D sections to calculate the compensational stacking index is always preferred for this kind of analysis, and doing that might reduce T_c . However, the outcrop exposure does not provide various locations where many continuous floodplain alternations free of channel sandstone bodies are available.

Straub and Pyles (2012) proposed that units as small as individual channel beds compensate for the topographic differences created by older beds. In contrast, units of channel stories and higher hierarchy (i.e., channel element and channel complex) also compensate for one another during their stacking. This concept is extended to floodplain aggradation cycles, which also exhibit features of compensational stacking.

Overall, these findings demonstrate that compensational stacking and differential compaction play essential roles in the vertical thickness variability of floodplain aggradation cycles. The location of morphodynamic elements on the Willwood Formation fluvial landscapes was influenced by previous sedimentation for at least 40 kyr and 15 m of vertical stratigraphy (i.e., two floodplain aggradation cycles). Crevasse splay and avulsion-belt deposits tend to cluster in low-lying areas governed by distal floodplain deposition in preceding times. A very long full compensational timescale of more than 120 kyr and 40 m of stratigraphy (i.e., at least six floodplain aggradation cycles) could relate to the interaction between compensational topographic filling with ongoing differential consolidation and compaction as it seems unlikely that the dynamic fluvial systems could not level topographic differences at shorter time scales. Vertical variability in the thicknesses of floodplain aggradation cycles is thus governed by variable topographic infilling of fluvial landscapes and subsequent consolidation and compaction. These are primarily autogenic processes that external dynamics could strengthen or diminish.

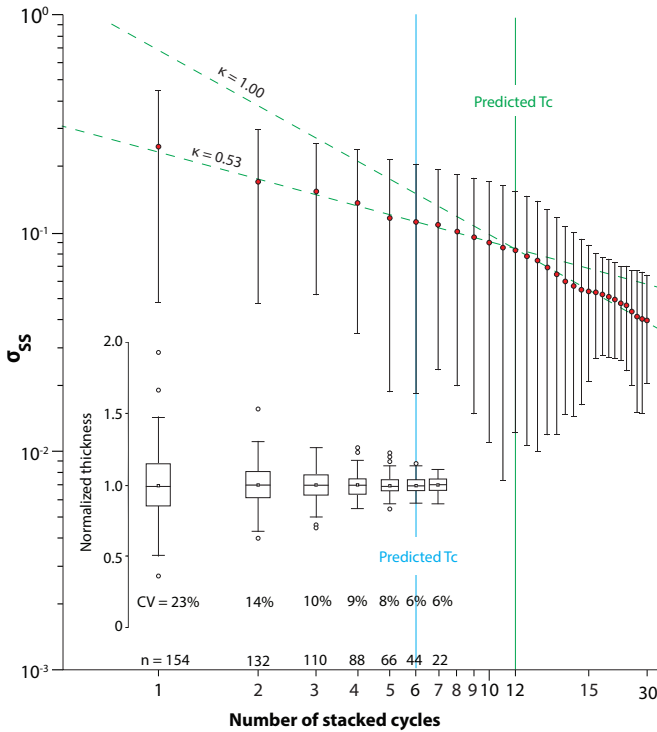


FIGURE 3.9 Two metrics for calculating the compensational timescale (T_c). The lower part shows the decay of coefficient of variance with an increasing number of floodplain aggradation cycles. The predicted T_c (blue line) corresponds to six floodplain aggradation cycles since CV no longer reduces and stabilises at 6%. The upper part shows the decay of σ_{ss} with an increasing number of floodplain aggradation cycles. Error bars represent the geometric standard deviation, red dots indicate the average σ_{ss} , green dashed trend lines represent the best linear fit, and the green dashed line indicates the predicted T_c that corresponds to twelve floodplain aggradation cycles.

The average thickness of individual floodplain aggradation cycles is observed to vary significantly in the stratigraphy (Fig. 3.4). There could be several reasons for this. First, if these floodplain aggradation cycles are driven by precession-scale climate change, as suggested in previous work (Abdul Aziz et al., 2008; Abels et al., 2013, 2016; van der Meulen et al., 2020), their deposition may represent different amounts of time since wavelengths of individual precession cycles can range between 19 and 23 kyr (Berger et al., 1992). However, the impact of this difference in precession component wavelength is expected to be minor, as the ratio of 23 kyr/19 kyr (about 1.2) is relatively small compared to the difference in the average thickness between floodplain aggradation cycles K and L (10 m versus 3.5 m). Alternatively, the study area of 10 km² may not be large enough, and river systems may have moved their courses over larger areas resulting in the absence of coarse-grained material during the deposition of some floodplain aggradation cycles, making them thinner. Moreover, vice versa, a dominance of coarse-grained material during other floodplain aggradation cycles makes them thicker. To further investigate this, larger datasets are needed to trace floodplain aggradation cycles over a more significant distance, which is challenging due to the limit of outcrop exposure and the difficulty in making a much larger digital outcrop model.

It is recommended to conduct alluvial stratigraphic analysis using composite stratigraphy, which averages several 1D sections. This approach allows for examining both the lateral depositional and compaction-related variability and the persistency and continuity of stratigraphy, as demonstrated by

Zhang et al. (2022). While the external climate and tectonic controls can influence internal depositional dynamics, it is argued that autogenic dynamics are responsible for most of the lateral and vertical thickness variability observed in the Willwood Formation alluvial stratigraphy. Thus, it is essential to interpret palaeoclimatic information derived from alluvial stratigraphic records in the context of considering significant lateral thickness variability of floodplain stratigraphy between lateral areas. To avoid misinterpretation, meter-scale, and kyr-scale variability in high-resolution palaeoclimate records of alluvial strata should not be interpreted in detail that suggests continuity of sedimentation. Instead, detailed patterns in such records can only be obtained by averaging multiple 1D parallel successions. Nevertheless, the considerable lateral variability would be significantly suppressed if analysing larger-scale stratigraphic patterns, such as combining several successive floodplain aggradation cycles as a stratigraphic assemblage. Therefore, it is essential to consider the scale of analysis, both lateral and vertical, when interpreting alluvial stratigraphy.

3.5 Conclusions

This chapter utilised a three-dimensional digital outcrop model to examine floodplain aggradation cycles' lateral and vertical thickness variability in the McCullough Peaks Area of the lower Eocene Bighorn Basin, Wyoming. In the lateral direction, the thicknesses of individual floodplain aggradation cycles may vary rapidly, which is more pronounced perpendicular to the palaeoflow than in the palaeoflow direction. This lateral variability is believed to result from the combined effect of differential consolidation and compaction and varied depositional rates depending on the proximity to the channel belts. Notably, such lateral variability archived in the stratigraphy differs from that seen in a modern-day fluvial landscape. The latter represents only one of the many snapshots in the geological history that generates each floodplain aggradation cycle. Palaeoflow direction significantly impacts such lateral variability in both numerical and field data. In the vertical direction, there are significant thickness variations among successive sedimentary alternations; thicker-than-average floodplain aggradation cycles are followed by thinner ones, as observed in one- and three-dimensional mapping. Such vertical thickness variability is counterbalanced by later-deposited floodplain aggradation cycles, during and after which both compensational stacking and differential compaction may play crucial roles. Fully compensational stacking occurs at the scale of at least six floodplain aggradation cycles. Results in this chapter suggest the necessity of using composite stratigraphy averaging several 1D sections, reducing the impact of the significant lateral thickness variability. Similarly, the significant vertical thickness variability will be less influenced by analysing larger-scale stratigraphic patterns. In other words, it is always important to consider the scale of analysis, both lateral and vertical, when interpreting alluvial stratigraphy.



4

Sandstone body character and river
planform styles of the lower Eocene
Willwood Formation, Bighorn Basin,
Wyoming, USA

Abstract

In the lower Eocene Willwood Formation of the Bighorn Basin, Wyoming, USA, channel dynamics were studied at a relatively low resolution throughout the basin over the geologic time from the Late Paleocene to the early Eocene. In the present chapter, a high-resolution study is reported to complement previous research at the basin scale. Efforts are made to document the characteristics and river planform styles of most sandstone bodies encountered through ca. 300 m of alluvial stratigraphy in a 10 km² area of the Deer Creek area of the McCullough Peaks, situated in the basin axis of northern Bighorn Basin. Four channel facies associations are recognised and ascribed to four river planform styles: crevasse channel, trunk channel, braided-like channel, and sinuous-like channel, with the latter two dominant types. Braided-like and sinuous-like channel sandstone bodies differ significantly in thicknesses, on average 6.1 m versus 9.0 m, but they have similar palaeoflow-perpendicular widths of on average 231 m and palaeoflow directions of on average 003°. Braided-like and sinuous-like river planform styles show no spatial dependency in the 10 km² study area. This chapter's results align with existing basin-scale depositional models composed of a single axial system fed by several transverse systems dominantly from the west. The feeding of these systems could be influenced by palaeoclimate changes, possibly controlling their contribution over time, thereby impacting river planform styles. At the same time, changing water discharge hydrograph, sediment load, and overbank cohesiveness may have equally driven the observed river planform style changes within the basin without a significant role of catchments.

Chapter 4 is based upon: Wang, Y., Baars, T.F., Sahoo, H., Storms, J.E., Martinus, A.W., Gingerich, P. and Abels, H.A., 2022. Sandstone body character and river planform styles of the lower Eocene Willwood Formation, Bighorn Basin, Wyoming, USA. *Sedimentology*, 69(7), pp.2897-2924. <https://doi.org/10/grb6x5> Author contributions can be found on page 187.

4.1 Introduction

Alluvial architecture illustrates fluvial channel bodies' size, shape, spatial arrangement, and associated facies in three dimensions (Allen, 1978; Bridge and Leeder, 1979). The architecture is controlled by both autogenic processes, such as channel avulsion and self-organisation (e.g. Mackey and Bridge, 1995; Hajek et al., 2010), and allogenic factors, such as climate, basin subsidence and uplifting, and base level (e.g. Shanley and McCabe, 1994; Holbrook et al., 2006; Hampson et al., 2013; Bijkerk et al., 2014). Extensive studies have been conducted on alluvial deposits using various approaches and datasets, including high-resolution three-dimensional seismic data (e.g. Posamentier et al., 2007), numerical modelling (e.g. Jerolmack and Paola, 2007; Karssenberg and Bridge, 2008; Wang et al., 2021b), and outcrop analogues (e.g. Fielding, 1986, 2006; Allen et al., 2013; Colombera et al., 2016, 2017; Ghinassi et al., 2016; Ghinassi and Ielpi, 2018). Outcrops provide data that span large hierarchical temporal and spatial scales, which can help interpret depositional environments, reconstruct palaeoclimates (e.g. Howell et al., 2014; Colombera et al., 2016; Paredes et al., 2016), and build subsurface predictive models (e.g. Bryant et al., 2000; Enge et al., 2007).

By investigating alluvial strata in the Bighorn Basin, Wyoming, USA, numerous studies have reported on a variety of aspects: e.g. palaeontology (Gingerich, 2010); palaeo-magnetism (Clyde et al., 1994); palaeosols (Bown and Kraus, 1981; Kraus and Gwinn, 1997; Kraus, 1999, 2002; Davies-Vollum, 1999, 2001; Abels et al., 2013; Wang et al., 2021b); and channel sandstone bodies, the focus of this chapter (Van Houten, 1944; Neasham, 1970; Neasham and Vondra, 1972; Kraus and Middleton, 1987; Bown and Kraus, 1987; Kraus, 1985, 1996; Willis and Behrensmeier, 1995; Kraus and Gwinn, 1997; Kraus and Wells, 1999; Davies-Vollum and Kraus, 2001; Clyde and Christensen, 2003; Kraus and Davies-Vollum, 2004; Foreman, 2014; Owen et al., 2017). The well-documented floodplain cyclicality in the Willwood Formation of the Bighorn Basin provides an opportunity to investigate the influence of orbital climate forcing on alluvial architecture (Abdul Aziz et al., 2008; Abels et al., 2013; Wang et al., 2021a). Also, extreme climate warming has been observed to impact alluvial architecture in the basin (Foreman, 2014; Van der Meulen et al., 2020; For more information about the Willwood Formation and the geological setting, see Chapter 2).

Generic relationships between channel and floodplain deposits were illustrated over basin scales, with thick sheet sandstones ascribed to meandering river processes (Kraus and Middleton, 1987; Kraus and Gwinn, 1997; Foreman, 2014). Moreover, the Bighorn Basin is suggested to host an axial river system and several transverse systems (Kraus and Middleton, 1987; Owen et al., 2019). Interaction between these systems could have influenced the geomorphology downstream of the interfingering sites. This hypothesis has been corroborated by data from Owen et al. (2019), analysing the downstream variation trends of channel proportion, geometry, and grain size. The channel sandstone bodies studied by Owen et al. (2019) are spread through the basin and of different stratigraphic levels. In this context, documentation of all sandstone bodies in one continuous succession in a single area could aid the understanding of changes in fluvial dynamics in space and time, further document the possible interaction between the axial and transverse systems, and validate or refine existing depositional models.

In this chapter, efforts are made to investigate the lower Eocene channel sandstone bodies in the Deer Creek area of the McCullough Peaks in the northern Bighorn Basin situated near the basin axis (see Chapter 2: Fig. 2.2, Kraus and Middleton, 1987). Sandstone bodies that occur in ca. 300 m of stratigraphy are targeted to analyse their geometry and internal characteristics, reconstruct

their related river planform styles, and interpret their character within the frame of the basin-scale geomorphology. This analysis combines field documentation with observations in a georeferenced digital outcrop model developed using an unmanned aerial vehicle (UAV) in a 10 km² area (for more information about the digital outcrop model see Chapter 2).

4.2 Methodology

4.2.1 Fieldsite documentation

Sandstone bodies were systematically documented in the field using a standard set of parameters, including grain size, lithology, sedimentary structure, geometry, boundaries, palaeoflow directions, and dimensions. Based on this documentation, lithofacies and lithofacies association classification schemes were established following the methods outlined by Allen (1983) and Miall (1985, 1996). Data were structurally collected with spreadsheets and short sedimentary logs to characterise each sandstone body type. The grain size was measured by observing the grains with a grain size chart under a hand lens. Dimensions of sandstone bodies were measured using Jacob's staff, flexible tapes, and a laser rangefinder when not directly accessible. The colour was described according to the methods detailed in the Soil Survey Manual (Ditzler et al., 2017). Palaeocurrent data and cross-set thickness were measured from dune-scale cross-stratification (mainly planar and trough cross-stratification). All documented sandstone bodies were referenced in a digital outcrop model where the outcropping extent was mapped (for more information about the digital outcrop model, see Chapter 2). The locations of the studied sandstone bodies in the digital outcrop model are provided in Supplementary Data Ch4S1.

4.2.2 Petrological analysis

Classification of sandstones follows the scheme by McBride (1963) that groups framework grains into (1) quartz plus chert and quartzite, (2) feldspar, and (3) rock fragments and accessory minerals. Thirty-two sandstone samples were collected from outcrops in the study area and made into thin sections in the thin section laboratory of Utrecht University. It should be noted that the specimen sampling is biased regarding the specimen number during the fieldwork when types of deposits were not identified yet. Therefore, specimens of some types were collected more than others. Covid-19 travel restrictions prevented further sampling in 2020 and 2021.

4.2.3 Formative bankfull depth estimation

Dune-scale cross-set thickness (S_m) has been empirically used to estimate the mean formative bedform height (h_m), as is shown in equation 1 (Bridge and Tye, 2000; Leclair and Bridge, 2001). Applying this method requires meeting the precondition that the coefficient of variation (ratio of standard deviation to mean) of the preserved cross-set thickness should vary between 0.58 and 1.18 (Bridge and Tye, 2000).

$$h_m = 2.9(\pm 0.7)S_m$$

Subsequently, the mean formative bankfull depth (d) can be estimated based on the empirical equation proposed by Bradley and Venditti (2017):

$$d = 6.7h_m \text{ (with 50\% prediction interval: } 4.4h_m \text{ to } 10.1h_m \text{)}$$

4.2.4 Statistical analysis

Two-sample t-tests were performed to assess whether there are statistically significant differences between different types of deposits in terms of channel sandstone body thickness and width. Palaeocurrent data was analysed as circular data using the R programming language, and the Rayleigh Test of Uniformity was implemented to check whether the distribution of the palaeoflow data of certain deposits is significantly different from the uniform distribution. Watson's Two-Sample Test of Homogeneity is employed to compare whether the distributions of the palaeoflow data of two types of channel deposits are significantly different.

4.3 Results

4.3.1 Lithofacies analysis

Based on detailed observation and description of grain size, lithology, internal sedimentary structures, and spatial positions in the sandstone bodies, 12 lithofacies are recognised in the field (Fig. 4.1 and Table 1). There are one conglomeratic lithofacies, named clast-supported conglomerate (G); nine sandy lithofacies, including massive sandstone (Sm), trough cross-stratified sandstone (St), planar/tabular cross-stratified sandstone (Sp), ripple cross-laminated sandstone (Sr), climbing-ripple cross-laminated sandstone (Scr), low-angle ($<15^\circ$) cross-stratified sandstone (Sl), sandstone with erosional scour and fill (Se), bioturbated sandstone (Sb), and convoluted sandstone (Sc); and two silty to muddy lithofacies: mudstones and siltstones (Fs) and laminated siltstones (Fl). Details of their character and interpretation are given in Table 1.

4.3.2 Facies association analysis

According to the organisation of lithofacies in the vertical succession and lateral distribution (Table 2), five sandy facies associations are classified, which fall into two major categories: channel facies associations and floodplain facies associations.

Channel facies associations

Facies Association 1: Small-scale crevasse channel sandstone deposits

Description:

Facies Association 1 (FA1) mainly comprises fine- to medium-grained sandstone bodies (Fig. 4.2) with a thickness range of 0.5-3 m and an average of 1.9 m ($n = 15$). Its indurated part shows a lenticular external geometry with concave-up margins in the transverse view (Fig. 4.2a) and ribbon-shaped geometry in the longitudinal view (Fig. 4.2b). Various lithofacies are present, including trough cross-stratified sandstone (St), planar/tabular cross-stratified sandstone (Sp), and ripple cross-laminated sandstone (Sr). Within FA1, trough cross-stratified sandstone (St), if present, is usually in the lower part, planar/tabular cross-stratified sandstone (Sp) in the middle part, and ripple cross-laminated sandstone (Sr) in the upper part. This facies association is generally encased within floodplain deposits with pedogenic features due to subaerial exposure. The contact between FA1 and floodplain fines is usually sharp, with floodplain fines passively draping the top of the sandstone body.

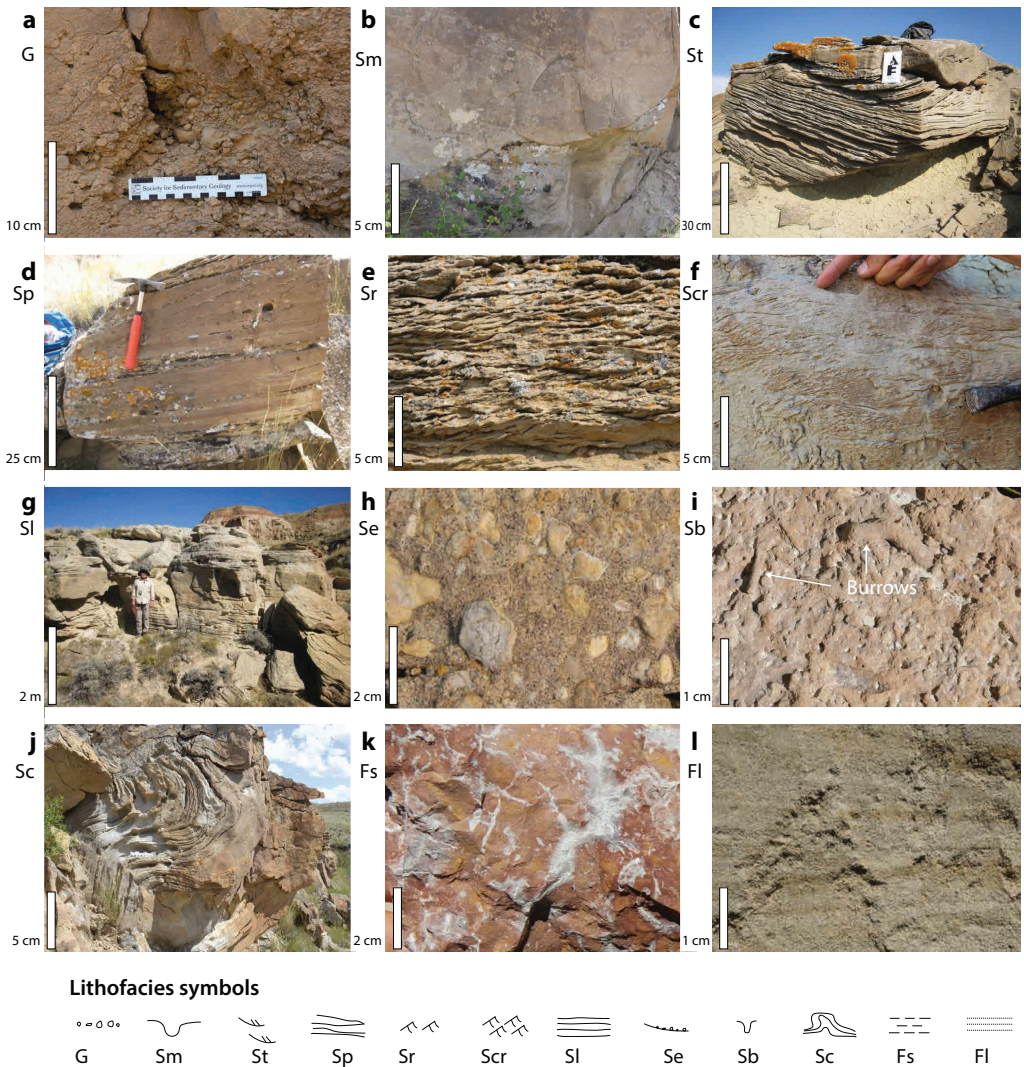


FIGURE 4.1 Lithofacies recognised in the study area. a) Clast-supported conglomerate (lithofacies G). b) Massive sandstone (lithofacies Sm). c) Trough cross-stratified sandstone (lithofacies St). d) Planar/Tabular cross-stratified sandstone (lithofacies Sp); hammer length = 25 cm. e) Ripple cross-laminated sandstone (lithofacies Sr). f) Climbing-ripple cross-laminated sandstone (lithofacies Scr). g) Low-angle (<math><15^\circ</math>) cross-bedded sandstone (lithofacies Sl). h) Sandstone with erosional scour and fill (lithofacies Se), with floating carbonate nodules as the lag deposits. i). Bioturbated sandstone (lithofacies Sb). j). Convoluted sandstone (lithofacies Sc). k). Mudstones and siltstones (lithofacies Fs). l). Laminated siltstones (lithofacies Fl). Legends for lithofacies are shown for logs in the below figures.

Lithofacies code	Description	Interpretation
Clast-supported conglomerate (G)	Poorly sorted, granule to small pebble conglomerate, with medium-grained angular sandstones as the matrix. The conglomerate fills erosional scours and can also be organized into 20 to 60 cm thick beds at the base of sandstone bodies	Intrabasinal clasts of floodplain mudstones or granules deposited by subcritical to supercritical traction flow
Massive sandstone (Sm)	Fine to medium-grained sandstone, well-sorted, no apparent sedimentary structures, a few decimetres in thickness	High rate of deposition, probably formed during high-discharge periods
Trough cross-stratified sandstone (St)	Fine to coarse-grained, well-rounded sandstone forming up to 50 cm thick cross-stratified beds. Preserved set thickness varying between 5 cm and 30 cm, often decreasing upward in the bed. Sets in the basal part of a sandstone body are often poorly sorted and may contain granules; sets in the top of a bed are better sorted. Claystone chips are common. Bed boundaries are slightly inclined (up to 2 degrees)	Subcritical flow, normal deposition rates, bedload deposition, dune migration
Planar/tabular cross-stratified sandstone (Sp)	Fine to medium-grained, well-rounded, and moderate to well-sorted lithic sandstone forming up to 30 cm thick cross-stratified beds. Preserved set thickness varying between 5 cm and 20 cm, often decreasing upward in the bed. Bed boundaries are slightly inclined	Subcritical flow, normal deposition rates, bedload deposition, plane bed formation
Ripple cross-laminated sandstone (Sr)	Very fine to fine-grained sandstone, well-sorted, ripple lamination with a set thickness of 2 to 5 cm	Ripple migration under the low-flow regime
Climbing-ripple cross-laminated sandstone (Scr)	Fine-grained sandstone, moderately to well-sorted, asymmetrical cross-lamination with climbing set boundaries, with a bed set thickness of 2 to 5 cm	Subcritical flow, faster deposition than ripple migration due to abundant sediments in suspension
Low-angle (< 15°) cross-bedded sandstone (Sl)	Fine to medium-grained sandstones, well-rounded, moderately to well-sorted, bed thickness of 0.1 to 1.0 m. Low-angle stratification with a long wavelength and low angle	Deposition under upper-flow-regime conditions during high-stage flooding events in nearby channels; or formed as part of a bar clinoform
Sandstone with erosional scour and fill (Se)	Fine to medium-grained poorly sorted sandstones, with sand-supported nodules (0.5 to 2.0 cm in diameter) filling the scours, thickness of 0.2 to 1.0 m	Supercritical flow causing the scour, high deposition rates, with nodules as lag deposits
Bioturbated sandstone (Sb)	Fine to medium-grained sandstone, moderately to poorly sorted, with vertical and horizontal burrows and trace fossils	Trace fossils formed by insects, dwelling, resting, crawling
Convolved sandstone (Sc)	Fine to medium-grained, well-rounded, moderately to well-sorted lithic sandstone. Preserved set thickness varying between 5 cm and 20 cm, often decreasing upward in the bed. Overturned-fold-shaped structures that modified or destroyed primary sedimentary structures, with a size of 20 to 60 cm	Water escape structures formed in rapidly deposited, poorly sorted sands
Mudstones and siltstones (Fs)	Clay to siltstone, with laminated or blocky structures, various matrix colours, common slickensides and nodules	Soil formation with chemical precipitation developed on former overbank fines
Laminated siltstones (Fl)	Well-sorted siltstones with ripple laminations	Settling from suspension and forming silty plug in the abandoned channel

TABLE 4.1 Description and interpretation of lithofacies in the McCullough Peaks stratigraphy.

Facies associations	Containing lithofacies
FA1 - Small-scale crevasse channel sandstone deposits	St, Sp, Sr
FA2 - Large-scale trunk channel sandstone deposits	G, St, Sp, Sr, Sc
FA3 - Braided-like channel sandstone deposits	G, Se, St, Sp, Sr, Sc, Sl
FA4 - Sinuous-like channel sandstone deposits	G, Se, St, Sp, Sr, Sc, Fl
FA5 - Sheet-like crevasse splay deposits	St, Sl, Sr, Sb

TABLE 4.2 Facies present in each facies association

Interpretation:

FA1 is interpreted to be the product of straight crevasse channels (Kraus and Gwinn, 1997; Clyde and Christensen, 2003; Gibling, 2006), also known as feeder channels of the avulsion complex (cf. Davies-Vollum and Kraus, 2001). The sharp contact with floodplain fines indicates an erosional base, the massive structure indicates rapid cut-and-fill processes, and cross-bedding suggests downstream traction of stream power. Similarly, at localities near the study area, this type of sandstone body is reported to be generally thinner than 3 m (Kraus, 1997; Clyde and Christensen, 2003) and referred to as ribbon sandstone bodies (Kraus and Middleton, 1987). In this chapter, all the FA1 sandstone bodies were observed to occur in isolation. At the same time, they can also be nested/stacked, as demonstrated by Davies-Vollum and Kraus (2001), who describe the geometry and architecture of these in detail in the central part of the Bighorn Basin.

Facies Association 2: Large-scale trunk channel sandstone deposits

Description:

Facies Association 2 (FA2) is mainly composed of fine- to medium-grained sandstone (Fig. 4.3), with a thickness range of 8-15 m and an average of 9.8 m (n = 5). FA2 deposits generally present channelised features with clear gradually-thinning channel wings (Fig. 4.3a). There is usually an erosional channel base with scouring characteristics, above which trough cross-stratified sandstone (St), planar/tabular cross-stratified sandstone (Sp), and ripple cross-laminated sandstone (Sr) dominate, with occasionally seen convoluted sandstone (Sc; Fig. 4.3b and c). At some locations, FA2 manifests as massive-weathering sandstone bodies that barely have any internal erosional surfaces but have sharp channel margins (Fig. 4.3d). FA2 is relatively rare (five out of ninety-two documented channel sandstone bodies) in the study area. Although not always, it mainly (three out of five cases) occurs at the same stratigraphic level as the sinuous-like channel sandstone deposits (FA4), which will be described below.

Interpretation:

FA2 is interpreted to have formed in the main threads of the drainage system under high sedimentation rate conditions. Large sandstone body thickness (>8 m), steep channel margin (e.g. Fig. 5e), and the erosional base of the sandstone body indicate deep and strong scouring. Nonetheless, its origin and planform style is not well understood due to the scarcity of FA2 in the study area and limited exposure quality, and more data are needed.

a**b**

FIGURE 4.2 Facies Association 1: small-scale crevasse channel sandstone deposit. a) UAV photo showing the channel body in transverse view. b) UAV photo showing the ribbon shape of the same channel body in longitudinal view. The two black arrows in subfigures a and b point at the same gravel rock debris on the ground.

Facies Association 3: Braided-like channel sandstone deposits

Description:

Facies Association 3 (FA3) is generally composed of medium-grained sandstones, with conglomerate (G) occasionally seen at the base as lag deposits (Fig. 4.4). It is usually multi-storied, and sharp erosional bases are present between stories. Within a single story, sandstone with erosional scour and fill (Se). Trough cross-stratified sandstone (St) is present in the lower part, planar/tabular cross-stratified sandstone (Sp) is in the middle part, and ripple cross-laminated sandstone (Sr) and low-angle ($<15^\circ$) cross-stratified sandstone (Sl) are in the upper part, occasionally replaced by massive sandstone (Sm; Fig. 6d). The dip direction of the accretion surfaces is generally parallel to measured palaeocurrent directions in cross-bedded sets.

Forty-eight FA3 sandstone bodies are documented in this study, with a thickness range of 4-8 m, an average thickness of 6.1 m, and a standard deviation of 2.4 m (Fig. 4.7a) as measured in the digital outcrop model. Their apparent widths were corrected using the average palaeoflow direction (003° ; Fig. 4.8a-d; Fabuel-Perez et al., 2009), yielding an average of 203 m and a standard deviation of 137 m (Fig. 4.7b). These braided channel sandstone bodies commonly have three to four stories, with a thickness range of 0.5-2 m and an average story thickness of 1.7 m ($n = 151$). The sandstone body aspect ratio, defined as the width/thickness ratio, has an average of 38 and a standard deviation of 28 (Fig. 4.7c). Dune-scale cross-sets in FA3 ($n = 45$) have an average preserved thickness of 22 cm, with a

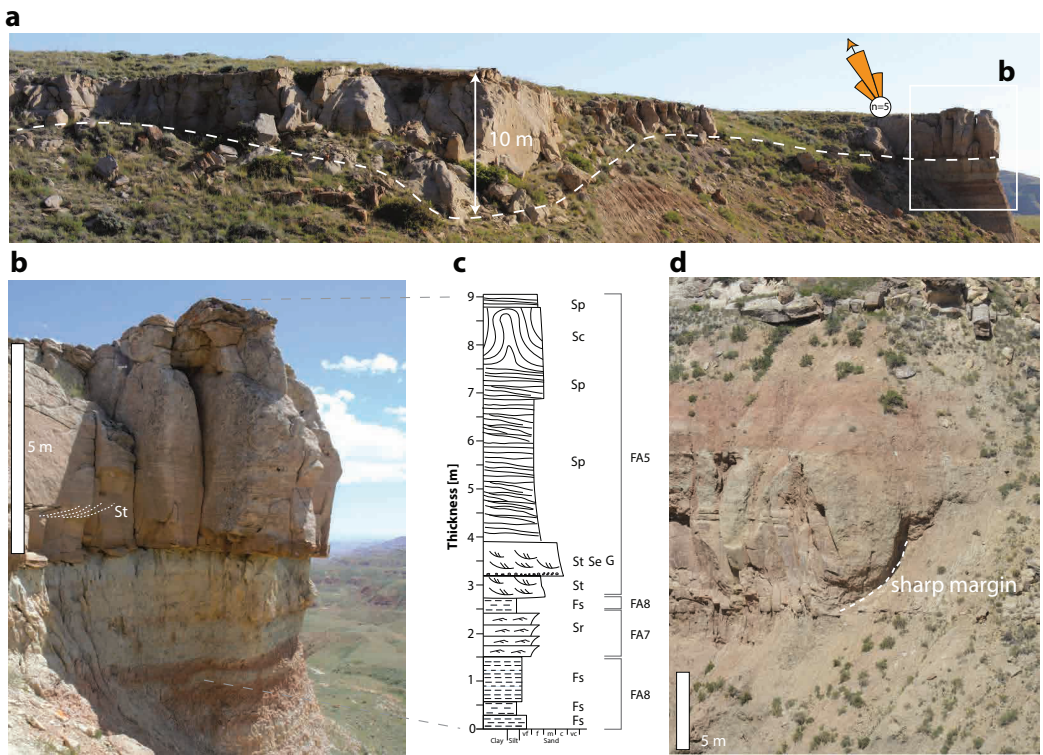


FIGURE 4.3 Facies Association 2: large-scale trunk channel sandstone deposit. a) Overview of the large-scale trunk channel sandstone deposits with a maximum thickness of ~10 m. b-c) Zoomed-in view and log of the right side of subfigure A showing detailed sedimentary structures and underlying floodplain fines. The white line marks the corresponding sedimentological log position. d) A second example of FA2 deposits with a maximum thickness of ~10 m with sharp channel margins eroding into floodplain fines and a thin splay bed in the lower part. For the legend, see Figure 4.1

standard deviation of 13 cm and a coefficient of variation (CV) of 0.59 (Fig. 4.7d). Using these dune-set data and employing existing empirical relationships (e.g. Bridge and Tye, 2000; Leclair and Bridge, 2001), the average bankfull depth is estimated to be 4.3 m ($22 \text{ cm} \times 2.9 \times 6.7$). The high CV (0.59) ensures the reliability of the estimation of the formative flow depth using cross-set thickness (Bridge and Tye, 2000). Planar/tabular cross-stratified sandstone (Sp) and low-angle ($<15^\circ$) cross-stratified sandstone (Sl) are dominant lithofacies in FA3, accounting for 51% and 15%, respectively (Fig. 4.7e). The palaeoflow rose diagram shows a mean flow direction of 016° and a standard deviation of 90° (Fig. 4.7f). The distribution of the palaeoflow data is significantly different from the uniform distribution according to the Rayleigh test of uniformity (0.29 with a p-value of 0).

Microscopic observation of twenty-eight thin sections shows that monocrystalline quartz grains in FA3 are generally subrounded to subangular and slightly spherical (Fig. 4.9), and they are classified together with polycrystalline quartz (quartzite) and microcrystalline quartz (chert) as “quartz” in

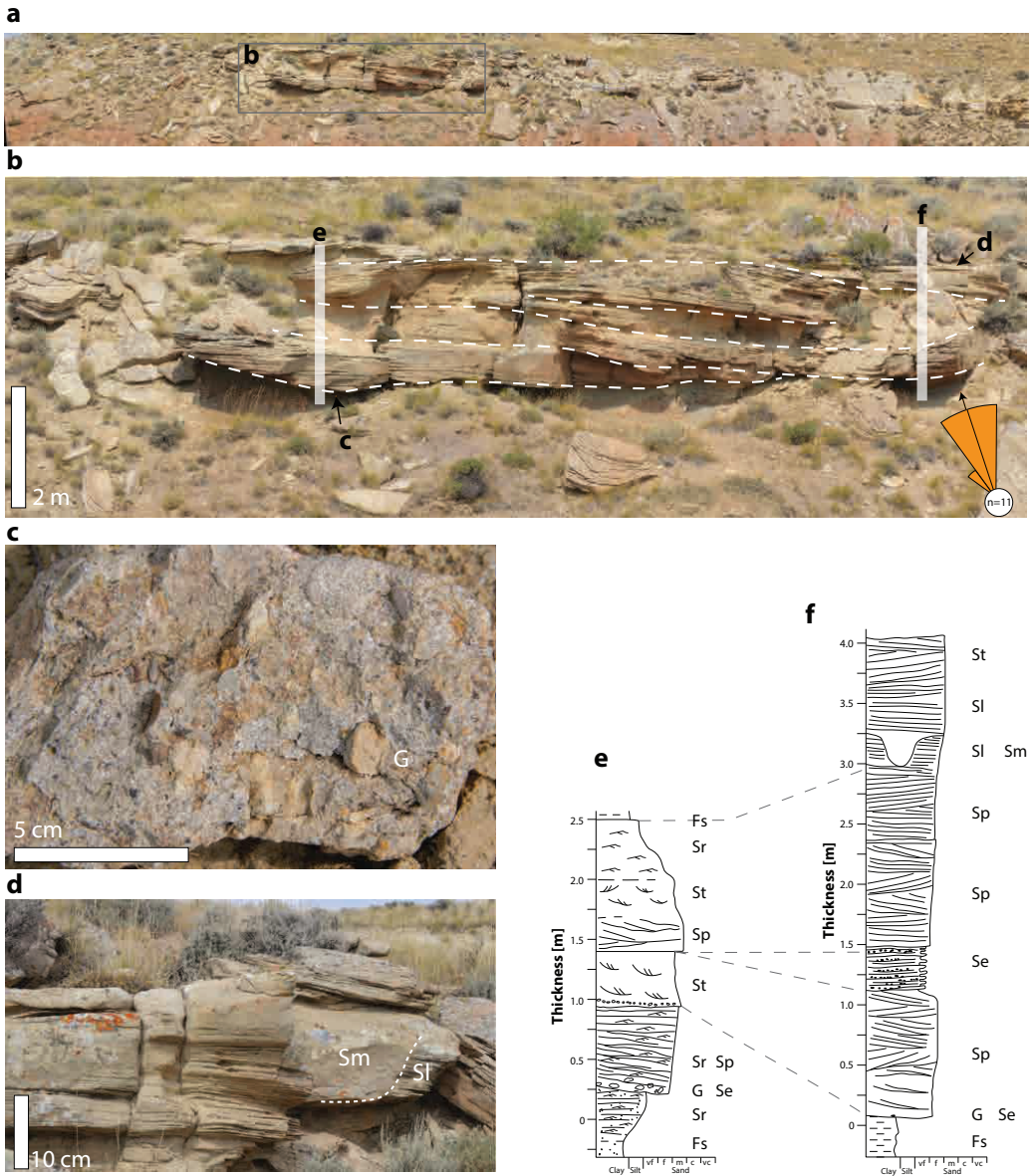
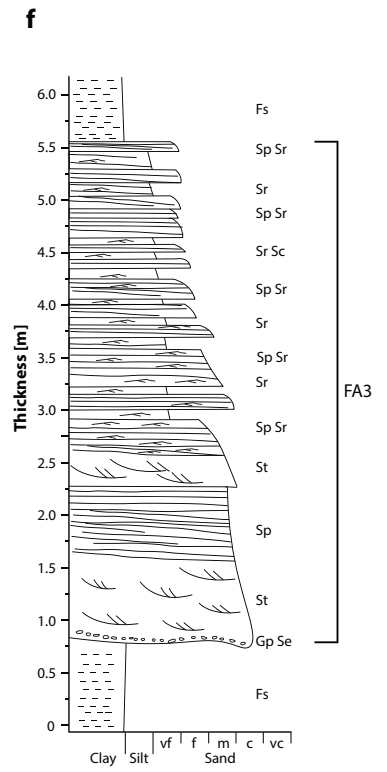
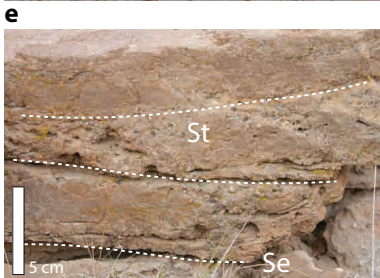
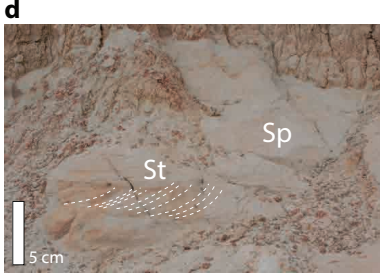
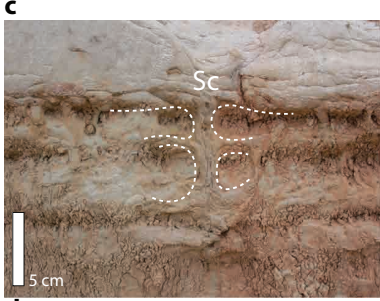
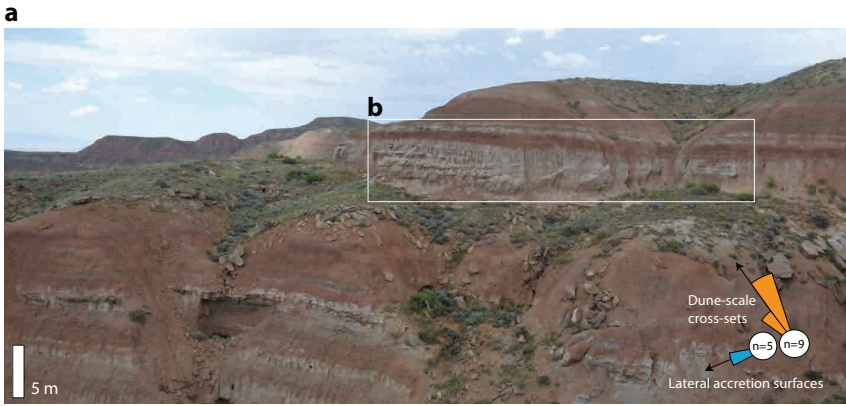


FIGURE 4.4 Facies Association 3: braided-like channel sandstone deposits. a-b) Overview and close-up view of FA3 deposits, where there are five stories with the thickness of each varying between 0.5 and 1 m. c) The bottom view of the channel base with floodplain nodules as lag deposits. d) Massive bank-breaching deposits (Sm; cf. Van den Berg et al., 2017) eroding low-angle cross-bedded sandstone (Sl). e-f) Sedimentary logs for locations in panel b, showing the vertical succession of lithofacies in FA3. For the legend, see Figure 4.1.



← **FIGURE 4.5** Facies Association 4: sinuous-like channel sandstone deposits. a) Overview photo showing the juxtaposition between FA4 and surrounding strata. b) Enlarged view of the FA4 deposits, where lateral accretion deposits are distinct, as indicated by dashed lines. Letters c-e of this subfigure indicate the positions of subfigures c-e. c) Convolute sandstone with clear water escape structures. d) Trough and planar cross-bedding with a dominant flow direction of 10°. e) Channel-floor deposits at the base of FA4. f) Composite sedimentary log illustrating the vertical succession of lithofacies in FA4. For the legend, see Figure 4.1.

the scheme developed by McBride (1963). Feldspar content varies widely, with potassium feldspar (e.g. orthoclase and microcline) more dominant than plagioclase (e.g. albite). Rock fragments include sedimentary, volcanic, and metamorphic components. Accessory (heavy) minerals are either igneous or metamorphic, including magnetite, zircon, tourmaline, and hornblende. Both calcite and silica cement are observed, with the former contributing to the mosaic granular framework and the latter causing euhedral to subhedral quartz/feldspar overgrowths.

Interpretation:

FA3 presents characteristics generally ascribed to the sedimentary product of braided river processes. This interpretation is supported by the predominance of medium to coarse-grained bedload material, the scarcity of lateral accretion deposits, the abundance of downstream accretion deposits, no fining upwards grain size profile, little or no fine-grained sediment and/or soil preservation, and the stacking of several single-story units within individual sandstone bodies (Leopold and Wolman, 1957; Bridge et al., 1986; Gibling, 2006; Sambrook Smith et al., 2006; Foreman, 2014; Hartley et al., 2016, 2018; Limaye et al., 2020). The presence of some fine-grained deposits below erosional surfaces suggests channel abandonment and reoccupation. Single-story units in FA3 are generally narrow and thin, indicating their short life spans and quick lateral coalescence of multiple channel stories (Gibling, 2006). In general, braided channels tend to occur in a range of environments associated with rapid and frequent variations in water discharge, high sediment load, coarse sediment grain size, high gradient, and erodible banks (Leopold and Wolman, 1957; Schumm, 1985; Summerfield, 1991; Bridge, 1993; Church, 2006; Ashmore, 2013; Limaye et al., 2020).

Facies Association 4: Sinuous-like channel sandstone deposits

Description:

Facies Association 4 (FA4) is generally composed of (1) poorly-sorted, subangular, coarse-grained trough cross-stratified sandstones (St) with granules (G) and sandstones with erosional scour and fill (Se) at the base, (2) large-scale inclined strata with moderate to well-sorted medium-grained trough cross-stratified sandstones (St) and planar cross-stratified sandstones (Sp) in the middle, and (3) fine-grained ripple-laminated sandstones (Sr) at the top (Fig. 4.5). The basal part is usually 0.5-1 m thick, while the middle and upper parts are generally >4 m thick. Dune-scale cross-stratification (Fig. 5d) and ripple-scale cross-lamination sedimentary structures are present. Accretion beds (Fig. 4.5b) are inclined approximately perpendicular to or at a large angle with measured palaeocurrent directions from cross-stratified bedforms. Water-escape structures are occasionally seen in convolute sandstone (Sc) within lateral accreted deposits (Fig. 4.5c).

A set of four well-preserved point bars constitutes a series of bends along a downstream-oriented sinuous channel belt in the map view, as corroborated by the laterally traceable palaeosol layer over

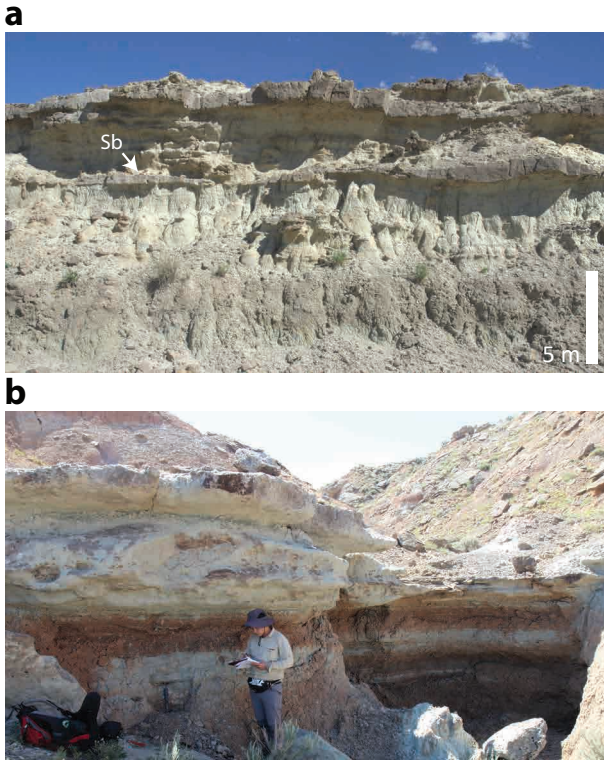


FIGURE 4.6 Facies Association 5: sheet-like crevasse splay deposit. The person for scale in panel b is ~1.8 m.

approximately 2.0 km on top of these point bars (Fig. 4.8h). Lateral accretion surfaces of these point bars all dip in the direction at a large angle with the measured palaeocurrent directions from cross-stratified bedforms. Individual point bars of this set are 0.2-0.5 km wide, 0.1-1.2 km long, and 7.0-11.0 m thick, presenting features both parallel and perpendicular to the palaeoflow direction. The map view of these point bars using their three-dimensional coordinates from the digital outcrop model makes it possible to calculate the channel sinuosity index, which is 1.8 and thus falls in the category of meandering river planform (Williams, 1986).

Thirty-nine sandstone bodies with FA3 are documented. The average thickness is 9.0 m, while the standard deviation is 2.7 m (Fig. 4.7a). Apparent field measurements of these sandbodies are corrected against the average palaeoflow direction (003°; Fig. 4.8e-h), yielding an average value of 266 m and a standard deviation of 203 m (Fig. 4.7b). The sandstone body aspect ratio averages 31 and has a standard deviation of 21 (Fig. 4.7c). Preserved dune-scale cross-sets in FA4 ($n = 11$) have an average thickness of 26 cm with a standard deviation of 7 cm and thus a coefficient of variation (CV) of 0.29 (Fig. 4.7d). From these data and the application of existing empirical relationships (Bridge and Tye, 2000; Leclair and Bridge, 2001), the average bankfull depth is calculated to be 5.1 m ($26 \text{ cm} \times 2.9 \times 6.7$), which is consistent with the thickness of the inclined strata (commonly > 4.0 m). The low CV (0.29, required to range between 0.58-1.18) renders it uncertain to estimate the formative flow depth using preserved cross-set thickness (Bridge and Tye, 2000). Planar/tabular cross-stratified sandstone (Sp) and trough

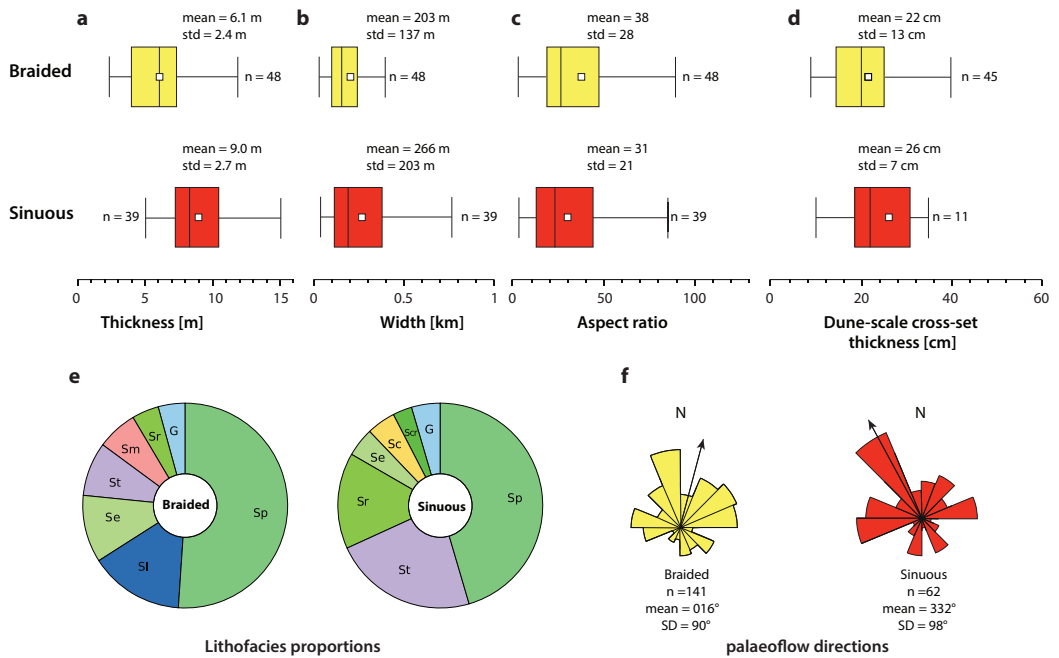


FIGURE 4.7 a) Thicknesses, b) widths, and c) aspects of braided-like and sinuous-like channel sandstone bodies. d) Thicknesses of dune-scale cross-sets. e) Relative abundance of different lithofacies within braided-like and sinuous-like channel sandstone bodies (abbreviations are listed in Table 4.1). f) Rose diagrams of palaeoflow directions. Note the significantly thinner and insignificantly narrower braided-like channel sandstone bodies than sinuous-like counterparts, the similarity and difference between relative lithofacies abundance, and the similarity and difference between palaeoflow directions.

cross-stratified sandstone (St) are predominant lithofacies in terms of the lithofacies proportions in thickness, accounting for 45% and 23%, respectively (Fig. 4.7e). The palaeoflow measurements ($n = 63$) present a mean flow direction of 332° , with a standard deviation of 98° (Fig. 4.7f). The distribution of the palaeoflow data in FA4 is significantly different from the uniform distribution according to the Rayleigh test of uniformity (0.23 with a p-value of 0.04).

Compared with FA3 braided-like channel sandstone bodies, sinuous-like counterparts are significantly thicker ($t = 5.3$, $p = 0.9 \times 10^{-7}$) and insignificantly wider ($t = 1.4$, $p = 0.16$). However, dune-scale cross-sets in FA4 sinuous-like channel deposits are not significantly different from those in FA3 braided-like channel deposits ($t = 0.6$, $p = 0.5$), although the average preserved thickness of the former is higher than that of the latter. In terms of palaeoflow measurements, there is no significant difference between braided-like and sinuous-like channel deposits at a 0.05 level of significance according to Watson's Two-Sample Test of Homogeneity, which is likely attributable to the large standard deviations of both measurements (90° and 98° , respectively).

There are three available thin sections for FA4 sandstone bodies. Compared with FA3, FA4 is finer overall and has higher quartz and chert abundances (Fig. 4.9c and d).

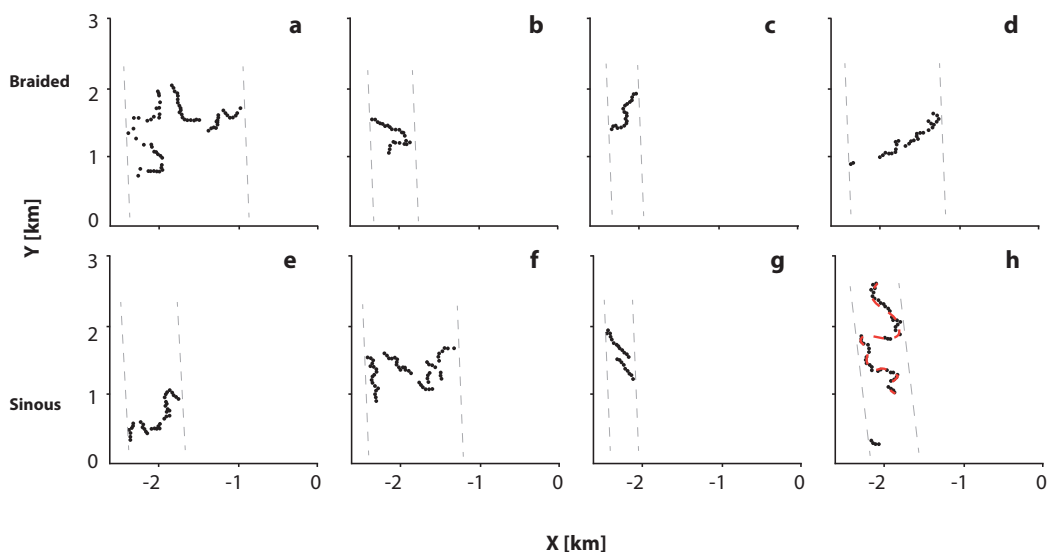


FIGURE 4.8 Four examples showing how widths of braided-like channel sandstone bodies are measured (a-d) and four of sinuous-like channel sandstone bodies (e-h). The black dots indicate the presence of the sandstone body at the outcrop surface, and two dashed boundary lines are along the average palaeoflow direction (004°). A sinuosity index is calculated in subfigure H, indicated by the red dot line.

Interpretation:

FA4 presents the characteristics that are generally ascribed to sinuous river processes. Accretion beds are aligned broadly perpendicular to the overall palaeoflow direction. They are inferred as lateral accretion beds (Fig. 4.5b). These lateral accreted deposits result from the reduced shear stress associated with helicoidal flows, which leads to erosion in the outer bend and lateral migration of the point bar located in the inner bend in the same direction (Bridge, 1993). The lower coarser-grained segment of the sandstone bodies represents the channel lag interval. Sinuous channels tend to occur in environments associated with perennial flow, relatively low sediment load, low gradient, and cohesive overbank materials (Leopold and Wolman, 1957; Schumm, 1985; Church, 2006).

Nevertheless, recent progress in understanding high-sinuosity rivers has been contesting these generic models. For instance, many more sandy sinuous systems have been documented in the laboratory and depositional basins (e.g. Braudrick et al., 2009; Hartley et al., 2015, 2018), indicating the low sediment load is not necessarily a prerequisite for sinuous river channel development. Therefore, no single factor can be determined to contribute to sinuous river channel development definitively, and a combination of several factors should be implemented for higher-certainty interpretation.

Floodplain facies associations

The floodplain deposits have been extensively described in numerous studies (e.g. Kraus, 1987; Kraus and Bown, 1993; Kraus and Gwinn, 1997; Kraus and Hasiotis, 2006; Abdul Aziz et al., 2008; Abels et al., 2013; Wang et al., 2021b). Here, only the sandy floodplain facies association is documented.

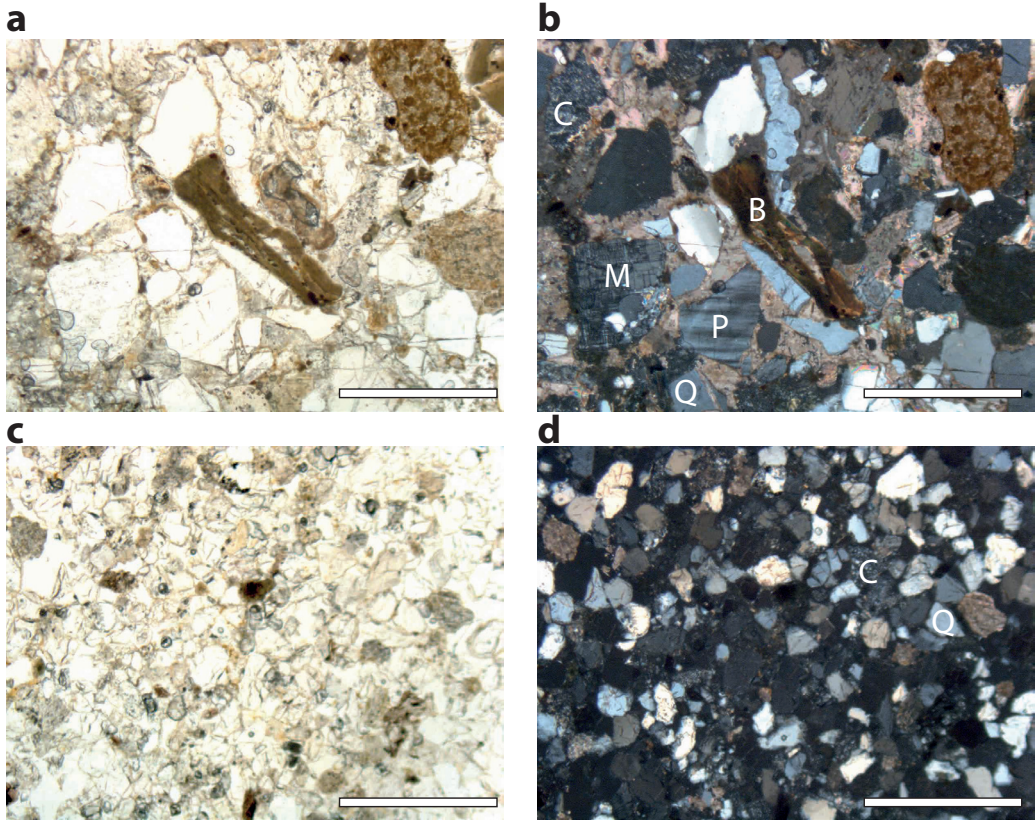


FIGURE 4.9 Petrographic characteristics of braided-like and sinuous-like channel sandstone deposits. a-b) Thin sections of braided-like channel sandstone deposits under plane- and orthogonally-polarised light. c-d) Thin sections of sinuous-like channel sandstone deposits under plane- and orthogonally-polarised light. B = biotite; C = chert; M = microcline; P = plagioclase; Q = quartz. The white bar for scale is 500 µm.

Facies Association 5: sheet-like crevasse splay deposits

Description:

Facies Association 5 (FA5) consists of very fine- to coarse-grained sandstones (Fig. 6a). It is often composed of multiple beds, with the thickness of an individual bed ranging from 0.1 m to 0.5 m. FA5 sediments are, in general, well sorted. Trough cross-stratified sandstone (St), low-angle (<15°) cross-stratified sandstone (Sl) and ripple cross-laminated sandstone (Sr) are the most dominant lithofacies, typically presenting upward coarsening trends. The lateral extent of FA5 can be up to a few kilometres as measured from the digital outcrop model and traced in the field, which depends on the direction in which it is measured. Burrows are observed to be oriented in random directions (Facies Sb in Fig. 4.1). The palaeocurrents measured in FA5 deposits are generally oblique to the main channel from which the deposit originates. FA5 deposits are prevalent throughout the entire stratigraphy, forming the ‘heterolithic’ deposits of Abels et al. (2013).

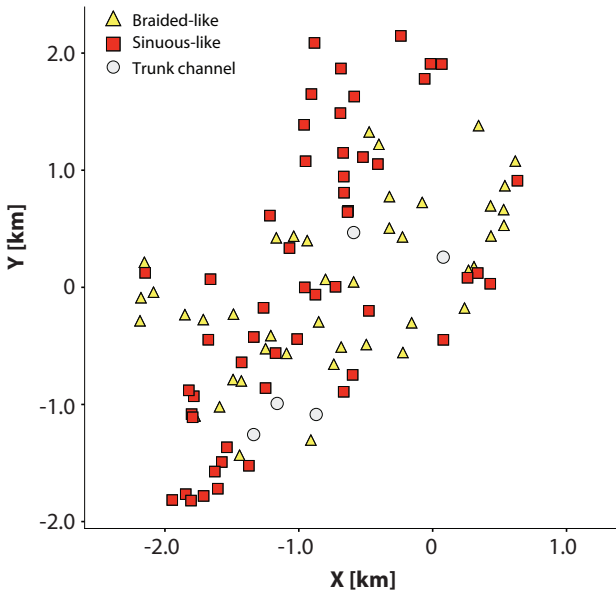


FIGURE 4.10 Projection of sandstone bodies in map view.

Interpretation:

FA5 is interpreted to represent unconfined flow conditions on the floodplain as part of a splay complex formed during the erosion of the channel levee (Davies-Vollum and Kraus, 2001; Fisher et al., 2007). Multiple beds may represent multiple events of crevasse processes. FA5 has been commonly referred to as heterolithic deposits produced by crevasse splaying and overbank flooding processes (e.g. Kraus and Aslan, 1993; Kraus and Wells, 1999; Abels et al., 2013; Foreman, 2014).

4.3.3 Spatial distribution of channel sandstone bodies

The highest point of a channel sandstone body in the three-dimensional digital outcrop model is assigned as the representative point for this sandstone body. Thus, it becomes feasible to project the locations of all the channel sandstone bodies in the three-dimensional space, including five large-scale trunk channel sandstone bodies (FA2), 48 braided-like channel sandstone bodies (FA3), and 39 sinuous-like channel sandstone bodies (FA4). Crevasse channel sandstone bodies (FA1) are not projected because they cannot consistently be confidently recognised in the field when direct access is unavailable nor in the digital outcrop model because of their relatively low thickness. Large-scale trunk channel sandstone deposits (FA2) are relatively rare (5 out of 92) and thus will not be analysed in detail below. Therefore, the main focus will be on FA3 and FA4, even though it may be possible that the FA2 systems may have played a relatively significant role at the basinal scale.

From the horizontal XY plane of Figure 4.10, FA3 and FA4 occur in an intercalated fashion. In other words, laterally (along the XY horizontal plane), FA3 or FA4 are not confined to certain portions of the study area and appear randomly distributed. Projection of the channel sandstone bodies from three-dimensional space onto the YZ plane shows a pseudo-downstream-oriented stratigraphic profile, but it is not done here as it requires adjustments to tectonic tilt, faults, and integration with floodplain stratigraphy. This analysis is partly done in Chapter 6.

4.4 Discussion

4.4.1 River planform identification

Results from the integrated field analysis allow for a discussion on the difference in flow conditions associated with sandstone bodies of different river styles. As mentioned in Section 4.3, the focus of this chapter is on FA3 ($n = 48$) and FA4 ($n = 39$) channel sandstone bodies, features of which point to braided-like and sinuous-like river planform styles, respectively. Nonetheless, the above interpretation of river styles is inevitably influenced by the limitations of available outcrop and our inherent inability to distinguish river planform morphology from near-vertical outcrop sections. Lithofacies and their associations are the most direct and helpful indicators of river planform morphology, but they are not necessarily definitive. In other words, the braided-like and sinuous-like morphology can be caused by different factors that result in a similar product.

Lateral accretion sets are regarded as the key to the distinct separation of braided and sinuous systems (Davies and Gibling, 2010; Hartley et al., 2018), but their absence in the outcrop sections does not always imply a braided planform style, which brings uncertainties in identifying braided channel deposits. Holbrook and Allen (2021) report a case of a braided river that meanders, which means the above interpretations may be biased if only parts of the outcrop are observed. Moreover, since braided and sinuous rivers constitute a continuum in river planform styles, the study area may also be situated in a transitional zone between sinuous- and braided-river-dominated zones, and thus the two main interpreted river planform styles may not be too far from each other. Therefore, what is documented in this chapter may not be the absolute end members (i.e. sinuous and braided river planforms); instead, the basin may have mixed systems. A detailed stratigraphic analysis is needed to elucidate the stratigraphic occurrence of the two seeming end-members recognised in this chapter. Initial observations suggest occasional close stratigraphic proximity of FA3 and FA4 sandbodies, while intervals dominated by one of the two Facies Associations also seem to occur.

Another critical issue in our interpretation is the potential over-reliance on the river planform attribution. For instance, the low-angle cross-bedded sandstone (Facies S1) recognised in the FA3 braided-like channel deposits is inferred above to be formed in the upper flow regimes (Lorenz and Nadon, 2002; Fielding, 2006), and an increase in the upper flow regime structures is suggestive of braided river morphology. However, Facies S1 could also be a part of the bar clinoform that does not require upper flow conditions (Ethridge and Schumm, 1978; Foreman et al., 2012). Moreover, as noted by many researchers (e.g. Davies and Gibling, 2010; Gibling and Davies, 2012; Santos et al., 2016; Hartley et al., 2018), it is not easy to distinguish between braided and sinuous river planforms if the deposits are coarse-grained, because they may have very similar characteristics. In this context, it might be more conservative and objective to attribute FA3 and FA4 to two scenarios of fluvial deposition: one that is more perennial or uniform in discharge and one that is more ephemeral or peaked in discharge (Plink-Björklund, 2015; Fielding et al., 2018). This interpretation would pertain to our dataset but avoid invoking whole-scale changes in planform morphology, given that the braided-like and sinuous-like channel sandstone bodies are not significantly different regarding width, aspect ratio, and palaeoflow direction. However, they do significantly differ from each other in thickness (Fig. 4.7).

Disregarding the fully acknowledged difficulties in attributing these fluvial deposits to two end-member river planforms, we further refer to FA3 as braided-like and FA4 as sinuous-like river styles

for the simplicity of the below general discussion while still referring to the fact that these are not strictly the end-members of a continuum of river planform styles.

4.4.2 Bighorn Basin river styles and flow conditions

As discussed above, all the interpreted river styles are based on the authors' best knowledge on the available outcrop data. Owing to the dominant abundance and geological importance, FA3 and FA4 deposits are the focus of discussion, while it is acknowledged that FA2 needs further study.

FA3 braided-like channel sandstone deposits and FA4 sinuous-like channel sandstone deposits present similarities and differences. First, the most dominant lithofacies in both of them is the planar cross-stratified sandstone (Sp; Fig. 4.1d), which is the result of straight crested bedforms in the lower flow regime with intermittent to continuous sand motion and subcritical water flow conditions (Harms and Fahnestock, 1960; Coleman, 1969; Bourquin et al., 2009; Went and McMahon, 2018). The second most dominant lithofacies in FA3 braided-like channel sandstone deposits is low-angle (<15°) cross-bedded sandstone (Sl), which is formed in upper flow regimes, accompanied by high sediment concentration and continuous sand motion (Harms and Fahnestock, 1960; Coleman, 1969; Bourquin et al., 2009; Went and McMahon, 2018). In contrast, the second most dominant lithofacies in FA4 sinuous-like channel sandstone deposits is trough cross-stratified sandstone (St), which results from linguoid bedforms that mainly develop in the subcritical lower flow regimes. Based on the two most dominant lithofacies in FA3 and FA4, the flow velocity that produces FA3 braided-like channel sandstone deposits is generally higher than that of FA4 sinuous-like channel sandstone deposits. From the perspective of Froude number calculation (Kennedy, 1969), FA3 braided-like channel sandstone deposits should be formed in a condition of either higher velocity or shallower water depth or a combination of than FA4 counterparts.

The narrow and thin single-story units in FA3 indicate short life spans and quick lateral coalescence of multiple channel stories that may result from multiple phases of ephemeral flow (Gibling, 2006) or spike-like discharge conditions (Fielding et al., 2018). In contrast, the lateral accretional surfaces and the sinuosity index up to 1.8 (Fig. 7 and 8) in FA4 suggest more stable, perennial water flow conditions. More importantly, FA3 braided-like channel deposits are significantly thinner and insignificantly narrower than FA4 sinuous-like channel deposits, which indicates FA3 may be formed in flashy-discharge conditions instead of continuously high-discharge conditions (Fielding et al., 2018).

The insignificant difference in palaeoflow directions between FA3 and FA4 suggests they may have developed in channel belts with similar downstream orientations. Measurements of palaeoflow directions in FA4 sinuous-like channel sandstone deposits are not uniform, and this is expected because they vary with the locations with reference to the meander bend and should show a large spread when plotted altogether. Meanwhile, those in FA3 braided-like channel sandstone deposits are also different from the uniform distribution, and they have a significant circular deviation (standard deviation = 90°) and present a dispersal pattern as the FA4 sinuous-like channel sandstone deposits do (standard deviation = 98°). Pryor (1960) suggested that the slope of the depositional surface is the most critical factor controlling the circular deviation and dispersal pattern of the palaeoflow data, with a more significant slope contributing to more consistent palaeoflow data. Therefore, it can be inferred that the slope was gentle for both FA3 and FA4 deposition. In this context, discharge differences might mainly contribute to the river planform style change (Leopold and Wolman, 1957).

Nevertheless, a wide range of palaeocurrents is also expected in braided rivers when there is local

flow deflection around bars (Miall, 1994). Therefore, the hypothesis of slope gentleness needs more analysis before argumentation. Moreover, it is worthwhile to note that palaeocurrent dispersal alone cannot be used as a criterion to distinguish sinuous and braided channel deposits (Jordan and Pryor, 1982; Ghinassi and Ielpi, 2015; Ghinassi et al., 2016; Hartley et al., 2018).

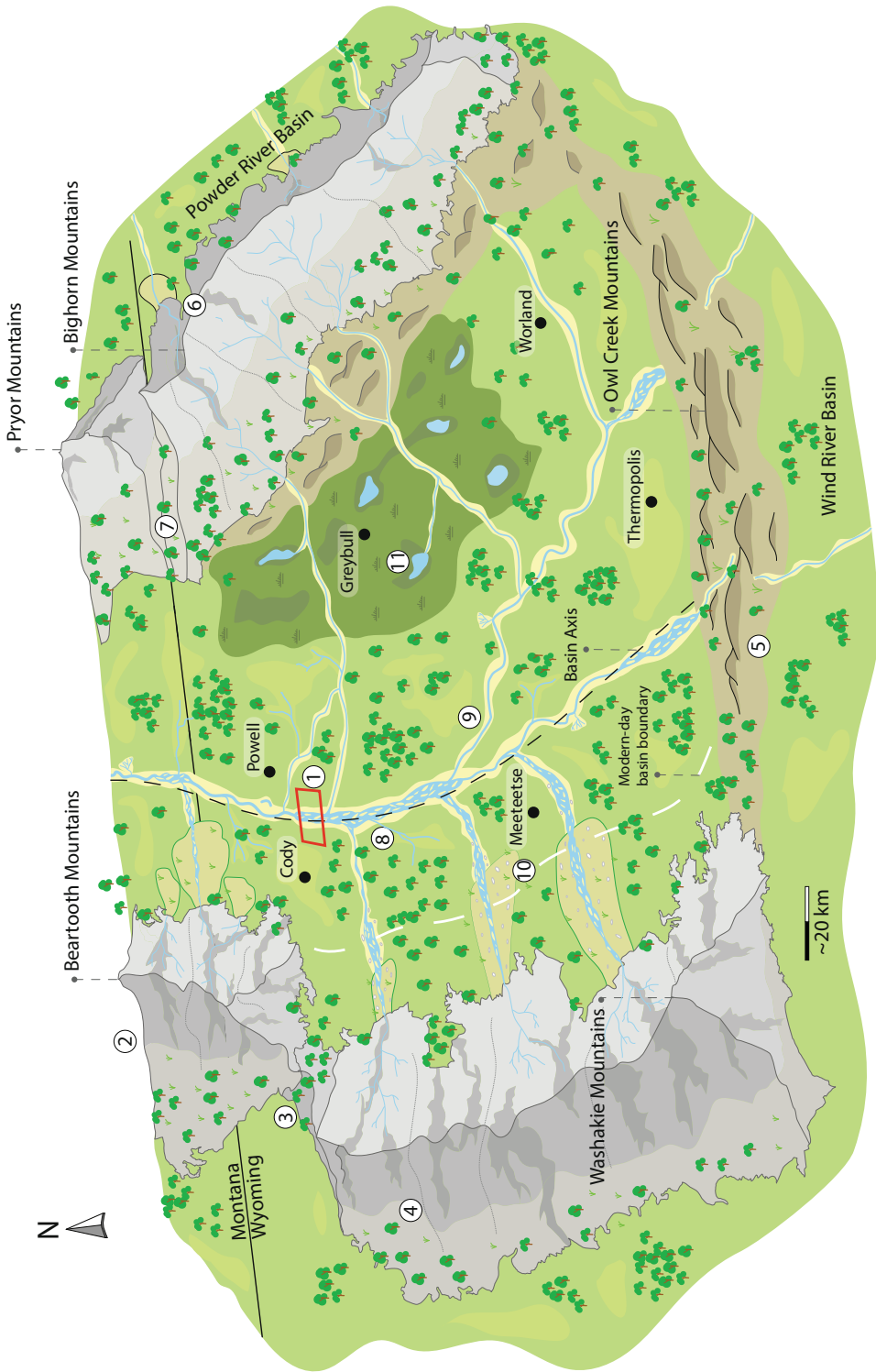
4.4.3 Geomorphic zonation of the Bighorn Basin

Literature shows that braided rivers evolve into sinuous rivers when certain thresholds in water and sediment discharge and/or slope are exceeded (Leopold and Wolman, 1957; Bridge, 2003). As analysed in the above section, the study area might represent a gentle slope during the deposition of FA3 and FA4, and thus the discharge condition may play a critical role in determining the river planform styles. The study area is far from the southern Owl Creek Mountains (see Chapter 2 for an overview of the basin setting), and if that is the only catchment, sinuous rivers should develop in the study area according to the geomorphic zonation theory in river basins (Schumm, 1985). However, in the study area, braided-like channel deposits occur in many cases (forty-eight FA3 versus thirty-nine FA4). Existing data suggest that there might have been multiple feeding systems influencing the study area from the western catchments (Kraus, 1980; Wing and Bown, 1985; Owen et al., 2019). Given the proximity of the study area to the western catchment and the high gradient from the western basin margin relative to the southern and eastern margins in the early Eocene, the study area will likely have been fed by multiple western systems that confluence with an axial system flowing from south to north, as has been demonstrated in Owen et al. (2019). Similar depositional models that include transverse and axial river systems have been reported in modern and ancient outcrop analogues as well as flume experiments (e.g. DeCelles et al., 1991; DeCelles and Cavazza, 1999; Weissmann et al., 2015, 2016; Giles et al., 2018; Kim et al., 2011; Connell et al., 2012).

The southern and eastern catchments are thought to have been lower and possibly more dominated by the reworking of Mesozoic fines (DeCelles et al., 1991). With the feeding of basement-rich western source materials into the axial system of the basin, the sinuous systems may have been alternated or changed into braided systems downstream where discharge was temporarily increased. Quantitative basinal data are provided by Owen et al. (2019), where a wide axial fluvial system is identified that characterises reverse downstream distributive fluvial system trends (i.e. decreasing channel portion and dimension as well as grain size), and they ascribe this to influences of transverse systems of variable size at different sites with respect to the axial system. This chapter's results could align with the interfingering between an axial system and possibly the Absaroka or Washakie transverse systems regarding sediment and discharge, while the study site is probably too far downstream to see the direct interfingering site of these systems as suggested by our and basin-wide palaeocurrent data.

The Washakie Range, now partly covered by the Absaroka Mountains, was present during the deposition of the Willwood Formation and is hypothesised to have been an important catchment for the transverse system (Owen et al., 2019). This suggestion is supported by the presence of Palaeocene-aged fanglomerates in the basin's western margin (Kraus, 1984). There could also have been an "Absaroka" transverse system north of the Washakie system (van Houten, 1944; Sundell, 1990), which is more proximal to the study area and could have played a more important role as a transverse system directly feeding the study area.

The study area is relatively small compared with the basin size, and thus data from other studies are needed to provide information at other basin sites. Willwood sheet sandstones documented very



← **FIGURE 4.11** Schematised palaeogeographic model of the Bighorn Basin during the early Eocene. Avulsion is a prevailing behaviour of the Willwood system, but it is only sporadically portrayed here not to obscure the river planform style alternation. Annotations for elements marked with numbers in the figure are as follows: (1) The McCullough Peaks study area. (2) The Beartooth Mountains with a very steep eastern flank (Bown, 1980) and several ephemeral coarse-grained alluvial fans and braid-plain deposits (DeCelles et al., 1991). (3) The space between the Washakie Mountains and the Beartooth during Eocene is uncertain in the literature due to the covering of the Absaroka Mountains. (4) Washakie Mountains are not present today (Kraus, 1985), because they are covered by volcanic Absaroka Mountains (Sundell, 1990). Its exact extent is currently unknown, and several hypotheses exist (van Houten, 1944; Kraus, 1985; Sundell, 1990; Lillegraven, 2009; Owen et al., 2019). (5) The Owl Creek Hills were relatively gentle in Eocene (Wing & Bown, 1985; Hoy & Ridgway, 1997). (6) Unlike the present day, the Bighorn mountains were much smaller and not fully formed in the Eocene (Hoy & Ridgway, 1997; Yonkee & Weil, 2015). The small fine-grained sediment input from the Bighorn Mountains into the Bighorn Basin is speculated to be present (Kraus & Middleton, 1987), but this is uncertain given the large distance and gentle topography from the mountains to the axis and the absent palaeocurrent records from the east (Owen et al., 2019). (7) Pryor Gap could be an exit for the rivers during the Eocene (Blackstone, 1940). However, there are no constraints on when it opened. (8) Braided channel belt with downstream accretion deposits. (9) Sinuous channel belt with crevasse splay, local/regional avulsion, and point bars. (10) Fanglomerates on the alluvial fan (Kraus, 1983, 1984; Malone et al., 2017; Syzdek et al., 2019), indicating a near-source system. (11) Poorly drained floodplain, swampy, and/or lacustrine environments in front of the Bighorn Mountains indicated by organic-rich beds and gley palaeosols (Wing & Bown, 1985; Davies-Vollum & Wing, 1998; Davies-Vollum, 1999, 2001).

close to the study area (cf. Friend, 1983; Kraus and Middleton, 1987) are believed to be generated by laterally mobile or meandering streams in the major axial system as corroborated by the presence of lateral accretion surfaces (Kraus and Middleton, 1987), the wildly varied palaeoflow direction in vertically adjacent stories (Kraus and Middleton, 1987), and sequences of depositional facies in the sheet sandstones (Kraus, 1980). The work by Foreman (2014) suggests that the Paleocene-Eocene “boundary sandstone”, two million years older than the Willwood strata studied here, was meandering in origin in the Sand Coulee area, which is further downstream to the north of the study area. The sedimentological work by Owen et al. (2017) suggests the presence of five channel body geometries, including massive (M), semi-amalgamated (SM), internally amalgamated (IA), offset stack (OS), and isolated (I) forms. According to the included lithofacies associations in these geometries, M is dominantly braided, SA is primarily braided while secondarily meandering, IA is primarily meandering while secondarily braided, and OS and I are mostly meandering (Owen et al., 2017). Projections of these channel body geometries onto the basin map suggest the potential presence of transverse systems at the Beartooth Mountains and the intersection between the current Absaroka Mountains and the Owl Creek Mountains (see Fig. 12 of Owen et al., 2017). The downstream increasing IA proportion and decreasing I and OS proportions, particularly obvious near the study area, suggest the interference of transverse systems with the axial system. In other words, the axial system should be more dominated by the meandering river planform at the northern part of the basin, but instead, the braided river planform is observed to increase due to the input from the transverse system, as evidenced by both the basin-scale study of Owen et al. (2017) and the more local study reported here.

Based on the above analyses and existing literature, the palaeogeography of the Bighorn Basin

during the early Eocene is refined in map view (Fig. 4.11), representing field observations of this chapter and data from previous studies, particularly the basin-scale depositional model of Owen et al. (2019). Detailed annotations of elements in this map are listed in the figure caption, with reference to published literature and this chapter. The presented palaeogeographic model represents one possible scenario where FA3 braided channel deposits dominate the study area during high or ephemeral discharge conditions (Fielding et al., 2018). Other scenarios are plausible when the study area hosts FA4 sinuous channel deposits, probably during the low/perennial discharge conditions based on the analysis in Section 5.1.

To summarise, water discharge in the main stream is determined by contributions from axial and transverse systems at the upstream part of the study area, and high/ephemeral discharge conditions favour FA3 braided-like channel development. In contrast, low/perennial discharge conditions favour FA4 sinuous-like channel development (cf., Fielding et al., 2018).

4.4.4 Controls on river planform styles and geomorphic zonation

River planform styles depend on several controlling conditions, including water discharge, transport material (bedload vs. suspended load), sediment concentration, valley gradient, and bank material strength (Schumm, 1985; Church, 2006). In an equilibrium-state river channel, sediment concentration is in balance with the valley gradient (Muto et al., 2007; Wang et al., 2021a). Upstream factors also influence these controlling conditions, and the sediment concentration can, at times, be greater than the transport capacity determined by valley gradient and stream power. When this happens, aggrading and braiding fluvial conditions tend to occur (Schumm, 1985; Church, 2006; Muto et al., 2007). In contrast, the river will tend to entrain sediment and degrade when sediment concentration is lower than the transport capacity. The channel's preferred mode of transient degradation is to become more sinuous until the channel gradient is reduced to the required value (Bettess and White, 1983) unless bank strength prevents it from reaching the equilibrium gradient (Church, 2006).

Nevertheless, sinuous systems are also reported in aggrading schemes (e.g. Willis and Tang, 2010; Ghinassi et al., 2014; Van de Lageweg et al., 2015), which should be noted in linking the river planform type and depositional setting during the outcrop interpretation. Therefore, the climatically-controlled sediment concentration can change river planform style by shifting the geomorphic zonation boundaries between two adjacent river styles toward upstream or downstream directions (Holbrook et al., 2006). Understanding what timescale this process is occurring needs more study. Climate changes, possibly related to astronomical forcing, may have been a dominant contributor to river planform changes. Alternatively, tectonics could also have played an important role in controlling the river planform styles since it can uplift the source area, introduce sediment into the system, and regulate stream style and process by influencing slope, sediment supply, and even discharge (Kraus and Middleton, 1987). The Bighorn Basin was tectonically active during the Paleocene and Eocene. The relatively constant basin subsidence rates (Abels et al., 2013; Foreman, 2014) could suggest that climatic factors might have been more dominant, resulting in the alternation of river planform styles over certain timescales, although the influences of short-term tectonic fluctuations cannot be ruled out.

The early Eocene river systems in the Bighorn Basin experienced substantial climate alternations likely driven by orbital forcing (Abels et al., 2013), and changes may embody these climate alternations in temperature, precipitation, vegetation cover, bank erodibility, suspended load/bedload ratio,

and seasonal contrast (Vandenberghe, 1995, 2003). It is anticipated that some other proxies may provide constraints for inference of the above-mentioned climate alternations, particularly the hydrodynamic conditions. However, sandbody data are not yet integrated with other proxies during the early Eocene, such as palaeosol data, in the Bighorn Basin studies to support palaeoclimatic reconstructions. Foreman (2014), however, has integrated sedimentological data with geochemical, palaeoichnological, and palaeobotanical proxy records to characterise the climatic shift of PETM, providing interesting and inspiring insights. Therefore, a detailed stratigraphic analysis is needed to establish a possible precession- or eccentricity-scale relation stratigraphically and statistically between floodplain aggradational cycles and channel sandstone bodies of different river planform styles to improve the climatic reconstruction in the Bighorn Basin. This analysis is partially conducted in Chapter 6.

4.5 Conclusions

This chapter presents a comprehensive sedimentological analysis of outcrops of the lower Eocene Willwood Formation in the McCullough Peaks area of the northern Bighorn Basin, USA, using field-documented data and UAV-digital outcrop model measurements. A total of four channel lithofacies associations are recognised, which are interpreted to be deposits of four river planform styles: crevasse channel, trunk channel, braided-like channel, and sinuous-like channel, respectively, with the latter two styles as dominant ones. Braided-like and sinuous-like channel sandstone bodies differ significantly in thicknesses, being on average 6.1 m versus 9.0 m, they have similar widths of 231 m and palaeoflow directions of on average 003°. They are different in lithofacies compositions and proportions, but planar cross-stratified sandstone is the most dominant lithofacies in both types of deposits. The alternating presence of sinuous and braided river styles recorded in the outcrop offer insights for the refined reconstruction of a palaeogeographic model for the early Eocene period. In the schematised model, several transverse systems confluence with an axial system roughly following the basin axis in line with previous reconstructions. In addition to the importance of understanding the depositional patterns of the Bighorn Basin, this chapter efficiently synthesises traditional sedimentologic data collection often hampered by small sample sizes with UAV-based digital outcrop models that can contribute to a significant increase in data. This innovation is expected to provide a template for future data collection that can substantially increase the sample size of sedimentologic studies to eliminate data biases to a large extent.



5

Stratigraphic relation between river channels and channel sandstone bodies with floodplain sedimentary environments and stratigraphy in the Willwood Formation of the Bighorn Basin, Wyoming, USA

Abstract

Understanding river channel sands and their relationship with their floodplain deposits is essential to accurately interpret alluvial systems to assess the quality of subsurface reservoirs. Floodplain deposits can be used to reduce the uncertainty in estimating sandstone body geometry, connectivity, and occurrence. However, studying the interrelation of channel and floodplain sediments has been difficult due to limitations in outcrop quality, workers that are either specialists in sandstones or fines and due to low resolution of age and stratigraphic control. Despite these challenges, conceptual models of channel-floodplain stratigraphic relations remain the basis for interpreting alluvial stratigraphies and producing static reservoir model scenarios. This chapter attempts to unravel the stratigraphic relation between the channel and channel sandstone body and the adjacent floodplain sediments and stratigraphy in the Willwood Formation of the Bighorn Basin, Wyoming, USA. Field outcrops are relatively continuous and of good quality in the study area. Floodplain aggradation cycles in the Willwood Formation are ~7 m-thick and consist of avulsion-belt heterolithics and overbank fines. The sandy heterolithics are deposited by crevasse splays and the fines by true overbank flooding deposition on which well-developed palaeosols developed. Thirty-five channel sandstone bodies are related to their adjacent floodplain stratigraphy at dm- to m-scale vertical resolution. The channel sandstone bodies incise stratigraphically from the middle or top of the avulsion-belt deposits within the avulsion-belt – overbank floodplain aggradation cycles, and on average, the incision depth is 80% of the total sandstone body thickness. On average, the channel sandstone bodies are 0.9 to 1.3 times as thick as the related floodplain aggradation cycles. Two channel sandstone bodies incise, fill, and incise again with only decimetres of floodplain stratigraphy separating the two incisions, suggesting that either incision on these floodplains was relatively easy to produce or there is more time in the avulsion-belt phase than previously assumed. Two depositional models are discussed for the deposition floodplain aggradation cycles and their relationship with channel sandstones. In one model, channel aggradation creates superelevation and generates channel avulsion. The other model consists of phases of fluvial activity with channel incisions, infill and avulsion and phases of fluvial inactivity and relative channel stability with overbank deposition. Both models can be interpreted to be allogenic and autogenic driven. The examples in this chapter demonstrate that the resulting stratigraphy exhibits a preferential zonation of channelised sandstone bodies in the base of a floodplain aggradation cycle and a potentially positive effect on vertical connectivity. Integrating such conceptual models and channel-floodplain stratigraphic relationship into subsurface reservoir characterisation help improve the vertical probability estimation of channel sandstone occurrences on the high-resolution floodplain aggradation cycle scale.

Written by: Baars, T.F., Martinius, A.W., Abels, H.A.

Author contributions can be found on page 187.

5.1 Introduction

Alluvial stratigraphy chiefly consists of channel sands and surrounding floodplain fines. Both channel sands and floodplain sediments have received ample study over the last decades resulting in a rich knowledge-base unravelling dynamics and controls on alluvial systems. (e.g. Fielding et al., 1986; Martinius et al., 2002; Owen et al., 2017; Wang et al., 2022 and Kraus and Gwinn, 1997; Muller et al., 2004; Kraus and Alsan, 2009; Lelpi et al., 2018 respectively). How channels relate to the adjacent floodplains at morphological and geologic time scales has received interest because it places each system into a more holistic interpretation. The relationship between the floodplain and channel is studied in modern-day settings (e.g. Lecce, 1996; Walling and He, 1998; Thonon et al., 2007; Valenza et al., 2022) and integrated into numerical models (e.g. Mackey and Bridge, 1995; Nicholas and Mitchel, 2003; Hajek and Edmonds, 2014). However, detailed studies in the geological record studies have been few (e.g. Kraus, 1996; Varela et al., 2021). This low amount is because studying their exact interrelation has shown to be difficult. Limitations in outcrop quality prevent the channel margins from being related to their adjacent floodplain stratigraphy because sedimentologists are often specialists in either channel or floodplain sediments and because age and stratigraphic control is commonly at such a low resolution that it cannot be shown when which channel was active compared to the adjacent floodplain stratigraphy. Nevertheless, conceptual models about channel-floodplain stratigraphic relations in upstream and downstream controlled systems remain the baseline from which alluvial stratigraphies are interpreted. Such models are important for understanding the sedimentary environmental evolution and control of deposition and may help improve the characterisation of subsurface reservoirs.

In low net-to-gross alluvial systems, the floodplain fines comprise most sediment content (ca. <30% sand content, e.g. Larue and Hovadik, 2006). Generally, these systems have a low gradient and are dominated by high aggradation rates with rapid lateral movement of channels (Bridge and Tye, 2000). Commonly these floodplain fines are interpreted to show an increasing maturity further away from a channel (e.g. Bown and Kraus, 1987; Valera et al., 2021), and thus there is a strong lateral gradient palaeosol maturity and development. However, with rapid lateral movement of the channels, often the floodplain fines are alternating with stratified, coarser-grained (silt to medium-sand), forming floodplain aggradation cycles consistent on a kilometre-scale (e.g. Allen 1974; Willis and Behrensmeyer, 1994; Kraus and Gwinn, 1997; Atchley et al., 2004; Abels et al., 2013; van der Meulen et al., 2020, Chapter 3). In the past, several conceptual models for depositing such cycles and the relationship between alluvial channels and their floodplains have been suggested. For example, Allen (1974) describes the lateral continuous carbonate horizons in the Lower Old Red Sandstone, United Kingdom, suggesting that these sites on the floodplain were denied river-borne sediments for extended periods. Allen (1974) proposed several models for depositing these carbonate beds based on horizontal and vertical river movement. Migration, avulsion, and merging of rivers can drastically change the aggregation rates on the overbank and can be forced by both local channel movement and external climate-induced upstream or downstream changes in the forcing patterns. Similarly, Willis and Behrensmeyer (1994) observed palaeosols-bounded cycles in the Chinji Formation, Pakistan, which they also attribute to episodic vertical aggradation of the entire floodplain and suggest that deposition controlled by the growth of alluvial ridges followed by rapid deposition associated when channel avulsed.

To observe, understand, and model the relationship between floodplain developments and alluvial architecture in low-gradient fluvial systems, floodplain aggradation cycles in the Early Eocene Willwood Formation, Wyoming, USA, are investigated (for more information about the Willwood Formation and the geological setting, see Chapter 2). Chapter 3 of this thesis and previous research (Kraus, 1987; Abdul Aziz et al., 2008; Abels et al., 2013, Van der Meulen et al., 2020) shows floodplain fines display a lithological alternation arrangement on a scale of 3-12 meters and average ~7 m. Intervals of red and purple well-developed palaeosols developed on floodplain fine clastics alternate with heterolithic, sandy intervals with moderate to weak palaeosol development (see Chapter 2: Fig. 2.3). The heterolithic deposits are interpreted as avulsion-belt deposits with a high aggradation rate. In contrast, the fines with well-developed palaeosols are interpreted as true overbank deposits with a low aggradation rate.

Channel avulsion occurs due to the elevation of the channel higher than its floodplain caused by uneven sediment deposition (e.g. Bryant et al., 1995; Mohrig et al., 2000; Jerolmack and Paola, 2007). The levees close to the channel build up more quickly than the floodplain further away, leading to a superelevation of the channel and making it prone to avulsion. A trigger can cause crevassing and rapid deposition of sand and mud on the floodplain, followed by channel relocation. Using integrated stratigraphic age constraints, the cycles observed in the Willwood Formation have an estimated period of 21 kyr. This period forms the basis of the suggestion that the floodplain aggradation cycles and avulsion patterns could be externally forced by precession-paced climate changes (Kraus and Aslan, 1993; Abdul Aziz et al., 2008; Abels et al., 2012; 2013). Given this, Abels et al. (2013) proposed a model in which a well-developed palaeosol is related to periods of relative channel stability when gradients between channel belts and floodplains were low, and a moderate to weak palaeosol development relates to episodes of regional wide channel avulsion that occurred when channels became superelevated above the floodplain. However, contrary to this, the floodplain aggradation cycles in the Willwood Formation are also interpreted to be the result of autogenic channel behaviour alone, as numerical modelling suggests similar time scales for autogenic avulsion patterns (Hajek et al., 2010; 2012; Hajek and Straub, 2017).

The present chapter investigates the interaction between channels and their floodplain, and the embedding of channels in models proposed for the floodplain aggradation cycles in the Willwood Formation. This analysis is done in the Deer Creek and Gilmore Hill area of the McCullough Peaks of the northern Bighorn Basin (See Chapter 2: Fig. 2.2). To do so, channels are observed and documented in the field and digital outcrop models, focusing on the channel margins and interaction with floodplain deposits. Floodplain aggradation cycles are defined based on one-dimensional outcrop and three-dimensional digital outcrop data in a similar approach to Chapter 3. Fluvial style, Incision dimensions and stratigraphic position are documented in a similar approach as in Chapter 4. Subsequently, models for floodplain aggradation cycles are evaluated and refined, whereafter, the implications for reservoir architecture and the potential as subsurface analogue are discussed.

5.2 Methods

5.2.1 Trenched section

In the Gilmore Hill area, a stratigraphic section was measured by digging trenches approximately 1 meter deep to expose fresh rock samples. The section is constructed as a composite of several smaller

Facies association	Features	Interpretation
1	Fine to medium sand, 0.5-3 m thickness, a lenticular external geometry	Small-scale crevasse channel sandstone deposits
2	Fine to medium sand, 8-15 m thickness, channelized features with thinning channel wings	Large-scale trunk channel sandstone deposits
3	Medium sand with conglomerate at the base, 4-8 m thickness, commonly have three to four storeys	Braided-like channel sandstone deposits
4	Medium sand, 5-15 m thickness, lateral accretion surfaces	Sinuuous-like channel sandstone deposits
5	very-fine to coarse sand, 1-6 m thickness, multiple beds of 0.1-0.5 m	Sheet-like crevasse splay deposits

TABLE 5.1 Sandstone bodies classifications used in this Chapter. Based on facies associations from Chapter 4 and the Deer Creek area.

trenches (for the locations, see Supplementary Data Ch5S1). This composite section enables the construction of a one-dimensional vertical section that excludes large sandstone bodies and shows only floodplain deposits and the targeted floodplain aggradation cycle. Logging was done based on documenting the grain size, matrix colour, size and colour of mottling, the presence, abundance, and size of carbonate nodules, and the presence and abundance of slickensides. The field descriptions of the palaeosols are based on methods detailed in the Soil Survey Manual (Soil Survey Division Staff, 2017).

5.2.2 Floodplain aggradation cycles

To identify the floodplain aggradation cycles, a Soil Development Index (SDI) was constructed. Abels et al. (2013) proposed that this index curve provides a quantitative estimation of the level of pedogenic development of overbank deposits. The SDI methodology allows to recognition of soil development stages based on three key criteria: (1) palaeosol B-horizon thickness, (2) a simple assessment of the intensity of horizon development and (3) the amount of rubification of the palaeosol. For each individual palaeosol profile, these parameters are assigned a score between 0 and 1, depending on the intensity. Next, the scores are standardised using two standard deviations of the entire section. Subsequently, the index per soil averages the three standardised parameters plus 1.0 to make the SDI positive between 0 and 2. SDI values below 0.5 are weakly developed palaeosol, intermediate pedogenesis yields SDI values between 0.5 and 1.0, and an SDI >1.0 indicates intense pedogenesis.

Based on the SDI score, boundaries of floodplain sedimentary aggradation cycle transitions were placed at the tops of the interval showing the most intense pedogenesis. Some cycles are straightforward to identify due to their distinct red or purple palaeosol and light sandy base. However, others have a higher content of heterolithic deposits and less pronounced palaeosol development in a one-dimensional view. The floodplain aggradation cycles were identified in the digital outcrop models using the methodology described in Chapter 3.

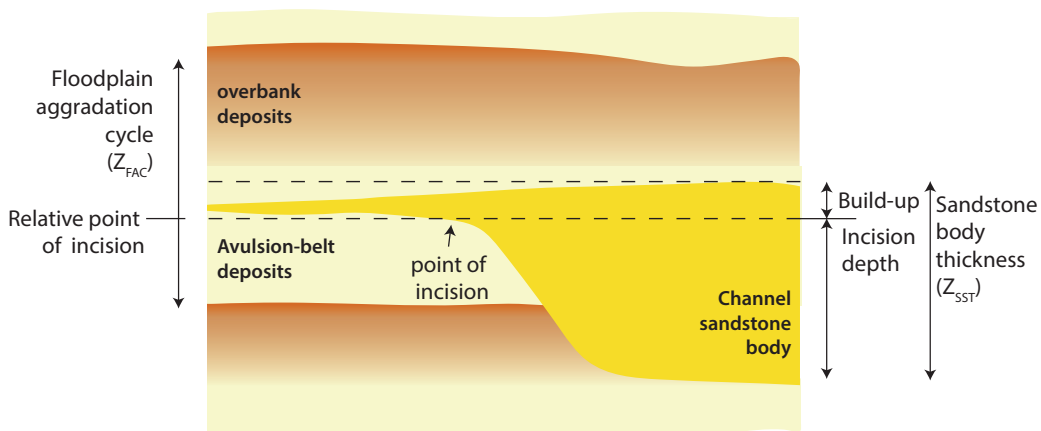


FIGURE 5.1 Schematic diagram of an incised channel with inset in the floodplain aggradation cycles, illustrating the terminology used in this paper. The floodplain aggradation cycle thickness, Z_{FAC} is used to calculate the relative point of incision [%] of the channel sandstone body in the cycle. Sandstone body thickness, Z_{SST} is divided into thickness of incision and build-up above the point of incision.

5.2.3 Digital Trenches

Sixteen lithostratigraphic logs have been created based on the Gillmore Hill digital outcrop model (for more information about the digital outcrop model see Chapter 2). The grain size (clay, silt, fine sand and coarse sand) and colour (grey, yellow, brown, orange, red, and purple) classification was determined based on visual analysis combined with the field experience of the trench data. These logs are intended to have a higher resolution than the tracing of avulsion and overbank deposits. In between the logs, individual crevasse splay and levee deposits were traced.

5.2.4 Stable carbon isotopes

A carbon isotope record was constructed for the Gillmore Hill trench section to embed the floodplain aggradation cycles in a relative timeframe and correlated between the Gillmore Hill and Deer Creek areas. This was possible because in both study areas, the Eocene Thermal Maximum 2 (ETM2, also known as H1) and Hyperthermal 2 (H2) events are documented (Abels et al., 2012; 2016, D'Ambrosia et al., 2017).

Pedogenic carbonate nodules were sampled at a 25 cm spacing where present after removal of the weathered surface. When sampling, the pedogenic carbonate structures' primary micritic parts were chosen, and the secondarily formed calcite spar was avoided as this can influence the stable isotope ratios. Carbon isotope excursion magnitudes are calculated as the difference between pre-excursion carbon isotope values and excursion values within the core of the main body. Standard errors are calculated using variability in background and excursion values. The data is provided in Supplementary Data Ch5S2

5.2.5 Channel sandstone body margins

The study of sandstone body margins and their interaction with floodplains was conducted through field observations, sketches, and drone photographs. Sandstone bodies were classified using the facies associations of Chapter 4 (Table 5.1). Thickness was measured at the thickest point of the sandstone body, and incision thickness was determined as the vertical distance between the channel base and the point of incision on the adjacent floodplain (Fig. 5.1). Although this might not be the exact initiation point of the channel, in a stratigraphic context this is the best estimate of the position of the channels in relationship with the surrounding floodplain. The height of the alluvial ridge, formed by the channelised sandstone body, was documented from the incision to its top and expressed in percentage (relative superelevation). These thickness measurements pertain to compacted stratigraphy and cannot be compared to current measurements.

Palaeoflow measurements were taken from dune-scale cross-stratification (primarily planar and trough cross-stratification). Palaeoflow measurements were derived from the documented sandstone body margins and other sandstone bodies without exposed margins. Per sandstone body, four to five measurements were averaged into one average palaeoflow direction. This analysis was only done for the Gillmore Hill area and compared to the palaeoflow measurements of the Deer Creek area discussed in Chapter 4.

The sandstone bodies were embedded in a floodplain-based stratigraphic framework as the documented sandstone body was correlated to the corresponding floodplain aggradation cycle. The thickness of the floodplain aggradation cycle was measured directly on the margin of the channelised sandstone body. Additionally, the relative position of the sandstone body incision in the floodplain aggradation cycles was documented. This level was calculated by determining the distance from the base of the floodplain aggradation cycles to the incision and expressing it as a percentage of the total cycle thickness at that location (Fig. 5.1). Lastly, it was documented whether the point of incision was positioned in the avulsion-belt or in true overbank deposits of the floodplain aggradation cycle.

5.3 Results

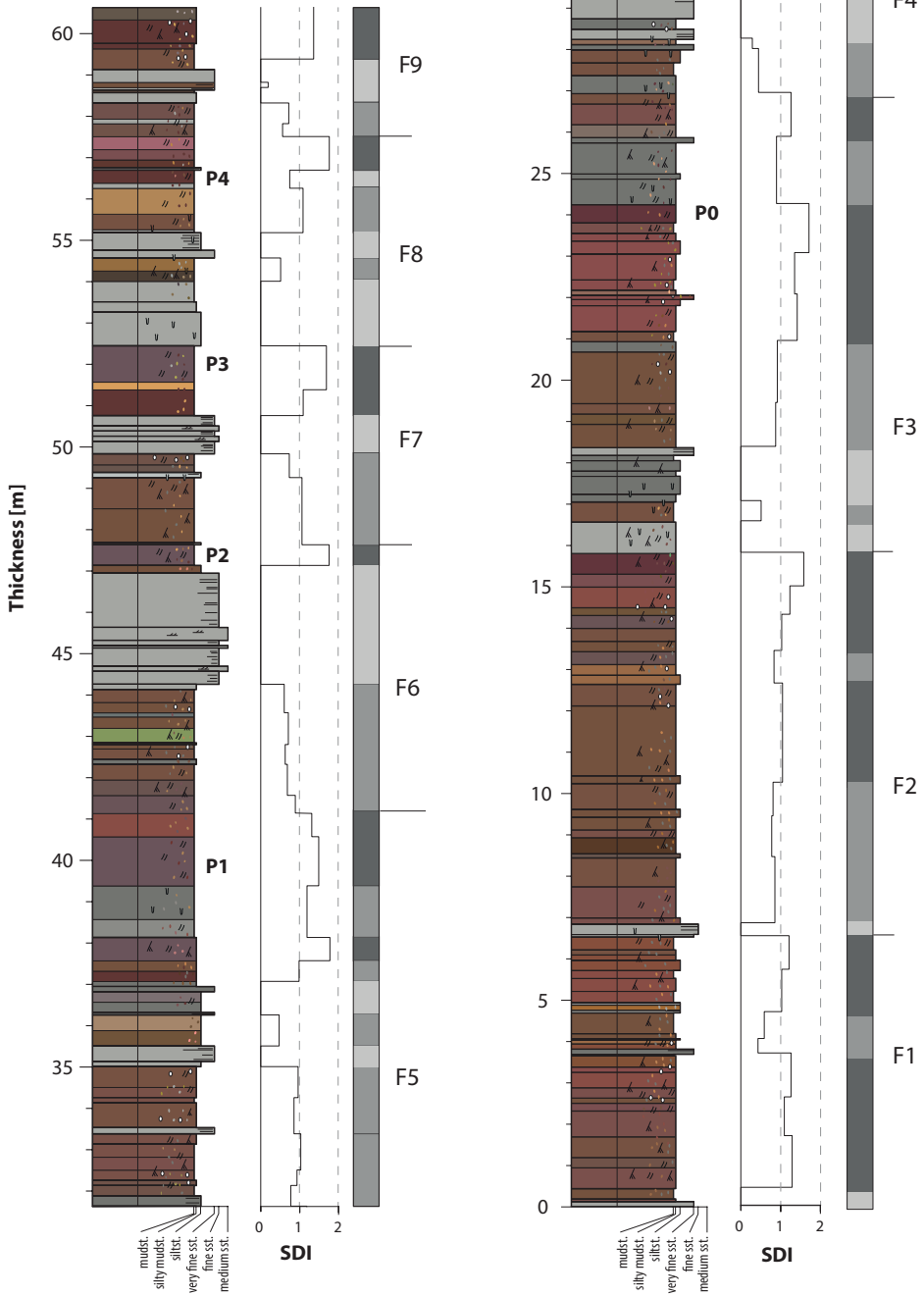
5.3.1 Floodplain stratigraphy

The stratigraphy of the Gilmore Hill area has been measured through a 60 m thick composite floodplain section. The pedogenic carbonate $\delta^{13}\text{C}$ record of the Gillmore Hill section has a baseline $\delta^{13}\text{C}$ value of -10.5‰ and displays a distinct carbon isotope excursion between 37 to 53 m (Fig. 5.3). This excursion displays a relatively sharp decrease towards values of -14‰ after which values gradually increase again to -10.5‰ . The excursion magnitude is 2.62‰ (standard error: 0.18), similar to the previously described section at Gilmore Hill, where a magnitude of 2.5‰ was documented (D'Ambrosia et al., 2017). Magneto- and biostratigraphic constraints allow relating this excursion to the ETM2 hyperthermal event with values slightly lower than the ETM2 excursion documented in the Deer Creek area (Abels et al. 2012; D'Ambrosia et al. 2017).

The floodplain stratigraphy displays alternations of heterolithic, sandy, pale-coloured sediments and fine clastic, red-coloured sediments related to avulsion-belt and true overbank deposition (Fig. 5.2), as described in Chapters 2 and 3. The Soil Development Index (SDI) was used to objectively identify these two depositional phases. Sand- and siltstones showing weak pedogenic development score SDI values below 1. Fine clastics showing distinct palaeosols score values above 1. Based on the

Legend

- | | | |
|---------------------|-------------------------|----------------------------|
| ⋈ Rhyzolithes | ••• Colour mottle | □ No/incipient pedogenesis |
| ○ Carbonate nodules | ∩ Burrow | ▒ Medium pedogenesis |
| // Slickensides | — Small-scale cross-bed | ■ Intense pedogenesis |



← **FIGURE 5.2** Simplified field log of the Gillmore Hill section showing stratigraphic thickness, grain size, matrix colour, bed induration as related to grain size, and sedimentary characteristics such as carbonate nodules, slickensides, and colour mottling. Distinct purple palaeosols are labelled. To the right of the Soil Development Index, a simplified intensity of pedogenesis bar is given. Based on the intensity of pedogenesis and recognition of overbank and avulsion deposits, floodplain aggradation cycles are labelled 1 to 9.

transition from high to low SDI, a total of seven complete floodplain aggradation cycles are identified (Fig. 5.2). These seven cycles have an average thickness of 7.1 m (SD 1.9), which is similar to the average thickness observed in the Deer Creek area in one-dimensional sections and based on the digital outcrop model (7.1 m; Abels et al., 2013; 6.9 m; Chapter 3).

As tracing in the digital outcrop model demonstrates, the seven floodplain aggradation cycles are continuously present in the Gilmore Hill area over a lateral extent of 2 km (oblique to the average palaeoflow; 308°). Lateral thickness measurements of the same floodplain aggradation cycles indicate a thickness variability of 3.3 to 11.2 m. On average, the avulsion-belt deposits comprise 59% of the cycles (Table 5.2).

The Gilmore Hill floodplain stratigraphy presents several distinct lilac to purple palaeosols. These palaeosols are laterally extensive through the whole area and were visually traced beyond the whole Gilmore Hill digital outcrop model towards the west, where D'Ambrosia et al. (2017) sampled the White Temple section (In between the Deer Creek and Gillmore Hill area). The most pronounced lila to purple soils are labelled P0 to P4 (Fig. 5.2). These strong palaeosols form the top of the floodplain sedimentary aggradation cycles. P1 and P2 occur in the ETM2 $\delta^{13}\text{C}$ isotope excursion, while P3 occurs at the top of the recovery interval of this event. At Deer Creek, the ETM2 floodplain stratigraphy is similarly characterised by lila to purple palaeosols (Abels et al. 2012; 2016).

5.3.2 Crevasse-splay and Avulsion-belt deposits

In the heterolithic avulsion-belt deposits, several centimetres to decimetre thick splay deposits are present, which commonly occur as two to four stacked events over 1 to 2 m thick intervals and are separated by centimetre thick mud rocks (Fig. 5.4). The level pedogenic overprint (visual, based on the outcrop photographs) of individual splays laterally increases when more distal from source channels; however, the stacked composite of individual splays can be traced continuously. Tracing shows a strong continuity over at least 2 km and a wider extent than the digital outcrop model.

5.3.3 River channels and channel sandstone bodies

Fifty-six sandstone bodies have been documented in the Gillmore Hill area and ninety-two in the Deer Creek area (Chapter 4). However, in most channel bodies, the margins are not exposed or unclear due to the cover of vegetation or Holocene alluvium.

Thirty-five of these sandstone bodies display well-exposed channel margins and have been studied. Twenty-three are located in the Gilmore Hill area, and twelve are located in the Deer Creek area (for their locations, see Supplementary Data Ch5S1). Twenty-four of the channel sandstone bodies are interpreted to be the result of sinuous-like channels (FA4), four are interpreted as small-scale crevasse channels (FA1), and seven as the result of braided-like channel styles (FA1). No outcropping margins were observed of the large-scale trunk channels (FA2).

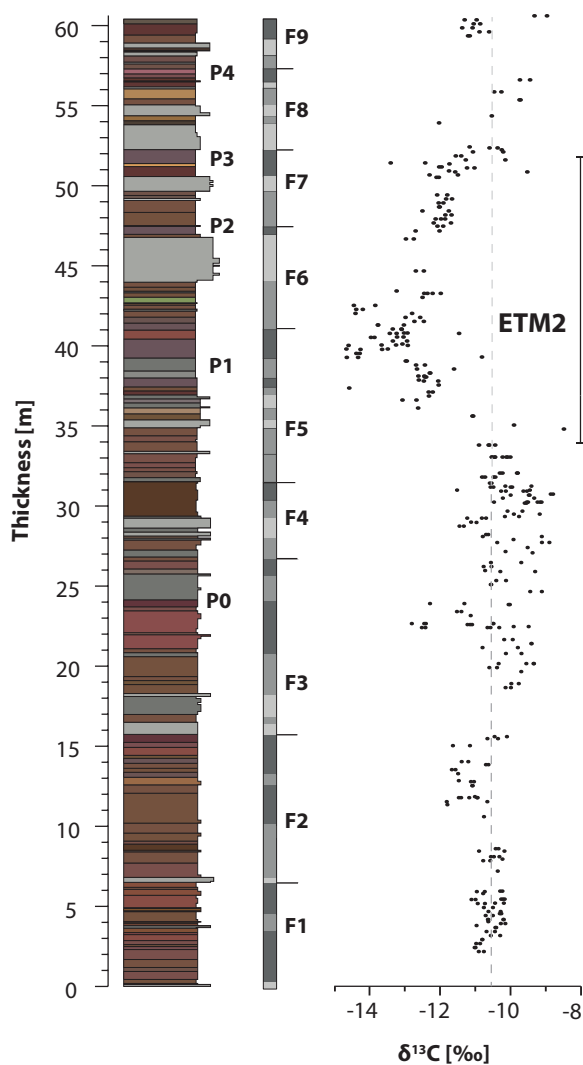


FIGURE 5.3 The pedogenic carbonate $\delta^{13}\text{C}$ data expressed in per mille on the VPDB scale. The stippled grey line represents the baseline of 10.5‰. The negative carbonate excursion is interpreted to represent the ETM2 excursion and is similar other records in the area (Abels et al., 2016; D’ambrosia et al., 2017). On the left, the lithostratigraphic log and floodplain aggradation cycles are displayed (see Fig. 5.3).

On average, the observed channel sandstone bodies have a thickness of 7.6 m (SD 2.2) and incise 6.4 m downward, and the build-up above the incision point is 16% of the total sandstone body thickness in compacted stratigraphy (Table 5.2). Palaeoflow measurements from fifty different sandstone bodies (including those that do not display clear margins) in the Gillmore Hill area indicate a mean palaeoflow direction of 308° with a standard deviation of 65° (Fig. 5.5). A similar broad spread of flow direction is observed in the Deer Creek area (Chapter 4), where the flow was 003° .

Two examples of channel margins are shown in Figure 5.6, while all observed channel margins are provided in Supplementary Data Ch5S3. Most of the documented channel margins ($n=28$) are incising from avulsion-belt deposits. Some channels ($n=7$) are also incising from the base of the avulsion-belt deposits. On average, the stratigraphic point of incisions occurs at 22% of the floodplain sedimentary

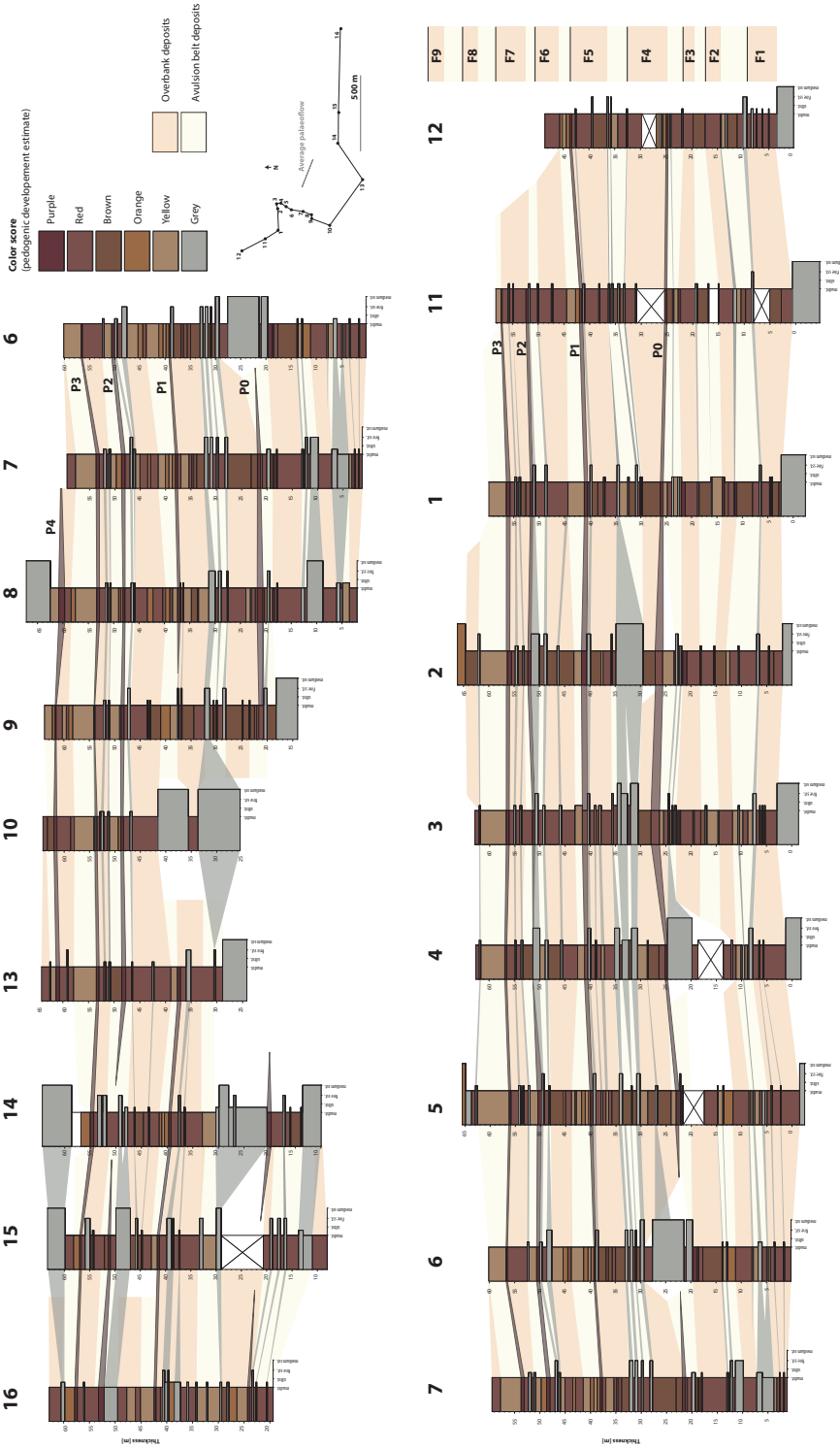


FIGURE 5.4 A fence panel generated from the digital outcrop model with stratigraphic logs estimated from outcrop photographs and knowledge of trench data. Correlations between crevasse splays and levee deposits are made from tracing in the digital outcrop model. Purple marker beds P0-4 are highlighted.

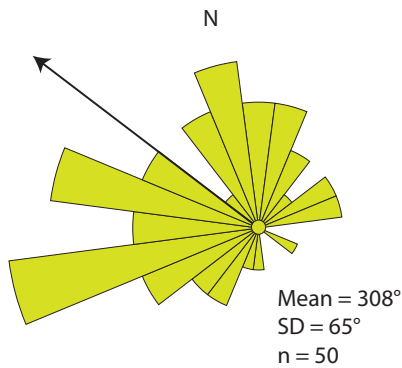


FIGURE 5.5 Rose diagram of palaeoflow directions of 50 sandstone bodies in the Gillmore Hill area. Both sinuous-like and braided-like palaeoflow measurements are combined. Palaeoflow measurements were taken from dune-scale cross-stratification (primarily planar and trough cross-stratification)

aggradation cycle counted from the top of the overbank phases. Individually this number may vary, showing a standard deviation of 17%. Commonly, it is found that crevasse splay deposits precede a channel margin.

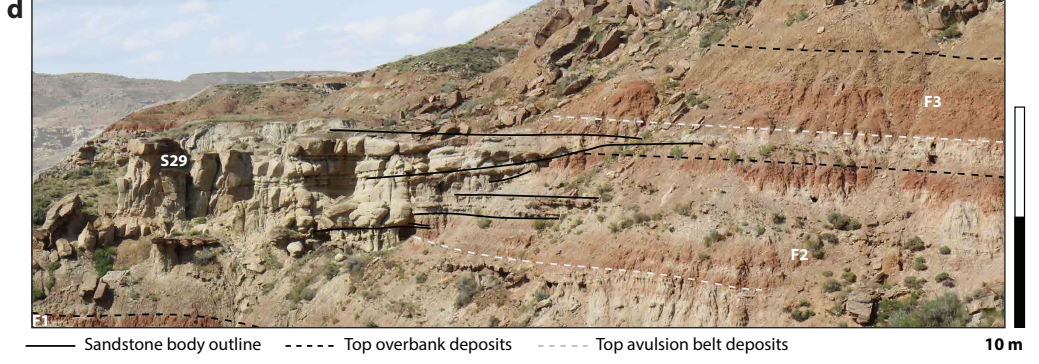
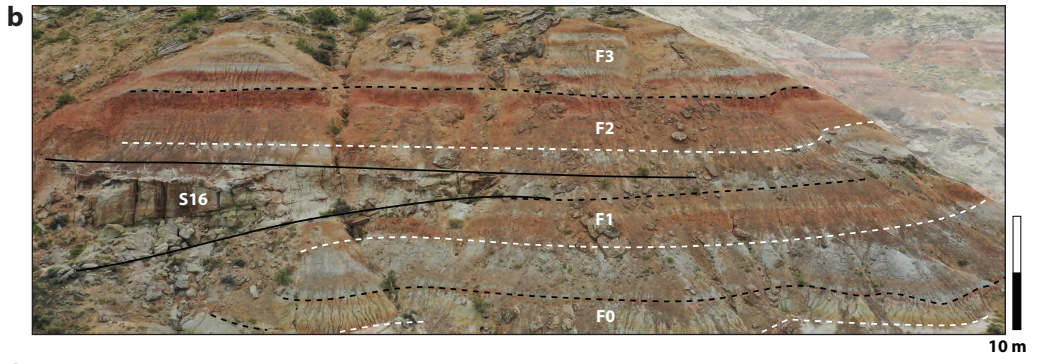
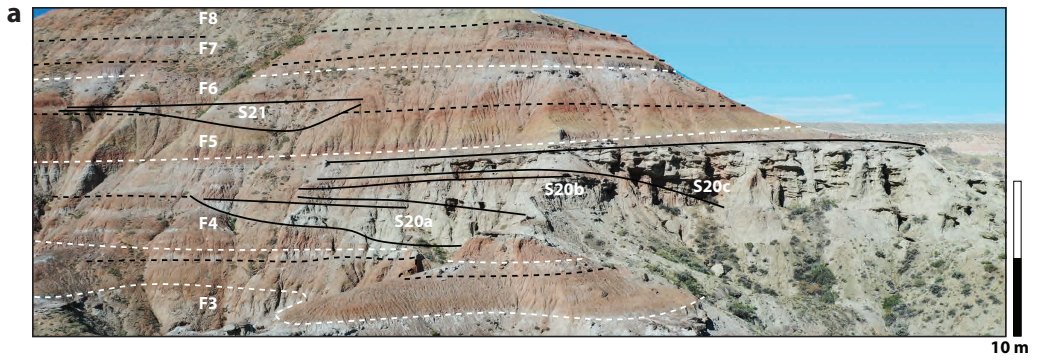
Three channels have been documented to have a point of incision in lateral extensive overbank deposits. Two are crevasse channels, and one is sinuous-like (S5; Supplementary Data Ch5S3). In the latter, near the channel, the palaeosols are weakly developed, while laterally, these rapidly turn into well-developed soils at a scale of 100 m perpendicular to palaeoflow.

In the seven braided-like channel margins, the relative point of incision is harder to determine as the margins are showing interference with the surrounding floodplain deposits (Fig. 5.6c). The top incision of the braided-like channel occurs slightly higher in the floodplain sedimentary aggradation cycle (30%, std: 17%) compared to their sinuous-like counterpart (Table 5.2).

One sinuous-like multi-storied sandstone body in the Deer Creek area (S29; Fig. 5.6d) has been observed to deposit sediments in two consecutive avulsion-belt phases. The sandstone body is interpreted to be aggrading and interfering with the overbank deposits between these two phases.

Frequently (n=11), moderately developed palaeosols separate individual sandstone bodies or sheet-splay events. This separation is well illustrated in the case of sandstone body S20 (Fig. 5.6a),

→ **FIGURE 5.6** Four examples of channel incisions and margins in the Gillmore Hill area. a) a sinuous-like channel sandstone (S20) incising (black outline) into overbank fines. The channel originates in the avulsion-belt deposits of floodplain sedimentary aggradation cycle F5 and forms the complete avulsion-belt deposits (~4m) at this site. The sandstone body has multiple stories that are separated by moderate developed palaeosol deposits in the margin. This indicates that channel abandonment and reactivation happened at least two times in one avulsion phase. Above this, a small-scale cut and fill is observed (S21). b) a sinuous-like channel sandstone (S16) incising into the overbank fines. Here the incision forms the base of the avulsion phase. Above the top of the channel, a moderately developed palaeosol is topped by a sheet splay deposit forming the top of the avulsion-belt deposits of F2. c) a braided-like channel sandstone (S2) displaying an aggradation style and interfering with the floodplain sedimentary aggradation cycle. d) a sinuous-like channel sandstone (S16) from the Deer Creek area with displaying aggradation style. The body likely originates in the avulsion-belt of F2 and remains aggrading through the overbank phase. Here, levees and/or splays cause a local lesser pronounced overbank phase. The highest point of the sandstone body forms the base of the avulsion phase of cycle F3. In supplementary data Ch5S3 the accompanying non-interpreted images can be found.



—— Sandstone body outline - - - - Top overbank deposits - - - - Top avulsion belt deposits

Channel overbank relationship

Floodplain sedimentary aggradation cycle

Channel sandstone body

Sandstone	Location	Facies association	Channel sandstone body			Buildup above point of incision [%]	Multi-story	Floodplain sedimentary aggradation cycle			Phase	Relative point of incision in FSAC [%]		
			Thickness [m]	Incision depth [m]	Incision			FSA Thickness [m]	Overbank deposits [m]	Avulsion belt deposits [m]			Relative avulsion belt [%]	
1	GH	FA4	8.9	7.0	21	Y	Y	1	8.9	4.0	5.9	66	Avulsion	19
2	GH	FA3	6.3	4.2	33	Y	Y	-1	6.5	3.6	2.9	45	Both	80
3	GH	FA4	6.2	4.8	23	n	n	3	6.4	3.6	2.8	44	Avulsion	6
4	GH	FA4	7.2	5.9	18	Y	Y	4	9.7	3.8	5.9	61	Avulsion	32
5	GH	FA4	5.2	5.1	2	n	n	3	7.2	2.5	4.7	65	Overbank	72
6	GH	FA4	7.5	6.5	13	?	?	5	9.0	2.0	7.0	78	Avulsion	41
7	GH	FA4	12.0	9.7	19	Y	Y	4	7.9	2.9	5.0	63	Avulsion	44
8a	GH	FA4	9.3	6.4	31	Y	Y	4	8.4	3.2	5.2	62	Avulsion	17
8b	GH	FA4	6.9	6.3	9	n	n	4	8.4	3.3	5.1	61	Avulsion	24
9	GH	FA1	7.5	7.3	3	?	?	2	8.7	3.1	5.6	64	Avulsion	14
10	GH	FA4	10.2	9.3	9	n	n	2	9.1	3.5	5.6	62	Avulsion	11
11	GH	FA4	10.1	9.9	2	n	n	3	8.7	2.9	5.8	67	Avulsion	7
12	GH	FA4	8.0	7.2	10	?	?	7	7.2	3.1	4.1	57	Avulsion	14
13	GH	FA4	6.9	5.4	22	n	n	2	4.6	1.3	3.3	71	Avulsion	52
14	GH	FA4	8.3	7.5	10	n	n	2	4.0	1.8	2.2	55	Avulsion	43
15	GH	FA1	4.4	4.2	5	n	n	3	3.3	2.0	1.3	39	Avulsion	3
16	GH	FA4	8.3	8.0	4	n	n	4	5.6	3.4	2.2	39	Avulsion	2
17	GH	FA4	6.9	6.4	7	n	n	8	6.3	3.1	3.2	51	Avulsion	2
18	GH	FA4	8.0	7.3	9	?	?	2	7.2	1.8	5.4	75	Avulsion	22
19	GH	FA1	4.5	4.3	4	n	n	7	5.7	2.9	2.8	49	Overbank	56
20a	GH	FA4	14.0	13.2	6	Y	Y	5	10.5	4.6	5.9	56	Overbank	57
20b	GH	FA4	-	-	-	Y	Y	5	-	-	-	-	Avulsion	36
20c	GH	FA4	-	-	-	Y	Y	5	-	-	-	-	Avulsion	13
21	GH	FA1	3.1	2.9	6	n	n	6	6.9	3.0	3.9	57	Avulsion	1
22	GH	FA4	7.8	6.1	22	?	?	6	5.8	2.3	3.5	60	Avulsion	34
23	GH	FA4	6.5	4.5	31	?	?	7	5.5	1.7	3.8	69	Avulsion	11
24	DC	FA3	5.6	4	29	Y	Y	P3	5.6	2.6	3.0	54	Overbank	4
25	DC	FA4	9.1	7.9	13	?	?	P11	11.2	2.7	8.5	76	Avulsion	4
26	DC	FA4	10.9	10.1	7	n	n	K	9.8	4.9	4.9	50	Avulsion	12
27	DC	FA4	9.2	8.3	10	n	n	I	8.3	4.1	4.2	51	Avulsion	28
28	DC	FA4	7.6	5.6	26	?	?	R	7.3	3.2	4.1	56	Avulsion	18
29	DC	FA4	7.3	7.1	3	Y	Y	O	3.5	1.6	1.9	54	Both	14
30	DC	FA3	6.3	4.5	29	Y	Y	Q	8.5	1.2	7.3	86	Avulsion	69
31	DC	FA3	5.3	3.6	32	Y	Y	P8	5.2	1.6	3.6	69	Avulsion	44
32	DC	FA3	4.6	2.7	41	Y	Y	P3	6.5	3.4	3.1	48	Avulsion	8
33	DC	FA3	7.1	5.5	23	Y	Y	P12	9.2	5.3	3.9	42	Avulsion	66
34	DC	FA3	7.2	6.1	15	Y	Y	U	6.8	3.5	3.3	49	Avulsion	60
35	DC	FA4	10.6	3.4	68	n	n	P6	5.1	2.0	3.1	60	Avulsion	27
			mean	7.6	6.4	16			7.1	2.9	4.3	59		27
			SD	2.2	2.3	14			1.9	1.1	1.6	11		23

← **TABLE 5.2** Statistics of the channel margin observations with facies association thickness, incision depth and build-up above the point of incision. The corresponding floodplain aggradation cycles are given with the total thickness and thickness of overbank and avulsion-belt deposits. Channel overbank relationship is given by embedding in phase and the relative point on incision compared to floodplain sedimentary aggradation cycles. Abbreviations GH: Gillmore Hill, DC: Deer Creek., SD: Standard deviation

where complete incision and infill occurs three times (S20a, S20b, and S20c) in the same overall channel sandstone body. Decimetre-thick, moderate palaeosol deposits lateral to the channel margins separate these stories. Such clear separation by floodplain intervals in the margins of multi-storeyed sandstone bodies is observed in four different sandstone bodies (S1, S8, S20, S22). Additionally, splay deposits are observed above the main channel body separated by decimetre scale moderate developed palaeosol (such as S16; Fig. 5.6b). In total, seven of the documented sinuous-like sandstone bodies show such separation (S1, 4, 14, 16, 18, 24, and 30).

5.4 Discussion

5.4.1 Floodplain consistency

Lateral consistency in avulsion-belt deposits of the Willwood formation has been observed by multiple authors. In digital outcrop models the consistency is shown stable on a 2–5 kilometre range (Chapter 3) and based on one-dimensional correlations a consistency up to 10 kilometres is proposed (Kraus and Aslan, 1993; Kraus and Wells, 1999, Abels et al., 2013; van der Meulen et al., 2020). In this Chapter, similar patterns are observed as the identification of floodplain aggradation cycles in the Gillmore Hill area digital outcrop model display traceability of avulsion-belt deposits at a 2 km scale. Additionally, the average 7.1 m thickness of the floodplain aggradation cycles in the Gillmore Hill area is consistent with the 6.8 m documented in the Deer Creek area (Chapter 3).

The regional consistency and similar thickness of the floodplain aggradation cycles demonstrates that alluvial sedimentation occurred at a similar pace in the Deer Creek area and Gillmore Hill area and avulsion-belt sediments occurring every 7 m would suggest a reorganisation of rivers at a timescale at which 7 m of stratigraphy is preserved. Abels et al. (2013) propose that this is related to precession-driven climate change causing a phase of avulsion levelling superelevation of the channel belts. Superelevation of the channel belts, in turn, originated from the initial so-called overbank phase, during which channels and channel belts were relatively stable in position and gradually aggraded (see Fig. 7 in Abels et al., 2013).

To fully solve the question of the degree of floodplain aggradation cycle consistency, a correlation between the Gillmore Hill and Deer Creek areas needs to be made accompanied with an accurate age control. Allogenic control on the overbank-avulsion floodplain aggradation cycles would imply that these cycles occur synchronously within the areas while autogenic control could imply a diachronous occurrence (Kraus and Aslan 1993). Therefore, without that correlation, the consistency of the cycles between the Gilmore Hill and Deer Creek areas could still be in line with both allogenic and autogenic control. In this chapter, the choice is to focus on the geometric character of, and stratigraphic relation and sedimentary origin between the channel sandstone bodies and the floodplain cycles.

5.4.2 Avulsion patterns

Independent of the question whether overbank-avulsion floodplain aggradation cycles are controlled by autogenic or allogenic forcing, a high degree of consistency in floodplain aggradation cycles would indicate association with large lateral displacements of avulsion deposits. Abels et al. (2013) suggest that such behaviour could be related to large regional channel avulsions. Regional avulsion is defined as an avulsion where the flow deviates from the parent channel into an avulsion and creates an entirely new channel in a new location on the floodplain. Opposite to this, local avulsion, defined as the reconnection of a new channel with the same main channel further downstream, could also occur. Edmonds et al. (2016) proposed an empirical relationship between local avulsion range and length with channel-belt width. Using the documented sandstone body width from the Deer Creek Area (Chapter 4), a local avulsion range of ~500 m perpendicular and ~3 km parallel to the palaeoflow direction is estimated. Such lateral extent is similar to the spatial correlation of floodplain aggradation cycle thicknesses based on variogram analysis (~600 m perpendicular and ~1.3 km parallel) as calculated in Chapter 3. While local avulsion patterns cannot be excluded, the similar patterns in both areas make regional avulsion patterns more plausible. Most likely, however, both have occurred.

Furthermore, the channel margins in the Gillmore Hill and Deer Creek areas are predominantly embedded in the top or middle part of the avulsion belt deposits. As they are frequently preceded by crevasse splays and other coarser floodplain deposits the avulsion style is similar to the model described by Smith et al. (1989; their Fig. 6) and could be classified as stratigraphically transitional incisions (Jones and Hajek, 2007). This suggests that the channel avulsion could have a gradual and progradational style, growing downstream.

The presence of palaeosols and subsequent splay deposits covering channels suggests that there were breaks in sedimentation and development of new palaeosol profiles in the avulsion belt deposits. The presence of multiple stories in channel bodies separated by decimetre scale moderately mature palaeosols also suggests the likelihood of multiple avulsion events within one floodplain sedimentary alternation and a rapid incision and filling of the channel belt. According to modern data from field observations, models, and experiments, the frequency of avulsions can range between 1 to 4 thousand years (Mohrig et al., 2000; Stouthamer and Berendsen, 2001; Jerolmack and Mohrig, 2007; Hajek and Wolinsky, 2012). In the case of the Willwood Formation, if it is assumed that the floodplain aggradation cycles are driven by precession (Abels et al., 2013), which represents roughly 21 kyr, it is possible that several avulsion events could occur within one single floodplain sedimentary alternation. The multi-storied sand bodies and incisions could also result from a positive feedback loop, as heterolithic deposits with less pedogenic development and vegetation cover have lower sediment cohesion due to less consolidation and clay binding. This could make the incised and infilled channel locations more susceptible to erosion and trigger additional annexational-styled avulsions.

It is difficult to determine the exact time represented in overbank and avulsion belt deposits, as accurately dating on a high-resolution scale (< 10 m) remains a challenge due to the limited temporal resolution of current methods and the degree of homogenisation that occurred in the palaeosols. Commonly, it is assumed that the palaeosols represent most of the time in a floodplain sedimentary alternation because one of the main factors for strong pedogenic development, is time (Kraus and Aslan, 1993; Kraus et al., 1999). However, the possibility of multiple avulsion events in a single avulsion phase may indicate a longer duration of deposition during this phase than previously estimated.

5.4.3 Channel incision and aggradation

Avulsion-belt splay deposits frequently precede channel sandstone bodies, and the channelized sandstone bodies incise from the top or middle of the avulsion-belt deposits within the floodplain aggradation cycles. Only one documented sandstone body displays aggradation and interfingering with floodplains deposits. The incisional sandstone bodies originate from the avulsion-phase that the incisions start from. They could be the avulsing rivers described in depositional model by Abels et al. (2013). For the aggradational sandstone bodies, it is hypothesised that the preceding avulsion-phase forms the origin of the rivers that gradually build-up towards the next avulsion-phase.

Such aggradation is not documented in the Gilmore Hill area, which is positioned towards the eastern basin margin. Aggradational bodies are likely to be more common in the Deer Creek area, which is positioned on the basin axis (Finn et al., 2010). It is suggested, therefore, that the axial alluvial systems were more dominantly aggrading, while the marginal systems were more often incising under the influence of changing water and sediment fluxes. However, to substantiate such claims, more data is needed to distinguish between marginal and basinal settings, and between braided and sinuous systems, and to unravel transverse versus axial river systems.

5.4.4 Channel – floodplain relationship

Regional driven avulsion

As previously discussed, Abels et al. (2013) proposed a model for the deposition of floodplain sedimentary alternations in which well-developed palaeosol deposits are related to periods of relative channel stability when gradients between channel belts and floodplains were low (i.e. overbank phase), and the avulsion belt deposits relate to episodes of increased avulsion frequency that occurred when channels became superelevated above the floodplain (i.e. avulsion phase). Observations presented in this chapter are partly in line with this proposed model as most channels observed originate in the avulsion belt deposits, and a similar avulsion style is attributed to the channels.

Furthermore, the occurrence of phases of avulsion implies that channel build-up is halted, and channels relocate to start build-up at a new location. In that case, the stratigraphic thickness of floodplain aggradation cycles would relate to the thickness of the coeval sandstone bodies and such a relationship is documented. The average sandstone body thickness in the Gilmore Hill area is 1.09 times thicker than the average floodplain aggradation cycle: 7.6 m versus 7.1 m respectively. In the Deer Creek area, channel sandstone bodies are 1.30 times thicker than the floodplain aggradation cycles (8.9 m versus 6.8 m; Chapters 3 and 4). However, this averaged data includes braided and meandering channels combined. While not many braided channels are included in the Gilmore Hill data set, braided-like sandstone bodies in the Deer Creek area (on average 6.1 m thick; Chapter 4) have an average sandstone body thickness to floodplain aggradation cycle thickness ratio of 0.88, while sinuous-like sandstone bodies (on average 9.0 m thick; Chapter 4) have a ratio of 1.32.

In the proposed model by Abels et al. (2013) channels are stable during the overbank phase and have an amalgamated character. However, in this chapter, only one major sandstone body displays aggradation, and two other bodies are documented to be laterally embedded in well-developed palaeosol deposits. Part of this absence could be explained by the fact that the Gilmore Hill and Deer Creek areas are simply not covering enough lateral extent to observe more channels embedded in mature palaeosol deposits.

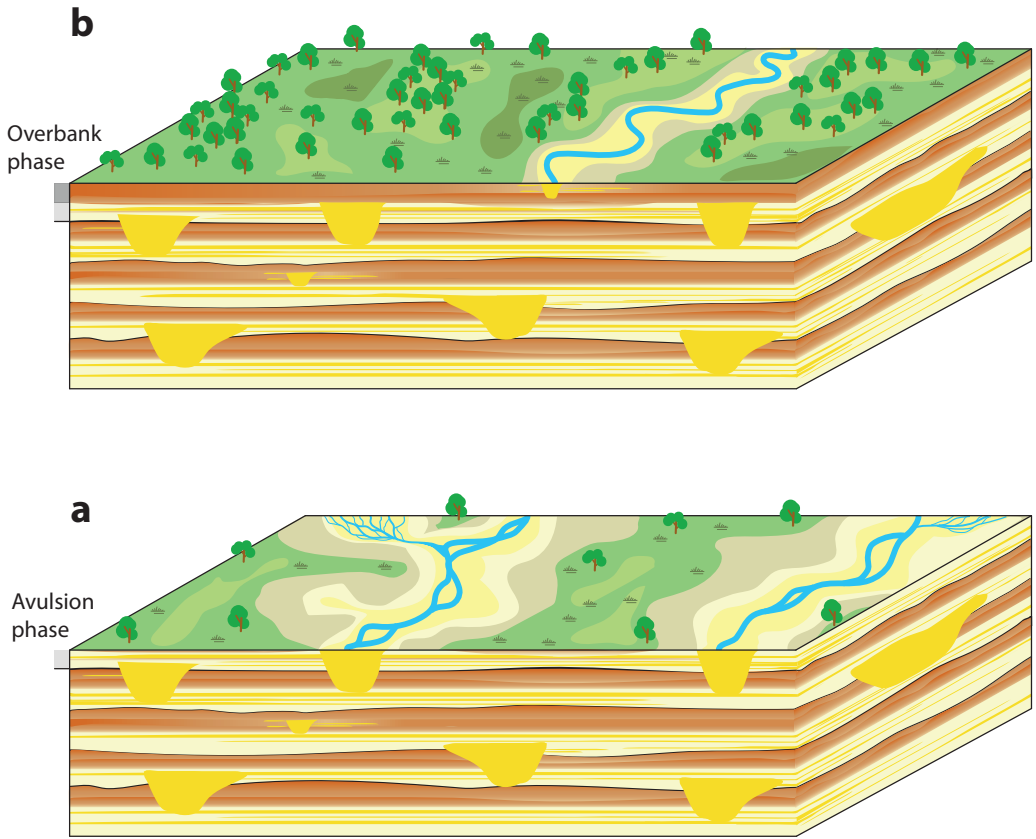


FIGURE 5.7 A schematic overview showing the sedimentary responses to the proposed morphological landscape changes. a) The avulsion phase, where regional avulsion occurs and avulsion frequency increases, leading to the deposition of heterolithic deposits and widespread weak to moderate developed overbank fines. b) the overbank phase, where channel movement is more stable, and the frequency of regional avulsion decrease. It is still possible to have local, minor avulsions. Possibly this stability can be induced by overbank stability and vegetation cover on the overbank.

The new data also suggest that the avulsion belt deposits can consist of multiple incisions relatively close to each other and, thus, encompass multiple avulsion events. Therefore, the avulsion belt deposits could not only be a product of singular avulsions but also be related to an increase in avulsion frequency. This would result in a lateral constant overlapping sheet of avulsion belt deposits interfering with each other, covering a large lateral extends. Observations in lateral changes in thickness and facies characteristics of the avulsion belt deposits can be attributed to autogenic local differences of individual avulsion events (Kraus and Aslan, 2009; Chapter 3).

Clastic phase model

With the likely absence of major channels during the overbank deposits and the occurrence of multiple incisions during one avulsion phase, an alternative model can be developed. Wang et al. (2020) show that cyclic variation in the ratio of sediment load and water discharge can produce alternations consisting of aggradation and non-deposition phases similar to the floodplain sedimentary alternations observed in the Willwood Formation. This would suggest that the cyclic behaviour could be controlled by upstream allogenic forcing, not intrinsic to the depositional system itself.

Dyer-Pietas (2020) shows that during the Eocene in the nearby Green River Formation, Wyoming, lacustrine debris flows were controlled by precession forcing and increased precipitation caused by monsoonal amplification during precession minima. Similarly, in the Willwood Formation, such hydrological variance could have led to an increase in siliciclastic material input by increasing sediment load, bedload particles, and weathering, or an increase in water discharge. Furthermore, it has been shown that precession also can have an impact on vegetation type and density. Based on numerical modelling, Tuenter et al. (2007) proposed a change in vegetation cover correlated to precession minima with increased grass precipitation, while during maxima, increased tree vegetation occurred. Such changes in vegetation cover could significantly impact channel stability and erodibility. Plant growth can cause a fluvial system to organise itself into distinct stable channel and non-channel areas (Tal and Paolo, 2010) and increased channel bank vegetation results in bank stability and lower erodibility of the bank sediments. However, the temporal resolution of the palynological record is not high enough to prove such a hypothesis for the Willwood Formation.

An alternative model is proposed based on siliciclastic input variability and landscape stabilisation patterns (Fig. 5.7). In this model, a phase of increased siliciclastic input and/or water discharge could lead to increased aggradation of channels, increasing the rate at which superelevation is achieved and subsequently triggering avulsion. Such a siliciclastic phase would align with observing multiple avulsion events within one avulsion belt deposit. Additionally, here grassland vegetation would positively influence the tendency to avulse. The second phase of the model, a decrease in siliciclastic input and/or water discharge, combined with a change to a more forested landscape, would lead to smaller, more confined channels and stabilisation of the landscape. Such a model differs from the previously proposed models in that channels are smaller and less present during the overbank phase than in the avulsion phase and would better fit the absence of large, aggrading channels during the overbank phase.

Autogenic forcing mechanisms

Abels et al. (2013) have shown that the average sedimentation rate of the floodplain sedimentary alternations in the Willwood Formation overlaps with the pacing of the precession cycle. Moreover, climatic change potentially has a large impact on preserved fluvial depositional and stratigraphic variations in alluvial architecture as shown by various authors (e.g. Valero et al., 2017; Noorbergen et al., 2020; Lanci et al., 2022; Sharma et al., 2023). In this study, it is proposed that allogenic, upstream control forms a significant forcing factor on alluvial stratigraphy. Nevertheless, autogenic control cannot be ruled out entirely because time scales for autogenic-controlled avulsion patterns are proposed to be similar to short-term allogenic controls (Hajek et al., 2010; 2012; Hajek and Straub, 2017). Modern-day avulsion belt deposits range from 5 up to 60 km in length and from 1 to 50 km in width (Valenza et al., 2022), which is significantly larger than the range of correlation obtained in this

outcrop-based study. Despite this, the observed multiple incisions and channel relocations within one avulsion belt deposit seem to suggest that allogenic controls played a more dominant role.

5.4.5 Implications for subsurface reservoir modelling

The stratigraphic architecture of the studied low net-to-gross fluvial succession of the lower Eocene Willwood Formation can be partially reconstructed through the vertical cyclic stacking of avulsion-belt and overbank deposits in the floodplain succession. The recognition of these patterns has the potential to improve well correlation and reservoir characterisation in the subsurface. This value is not very different with an autogenic or allogenic driving mechanism behind it because the consistency of the cyclicity at 2-5km scale is demonstrated. An autogenic control would create diachroneity of strata, but the data from this chapter and Chapter 3 suggests that this occurs at a larger scale than 5 km.

Channel sandstone bodies seem to have a thickness relation with the related floodplain aggradation cycles between 0.88 and 1.30. Moreover, the use of the ratio between both (Z_{sst}/Z_{fac}) may hold predictive value for the subsurface low net-to-gross intervals as this could enable estimation of average sandstone body thickness (non-amalgamated) based on floodplain intervals. This ratio should be further studied to distinguish between basin margins and axes, and downstream or upstream-controlled systems.

In the Gilmore Hill area, the incision depth produces about 80% of the total thickness of the sandstone body indicating that the incision depth strongly controls sandstone body thickness. Incision depth could be less-well related to the floodplain sedimentary aggradation cycle thickness, although particularly when allogenically driven, the external driving mechanism fills the incisions and drives the system towards the overbank phase. Thus, the rate at which incision develops and the time available for incision could still be related to the thickness of the overbank-avulsion cyclicity if there is a time-control behind the cycles, such as precession forcing.

Stratigraphically, it is documented herein that the channel sandstone bodies are predominantly occurring with their tops and bases in the avulsion-belt deposits as part of the floodplain sedimentary aggradation cycles. Avulsion-belt deposits could improve vertical connectivity of channel sandstone bodies, and their continuous stratigraphic relation with channel sandstone bodies would improve sandstone body connectivity. The avulsion-belts of the Willwood Formation are typically aggradational, with distal, fine-grained crevasse splay deposits at their bases gradually coarsening upward towards proximal crevasse delta deposits, including crevasse channels (Davies-Vollum and Kraus, 2001). Most meter-scale avulsion-belt deposits range from silt to very fine sandstone at their bases towards very fine sandstone to coarse sandstone at their tops. Lateral variability is strong in the avulsion-belt deposits, with crevasse channels mostly not larger than 10-20 m in width (Davies-Vollum and Kraus, 2001) and crevasse deltas filling the available space on the floodplain. Crevasse splays, however, can be continuously traced throughout the Gilmore Hill and Deer Creek outcrop models and display a consistency of up to 2 km (Fig. 5.4). Porosity and permeability ranges and distribution patterns have not been studied; however, it is expected that the connectivity of this pseudo-three-dimensional correlation would increase if a full three-dimensional volume is considered (Laure and Hovadik, 2006)

The predominantly fixed position of the sandstone bodies at the base of the floodplain aggradation cycles suggests the presence of a control that drives sandstone body position in the stratigraphy in a cyclic manner. Therefore, if floodplain cyclicity is detected, this can have a predictive value for preferred sandstone body occurrence. The occurrence of separate channel sandstone bodies in

stratigraphy with every floodplain aggradation cycle is expected to reduce channelised sandstone body connectivity. It creates a more bedded stratigraphy. This vertical spacing would produce less stochastic connectivity due to floodplain fines separating sandstone bodies. The fact that sandstone body connectedness may be improved by layer-cake, laterally continuous avulsion-belt deposits at their bases and tops, as discussed above, could work as a counterbalance against this.

5.5 Conclusions

Floodplain aggradation cycles in the Willwood Formation display systematic variations in aggradation rate and stability. These are expressed as stratigraphic variations of heterolithic deposits with weak pedogenesis (avulsion phase) and palaeosols with strong pedogenesis (overbank phase), and are documented to have an average thickness of ~7 m. The kilometre-scale lateral consistency and occurrence in multiple parts of the basin of the deposits suggest that periods of channel avulsion and stability could be present. Thirty-five channel sandstone bodies placed accurately in their encasing and adjacent floodplain stratigraphy at dm- to m-scale vertical resolution in two areas spaced 17 km apart. The stratigraphic initiation point of channel sandstone body incision lies in the middle or top of the avulsion-belt deposits within a floodplain aggradation cycle. Total incision depth from this stratigraphic point is on average 6.4 m or 80% of the total sandstone body thickness. One channel is documented to have an aggradational style and occurs in a more basin-central position. On average, the channel sandstone bodies are 0.9 to 1.3 times as thick as the related floodplain aggradation cycles. Furthermore, two channel sandstone bodies are documented that incise, fully fill, and incise again with only decimetres of floodplain stratigraphy separating the two incisions. This suggests that either incisions were relatively easy to produce, or there was more time available during the avulsion phase than previously assumed. Based on these observations, two depositional models are discussed for the deposition floodplain aggradation cycles and their relationship with channel sandstones. The first is a model driven by channel aggradation, superelevation and avulsion, and the second is a model which has phases of fluvial activity typified by channel incision and infill and phases of fluvial inactivity and channel stability during which overbank deposition occurred. In this study, it is envisaged that an allogenic driver controlled both models. Both models can, however, also be interpreted to be controlled by a combination of allogenic and autogenic factors. In the context of the Willwood Formation serving as an analogue for a subsurface low net-to-gross reservoir, the differentiation is assumed to have a negligible impact on reservoir assessment as the lateral continuity of the floodplain aggradation cycles is constant at a 2-5 kilometre scale for both cases. The examples in this study demonstrate that the resulting stratigraphy exhibits a preferential position of channelised sandstone bodies in the floodplain aggradation. Therefore, the detection of floodplain cyclicity can point to sandstone body cyclicity. Integrating such conceptual models and channel-floodplain stratigraphic relationship into subsurface reservoir characterisation can potentially improve the vertical probability estimation of channel sandstone occurrences at the scale of high-resolution (10 m) floodplain aggradation cycles.



6

Long-term alluvial changes driven by
orbital eccentricity in the lower Eocene
Bighorn Basin, Wyoming

Abstract

Over time, palaeoclimatic changes must have considerably impacted rivers and floodplains as discharge profiles, sediment load, and vegetation covers drastically changed. An astronomically modulated cyclic climate is thus expected to influence fluvial processes and the corresponding sedimentary records strongly. These changes are well-documented in the floodplain record of the Willwood Formation of early Eocene Bighorn Basin, Wyoming, USA, where floodplain cyclicity is expressed as an alternation of heterolithic deposits with weak pedogenesis and palaeosols with strong pedogenesis and is correlated to a precession-paced forcing. As rivers form the source of floodplain sedimentation, channelised sandstone deposits are also expected to respond to orbital forced climate variability. This chapter presents an analysis of the stratigraphic distribution of channelised sandstone bodies. The floodplain cyclicity's stable spatial consistency allows the generation of a stratigraphic framework upon which 86 channelised sandstone bodies were populated. The sandstone body distribution could be compared to an astronomical target curve using stable isotope records. This revealed that sandstone body planform style and floodplain character changed along with the 400 kyr long-eccentricity cycle. An eccentricity maximum is correlated to a period of sinuous-dominated river planform style where more distinct, well-developed red palaeosols developed. Conversely, an eccentricity minimum is correlated to a period of braided-dominated river planform style and less pronounced, grey to drab palaeosols, often intermingled with more sandy deposits. At the same time, braided and sinuous channel sandstone deposits occasionally occur in close stratigraphic proximity, suggesting that river planform styles also change at shorter periods or that the system had intrinsic planform changes in proximal to distal space in one moment in time. This chapter shows that the link between orbital eccentricity climate forcing, river planform styles and floodplain character can provide a strong instrument for future alluvial stratigraphic analyses. This suggests that similar patterns can be found in subsurface reservoirs where orbital forced changes in river planform style can influence channel geometry, connectivity, and lithological heterogeneity.

Written by: Baars, T.F., Wang, Y, Martinius, A.W., Abels, H.A.

Author contributions can be found on page 187.

6.1 Introduction

Alluvial stratigraphy carries informative signatures of basin-wide allogenic signals (e.g. climate, tectonics, and eustasy) and autogenic processes that are intrinsic to the sedimentary environment (Blum and Törnqvist, 2000; Romans et al., 2016; Hajek and Straub, 2017). Autogenic processes in alluvial systems can act completely independent of external change and may react to seemingly minor events such as ice rafting and tree stump blockage of river channels, triggering channel bifurcation and avulsion (e.g. Gibling et al., 2010). At the same time, these processes may also strongly react to external influences, such as variations in sediment load or water discharge, fluctuations of base-level, or changes in vegetation cover and bank cohesiveness (Gibling and Davies, 2012). These responses are well-documented for extreme climate events, such as the Paleocene-Eocene Thermal Maximum (PETM) and Permian-Triassic extinction event (e.g. Arche and López-Gómez, 2005; Foreman, 2014; Colombero et al., 2017). However, it is less understood if alluvial stratigraphy can record allogenic signals of lesser extreme climatic events, such as orbital forced climatic variability.

Orbital climate forcing has been demonstrated extensively in the relative continuous marine and lacustrine sedimentary archives (Zachos et al., 2001; Machlus et al., 2008; Nie et al., 2017), yet the alluvial realm is subject to fragmentary sedimentation and stratigraphic incompleteness (Fielding and Webb, 1996; Hilgen et al., 2015). Depending on signal robustness, it is theorised that orbital forced cyclic patterns could potentially be preserved in the stratigraphic record (Wang et al., 2022). For base-level driven systems, fluvial cyclicity is documented and used to describe changes in channelised sandstone body architecture (Atchley et al., 2004; Hampson et al., 2013), and in upstream settings, without a dominant base-level component, similar suggestions are made (Jirásek et al., 2018; Noorbergen et al., 2020; Opluštil et al., 2022; Sharma et al., 2023).

The recently reported floodplain cyclicity of the Willwood Formation in the Bighorn Basin, Wyoming, USA, provides an opportunity to further investigate the impact of orbital climate change on upstream-controlled alluvial stratigraphy (Kraus, 1987; Abels et al., 2013; van der Meulen et al., 2020). Here floodplain cyclicity is expressed as an alternation of heterolithic deposits with weak pedogenesis and palaeosols with strong pedogenesis. These cycles are related to variability in aggradation rate induced by an allogenic, precession-paced forcing mechanism (Kraus and Aslan, 1993; Abul Aziz et al., 2008; Abels et al., 2013; For more information about the Willwood Formation and the geological setting, see Chapter 2). Based on detailed mapping and characterisation of palaeosols in digital outcrop models, insights are gained into the floodplain aggradation cycles' spatial consistency and variability (Chapter 3) and depositional models are proposed for the interaction and relationship between the floodplain and channelised sandstone bodies on the precession scale (Chapter 5).

Furthermore, previous study on outcrop and digital outcrop identified two dominant end-member planform styles in channelised sandstone bodies: sinuous-like and braided-like (Chapter 4; Wang et al., 2022). It remains unknown how these two planform styles are positioned in stratigraphy and how they impact large-scale (100-200 m) alluvial architecture. Several authors suggest that orbital forcing of eccentricity can significantly impact the alluvial architecture on a large scale (e.g. Smith et al., 2014; Valero et al., 2020; Sharma et al., 2023), and given the proposed precession control on floodplain deposition such patterns are also expected to occur in the Bighorn Basin. If so, the repetitiveness of orbital forcing would allow a better assessment of alluvial architecture as regularity and predictability of sandstone bodies could be considered. Such recognition could significantly impact subsurface reservoir characterisation as variability in architectural elements implies different properties and

geometries.

This chapter investigates the stratigraphic distribution of channelised sandstone bodies in the Willwood Formation. To do so, the Deer Creek area of the McCullough Peaks is studied (see Chapter 2: Fig. 2.2). Floodplain aggradation cycles are used to create a stratigraphic framework upon which sandstone bodies are populated and compared to an astronomical target curve. At the same time, other methods for stratigraphic visualisation of the digital outcrop model and sandstones are explored. Based on the framework, the vertical variability in river planform style and floodplain characteristics are analysed and compared to an astronomical target curve, and the impact of eccentricity forcing on alluvial architecture is discussed.

6.2 Methods

6.2.1 Floodplain stratigraphic framework

A floodplain-based stratigraphic framework was constructed using the laterally continuous floodplain aggradation cycles. Forty-four floodplain aggradation cycles were previously traced (Chapter 3) in a UAV-based digital outcrop model (for more information about the model, see Chapter 2). The model covers an area of approximately 10 km² and a stratigraphic interval of approximately 300 m. The framework was placed on a two-dimensional plane with a north-south orientation. A composite stratigraphic thickness for the interval was calculated by taking the average thickness of the floodplain aggradation cycle (7 m; Abels et al., 2013; Chapters 3 and 5) and multiplying this by the total amount of floodplain aggradation cycles.

6.2.2 Palaeosol intensity

The redness colour record (also known as a*) was used to illustrate the intensity of the palaeosols in the floodplain aggradation cycles. The colour record can be seen as a proxy for soil development because lesser-developed pedogenic, sandy intervals are relatively light, while palaeosols-rich, well-developed intervals are dominantly red. Better-defined floodplain aggradation cycles are expressed by more distinct and intense red and purple colours (Abels et al., 2013). This results in a higher score on the redness colour record for strong red palaeosols. However, purple palaeosols score low in the redness record.

The colour reflectance record produced by Abels et al. (2013, 2016) was used. This record was taken from one-dimensional trench data in the same study area and was measured at 10 cm vertical resolution using a portable photospectrometer (Minolta CM 508i, Minolta Co. Ltd., Japan). Values from the record range between -2 and 13 and an arbitrary cut-off value of 7.5 was applied to the colour record (Fig. 6.1). Values above this threshold were defined as intense red.

6.2.3 Sandstone body integration

Channelised sandstone bodies have previously been described and classified in the study area (Chapter 4). The two planform styles have been identified in the digital outcrop model and were populated in the floodplain-based stratigraphic framework. The stratigraphic positioning of the sandstone bodies was defined at two subsequent floodplain aggradation cycles, as it was not always possible to correlate the body to a single floodplain aggradation cycle. A third group of channelised sandstone bodies with a planform style of large-scale trunk channels was excluded from the analysis, as only five were identified.

Sandstone bodies' apparent width was measured in the digital outcrop model and corrected to true width using the regionally averaged palaeoflow direction of N 004° (Chapter 4). In the framework, the width and thickness of the sandstone bodies were proportionally scaled to their dimensions. It is important to note that channel architecture may not be fully exposed or preserved, and individual channels may exhibit different flow directions than the average, introducing uncertainties.

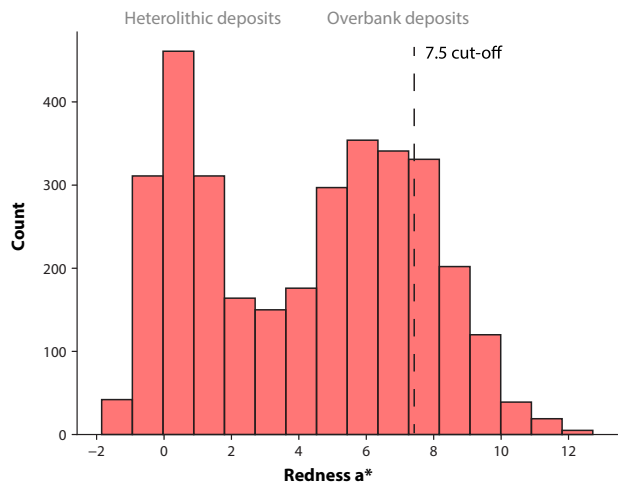
6.2.4 Correlation with astronomical curve

To compare observations with an astronomical solution, the populated floodplain-based stratigraphic framework was aligned with carbon isotope records from the same study area and stratigraphic interval (Abels et al. 2012, 2016). Next, the Willwood Formation stable isotope record and floodplain aggradation cycles were correlated to the marine realm using the stable isotope record of ocean drilling project site 1262 (Zachos et al., 2010). This correlation was done using two hyperthermal events as tie points (ETM2 and H2; Abels et al., 2012, 2016) and was linearly stretched to match the count of floodplain aggradation cycles with the age of the marine record. The assumption was made that a floodplain aggradation cycle represents a period of 21 kyr (Abels et al., 2013), and that there was average constant basin subsidence (Secord et al., 2006; Clyde et al., 2007; Foreman, 2014). Subsequently, the framework was aligned with a normalised eccentricity curve based on ocean drilling project site 1262 (Zeebe and Lourens, 2019).

6.2.5 Two-dimensional digital model view

The digital outcrop model was used to generate two-dimensional sliced views of the sandstone distribution and estimate net-to-gross levels. The model's XY plane was rotated to the regionally averaged palaeoflow direction of 004°, whereafter it was sliced in 250 m segments parallel with and perpendicular to the average palaeoflow (Fig. 6.3f). The segments were projected on a two-dimensional plane (XZ or YZ axis), showing the segment's maximum outcrop outline and positions of the channelised sandstone bodies. No floodplain aggradation cycles were used in this approach, and the Z axis is shown in meters above sea level. A crude net-to-gross estimate was made by calculating the percentage of outcrop covered by channelised sandstone bodies.

FIGURE 6.1. A histogram showing the distribution of the redness colour reflectance record of the Deer Creek area. A bi-modal distribution can be observed where the lesser red values (left) correspond to floodplain heterolithic deposits, and the stronger red values (right) correspond to palaeosols. The increase in redness corresponds with the level of pedogenic development, and an arbitrary cut-off of 7.5 is used to identify well-developed palaeosols.



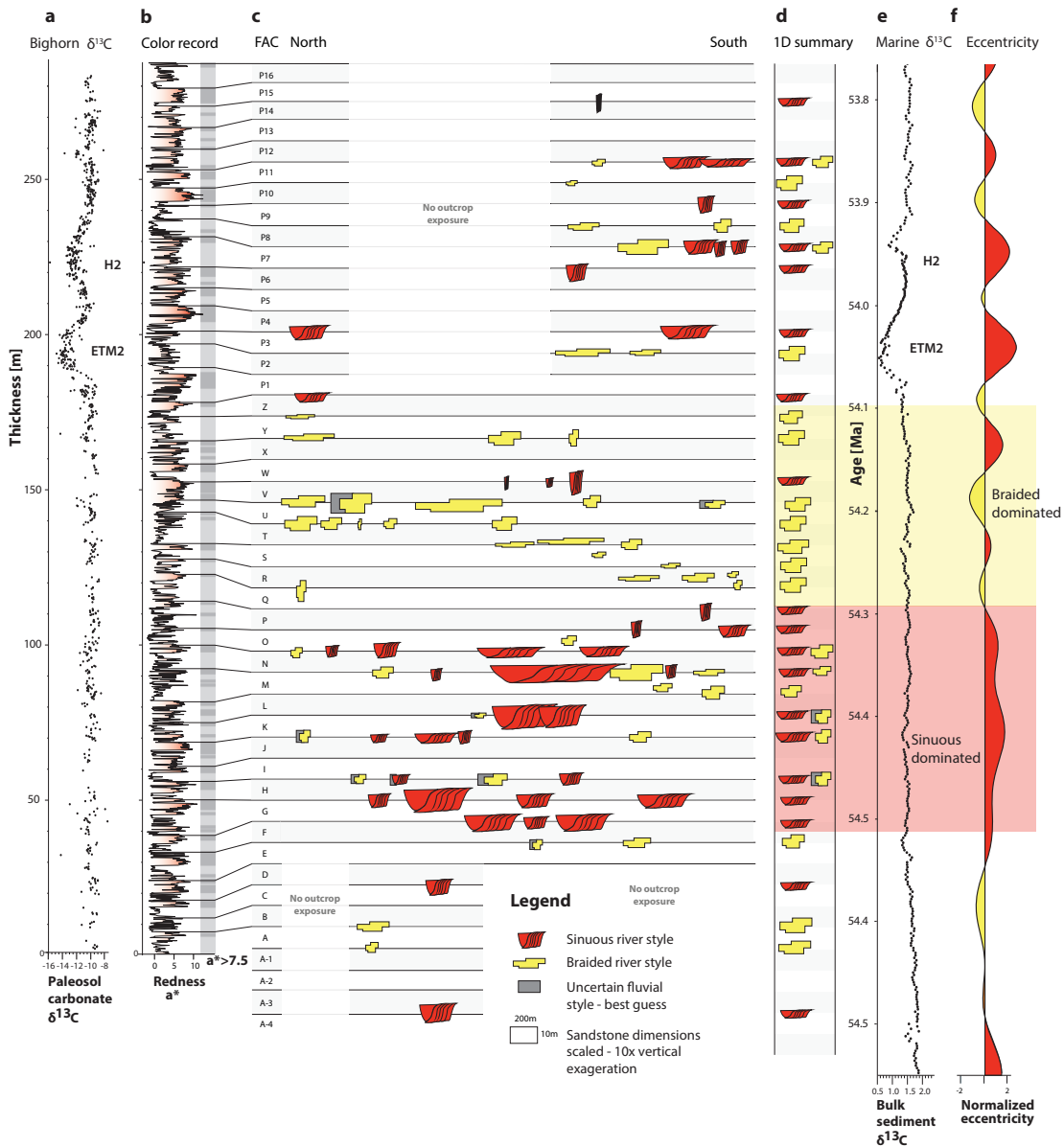


FIGURE 6.2 Stratigraphic occurrences of channel sandstone bodies in the lower Eocene Willwood Formation. a) the Bighorn Basin stable carbon isotope record with the hyperthermal events ETM2 and H2 from Abels *et al.* (2016). b) The redness colour reflector record (left; Abels *et al.*, 2013, 2016), and a cut-off end-member column with values above 7.5 in dark grey and below in light grey (right). c) Channelised sandstone bodies identified in the digital outcrop model positioned in a floodplain-based framework. The interpreted planform rivers are differentiated by colour, and the sandstones are proportionally scaled to thickness and width. d) A summary of interpreted planform river styles for each floodplain aggradation cycle. e) the stable carbon isotope stratigraphy at ODP site 1262 by Zachos *et al.* (2010) correlated using the ETM2 and H2 hyperthermal events. f) The normalised eccentricity target curve based on ODP site 1262 from Zeebe & Lourens (2019).

6.3 Results

6.3.1 Stratigraphic trends

A total of 86 sandstone bodies were populated in the floodplain-based stratigraphic framework (Fig. 6.2), of which 50 are classified as braided and 36 as sinuous. Both planform styles occur continuously throughout the stratigraphy. The planform styles occasionally coexist at similar stratigraphic positions at a scale of two floodplain aggradation cycles. This can also be seen in the two-dimensional slices of the digital outcrop model, where they occur relatively close to each other (for example, Fig. 6.3a, 1550 m). Vertical clustering is recognised on a larger scale, with two intervals dominated by either a braided or a sinuous planform style.

The first interval spans eleven floodplain aggradation cycles (cycles C to P) and covers 98 m of composite stratigraphic thickness. Twenty-five sinuous bodies (on average, 323 m wide, 9.3 m thick) and thirteen smaller, braided channel bodies (on average, 230 m wide and 5.9 m thick) were documented here. This interval is also observed in the two-dimensional sliced model (Fig. 6.3c and d, 1575- 1475 m). Based on the visual interpretation of the digital outcrop model, floodplain aggradation cycles in this interval have pronounced red, red-purple, and purple, well-developed palaeosols (cycles D to L). This is also seen in the colour reflectance record, where intense red values comprise 16% of the thickness over this interval.

The second interval spans ten floodplain aggradation cycles (cycle Q to Z) and is 70 m thick. Here, twenty-three braided channel sandstone bodies (on average, 230 m wide, 5.9 m thick) dominate over three small sinuous bodies (on average, 62 m wide, 7.2 m thick). This interval is also observed in the two-dimensional sliced model (Fig. 6.3d and e, 1575-1650 m). Floodplain aggradation cycles in this interval have less pronounced, grey to drab palaeosols, often intermingled with more sandy deposits (Cycles Q to U). In the colour reflectance record, this is documented by a lower percentage of intense red colours, as 12% of the interval comprises of intense red colours. The sand-rich and less pronounced palaeosols also make the floodplain aggradation cycles more challenging to trace laterally.

Below these two intervals, outcropping sandstones are limited (cycle D to A-4), and no trends are observed. Above the intervals, a mix of both planform styles was documented, with eleven sinuous-style sandstone bodies and seven braided-style sandstone bodies.

The populated floodplain-based stratigraphic framework was compared with the marine astronomical target curve (Fig. 6.2). This comparison reveals that the sinuous-dominated interval coincides approximately with a maximum of the 400 kyr long-eccentricity cycle. In contrast, the braided-dominated interval coincides approximately with a long-eccentricity minimum. At the 100 kyr short-eccentricity scale, comparing sandstone bodies of different fluvial styles shows no correlation.

6.4 Discussion

6.4.1 Uncertainty in classification and floodplain-based framework

The floodplain-based stratigraphic framework allows for a relatively high resolution (± 7 m) stratigraphic zonation. However, there are still uncertainties accompanying the framework and sandstone integration. Sandstone bodies are positioned between two subsequent floodplain aggradation cycles as it is not always certain where to stratigraphically place the sandstone bodies with respect to the floodplain aggradation cycles. This positioning is due to unclear channel-floodplain contacts obscured by recent debris, vegetation, and insufficient model resolution. For a more accurate

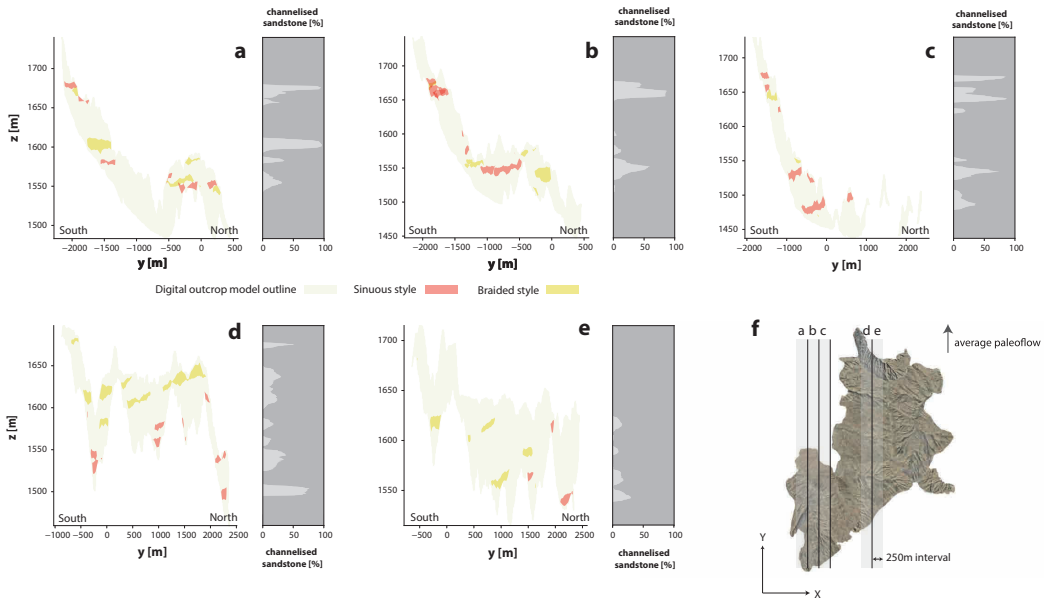


FIGURE 6.3 Two-dimensional slices of the digital outcrop model along average palaeoflow. a-e) The outcrop outline and sandstone bodies with differentiation between interpreted planform style by colour. On the left, estimated net-to-gross levels are shown. f) a map view of the digital outcrop model and the corresponding location for each section.

population, similarly detailed work would be needed as for the 35 sandstone bodies examined in Chapter 5. However, not all sandstone bodies show the quality of channel margins needed to successfully execute such an exercise. Additionally, the correlation framework might have under- or overestimated the number of individual floodplain aggradation cycles, as in some panel sections and intervals, they can be challenging to identify (for example, the sandy, less pronounced cycles Q to U).

These uncertainties result in a stratigraphic resolution of two to three floodplain aggradation cycles or 14-21 meters. If assumed that the floodplain aggradation cycles are precession-paced, short-eccentricity would be expected on a 35 m scale (5:1 ratio) and long-eccentricity at 140 m (20:1 ratio). Therefore, the floodplain-based framework is robust enough to detect trends at the long-eccentricity scale. At the 100 kyr short-eccentricity scale, comparing sandstone bodies of different fluvial styles is at a thickness range near the resolution of the stratigraphic framework and more difficult; consequently no correlation is found.

Furthermore, an end-member model was used to simplify the classification of the sandstone bodies. Identification of sandstone body classes in the digital outcrop model may not always be accurate due to the model's resolution. It is also recognised that the study area may host both sinuous and braided planforms in the same sedimentary units, as evidenced by their coexistence in certain intervals. Additionally, transitional planform styles may occur (Church and Ryder, 1972; Parker et al., 1976). Nevertheless, the two identified intervals have an abundance in the dominant planform style (sinuous-dominated: n=23 vs 3, braided-dominated: n=25 vs 11). Consequently, uncertainty regarding misidentification based on digital outcrop data or transitional planform styles are deemed minor.

6.4.2 Impact of eccentricity river style

An acceptable correlation between dominant river styles and long-eccentricity is found, which makes it tempting to consider the role of eccentricity in controlling river styles in the early Eocene Bighorn Basin. Tectonics or eustatic variations could also be possible explanations for these changes. However, constant basin subsidence is assumed (Secord et al., 2006; Clyde et al., 2007; Foreman, 2014), and tectonics tend to act on a scale of millions of years (e.g. Allen, 2008, Clift and Jonell, 2021). Furthermore, tends the impact of tectonic forcing to be attenuated during sediment transport as it primarily affects sediment supply and not precipitation (Simpson and Castelltort, 2012). Furthermore, eustatic variations are unlikely to have significantly impacted the Willwood Formation because the basin was geographically separated and far away from the palaeo-shoreline (Foreman, 2014).

Short- and long-eccentricity are documented to have a strong imprint on the Cenozoic climate (e.g. Westerhold et al., 2011). While the orbital forcing has a minor effect on the total annual insolation (Laskar et al., 2011), eccentricity forcing dominantly acts on climate systems as an amplitude modulator of precession. This modulation results in greater and lesser seasonal contrasts during eccentricity maxima and minima, respectively (Hilgen et al., 2015), and variability in the basin and catchment expressed in discharge and/or sedimented load can be expected to change (e.g. Tuenter et al., 2007; Smith et al., 2014). In this way, the scattered occurrence of braided channels in the sinuous-dominated interval might be related to a flashy discharge pattern during times of high seasonal contrast (eccentricity maxima), while the braided-dominated interval might be related to continuous high discharge conditions during periods with low seasonal contrast (eccentricity minima, Fielding et al., 2018; Manna et al., 2021). However, eccentricity may also control climates more remotely or globally, and climatic teleconnections can also change local climate via changes in vegetation for example (e.g. Lawrence et al., 2003). Vegetation may play an important role in determining sediment availability in the catchment and bank erodibility in the basin, and cause planform style changes (Vandenberghe et al., 1995, 2003; Tal and Paolo, 2010).

In the context of this research, no sufficiently convincing data has been collected to relate the observed changes to either local or global processes, also because the phase relationship between insolation variation and terrestrial palaeoclimate remains enigmatic. At this moment, the only observation that can be made is that a sinuous-dominated interval occurs during a long-eccentricity maximum and a braided-dominated interval during a long-eccentricity minimum, and how this observation fits with the proposed allogenic, precession-paced deposition of the floodplain aggradation cycles of in the Willwood Formation.

6.4.3 Impact of eccentricity floodplain style

Changes in the character of the floodplain record accompany the large-scale changes in planform style. The sinuous-dominated interval is characterised by pronounced, well-developed palaeosols and relatively more intense red colours, while less red-pronounced, sandier palaeosols characterise the braided-dominated interval. However, as noted before, the redness record is non-responsive to purple palaeosols, while these colours are attributed to well-developed palaeosols (Kraus, 1987; Kraus and Aslan, 1993). Further examination of the digital outcrop model shows that the purple palaeosols occur less frequently during the braided-dominant interval than during the sinuous-dominated interval. Therefore, if purple colours are considered, the difference in palaeosol expression would increase further during the two intervals.

Generally, these well-developed palaeosols can be linked to increased seasonality in the Bighorn Basin (Kraus et al., 2002; Abels et al., 2013), and this fits with the observation that well-developed palaeosols occur during the eccentricity maximum, providing an additional indication of orbital forced climate change on a long-eccentricity pace. Furthermore, similar observations are made by Abels et al. (2013), who suggested that the 100 kyr short-eccentricity curve expression is depicted in more distinct cycles with red and purple colours occurring in groups of three or four cycles.

6.4.4 Hyperthermal events

One would expect that the hyperthermal events, ETM2 and H2, had a considerable impact on fluvial style as these extreme climatic events are shown to have a significant impact on the faunal life in the Bighorn Basin (D'Ambrosio et al., 2017). Furthermore, the more substantial PETM hyperthermal event is associated with a change in fluvial style in several other basins (Foreman, 2011; 2014; Colombera et al., 2017; Barefoot et al., 2022). However, in this chapter, no straightforward linear response to either of the hyperthermal events is identified, as a mix of sinuous and braided channel styles is documented (Fig. 6.2). In contrast, a more linear relationship is found outside these events. Chapter 5 documents a similar mix of planform styles in the Gillmore Hill area, which also covers the ETM2 and H2 events. The ETM2 and H2 do not seem to behave like less intense versions of the PETM event; the latter is typified by the presence of a thick, amalgamated braided-like sandstone body in the Willwood Formation (Foreman et al., 2014). Potentially, the scale of the events was not large enough to cross a threshold for such a drastic change in depositional style.

Impact on alluvial architecture and subsurface characterisation

The controlling effect of orbital eccentricity on river planform style could be applied to improve and predict reservoir distribution in the subsurface. Intervals of different connectivity, lithologic heterogeneity, and net-to-gross levels may be pinpointed this way, and different near-field exploration and exploitation strategies could be used for the different intervals.

Using the Willwood Formation as a reservoir analogue, the observed changes in fluvial style from a dominant sinuous to a dominant braided style imply a change in the properties of sandstone bodies. The sinuous-like bodies have a larger degree of internal heterogeneity such as frequently occurring fine-grained lateral accretions surfaces as well as clay plugs (Chapter 4, Wang et al., 2022). In braided-like channels, the degree of internal heterogeneity is smaller, and the higher flow energies associated with these channel styles cause an overall coarser preserved grain size range (Chapter 4, Wang et al., 2022). These differences could potentially have an increased effect on the porosity and permeability of the braided-like sandstones compared to their sinuous counterparts (e.g. Jordan et al., 1992; Donselaar et al., 2017). The spatial distribution of the sinuous sandstones is often more isolated and variable, while the lower sinuosity braided sandstone bodies tend to be laterally more continuous and potentially traceable with less uncertainty if the assumption is made that average palaeoflow as a good measure for channel direction.

The coinciding change of floodplain characteristics with the change in sandstone body architecture may from an important marker for identifying such change in the subsurface. Especially in, low net-to-gross systems, typified by the presence of abundant floodplain sediments, variability in floodplain characteristic on a larger-scale (100-200 m) could indicate for orbital forcing on floodplain and sandstone architecture. However, identifying the key floodplain indicators that can support the argument for correlation and identification of a change in fluvial style and associated sediment properties is not straightforward. Such observations need to be accompanied by observation related

to the sandstone bodies themselves and their distribution pattern in the floodplain-based stratigraphic framework.

6.4.5 Digital model-based sandstone body distribution

The two-dimensional segments of the digital outcrop model form an alternative approach to analyse the stratigraphic sandstone distribution of the Willwood Formation. Similar patterns are found compared to the floodplain-based stratigraphic framework which show that the two documented intervals are present independent from the floodplain-based alignment. Based on the two-dimensional segments, there are no significant net-to-gross differences between the two planform styles (Fig. 6.3). However, this exercise is still a first effort, and uncertainties accompany the method. Only channelised sandstone bodies are used to calculate the net-to-gross ratios. Crevasse splays and other non-channelised sandstones are not incorporated while they form a significant part of the deposits. The question remains how these deposits influence the connectivity, but this has not been a topic for this chapter. The effort presented here shows the potential to achieve a more detailed characterisation of channel distribution in a pseudo-three-dimensional space and that spatial information on large-scale sandstone body architecture can relatively easily be collected. However, to fully achieve the potential, more research is needed.

6.5 Conclusion

This chapter used continuous lateral traceability of floodplain aggradation cycles in the Willwood Formation in the Bighorn Basin, Wyoming, USA, to create a stratigraphic framework in which sandstone bodies could be populated. The relatively minor thickness of 7 m of the floodplain aggradation cycles allowed for a high-resolution stratigraphic zonation over 300 m and 44 floodplain aggradation cycles in a digital outcrop model. Sandstone bodies show a continuous occurrence of two planform styles used to simplify natural variability, sinuous-like and braided-like, throughout stratigraphy. The planform styles coexist at similar stratigraphic positions at a scale of two floodplain aggradation cycles. However, on the longer term (approximately 80 m), an interval dominated by sinuous channel sandstone bodies and an interval dominated by braided channel sandstone bodies occurs. Independent of the floodplain framework, two-dimensional snapshots of stratigraphy display the same intervals of dominant styles. Additionally, the floodplain record during these intervals changes with intensity in redness of palaeosols increasing in the sinuous-dominated interval. Alignment with the marine realm via the stable isotope record allowed for comparison with a target eccentricity curve, revealing that both intervals coincide with long-term eccentricity pacing. This observation further strengthens the idea that the early Eocene alluvial system of the Willwood Formation was influenced by orbital climate change. However, the exact forcing and causal relationship between the forcing and change in planform style remains enigmatic. Nonetheless, it is theorised that such changes could significantly impact sandstone body style and distribution, and it is likely that orbital signals can also be found in other alluvial systems. Extrapolation of the observations to the subsurface can help improve the characterisation of alluvial architecture and help identify intervals with different sandstone body geometry, connectivity, and lithological heterogeneity.



7

A cyclostratigraphic framework of the Upper Carboniferous Westoe and Cleaver formations in the southern North Sea Basin as a methodology for stratigraphic reservoir characterisation

Abstract

Orbital driven climate control on sedimentation produces regional, stratigraphically repetitive characters and so cyclostratigraphic correlation can improve correlation and identify stratigraphic trends in borehole sections. This concept is commonly used to correlate marine and lacustrine strata. However, in the alluvial domain, its use is more challenging because internal, local dynamics controlling sedimentation may interfere with the expression of cyclic climate forcing. Intervals of low net-to-gross may be important for successful application in this domain as they tend to better document regional changes. This chapter applies climate-based stratigraphic correlation concepts to improve well correlations, characterise vertical sand distribution, and identify potential reservoir targets in a generally low net-to-gross interval. Coarsening upward sedimentary repetitions (cyclothems) are identified and correlated with high certainty in nineteen well sections in the upper Carboniferous Westoe and Cleaver formations of the Silverpit Basin. Local sedimentary dynamics provide variability in the character of the cyclothems and several types of cyclothem are classified. Correlation of sections using cyclothems recognised on wireline logs is done twice: once manually and once semi-automatically. The semi-automated correlation is based on calculation of deviation curves which depict stratigraphic changes that are less dependent on absolute wireline values and follow vertical trends more clearly. The correlations provide composite stratigraphies that are analysed using vertical proportions curves. Both approaches yield similar results in terms of stratigraphic trends. However, for detailed correlation of wells, the manual correlation is better at accounting for any local variability within the system. The same two zones of higher net-to-gross ratios are found using both correlation methods. These are linked to palaeoclimatic changes driven by long eccentricity and the proposed climate stratigraphic model has predictive value for identifying sandstone occurrence. The climate-based stratigraphic correlation improves the assessment of reservoir distribution and properties on small (10-20 m thickness) and large (100-200 m thickness) stratigraphical scales.

Chapter 7 is based upon: Baars, T.F., Huis in 't Veld, R., Zhang, L., Koopmans, M., McLean, D., Martinius, A.W., Abels, H.A., 2023, A cyclostratigraphic framework of the Upper Carboniferous Westoe and Cleaver formations in the southern North Sea Basin as a methodology for stratigraphic reservoir characterization, *Netherlands Journal of Geosciences*, 102, p. e9. <https://doi:10.1017/njg.2023.8>. Author contributions can be found on page 187.

7.1 Introduction

Stratigraphic correlation and prediction of subsurface reservoirs in low net-to-gross fluvial deposits is challenging, particularly when limited data are available to produce stratigraphic models. Such sedimentary systems are often characterised by extensive floodplains with localised, major and minor channels. Numerous studies have focused on characterising and predicting such reservoir architecture via the characterisation and correlation of sandstones (e.g. Bridge et al., 2000; Törnqvist and Bridge, 2002; Sahoo et al., 2020). However, the formation of channel belts is typified by internally-driven, "autogenic" processes, such as channel avulsion, crevasse splaying, and channel migration (e.g. Beerbower, 1964; Smith et al., 1989; Stouthamer and Berendsen; 2007). These processes lead to lithological heterogeneity and poor three-dimensional sandstone connectivity. The correlation potential of sandstones is therefore relatively low using only wireline data.

True overbank deposits tend to include regionally consistent characters. Continuous floodplain surfaces related to palaeosols or coals seams can be used to subdivide and correlate stratigraphy. These deposits better record external, "allogenic" processes such as tectonics or base-level and climate changes related to orbital cycles (Davydov et al., 2010; Jirásek et al., 2018; Noorbergen et al., 2018; Opluštil et al., 2019). Orbital forcing results in consistent vertical spacing of features and provides a tool for cyclostratigraphic correlation (e.g. De Jong et al., 2007; 2020; Nio et al., 2014). However, although used for correlation, the underlying climatic forcing mechanism remains mostly unused in reservoir modelling. The repetitive patterns of orbital forcing may hold valuable predictive capabilities where trends are laterally consistent. Recognising orbital forced patterns and integrating underlying conceptual models in subsurface workflows could improve well-to-well correlations. It may also allow identification of channel sandstone-prone stratigraphic intervals at a resolution not available by other means.

A suitable target to elaborate the cyclostratigraphic methodology is the Euramerican Upper Carboniferous deltaic and fluvial systems. These are well known for their repetitive nature and lateral continuity of coal seams. The cyclic arrangement of these sediments was recognised in the early 19th century (Weller, 1930; Wanless and Weller, 1932) and referred to as "cyclothems". Cyclothems comprise an array of clastic, organic, and chemical/biochemical lithologies and are often interpreted the products of alternations between non-marine and marine depositional conditions. For a summary, see Fielding (2021). The concept of cyclothems has been applied to a broad range of sedimentary successions, including successions without marine strata. The most widely accepted forcing mechanism for cyclothems is base-level change via glacio-eustatic control (e.g. Ramsbottom, 1973; Hampson et al., 1999; Heckel, 2008; Gibling and Rygel, 2008; Fielding et al., 2020; Fielding, 2021). Glacio-eustasy is driven by (palaeo-)polar ice volume changes controlled by orbital forcing, and radioisotopic dating of several sequences of cyclothems confirms such a link to orbital forcing (e.g. Davydov et al., 2010; van der Belt et al., 2015). Besides base-level changes, upstream sediment fluxes, and variations in mid-stream water and vegetation levels have also been proposed as mechanisms for cyclothem formation (Jirásek et al., 2018; Opluštil et al., 2019, 2022).

Smith and Joeckel (2020) demonstrated the potential for improved reservoir characterisation with a stratigraphic framework based on cyclothem correlations. In this example, limestones alternate with mudstones following coastline movement and display little lateral variation in cycle character. In the more fluvial domain, cycle character is more variable. The autogenic dynamics of a fluvial system cause lateral variation on the floodplains and the characteristics of any one cyclothem can be laterally

divergent. The ability to recognise and decouple autogenic and allogenic imprints in cyclothems is essential in these systems.

The present chapter aims to evaluate the potential of climate stratigraphy for improved reservoir quality assessment in low net-to-gross deltaic to fluvial systems using cyclothems. To do so, the dominantly fluvial Westoe and Cleaver formations (Maurits Formation in the Dutch sector) in the Silverpit Basin (Southern North Sea) are chosen (Fig. 7.1). Cyclothems are well-documented here as sequences of claystone, mudstone, siltstone, sandstone, and coal arranged in vertically stacked packages with coarsening upwards trends (O'Mara and Turner, 1999; Fig. 7.4b). The thickness of these repetitions does not vary markedly across the floodplain, ranging up to 15 m (Quirk, 1993; O'Mara and Turner, 1999). They are interpreted as shallowing-upward successions starting with lake deposits overlain by crevasse splay and minor delta deposits, and eventually mire accumulations. A depositional mechanism related to base-level fluctuation is proposed where the lake deposits were gradually filled in response to an upwards decrease in accommodation space due to base-level fall. Subsequently, the infill was capped by the formation of mires which sustained until drowning by base-level rise (O'Mara and Turner, 1999).

Current correlation methods, such as bio-, chemo-, and (sandstone) litho-stratigraphy, provide stratigraphical resolution in the order of 50-100 m (Pearce et al., 2010). Cyclothems with a thickness of <15 m, could provide much higher resolution for correlations. In this chapter: (1) cyclothems are identified per well, and variations in character are documented; (2) Manual and semi-automated methods are used to construct stratigraphic correlations based on the cyclothems; (3) The resulting horizontal and vertical sedimentary facies patterns are analysed; (4) These are combined with an analysis of sandstone occurrence and sandbody thickness and style; (5) Climate models are fitted to averaged stratigraphic trends, to identify stratigraphic intervals of higher reservoir potential.

7.2 Geological setting

The Silverpit Basin is one of several coal-bearing Carboniferous basins located north of the foreland of the Variscan Orogeny (Leeder, 1988). It is primarily located in UK offshore Quadrants 44 and 49, partly in the Netherlands Blocks D, E and J, and lies along the proximal northern margin of the more extensive Pennine Basin. Carboniferous strata ranging from Tournaisian to Westphalian (and possibly younger) were deposited as the basin formed a major sediment fairway from the northeast towards the south-southwest (Besly 1988; Collinson et al., 1993; Cole et al., 2005). The primary sediment source was across the Mid North Sea High in the north, with occasional input from the Variscan Orogen to the southeast (Morton et al., 2001; Besly, 2005). The depocentre is likely positioned in the southern part of Quadrant 44 (O'Mara, 1995)

The Westoe and Cleaver formations are Duckmantian (Westphalian B) to early Bolsovian (Westphalian C). Most sediments in these formations were deposited on a low-relief alluvial plain setting with a distant coastline under a palaeoequatorial, perhumid palaeoclimate (O'Mara and Turner, 1999). The succession is predominantly terrestrial and consists of clastic deposits ranging from sandstones to mudstones and coals. Sediment supply was by fluvial channels and overbank deposits fed by crevasse splay or minor delta systems that entered numerous inter-channel freshwater lakes (Haszeldine, 1983; Fielding, 1984a, 1986; Guion and Fielding, 1988). The Westoe Formation is a shale-dominated succession with high organic content, abundant coal seams, limited sandstone occurrence, and very little marine influence. In the Cleaver Formation, coal occurrence slightly decreases, and

sandstones and marine intervals are more common. Marine intervals are represented by thin marine mudstones (“marine bands”) interpreted as representing glacio-eustatic flooding events in sequence stratigraphic models (Calver, 1968; O’Mara and Turner, 1997).

The study interval is bounded between two regionally extensive major packages of stacked fluvial sandstones (Cameron et al., 2005). The lowest part of the Westoe Formation at the base of the study interval is characterised by the stacked sandstones of the Caister-Murdoch system that overlies the Vanderbeckei Marine Band (MB). The top of the study interval is defined at the lower Ketch member of the Ketch Formation. The Aegiranum MB is located below the lower Ketch member. The major marine bands are interpreted as high-stand deposits. These are followed by concentrations of sandstones, which reflect periods of non-deposition and erosion succeeded by stacking fluvial system infills during low-stands (Huis in ’t Veld et al., 2020). The base of the Cleaver Formation is identified by the Maltby MB Onshore sections in the Pennine Basin contain several thin marine bands indicating small marine incursions throughout the equivalents of the Cleaver Formation (Calver, 1968). In the lower part of the Duckmantian the flooding surfaces are lacustrine rather than marine, as is evident from the fossil record (Trueman and Weir, 1946; Calver, 1956; Eager, 1956; O’Mara and Turner 1997). Several timescales estimates, varying between 1.2 and 2.5 Myr, can be used for the duration between the formation of the Vanderbeckei MB and the Aegiranum MB, (Davydov, 2004, Menning et al., 2006; Van der Belt et al., 2015; Opluštil et al., 2016).

McLean et al. (1995), Besly (2005), and Waters et al. (2011) consider there to be a disconformity at the base Ketch Formation. The stratigraphy thins to the northeast and thickens to the southwest due to a rapidly subsiding basin depocentre in the southwest (Huis in ’t Veld et al., 2020). This thinning trend, combined with increasing rates of incision of the Ketch Formation northwards, leads to a disconformity at the base of the Ketch, but this is supposed to be minimal in the study area. The constant thickness of the Westphalian interval and the absence of large incisions on seismic interpretations suggest that regional subsidence was relatively high and exceeded the stratigraphic base-level fall (Leeder, 1988; Turner, 1993). Additionally, the high correlatability of marine excursions over Europe (Dusar et al., 2000) suggests that tectonic activity had a low impact on stratigraphic variability.

7.3 Methods

7.3.1 Data and transect

Two transects have been made perpendicular to the southwest thickening trend. In Transect One, fourteen wells cover a maximal lateral distance of 57 km from west to east. Transect Two, 12 km to the northeast, consists of five anonymised wells and spans approximately 15 km. Standard wireline suites of gamma-ray, density, sonic, and neutron-porosity logs were used for analysis. All wireline logs were corrected for environmental borehole conditions. The wells were adjusted for borehole and structural deviation and displayed at true stratigraphic thickness. The base of the Variscan unconformity was used as a zero horizon for the stratigraphic thickness. Structural dip above the unconformity is assumed to be minimal, and the depth above the Variscan unconformity was added to the TST. Well 44/23-14 was capped at the highest matching biostratigraphic marker since seismic interpretations indicate a fault gap.

The study workflow is shown in Figure 7.2. Three different approaches for the correlation of wells were applied: manual, semi-automatic, and stratigraphic thickness. The specific methods used in this

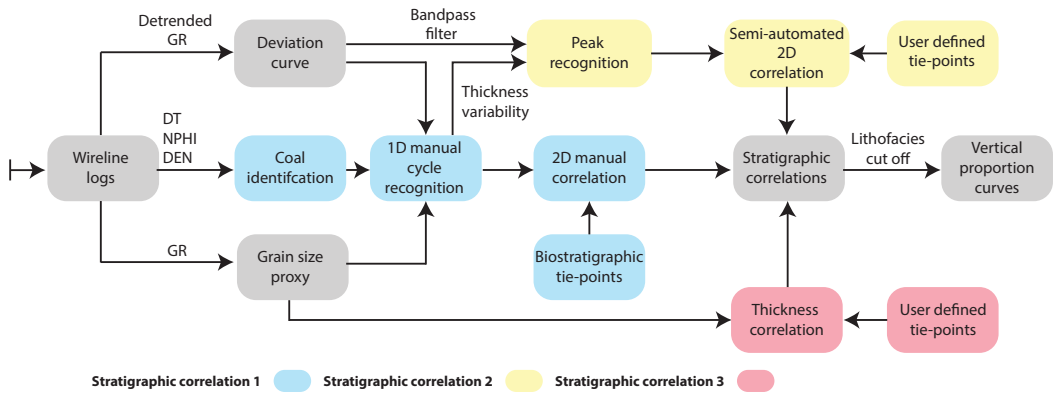


FIGURE 7.2 The workflow conducted in this study. Three different approaches to stratigraphic correlation are made: manual, semi-automatic, and stratigraphic thickness. The specific approaches are further explained in the text.

chapter are explained in the following paragraphs.

7.3.2 Existing stratigraphic markers

The transects are referenced to a well-established miospore biozonation for the area (McLean et al., 2005). Archive biostratigraphic control was available for six of the selected wells, and, for consistency, all biostratigraphic data used in this chapter were provided by one analyst (MB Stratigraphy Limited). Four biozones are defined within the study interval (W4a up to W5a; Fig. 7.1b). The biozones are defined, where possible, on the highest stratigraphical occurrences of zonal taxa (McLean et al., 2005). All samples are from ditch-cuttings material. Supplementary data S1 shows data for the wells with biostratigraphy, any uncertainty and comparison to the cyclostratigraphic framework.

Miospore species range limits are likely to be linked to palaeoclimatological changes such as marine incursions, and a close relationship between the biozonation and marine bands has been established (McLean et al., 2005). The Maltby MB and Aegiranum MB are related to the tops of the W4b and W5a biozones, respectively (Fig. 7.1b).

7.3.3 Integrated deviation curve

Because the lithological expression of a cyclothem can vary from place to place, identifying individual cyclothem was aided by applying a deviation filter (DC) to the gamma-ray logs (Nio et al., 2005). This method tracks spectral change and identifies “breakpoints” (i.e. points of change; Fig. 7.3). A similar approach has been successfully applied in the Southern North Sea for large-scale correlation of wells. (De Jong et al., 2006; 2020). For the calculation of the DC, an open-source Python script was used (Daely, 2019).

An L1 trend filter method (Kim et al., 2009) was used to remove large-scale trends and to amplify small-scale trends before applying the DC analysis. This method is a high-pass filter, filtering out the low-frequency components. The strength of the filter is controlled by a regularisation parameter that

balances the smoothness of the fit with the minimisation of smaller-scale variability between the actual signal and the smoothed series. A regularisation parameter of zero represents the original input signal, while the maximal regularisation parameter results in a linear signal. Twenty different filters were calculated with an exponentially increasing regularisation parameter between the maximal and minimal regularisation parameters. After calculating the L1-filters, the first twelve filtered high-frequency filters were combined, averaged, and subtracted from the original curve (Fig. 7.3b).

An autoregressive analysis in the form of a Maximum Entropy Analysis (MESA) was applied next (Burg, 1967). This fits an autoregressive model to the signal by using least squares method to minimise the forward and backward prediction errors based on a defined window length. In this chapter the window length was 7 m. The error of the predicted model compared to the detrended gamma-ray indicates the unpredictability of a signal. This error provides valuable information about the stratigraphic change of the record. Further integration of the curve is termed the deviation curve (DC), indicating the spectral trend attribute of the signal and identifying points of change. The DC was smoothed by a moving average (Savitzky–Golay filter, 6 m, 2nd polynomial; Savitzky and Golay, 1964).

7.3.4 Manual cycle identification

Gamma-ray logs are used as a substitute for grain size logs. Although grain size does not determine the natural gamma radiation, there is a dependency of mineral composition in grain size (i.e. Blatt et al., 1980; Martinius et al., 2002) which enables the recognition of coarsening- and fining-upwards trends. Coals can have similar low gamma-ray readings as sandstones, so the density curve was used for their identification. Coals generally have a significantly lower density and sonic travel time than other lithologies in the sections. A coal cut-off of $>2.00 \text{ g/cm}^3$ was used for most wells. Density readings were unavailable in wells 44/21-3 and 44/21-4. Here the neutron porosity ($> 0.45 \text{ m}^3/\text{m}^3$) and sonic ($> 80 \text{ } \mu\text{s}/\text{ft}$) readings were used, respectively.

A cyclothem boundary is defined at the base of a flooding surface. When coal is present, the boundary is placed at the top of the coal. However, cyclothem without coal development also occur. An approximated maximum geographical extent of 15-20 km was attributed to the coal seams which, due to palaeotopographic variations, are not expected to have developed consistently over the whole basin (Haszeldine, 1983; Fielding, 1984a). Therefore, a boundary was placed at the transition from coarse-grained to fine-grained material in cyclothem without coal development.

The DC was used for visual reference where cyclothem boundaries were difficult to identify. In addition, confidence levels were given to the interpretations. These are arbitrary scores of high, medium, and low based on the interpreter's confidence in identification. Cyclothem boundaries with an identifiable coal or a clear gamma-ray trend were classified as high confidence. Cyclothem boundaries without coal or with less well-defined gamma-ray profiles or low gamma-ray values were classified as medium to low certainty. This classification is displayed as solid and stippled lines in the wells (Fig. 7.7 and 7.8).

7.3.5 Manual well correlation

Biostratigraphy and characteristic lithological patterns provided initial correlation. This was followed by detailed correlations of individual cyclothem between wells. The initial biostratigraphy was not further used for correlation. The correlation exercise started at wells close to each other ($< 2 \text{ km}$).

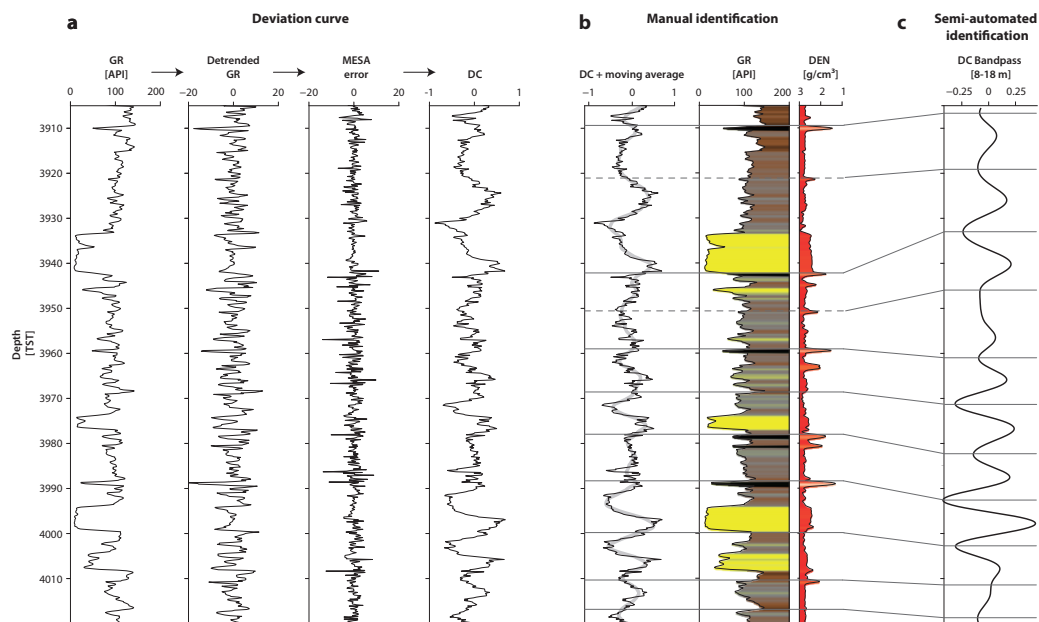


FIGURE 7.3 An example of the deviation curve methodology on the gamma-ray from well 44/22-8st. a) The construction of the deviation curve. From left to right: The input gamma-ray record. The stacked L1 trend filters amplify smaller-scale spectral change and remove large-scale trends of the gamma-ray. The error of the signal prediction by the Maximum Entropy Analysis (MESA). The integration of the Burg method's error shows the signal's spectral trend attribute and periods of change on the breakpoints of the curve and is called the deviation curve (DC). b) Manual identification of the cyclothem based on the gamma-ray and density record, combined with the visual aid of the deviation curve (moving average of the deviation curve is a Savitzky–Golay filter, 6 m, second polynomial). The colour fill of the gamma-ray is based on a continuous fill between 0 and 200 API values. Coals are coloured black and have a low API, like sandstone. Their identification is based on density values ($<2.00 \text{ g/cm}^3$). c) Semi-automated identification of cyclothem based on a gaussian bandpass filter (6-18 m) of the deviation curve. The peaks of the bandpass filter are used as cyclothem boundaries.

Information about any lateral variation in lithofacies was used as feedback for the correlation between wells that were further apart. The same certainty scoring was used for the correlation as for the cycle boundary identification. Here, the scoring was based on trends in multiple subsequent cyclothem. Similarity of patterns in the wells, such as the bundling of coal seams, allowed a high certainty of correlation. Otherwise medium to low confidence scores were given to the correlations.

As some correlated intervals lack confidence, it is unclear how the complete succession of cyclothem should be represented. For example, in places where a large, channelised deposit is present. Such gaps in correlation were accepted if both over- and underlying intervals could be correlated with medium to high confidence. In such poorly correlated intervals, the stratigraphic resolution was reduced, and low confidence correlation lines were excluded in subsequent analyses, as described below.

7.3.6 Semi-automatic identification and correlation

The correlation method described above is based on a manual interpretation and is subject to interpreter bias. Therefore, a second, semi-automated correlation effort was applied, matching the smoothed DCs of the wells. Using the cyclothem thickness range defined by the manual interpretation, a bandpass filter was used to filter and smooth the DCs. The peaks of the resulting filter were used for an automatic well-to-well correlation. Peaks were defined using the changes in amplitude of the smoothed DC. An initial calibration marker was chosen to align all wells. After alignment, the nearest peak to the calibration horizon was used as starting tie-point of the correlation, after which subsequent peaks in wells were matched.

7.3.7 Stratigraphic thickness correlation

A third correlation was constructed by aligning the wells based on their true stratigraphic thickness distance to a predefined calibration horizon. No other correlation markers were used. Here, the assumption was made that, over a thicker interval of stratigraphy, on average an equal thickness of strata represents an equal duration of deposition.

7.3.8 Compensational stacking

Compensational stacking is the tendency for sediment transport systems to preferentially fill topographic lows during deposition. This was estimated by calculating the coefficient of variation (Straub et al., 2009) over each well for an increasing cumulative. This was done based on the manual correlation and was calculated by:

$$CV = \frac{\sigma_c}{\mu_c}$$

σ_c is the standard deviation and μ_c the mean of the mean thickness over several consecutive cyclothem. Here the consecutive cyclothem range increases from one to the maximum continuously stacked number of cyclothem identified.

7.3.9 Average stratigraphic trends

If allogically forced then the correlated cyclothem boundaries represent coeval timelines. Given this, a composite stratigraphic thickness scale was constructed by calculating the mean thickness of each correlated cyclothem and adding the means cumulatively. All wells were placed on the new depth scale by linear interpolation between the correlated cyclothem boundaries. This was done for both the manual and the semi-automatic correlations.

Vertical proportion curves of lithotypes were created (e.g. Volpi et al., 1997) using the composite stratigraphic thickness scale. This allows for average stratigraphic trends to be interpreted. A simplified lithofacies model was used with differentiation between sandstone, coal, siltstone, and claystone. Coal content was estimated by the cut-off described above, while gamma-ray values were used to estimate sandstone (<60 API), siltstone (60-130 API) and claystone (>130 API) content. Lithofacies were calculated on wireline depth increments (15.24 cm), and the percentage of each facies was calculated on a 1 m interval for each well. Subsequently, the lithofacies percentages were averaged over all wells.

7.3.10 Base-level estimation

An index curve was made to classify environmental change and estimate the relative position of base-

level. This was done using lithofacies distribution of the constructed vertical proportions curve of the manual correlation. Each lithofacies curve was normalised. The sandstone and siltstone fractions were summed, as were the coal and claystone fractions. Subsequently, the grouped sandstone and siltstone fractions were subtracted from coal and claystone fractions. Bandpass filtering was performed on the index curve using the software package Acycle (Li et al., 2019). The assumption is that coal and claystone lithofacies correspond to mire, lacustrine or marine palaeoenvironments related to base-level highstands while sandstone and siltstone lithofacies correspond to floodplain palaeoenvironments related to base-level lowstands.

7.3.11 Sandstone characteristics and distribution

Sandstones which in part were below 60 API were measured for thickness, and categorised on shape based on the gamma-ray logs. A 3 m cut-off was used to exclude small, non-channelised (minor or single crevasse-splay deposits) sandstones. Three shape groups were recognised: coarsening-upward, fining-upward, and block pattern. Individual stories of channel bodies were measured where they could be identified.

7.4 Results

7.4.1 Cyclothem recognition and character

365 individual cyclothem were identified. 311 of these were given a certainty score of medium or high and are discussed below. Six cyclothem types were observed and defined (Fig. 7.4c, Table 7.1). The first (type C1) is a complete, “ideal” succession, coarsening upward from clay to sandstone with coal on top. Variations (types C2-C5) involve the absence or lesser development of a coal or sandstone parts. Most documented cyclothem have a coal seam but no pronounced sand deposit (types C2a-b). Cyclothem with a thin (<2 m) sandstone and no coal development (type C3) are also common, as are cyclothem without either a pronounced coal or a sandstone (C4). Cyclothem with a sandstone thicker than 2 m at their top are rare (type C5). Thick sandstones are more often found at the base of a cycle, directly overlying a coal seam (type C6).

Individual cyclothem thicknesses range from 3.7 m to 22.2 m (mean 11.0 m; median: 10.1 m; SD: 3.8 m; skewness: 0.75; Fig. 7.5a). There is no significant difference in thickness between most cycle types, other than those with sandstones at the base (type C6), which on average are thicker than the other types (t-test, $p < 0.01$). The vertical succession of cycle types changes quickly with no dominant successive pattern. The vertical variation in consecutive cycle thickness is reduced to 15% of the mean within five cycles (9.35 – 12.65 m; Fig. 7.5c). Cycles in the wells of Transect Two to the northeast are thinner (mean 8.9 m) than those of Transect One to the south and southwest (mean 11.2 m; Fig. 7.5b).

7.4.2 Sandstone character

A total of 99 sandstones have been documented in this chapters (Fig. 7.6a). Most have a blocky pattern ($n=61$) with fewer coarsening- and fining-upward sandstones ($n=23$ and $n=15$, respectively). Blocky pattern sandstones can occur as stacked units of up to four storeys, reaching a cumulative thickness of up to 30 m. They show a bimodal thickness distribution (Fig. 7.6b) with often single-story, isolated sandstones with a range of 3-6 m and stacked sandstones ranging from 8-12 m. The latter often have subtly serrated gamma-ray profiles, while the thinner blocky-pattern sandstones are described as

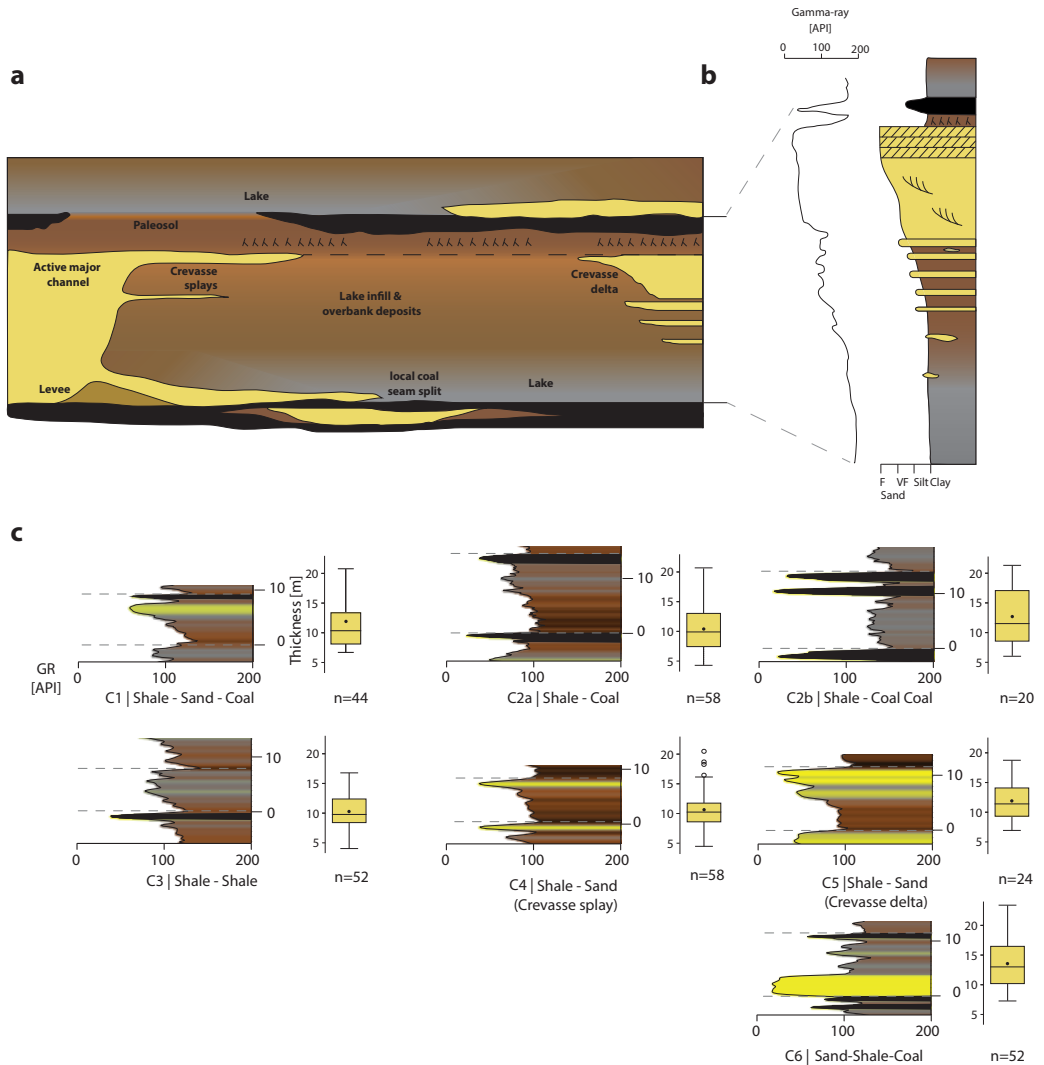


FIGURE 7.4 Cyclothems for the Southern North Sea Westphalian. a) A schematic drawing of facies recognised in the cyclothems with lateral differences illustrated. b) An idealised succession showing a gradual coarsening-upwards and then rapid fining-upward package moving from fine lake deposits followed by crevasse splay or crevasse delta progradation and subsequently floodplain deposits that are often organic-rich. The rapid upwards fining represents the drowning of the delta top by lake deposits under relative base-level rise (after O'Mara and Turner, 1999). c) Different types of cyclothems defined in this study and their corresponding thicknesses. Type C1 is defined as the ideal cyclothem. Note how a component is absent in each other type defined—for example, the coal in types C3, C4, and C5. See Fig. 7.3 for the key to the colour fill of the gamma-ray.

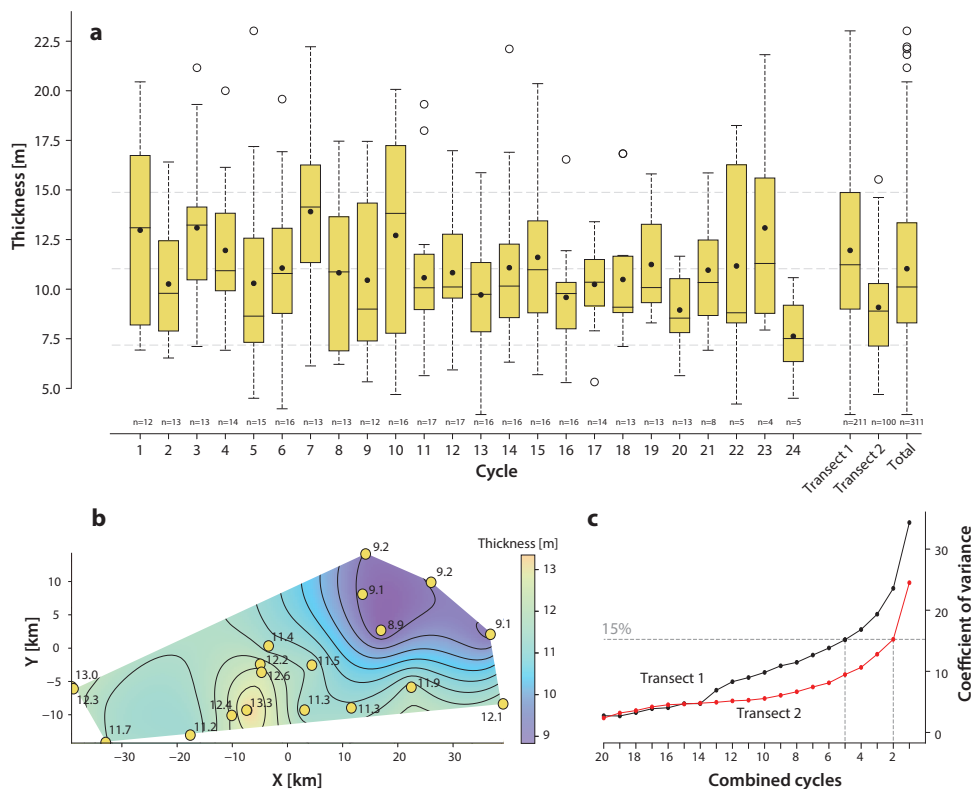


FIGURE 7.5 Cycle thickness statistics. a) Box plots illustrating the thicknesses of the first 24 correlated cycles and the total thickness based on 311 measurements. Cycle 25 has been excluded as it has only been identified twice. Black dots illustrate the mean thickness for each cycle. Dashed grey lines represent the mean and standard deviation of the total dataset. b) Plan view of the well's mean cycle thickness and interpolated thickness contours. Note how the cycle thickness is smaller in transect Two in the north of the study area. c) The coefficient of variance, an indication for the compensational stacking, is calculated for consecutive cycles over all wells and implies stable thickness variation (15%) near 2-5 cycles.

Type	Thickness [m]				Occurrence
	Mean	Min	Max	SD	
c1	10.9	6.4	20.5	3.8	44
c2a	10.1	4.0	20.4	3.7	61
c2b	12.6	5.9	21.2	4.5	20
c3	10.0	3.7	22.1	3.6	52
c4	10.4	4.2	20.0	3.3	58
c5	11.8	6.9	18.7	3.4	24
c6	13.1	6.9	23.0	3.9	52

TABLE 7.1 Cyclothem types (See Figure 4) and their thickness, variability, and occurrence.

more convex. Both the blocky pattern and fining-upwards sandstones tend to be thicker than the coarsening-upward sandstones (t-test, $p < 0.01$) which have a mean thickness of 4.3 m (Fig. 7.6a). Coarsening-upward trends are often seen in sands that are less than 3 m thick, but which are excluded from this chapter (Fig. 7.7 and 7.8). Net-to-gross ratios over all the studied wells are generally low, averaging 13% (min: 5%, max: 22%).

7.4.3 Cyclothem correlation

Manual correlation

The wells were first aligned based on miospore biozones and characteristic lithological patterns. The proximity of the wells allowed for high confidence in correlating lithostratigraphic patterns. The correlation started with three well clusters: 44/21-3, 44/21-7 (416 m), 44/23-8, 44/23-14 (1300 m); and 44/23-4, 44/23-7 (1900 m) and allowed the identification of a marker in the form of a thick coal seam overlain by a thicker sandstone package. This correlates with the top of biozone W4a (Cycle 6). More wells with increasing well spacing up to 12 km, were added using this marker or biostratigraphy. The resulting correlation panels are shown in Figures 7.7 and 7.8.

The biostratigraphic zonation and the constructed cyclostratigraphic correlation are generally in agreement (Fig. 7.9), particularly given the margins for error imparted to the biostratigraphic interpretations by sample distribution. The tops of biozones W4a, W4c, and W5a show a maximum offset of two cyclothem. The top of biozone W4b shows up to 3 cyclothem of offset. In well 44/23-13 the identification the top of the biozone is probably artificial (but would otherwise have an offset of five cyclothem), with the true top lost to erosion Variscan unconformity. The top of the biozone is defined by the top of the common occurrence of *Lycospora noctuina noctuina*. Any variation in records of this may reflect additional taphonomic controls on species abundance ranges (as compared to species total ranges) which may be exacerbated by practical factors such as the nature and distribution of ditch cuttings samples (e.g. McLean and Davies, 1999). The last occurrence of the *L. noctuina noctuina* provides a more consistent correlation with the cyclostratigraphic zonation. Accurate recognition of this biostratigraphic event is limited by the scarcity of the species at the limit of its range, meaning that in some cases this event may be artificially deep.

Semi-automatic and stratigraphic thickness correlation

A bandpass filter from 8-16 m was used to filter the cyclothem from the DC. The semi-automatic correlation was calculated twice. Once using the prominent marker coal seam as a calibration point (Fig. 7.10b) and once using the top of the Caister-Murdoch-System (Fig. 7.10c). The prominent coal seam was used as a calibration point for correlation based on stratigraphic thickness (Fig. 7.10d).

Individual cyclothem identified by this correlation are similar to and as well-defined as those identified manually. However, the stratigraphic positions of the cycle boundaries are different. This reflects a slight offset between the wireline data and the resulting DC, resulting in the boundary of a cycle being placed slightly above or below the manually defined boundary (Fig. 3c). In thicker sandstones (>10 m), the DC filter detects spectral change in sandstone shape. These changes are included in the automatic correlation, whereas they were treated as unknown intervals and were not used in the manual correlation.

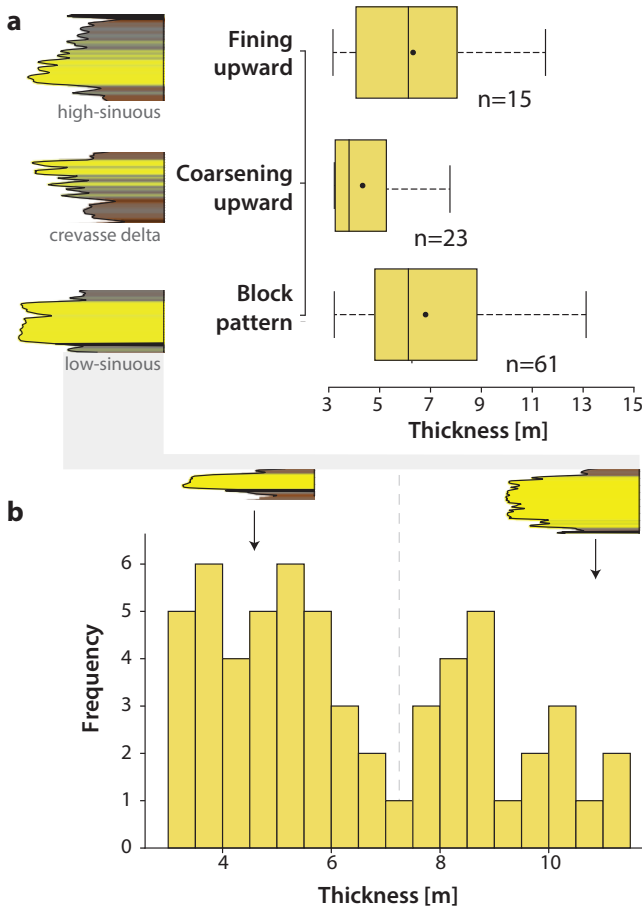


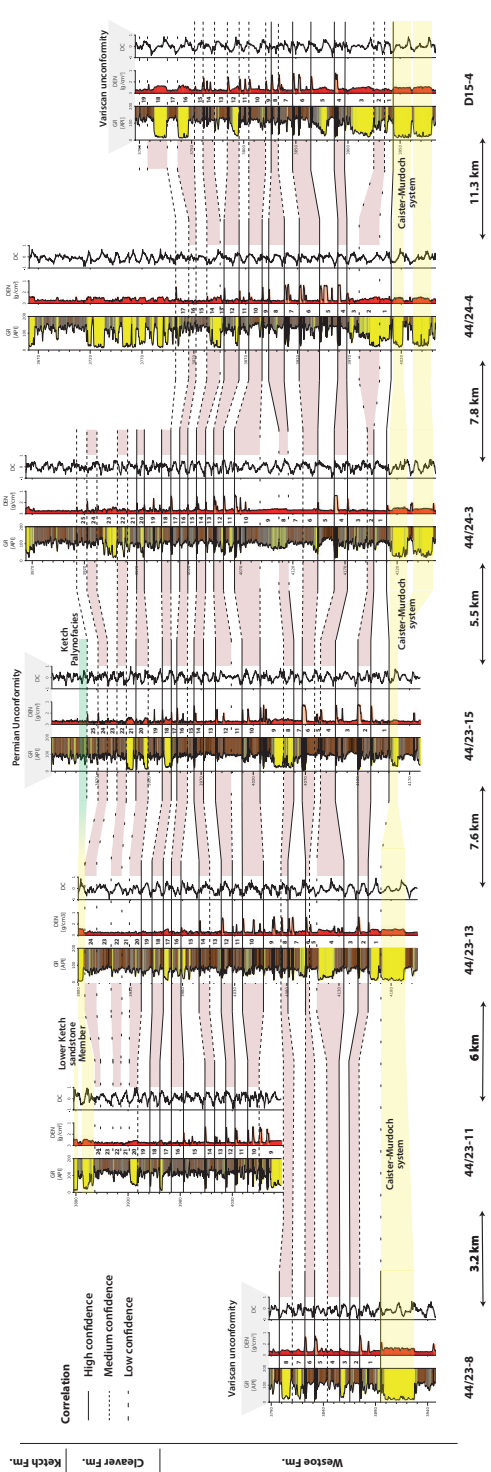
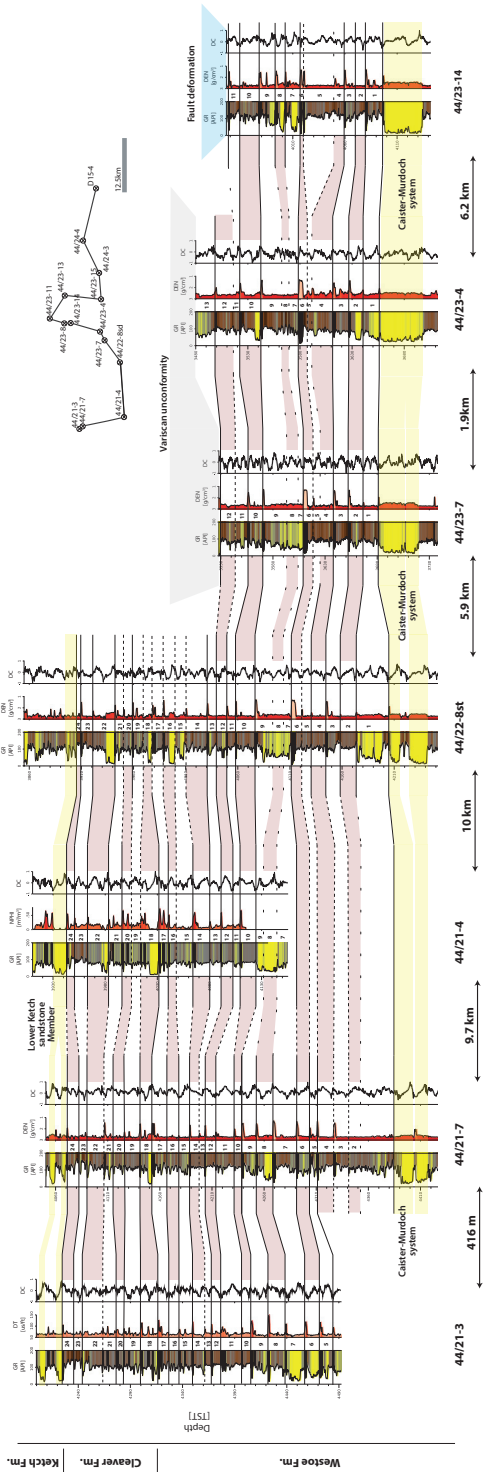
FIGURE 7.6 a) The measured thickness for sandstones >3 m. Based on the log shapes, the sandstones have been divided into three groups: block pattern, coarsening upwards, and fining upwards shapes. b) Histogram of the block pattern-shaped sandstones. Note the bimodal distribution of the sandstones with 3-6 m block patterns and the thicker, more serrated sandstones.

7.4.4 Resulting stratigraphy

Manual correlation

Twenty-five cycles are correlated over an average of 260 m of strata. Cycle thickness and thickness variability is higher in the lowest ten cyclothem (mean: 11.8; SD: 4.4) compared to those above (mean: 10.6; SD: 3.3) (Fig. 7.5a). Confidence scores are high up to cyclothem 16 or 17. After that, the scores decrease gradually towards the top of the correlation where individual sandstones tend to be more numerous. Coal seams are abundant in the first 16 cyclothem, above which they become less common, especially in the northern part of the study area. It is only in the most southwesterly part of the study area that coals remain common in the higher parts of the sections.

→ **FIGURE 7.7** The constructed cyclostratigraphic well correlation of Transect One. The gamma-ray, density and DC records are shown. See Fig. 7.3 for the key to the colour fill of the gamma-ray. Correlation lines are depicted with three confidence levels (high, medium, and low). Caister-Murdoch system and the Lower Ketch sandstone Member are highlighted in yellow. Grey indicates the Variscan unconformity.



Correlation

- High confidence
- - - Medium confidence
- · · Low confidence

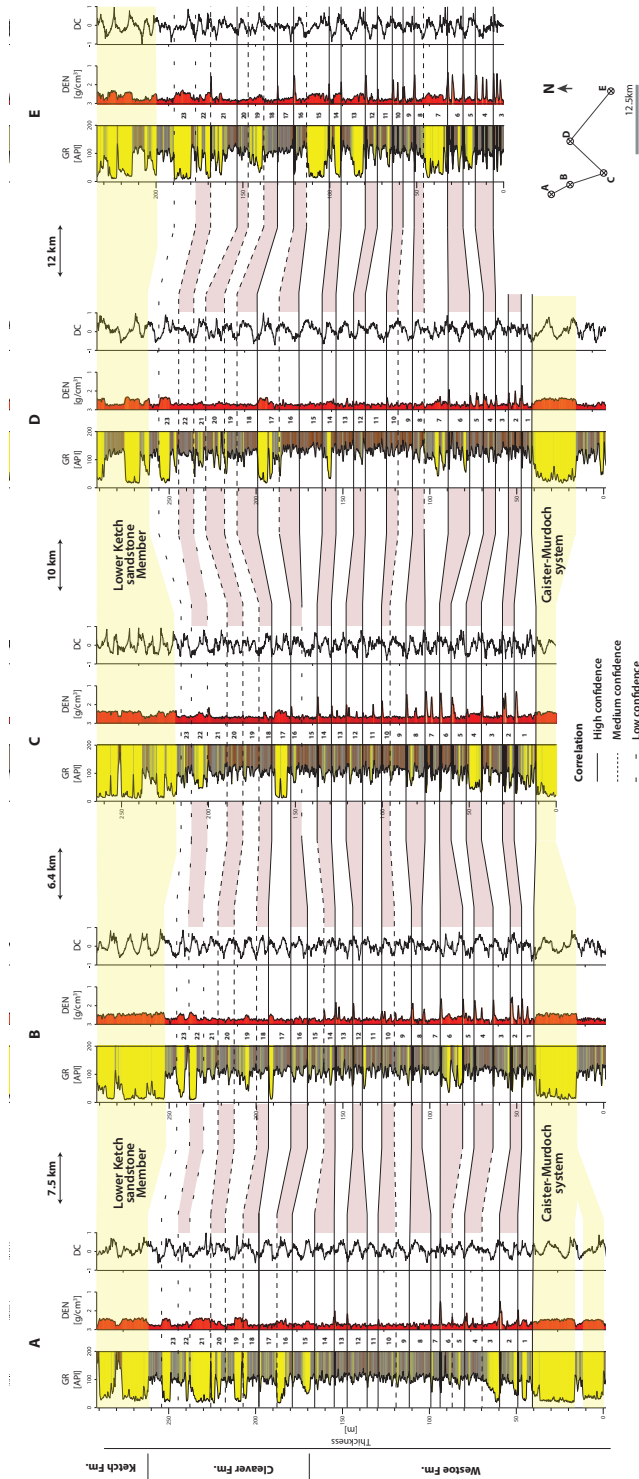


FIGURE 7.8 The constructed cyclostratigraphic well correlation of the Westoe and Cleaver formations for Transect Two. The gamma-ray, density and DC records are shown. See Fig. 7.3 for the key to the colour fill of the gamma-ray. Correlation lines are depicted with three confidence levels (high, medium, and low). The Caister-Murdoch system and the Lower Ketch Member are highlighted in yellow.

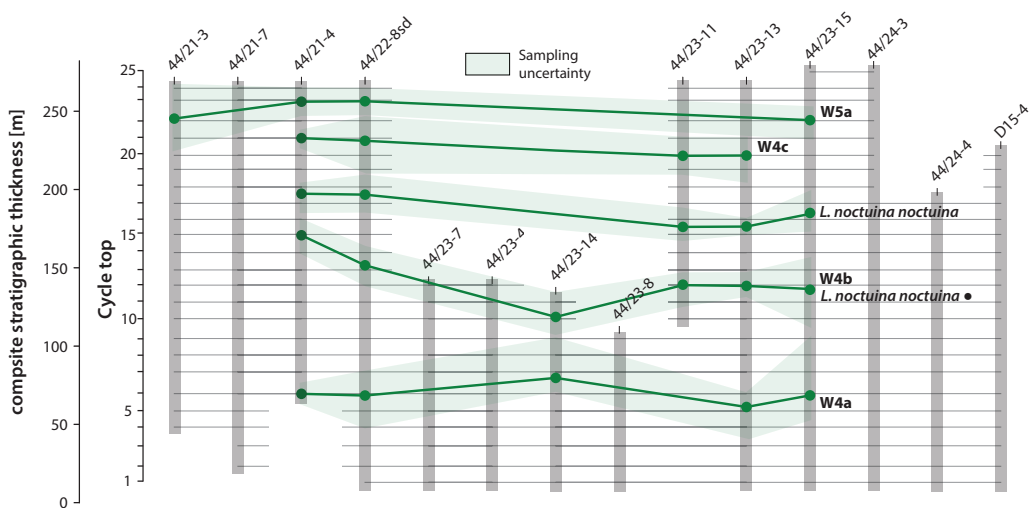


FIGURE 7.9 Comparison of biostratigraphic and cyclostratigraphic correlations. Wells are plotted on a composite stratigraphic thickness based on the cyclothem correlation. The green overlay represents the biostratigraphic sampling uncertainty.

The top of the correlation varies from cycle 23 up to cycle 25. In Transect One, most wells have a thicker sandstone interval on top of cycle 24. Above this interval the sandstone content becomes too dominant for further correlation. This event at the top of cycle 25 is interpreted as the base of the lower Ketch Member. This sandstone interval is absent in wells 44/23-15 and 44/24-3. Here the base Ketch palynofacies is used as a top marker resulting in one cycle offset (cycle 25). In well 44/24-4, no clear top is identifiable. The thick packages of concentrated sandstone from cycle 17 upwards in this well make cyclothem correlation impossible. This sandstone package may represent the local, deep incision by the lower Ketch Member (7 cycles, ± 77 m) although this seems unlikely, given the constant thicknesses of this interval over all of the other wells. It is also possible the section is faulted, causing an offset in correlation. Twenty-three cycles are correlated in Transect Two. The sandstone content becomes too dominant for further correlation above cycle 23 and this interval is interpreted as the lower Ketch Member.

The base of the correlation generally aligns with a thicker sandstone interval, identified as the Caister-Murdoch system. In 44/22-8st, 44/23-4, 44/23-13, and 44/24-4 there is another sandstone on top of the Caister-Murdoch system. There is clear separation between the sandstones with occasional development of coal and so the higher sandstones are interpreted as separate channels above Caister-Murdoch system.

Two intervals of increased sandstone content are identified (Fig. 7.10a). The first (in cycles 7, 8, 9) is of sandstone, c. 30 m thick, that is relatively constant laterally. It often contains multi-story (2-3 stacked) blocky-pattern sandstones where net-to-gross ratios are up to 30-40% (compared to 10-15% elsewhere). The base of the interval is marked by a relatively thick and laterally consistent coal seam forming the top of cycle 6. This coal is probably equivalent to the informal “Coal B” in legacy industry reports. The second interval (cyclothem 17, 18) is c. 20 m thick with an average net-to-gross

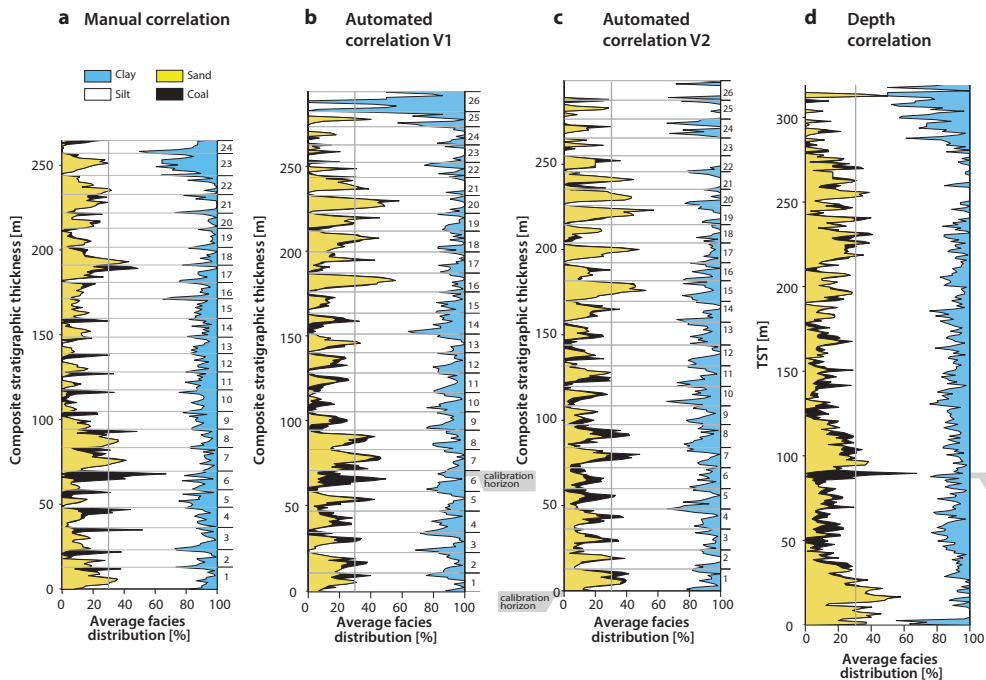


FIGURE 7.10 Comparison of vertical proportion curves based on different stratigraphic correlation methods. The facies have been divided into sandstone, coal, siltstone, and claystone. The lithofacies distribution has been calculated on a 1 m vertical spacing. a) Vertical proportion curve based on the manual correlation of cyclothems (see Fig. 7.7 and 7.8). b) Vertical proportion curve based on semi-automatic correlation method of cyclothems with a prominent coal seam as a tie-point. c) Vertical proportion curve based on the correlation of the semi-automatic correlation method with the top of the Caister-Murdoch system as a tie-point. d) Vertical proportion curve based on true stratigraphic thickness (TST) with a prominent coal seam as a tie-point but without further correlation between wells. Notice how both b, c and d indicate the increase of sand content near the calibration horizon. This zone is similar to the manual correlation. Clay and sand content intervals are well defined in the semi-automatic method (b and c), while this is less prominent in the manual method (a). The vertical grey arrow indicates the 30% level.

of 10-15% up to 40%. Here, the sandstone bodies are often thin (< 6 m) and single-story, separated by floodplain fines. Between these two intervals (cyclothems 10 to 16), there is an abundance of coal seams and fewer sandstones, which are predominantly coarsening upwards. A general increase in sandstone content characterises the interval above cyclothem 19. However, thick block pattern styled sandstones remain relatively scarce until cycles 23 to 24 and the interpreted base of the lower Ketch Member.

Combination of the vertical proportion curve with the biozonation allows location of marine bands in the cyclostratigraphic framework. The Maltby MB should lie between the top of *L. noctuina noctuina* and the top of common *L. noctuina noctuina* (McLean et al., 2005). Based on the average stratigraphy, the horizon of the Maltby MB is placed at the boundary between cyclothems 16 and 17. Here, the most southerly wells closest to the basin depocentre (44/21-3, 44/21-7, 44/21-4, 44/22-8st) have high gamma-ray values. The horizon of the Aegiranum MB is placed between cyclothems 23

and 24. An evident increase in high gamma-ray values is observed in multiple wells (44/21-3, 44/21-7, 44/21-4, 44/22-8sd, 44/23-15, 44/24-3, 44/23-13). Davies and McLean (1996) and O'Mara and Turner (1997) suggest that gamma-ray spectrometry can provide a proxy record for marine bands by enhancement in uranium-thorium ratios. Such signals were not identified close to the suggested marine band horizons or at any other depths.

Semi-automatic and stratigraphic thickness correlation

Twenty-six cyclothem are defined in both of the semi-automatic methods, one more than in the manual correlation. In the semi-automatic correlation, some wells appear shifted one cycle up or down compared to the manual correlation. A cyclic character is more clearly visible when comparing the vertical proportion curves of either of the semi-automated correlations than in the manual correlation (Fig. 7.10b and c). Individual coal seams appear less well-aligned in the semi-automated correlations and sandstones appear to have less stratigraphic overlap, and there are up to 20% higher net-to-gross averages. Both correlations suggest the same large-scale trends in sandstone distribution as the manual correlation, with two intervals of increased net-to-gross. As an independent calculation, the alignment of wells depth based on the true stratigraphic thickness shows a strong smoothing of all facies patterns, particularly at the cyclothem scale of 10-20 m.

7.4.5 Cyclothem duration

The interval between the Vanderbeckei MB and the Aegiranum MB (representing the Duckmantian Substage, Fig. 7.1b), as defined in the manual correlation, has been used to estimate the duration of a single cyclothem. This interval comprises twenty-three cyclothem, plus the Caister-Murdoch system. The studied wells indicate an average additional thickness of 60 m between the base of the Vanderbeckei MB and the top of the Caister Murdoch sandstone. Linear interpolation between the thickness of this interval and the average cyclothem thickness for the remainder of the Duckmantian suggests that it includes five or six additional cyclothem. This implies the presence of twenty-eight or twenty-nine cyclothem in the Duckmantian in the study area. With Duckmantian duration estimates ranging from 1.2 to 2.5 Myr, an individual cyclothem represents a period of between 41 kyr (1.2 Myr, 29 cyclothem) and 89 kyr (2.5 Myr, 28 cyclothem).

7.5 Discussion

7.5.1 North Sea Cyclothem

The term cyclothem describes an upward coarsening sequence of claystone to sandstone capped by coal (O'Mara and Turner, 1999). Most cyclothem, in the study wells lack some components of the complete cyclothem and different types of cyclothem have been defined accordingly. The most common cyclothem type is a coarsening-upwards shale capped by a coal, differing from the idealised sequence in the absence of sandstone in the top of the sequence. The common denominator of the cyclothem in the Westphalian of the Silverpit Basin is a coarsening upward sequence. A cyclothem containing all lithological elements (type C1) is the ideal or composite cyclothem, while the modal cyclothem is a sequence from shale to coal (cycle type C2a and C2b).

Differences in lithological character and thicknesses of cyclothem reflect local depositional geomorphology, which varied considerably. This is interpreted as an autogenic factor (Fig. 7.4a).

While the geographical extent of “minor” or crevasse deltas and coal mires can be substantial, their lateral continuity is unlikely to extend over tens of kilometres (Haszeldine, 1983; Fielding, 1984a; Fielding, 1984b). It should not be expected that the infill of a crevasse delta in a lake would result in a clear gamma-ray signal over a wide lateral distance. Such a feature would only cause a minor change in the gamma-ray trend when observed distal to the sediment source. Peat formation is also expected to occur at a distance from the sediment source (Ferm and Weisenfluh, 1989; O’Mara and Turner, 1999). Furthermore, autogenic processes such as differential compaction and channel switching can affect the lateral character of a cyclothem.

The documented thicknesses of the cyclothem are comparable to those reported by O’Mara and Turner (1999). Duff and Walton (1962) observed cyclothem with a similar thickness range of 4 to 20 m (average 11.5 m) in the Pennine Basin. They also recorded variations in cyclothem character, documenting a dominant coarsening upward sequence with the occasional absence of siltstones, sandstones, or palaeosols, similar to that seen in the present chapter. Further South, in the Dutch onshore on the other side of the Silverpit Basin depocentre, van der Belt et al. (2015) documented cyclothem ranging from 5 to 35 m with an average of 12.5 m. The continuous vertical and lateral detection of cyclothem in the study area and similar observations in other parts of the basin suggests a strong, basin-wide, allogenic forcing on deposition.

7.5.2 Sandstone type and occurrence

Wireline data alone does not provide enough evidence to allow interpretation of fluvial formation processes of the three major sandstone types, but it can be linked to outcrop analogues in the Pennine Basin. Fielding (1984b, 1986) described major and minor distributary channels in the Westphalian. Major distributary channels are broad, elongate, laterally extensive sandstone bodies with low sinuosity and widths of 2-10 km (Fielding, 1984b). Belts of such channels could be linked to the thicker block-shaped sandstones documented on wireline data in this chapter (Fig. 7.6). The stacking nature of these sandstone types is documented onshore. The thinner, more convex-shaped, block patterned sandstones can be interpreted as major crevasse channels. These coarse-grained deposits have a maximum thickness of 7 m and a lateral extent of roughly 2 km. Notably, the sharp boundary at the top of the sandstones suggests rapid channel abandonment. Fielding (1986) argues that such crevasse channels were active for prolonged periods and could transform into minor distributary channels. In contrast, he attributed sandstones with a fining-upward profile to high sinuosity channels. These are like the fining-upward sandstones documented in the present chapter. However, such channels in the Silverpit area are significantly thicker (up to 12 m) than the 6 m recorded by Fielding (1986). Sandstones with a coarsening-upward wireline profile most likely represent crevasse delta splays. The pronounced shape relates to the progradation of a crevasse delta into a lake or floodplain. Such overbank deposits have a limited lateral extent of a few hundred meters (Fielding, 1984b). Besides the documented thick (>3 m) sandstones, there are thin (0.5-2 m) single crevasse splays attributed to cycle type C4. The lateral extent of these crevasse splay sandstones is believed to be considerable, but they vary in thickness (Fielding, 1984b).

7.5.3 Manual cyclothem correlation

Neither coal seams nor crevasse delta or splay deposits can be correlated one-to-one between wells. The correlation here was not based on lithologies but on trends. Part of the ability to recognise

cyclothem trends and correlate despite lateral character changes is attributed to the use of the DC. With this curve, changes in the wireline record become less dependent on absolute values. While absolute values may change laterally and vertically, the DC filter depicts these changes as equal, allowing cyclic signal detection, as illustrated by the semi-automatic vertical proportion curves (Fig. 7.10 b and c). Further, when attempting a correlation exercise, it is essential to start in neighbouring wells where lateral changes are least, and confidence in correlation is highest. Information about lateral variations in lithofacies in these closely-spaced wells can be used as feedback when making correlations over greater distances.

Even with an understanding of the variability in the system, part of the correlation remains uncertain. This is often highest around thicker channel sandstones, where the preservation potential of cyclothems is lowest. Below channel sand bodies there may be gaps in the stratigraphical record due to incision. In the Pennine Basin, the maximum erosional relief of the major channels during the Westphalian is estimated at 6-10 m of compacted stratigraphy (Fielding et al., 1986). In the study area the Caister-Murdoch system has erosional relief of up to 15 m (O'Mara and Turner 1999). Sandstones frequently occur directly on top of coal seams. Primary compaction of coals (up to 47% of the total compaction) occurs rapidly, with average compaction rates of 5-24 mm/yr (Cahoon et al., 2000; Törnqvist et al., 2008; van Asselen et al., 2009). Such early lithification may suggest that even relatively young, buried peats could act as barriers to channel incision. Given this and the low relief of the Westphalian alluvial plain, it seems unlikely that channels could have removed more than two full cyclothems by incision. To address these issues intervals with thick sandstone bodies are scored with lower certainty than adjacent intervals. This results in a lower stratigraphic resolution for the sandstone-prone sections. However, the adjacent intervals (being constrained by biostratigraphic and lithostratigraphic markers) have higher certainty and so any stratigraphical gaps associated with sandstone incision do not represent problems for cyclothem correlation.

7.5.4 Resulting stratigraphy

There is a clear difference between the average cyclothem thickness in the southern (Transect One, 11.2 m) and northern (Transect Two, 8.9 m) transects. This reflects the southwestward increase in overall stratal thickness towards the basin depocentre. The change occurs over a relatively short distance of about 10 km. The orientation of the thickness change is perpendicular to a dominant northwest-southeast fault trend observed in the Silverpit Basin, thought to be related to the approaching Variscan deformation from the south (Leeder and Hardman, 1990). This may be an extension of the Elbe-Odra fault line (Smit et al., 2016) and may have been a hinge line that created more accommodation space on its south-southwest side. Alternatively, compartmentalisation of the foreland basin into small fault blocks with varying subsidence and accommodation space may account for the thickness changes. A similar feature is described for the Oligocene Boom Clay in the Campine area, Belgium where bed-to-bed correlations provided evidence differential subsidence of closely spaced fault blocks (Vandenberghe and Mertens, 2013).

The base of the correlation is bounded by the Caister-Murdoch system, and based on the cyclostratigraphic correlation, this lithological unit's position remains consistent. The position of the base of the lower Ketch Member differs being defined one cycle earlier in the Northeast (Transect Two). As with the change in cyclothem thicknesses, the overall study interval is thinner, in the Northeast. This is in line with the general northeast thinning trend of the Westoe and Cleaver

formations (Huis in 't Veld et al., 2020) and may reflect differences in accommodation space, with a larger sub-Ketch unconformity towards the north and consequent lower preservation potential in the upper part of the study interval.

7.5.5 Cyclostratigraphy compared to biostratigraphy

There is an average offset of 1-3 cyclothem or roughly 10-30 m between the biostratigraphy and the cyclostratigraphic framework. Several practical and geological factors impart margins of error on the use of miospores in the study. These include: sample density varies within and between the wells; all samples are from ditch cuttings that allow a maximum stratigraphical resolution of 3 m; the scarcity of species at the stratigraphical limits to their ranges can lead to false-negative results in the correct identification of a biostratigraphical event (species inception or extinction); and miospores are generally absent in medium- to coarse-grained clastics. Further, as different lithologies and facies provide different miospore assemblages (Neves, 1958) the stratigraphical ranges of many species in coal seam samples appear shorter than in clastic samples (McLean et al., 2005).

7.5.6 Semi-automated and stratigraphic thickness correlation

The semi-automatic and manual correlations are closely comparable. Individual cyclothem boundaries are often similarly defined, but cyclothem boundaries may be slightly offset. This is probably caused by a small “lag effect” of the DC on the wireline data and the use of a bandpass filter to smooth the signal (Fig. 7.3c) which may result in the misalignment of coal seam signals. However, the vertical proportion curves of the semi-automatic correlation (Fig. 7.10b and c) have a more distinctly cyclical pattern, reflecting the dominant influence of sandstones in the DC. The vertical proportion curves of the semi-automatic correlation result in apparent thinning of sandstone intervals and 20% higher net-to-gross ratios. They detect and suggest intervals of alternating sandstones and fine-grained clastics resulting in apparently low stratigraphic overlap of sandstones and laterally extensive, fine-grained clastics. These fine-grained intervals may act as flow barriers in a reservoir. When autogenic variability is taken into account, the manual correlation results in a model with more stratigraphic overlap of sandstones and suggests greater vertical sandstone connectivity. However, with its ease of use and faster output when looking at implementation into subsurface workflows and basin-wide trends, the benefits of the semi-automated method may outweigh the cost of any resultant uncertainties.

Using an equal thickness assumption, the calculated stratigraphic thickness correlation results in smoothed facies patterns. These are particularly evident at cyclothem scales of 10-20 m. Large-scale trends remain recognisable which is probably related to compensational stacking patterns within the system. The tendency for sediment transport systems to preferentially fill topographic lows produces an averaged equal thickness (Straub et al., 2009). Within two to five cycles (22 to 55 m), the average stacked thickness of cyclothem varies only by 1.65 m. Any patterns above this resolution appear to remain equal.

7.5.7 Controls on sedimentation

A depositional model driven by glacio-eustatic, base-level change explains the deposition of the cyclothem in the Silverpit Basin. Each cyclothem has a fine-grained, lacustrine, or marine bed at its base representing a (forth-order) base-level high-stand. Lacustrine or marine accommodation space is subsequently filled base-level fall (O'Mara and Turner, 1999; Huis in 't Veld et al., 2020).

However, glacio-eustasy will also have effected changes upstream. Palaeo-polar ice volume changes are also related to palaeo-tropical climatic variations with changes in rainfall and vegetation affecting upstream sediment supply and leading to cyclic behaviour in fluvial systems (e.g. Noorbergen et al., 2018; Opluštil et al., 2022). There is strong evidence that Pennsylvanian glacial-interglacial fluctuations produced significant climatic variations, with shifts from perhumid to semi-arid seasonal climates recorded in palaeotropical Euramerica (Cecil et al., 2003; Roscher and Schneider, 2006; DiMichele et al., 2010; Eros et al., 2012). Cecil et al. (2003) argue that changes in the position of the intertropical convergence zone caused relatively wet conditions in the palaeotropics during interglacials, while the climate was drier and more seasonal during glacials. Higher interglacial precipitation would stimulate peat development and, ultimately, the extended formation of lakes. Lower precipitation and enhanced seasonality during glacials would have decreased vegetation cover (DiMichele et al., 2010; Eros et al., 2012) resulting in higher sediment influx and the infilling of lakes with coarser-grained clastics. With the absence of clear marine conditions in the Westoe Formation (O'Mara and Turner, 1997) and probable upstream changes, both upstream and downstream controls, and likely combined, should be considered as mechanisms in the formation of cyclothem in the Silverpit Basin.

7.5.8 Cyclothem duration

The absence of sufficient chronological dating in the Silverpit Basin and the large variability in age control makes it challenging to identify an orbital forcing component in the depositional system. Different time scales, suggest a duration of between 41 and 89 kyr for cyclothem formation. In the Dutch onshore, van der Belt et al. (2015) identified cyclothem paced at a sub-eccentricity periodicity with dominant 21 kyr precession and interference of an obliquity component. For the central Appalachian Basin, Le Cottonnec et al. (2020) suggested cyclothem forcing by the interference of 34 kyr obliquity and 100 and 400 kyr eccentricity, while for Eastern European Basins a 100 kyr short-eccentricity is proposed (e.g. Davydov et al., 2010; Jirásek et al., 2018; Opluštil et al., 2022). In the Eastern European Upper Carboniferous, cyclothem are 50 to 100 m thick and commonly include multiple coal sequences. Jirásek et al. (2018) suggest the presence of obliquity or precession-controlled patterns on coal seam distribution within these thicker cyclothem.

Coal bundles which might suggest a larger-scale forcing were not observed in this chapter. However, the two large-scale trends of increased net-to-gross zones are separated by eleven cyclothem. This is also the case between the first interval and the Vanderbeckei MB. The constant spacing and the 11:1 ratio between the intervals are comparable to the ratio of the 34 kyr obliquity period during the Carboniferous (Collier et al., 1990) and the 400 kyr long-eccentricity cycles. Oligocene sedimentary records also show that glacio-eustasy has a strong obliquity component with long-eccentricity modulation (e.g. Wade and Pálike, 2004; Abels et al., 2007). This may suggest that the Silverpit Basin cyclothem had a strong obliquity-controlled component which was shorter than the estimated duration. However, there is a large uncertainty regarding age control. One could also argue for the existence of a 100 kyr short-eccentricity control, but a strong imprint of long-eccentricity (4:1 ratio) would be expected, which is not found.

7.5.9 Low net-to-gross targets

The two defined increased net-to-gross intervals, and the Caister-Murdoch system could be paced at a 400 kyr long-eccentricity interval (Fig. 7.11). Long-eccentricity modulation of glacio-eustasy (e.g.

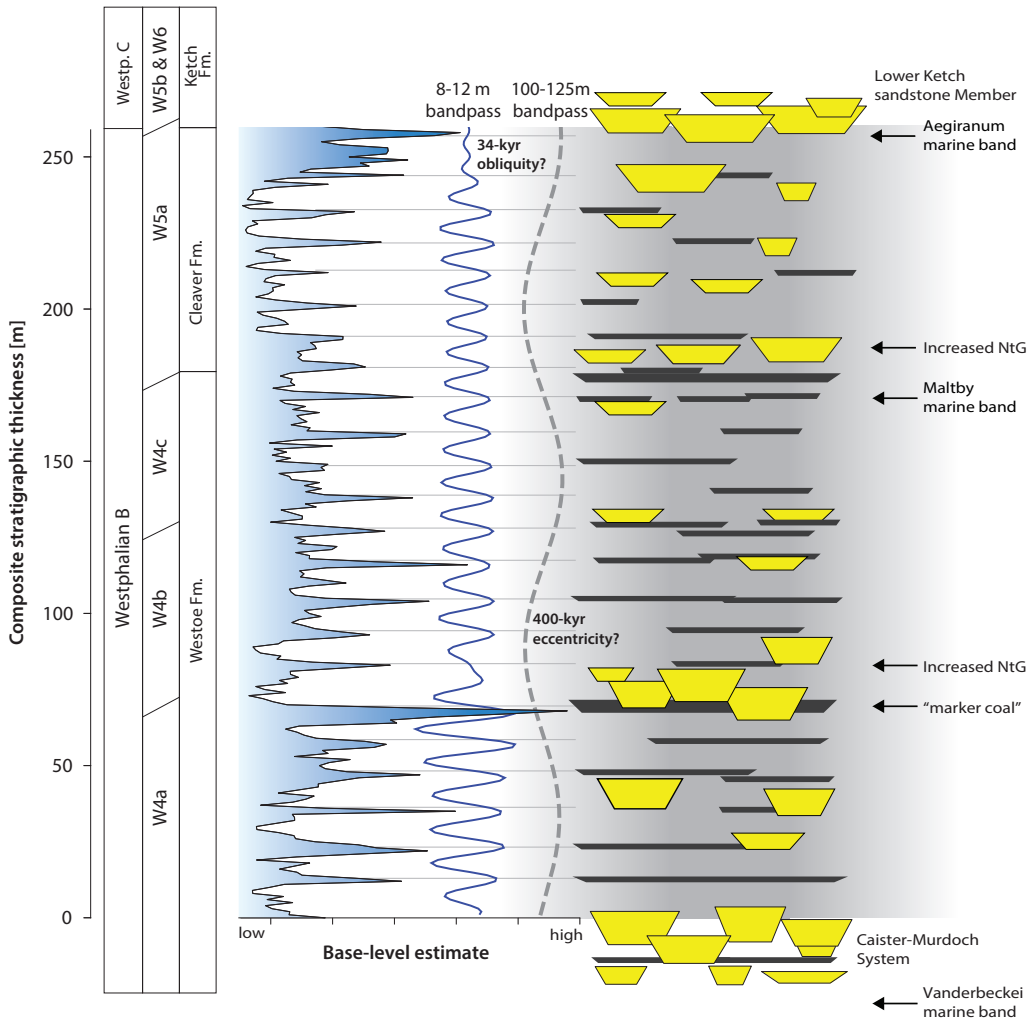


FIGURE 7.11 A base-level estimate curve based on the vertical proportions curve of the manual correlation. In blue, an 8-12 m and in grey, a 100-125 m bandpass filter is shown. The Caister-Murdoch sandstones and Ketch sandstones are indicated at the section's bottom and top, respectively. Based on the average stratigraphic trends, two zones with increased sand lithofacies are defined and shown on the right. These zones align with a 100-125 m bandpass filter and could possibly be controlled by a ~400 kyr long-eccentricity pacing.

Wade and Pälke, 2004; Abels et al., 2007) would have led to more extreme base-level fluctuations at specific intervals, and potentially resulting in incised valley fills. The Caister-Murdoch system was formed as an incised valley fill (Shanley and McCabe, 1994; Richie et al., 1998; Huis in 't Veld et al., 2020) or due to tectonic influence (O'Mara and Turner, 1999; Kusters and Donselaar, 2003). The vertical distribution and spacing of the Caister-Murdoch system, lower Ketch sandstone, and the two newly defined increased net-to-gross intervals suggests that it is unlikely that all of these sandstone-prone intervals were tectonically induced. Therefore, the two defined increased net-to-gross intervals could also represent incised valley fills.

Another explanation for the two-increase net-to-gross intervals can also be given. In the low-relief setting of the Silverpit Basin, a significant lowering of base-level could have changed the fluvial planform style towards the braided end of the alluvial spectrum. Such change is observed in the first low net-to-gross interval, where multi-storied block patterned sandstones are more common. Furthermore, greater extremes in base level fluctuation would also have led to enhancement of upstream sediment flux. This model would fit with the stratigraphical juxtapositioning of prominent coal seam markers and marine bands indicating enhanced wetter periods (Fig. 7.11).

Independent of the specific depositional model for the defined increased net-to-gross intervals, an orbital forced control would affect reservoir potential. Basin-wide forcing implies a more significant probability of the occurrence of sandstones within these stratigraphic intervals in the otherwise overall low net-to-gross Westoe and Cleaver Formations. Similar variations in net-to-gross ratios associated with long-eccentricity climate control are suggested for the Upper Carboniferous Upper Silesian (Opluštil et al., 2022) and Appalachian Basins (Le Cottonnec et al., 2020).

7.6 Conclusions

Repetitions of coarsening upward sequences, cyclothems, continuously occur in the Westoe and Cleaver formations in the Silverpit Basin in the Southern North Sea. These can be used for cyclostratigraphic correlation and identification of stratigraphic trends in this low net-to-gross interval. The average cyclothem thickness implies that a high-resolution correlation is possible but to achieve this the variability in thickness and lithological character, interpreted as local, autogenic components, must be considered. Five variations in cyclothem development are defined in relation to an ideal cyclothem consisting of a coarsening upwards sequence of shale to sandstone capped by coal and five variations. Manual and semi-automated methods for the correlation of wells are evaluated, and average stratigraphic trends are compared. The manual correlation demonstrates that wells can be correlated at a 10-20 m resolution, even over large well spacings. This correlation generally agrees with the available biostratigraphic control. The semi-automated method uses a deviation curve as an essential technique allowing identification of cyclothems relatively easily. However it is not as accurate as the manual correlation. The vertical proportions curve of the manual correlation indicates a higher level of stratigraphic overlap of sandstone bodies than expected for a fully cyclic-driven model. Similar trends are seen in the vertical proportions curve in the semi-automated method. Here, all sandstones relate to the same stratigraphic level. In the manually derived vertical proportions curve, claystones are stratigraphically more spread and represent fewer potential flow barriers than suggested by the semi-automated correlation. On balance, the ease of use and faster output of the semi-automated method outweighs the uncertainties produced. This is so particularly when looking at basin-wide trends for implementation into subsurface workflows. Both correlations identify two

laterally consistent intervals where net-to-gross increases from 10-15% to 30-40%. The lower interval in the Westoe Formation has the highest reservoir potential of the two. Here the sandstones are commonly stacked, multi-story units. These intervals are interpreted as being linked to a 400 kyr long-eccentricity control on base-level fluctuation and associated upstream changes in hydrology. Such an orbital forced control implies a stratigraphic predictive value. These intervals have a higher probability of sandstone occurrence and their recognition by cyclostratigraphic analysis may guide economic exploration in an otherwise low net-to-gross setting.



Top

Site
Date
Depth



NR01622098

Y	ELL	CORE NO.	BOX NO.	DEPTH (m)	CU
7	7-7	12	2 of 3	2908.00 2911.00	A

8

Implementation of cyclostratigraphic concepts and methodology in the Upper Triassic Lunde Formation to improve stratigraphic reservoir characterisation

Abstract

Floodplain deposits, especially palaeosols, are often overlooked when characterising alluvial reservoirs. However, they provide a significant database for the reconstruction of alluvial architecture and can compose an essential tool in characterising and correlating low net-to-gross, heterogeneous alluvial reservoirs. Palaeosols often capture different sedimentary processes than their sandstone counterparts and have distinct vertical and lateral arrangements. The approach in this chapter combines sedimentological and palaeopedological data with cyclostratigraphic analysis of floodplain fines. Palaeosols were studied in core intervals of the Upper Lunde Formation based on main pedofeatures such as soil cracks, colour, nodules, slickensides and rhizoliths. The palaeoenvironment is interpreted as a semi-arid climate with significant wet periods. Modern-day analogues and implications for processed-based modelling are discussed. Stratigraphic analysis of the floodplain fines reveals a stable alternation of high and weak to moderate pedogenesis with an average of 5.5 m thickness. These floodplain alternations are hypothesised to be formed by variability in the aggradation rate on the floodplain resulting from channel movement. Recognition in well-logs of the floodplain aggradation cycles allowed for a high-resolution floodplain-based stratigraphic framework over six wells and showed lateral consistent patterns over a 1-5 km scale. Stable isotope stratigraphy was used to identify tie points and correlate three additional wells over larger distances. The resulting stratigraphic zonation was compared to the existing reservoir zonation, and refinements were suggested. An orbital-forced precession-paced control is proposed and fitting thickness ratios between floodplain aggradation cycles, stable carbon isotope excursions, and low and high net-to-gross stratigraphy phases suggest orbital forcing as a controlling allogenic component on the Upper Lunde alluvial stratigraphy. However, without sufficient age control, there is no conclusive evidence. This chapter shows that implementing cyclostratigraphic concepts for stratigraphic reservoir characterisation can complement and improve existing models and that the floodplain sedimentary archive can be used as additional input for reservoir characterisation and modelling.

Written by: Baars, T.F., Martinius, A.W., Abels, H.A.

Author contributions can be found on page 187.

8.1 Introduction

Subsurface characterisation of alluvial successions and understanding of the occurrence, connectivity, and correlation of sandstone bodies in these successions is important for geo-energy production and carbon dioxide or hydrogen storage in many regions worldwide. This is challenging in low net-to-gross alluvial stratigraphy as these often feature isolated sandstone bodies with poor three-dimensional connectivity (e.g. Dalrymple et al., 2001; van Toorenburg et al., 2016; Varela et al., 2021) and it is difficult to correlate fluvial sandstones across a reservoir based on well data only (e.g. Donselaar et al. 2011; Ojik et al. 2011). The channels are often thin (<10 m) and challenging to identify on seismic data, and established marine biostratigraphic correlation methods cannot be used due to large distances to the shoreline and/or low vertical stratigraphic resolution. Therefore, there is a need for stratigraphic correlation concepts that consider the fluvial deposits themselves to predict sandstone stratigraphy.

Inherent to low net-to-gross alluvial systems is the abundance of fine-grained floodplain deposits with respect to their sandstone counterparts. Such ‘background sedimentation’ is commonly overlooked as it does not form the reservoir. However, the sedimentary archive within these deposits often encapsulates a unique point of view on deposition, climate, and past landscape (Kraus et al., 1999). Often palaeosols also have distinct vertical and lateral arrangements and form stacked multistorey complexes (e.g. Willis and Behrensmeyer, 1994; Abels et al., 2013; Varela et al., 2021), which are formed under a combination of autogenic and allogenic factors (e.g. Wright and Marriot 1993; Kraus, 2002).

Allogenic factors relate to basin-wide processes such as tectonics or base-level and climate changes related to orbital cycles. Typically, orbital forcing results in repetitive patterns which can be used for correlation (Davydov et al., 2010; Jirásek et al., 2018; Noorbergen et al., 2018; Opluštil et al., 2019). However, variability in these patterns is expected as autogenic processes, such as channel avulsion and crevasse splaying generally lead to local change (e.g. Kraus and Alsan, 1999; Kraus 1999; Hajek and Straub, 2017). Nonetheless, detected patterns in the floodplain sedimentary archive can be used for well correlation and constructing floodplain-based stratigraphic frameworks. Furthermore, floodplain sedimentation depends on their source channel deposits (e.g. Bridge and Leeder, 1979; Kraus, 2002; Törnqvist and Bridge, 2002). If allogenicly forced, basin-wide trends are also expected to occur in sandstone occurrence. Therefore, integrating underlying climatic-driven models can help improve reservoir characterisation, target potential hotspots in overall low net-to-gross intervals, and serve as input for static modelling scenarios.

To test the correlation potential of floodplain fines in the subsurface and study the implications on reservoir characterisation, the palaeosols of the Upper Triassic Lunde Formation were studied. The Lunde Formation is characterised by red and thick, cumulative palaeosols with single and variously stacked fluvial high-sinuuous sandstone bodies (Nystuen et al., 1989; Muller et al., 2004). Stratigraphic control in the Lunde Formation is poor, and well correlation and reservoir zonation are mainly based on seismic data and equal thickness assumptions (Olsen and Storemark, 2012).

The relatively high pedogenic carbonate content in the Lunde Formation in the Snorre Field allows additional stratigraphic constrain in the form of stable carbon isotope records. Late Triassic carbon isotope records are known for their fluctuations with abundant carbon cycle perturbations resulting in several carbon isotope excursions (Zaffini et al., 2017). These perturbations are likely caused by increased volcanic activity leading towards the end-Triassic mass extinction (Rigo et al., 2007, 2012). This volcanic activity suggests that the interval is a suitable target for carbon isotope excursions and,

thus, for establishing isotope-based correlation tie points. Furthermore, Cenozoic and Cretaceous records show that long- and short-term orbital forcing is detectable and abundantly present in stable carbon isotope records (e.g. Lourens et al., 2005; Boilila et al., 2014, Laurentano et al., 2018; Westerhold et al., 2020) implying that if orbital forcing would have acted on the Lunde Formation, an imprint of it can be expected in the carbon record.

This chapter applies cyclostratigraphic concepts and methodologies to the Lunde Formation through several steps. (1) Floodplain sediments are analysed and logged based on their sedimentological and pedogenic features, and an environmental interpretation is made accordingly; (2) The floodplain stratigraphic architecture is analysed in both core and well-log data for the use of detecting regional stratigraphic markers; (3) A high-resolution stable carbon isotope record is produced to study the imprint of climate variability in the record and generate tie points for well correlation; (4) A floodplain-isotope stratigraphic framework is constructed and compared to the existing reservoir zonation; (5) Stratigraphic trends are analysed, and climate models are fitted in order to provide scenarios for reservoir modelling.

8.2 Geological setting

8.2.1 Basin setting

The Lunde Formation is located in the Tampen Spur area of the northern North Sea and forms the top of the Triassic Hegre Group (Fig. 8.1). The Lunde Formation in the Snorre area is typified by an overall fining-upwards succession, with the top of the interval defined as a trend change from a fining-upward to a coarsening-upward succession. Within the studied cores, this transition is not covered. The formation was deposited in the central area of an approximately 200 km wide continental basin at a palaeolatitude of 33-35° north (Torsvik et al., 2002). This basin formed during a Late Permian to Early Triassic Rifting episode and underwent a thermal subsidence phase during the deposition of the Lunde Formation (Badley et al., 1988; Nystuen et al., 1989; Steel, 1993). The basin was linked to the Boreal Sea in the north (Müller et al., 2005) and the Tethys to the south-east (McKie and Williams, 2009), both located at a significant distance from the study area (several hundred kilometres). Drainage in the basin generally followed the basin axis towards the south-southwest (202°; Nystuen et al., 1989; Steel and Ryseth, 1990; Mjøs et al., 2005), transporting sediment from a Caledonian-aged source in the west (Mearns et al. 1989).

Establishing a chronostratigraphic framework for the Lunde Formation is difficult due to the sparsity of biostratigraphic markers. Biostratigraphic data suggest that the Lunde Formation was deposited during the late Norian to Rhaetian and covers a period of 4 up to 7 My (Nystuen and Fält 1995; Müller 2003). The Lunde Formation varies in thickness between 800 and 900 m, and in the present chapter, only the upper 250 m is studied. This upper part of the Lunde Formation is defined as low net-to-gross (<30% sandstone fraction) and interpreted as a wide alluvial plain with predominantly high-sinuuous to meandering streams (Nystuen et al., 2014). The palaeoclimate was warm and semi-arid (Nystuen and Fält, 1995; Müller, 2003). The thicknesses from the top of the middle part of the Lunde Formation to the top of the Statfjord Group is rather constant across a large number of wells in the Snorre field (Mjøs et al., 2005), suggesting that subsidence was rather uniform over a large area (20 km) during deposition.

Synsedimentary activity of the main faults during the upper Lunde Formation deposition in the

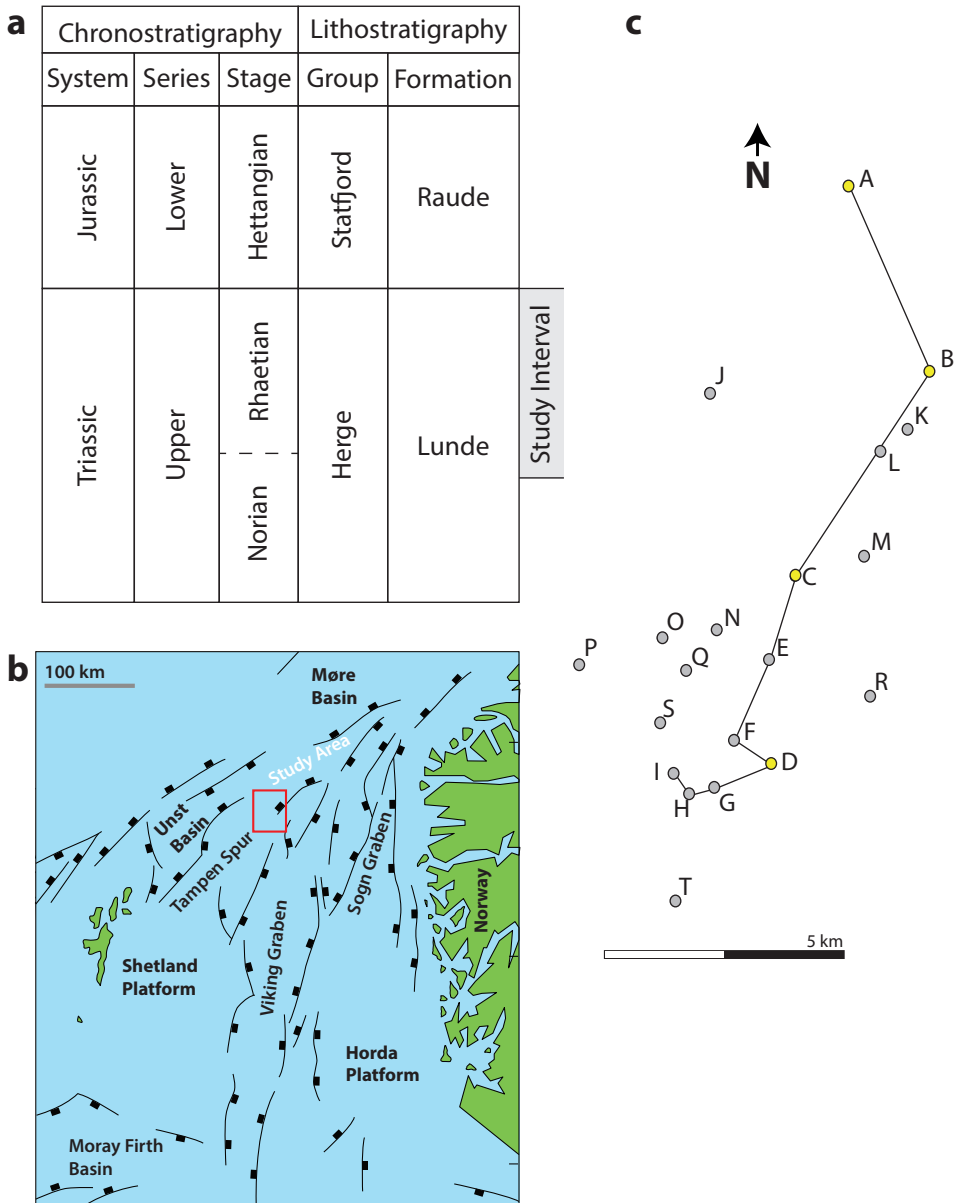


FIGURE 8.1 a) Chronostratigraphy and lithostratigraphy of the study interval in the Norwegian sector of the northern North Sea region (based on Nystuen et al., 2014 with ages from Gradstein et al., 2004). b) The structural features and basins of the northern North Sea with the study area highlighted by a red rectangle (modified after Nystuen et al., 2014). c) The relative position of all the wells used in the study. The transect used for well correlation is shown. The yellow highlighted wells are studies cored wells.

Snorre Field has not been observed based on the equal thickness recorded in the wells. The succession was uplifted and partly eroded during rifting in Late Jurassic to Early Cretaceous times. Uplift was followed by subsidence and burial during crustal cooling during the Early Cretaceous, and the studied succession became buried to depths of about 2.5 to 3 km.

8.2.2 Reservoir zonation

Due to an absence of good age control, stratigraphic zonation of the Lunde Formation has been challenging. The zonation was initially based on a sequence stratigraphic approach using correlation of base-level cycles (Mjøset et al., 2005). It was proposed that changes in base-level lead to changes in accommodation space (A) and/or sediment supply (S). Consequently, their relationship (A/S) resulted in repetitive patterns of sand occurrence and caliche (pedogenic carbonate) horizons which were used as markers for correlation. The top of the best-developed caliche and mudstone horizon often formed a zone boundary. Over the years, this zonation has been modified and adjusted as the zonation is continuously challenged by new data, such as improved seismic amplitude maps showing the extent of oil-filled sands intervals and 4D seismic data showing communication paths in the reservoir. Currently, the reservoir zonation is primarily driven by seismic correlation, and four main or “confident” reservoir zones are used as primary markers (personal communication, Sigrid Pillen, 2022). The seismic data show lithology contrasts and thicker sands (>10 m) with a shale below are recorded as an increase in acoustic impedance (density*velocity). When the sand is oil filled, this impedance will further enhance, and it will be brightened on the stacked far angles (25°-35°) of the seismic data.

The four confident horizons are labelled Top RZ-1, Top RZ-4, Top RZ-6 and Top RZ-9. They correspond to strong reflectors as the bases of thicker, often amalgamated, oil-filled sandstone packages. RZ-6 is believed to be correlated with the transition from carbonate-rich to carbonate-poor floodplain sediments. The seismic interpretation has been restricted to areas where a given horizon has been judged to be interpretable with a fair degree of reliability. The high level of structural fragmentation of the reservoir and high stratigraphic position of the oil-water contact (i.e. decreased seismic impedance below the oil-water contact) makes it challenging to trace all proposed reservoir zones with high certainty. For this reason, it was argued that a better technical solution is to model horizons from isochores rather than forcing speculative interpretations through seismic data (Olsen and Storemark, 2012). The isochores zonation is based on a constant thickness theory interpreted from gross thickness observations, stratigraphic correlations between cored wells, and the general North Sea subsidence model stating that the upper Lunde Formation was deposited during a passive thermal subsidence phase. This assumption results in a constant thickness of approximately 30 m per reservoir zone.

8.3 Methodology

8.3.1 Data and transect

Twenty-one wells were used in this chapter. All wells have been anonymised by name and depth. A transect has been made parallel to the average palaeoflow of nine wells (Fig. 8.1c). Four of these wells (A-D) are fully cored and have been analysed on floodplain sedimentology. The other five wells (E-I) are non-cored and were chosen due to their proximity to each other (<1 km). All wireline logs were

corrected for environmental borehole conditions. The wells were adjusted for borehole and structural deviation (average 10°) and displayed at true stratigraphic thickness. The study interval ranges from the top of RZ-4 to the top of the Lunde formation at the top of RZ-9. An additional twelve wells (J-T) were included in calculating average stratigraphic trends based on the existing stratigraphic reservoir zonation (discussed later in the methods).

8.3.2 Core descriptions

Logging of the cored wells was done by describing lithological and pedogenic features. Matrix and mottling colours were documented using Munsell colour codes (Standard Soil Colour Charts, Soil Survey staff, 1993). Mottling abundance and size were noted. The grain size was measured using a hand lens and grain-size reference cards. Occurrence, size and abundance of pedogenic carbonate structures were documented. Different pedogenic features were recorded. Alongside the descriptions, if identifiable, the soil horizons were labelled.

8.3.3 Stable carbon isotopes

Pedogenic carbonate nodules were sampled from the core for stable carbon isotope analysis. Two samples were taken at 25 cm intervals and drilled directly to powder using a microdrill. Small (<1 cm) pedogenic carbonate nodules were preferred during sampling and chosen when available. These structures cement relatively fast within the soil profile compared to the larger pedogenic carbonate structures resulting in less time-homogenised carbonised isotope values. Other pedogenic structures were sampled when the preferred small carbonate nodules were absent. The calcite structure type was noted with every sample (for more information, see Supplementary Data CH8S1). When sampling, the primary formed micritic parts of the pedogenic carbonate structures were chosen. The secondarily developed calcite spar was avoided as this can influence the stable isotope ratios.

Carbon and oxygen isotope ratios were measured at the Vrije Universiteit Amsterdam, the Netherlands, in their mass spectrometry laboratory. Gas (CO₂) was liberated from the samples in the solid phase by adding water-free phosphoric acid (100 % H₃PO₄) upon the carbonate under a constant temperature of 45°C in a clean vial flushed with Helium, whereafter Isotopic Ratio Mass Spectrometry was performed using the Finnigan MAT253. These isotope ratio measurements were normalised based on repeated measurements of in-house powdered carbonate standard (VICS), and analytical precision was calculated from the inclusion of three IAEA-603 standards.

A baseline, representing constant or 'background' intervals, was calculated by taking the average of the combined intervals over all wells. Carbon isotope excursion magnitudes were calculated as the difference between pre-excursion carbon isotope values and excursion values within the core of the main body. Standard errors were calculated using variability in background and excursion values. Floodplain stratigraphy

8.3.4 Soil profiles

Soil profiles and intervals were defined in the stratigraphic succession using the sediment characteristics of palaeosols and overbank deposits. An individual soil profile is defined as a single continuous interval of pedogenesis without significant, visible breaks. A break in pedogenesis can be caused by a phase of more rapid sediment accumulation, by less soil formation during a specific time driven by climate change, or by groundwater table changes (Kraus, 1999).

8.3.5 Soil development index

The intensity of pedogenesis was measured using a soil development index (SDI) to document the change in pedogenic development. Two approaches to this method were used. A soil profile method, as described by Abels et al. (2013) and as applied in Chapter 5, and a high-resolution method.

Soil profile method

The SDI methodology allows the recognition of soil development stages based on three key criteria: (1) palaeosol B-horizon thickness, (2) a simple assessment of the intensity of horizon development and (3) the amount of rubification of the palaeosol. Depending on the intensity, these parameters were assigned a number between 0 and 1. Next, the scores were standardised using two standard deviations of the total section. Then, the index per soil averages the three standardised parameters plus 1.0 to make the SDI positive between 0 and 2. A value of 0 indicates a lack of pedogenic alteration, and a value of 2 refers to high pedogenic alteration. A boundary of soil development was placed at the transition from below a value of 1.

The soil profile method applied here is based on the method defined for the lower Eocene Willwood Formation in the Bighorn Basin (Abels et al., 2013). Depositional conditions for the Willwood Formation differ from those of the upper Lunde Formation and are characterised by a semi-humid environment with more noticeable variation in soil colour (i.e., red, purple, brown vertisols) than in the Upper Triassic. Due to these colour differences, a different colour scoring has been used. Sediment matrix colours were grouped, and the level of rubification was compared to the intensity of pedogenic features. The grouping of sediment matrix colour in terms of pedogenic intensity was subsequently done by correlating the colours with the intensity of pedogenic features. This showed that high brightness colour correlates to better-developed palaeosol features (e.g. Munsell 10R-4/6), and low brightness colours correlate too weak to moderate palaeosol features (e.g. Munsell 5YR-5/6). The colour binning used is shown in Table 8.1

High-resolution method

In the high-resolution SDI method, the horizon development intensity has been calculated at 10 cm resolution instead of calculating a value for each B-horizon. The advantage of this approach is the better depiction of vertical changes, less biased towards soil profile recognition, and easier to generate for a non-specialist. For constructing this index curve, the intensity of different pedogenic features was combined with the grain size and the matrix colour (Table 8.2; Supplementary Data Ch8S2). The documented pedogenic features were the mottling intensity, slickensides intensity, rhizolith intensity, pedogenic carbonate intensity and size (small $1 < \text{cm}$; medium $1\text{-}2 \text{ cm}$; large $>2 \text{ cm}$), and preserved lamination presence (Table 8.2). After reviewing all the core material, an arbitrary scoring was applied for the intensity ranging from 0-3 for low, medium and high. The same matrix colour scoring was used as in the soil profile method. All parameters were standardised using two standard deviations of the total section. Subsequently, the index curve is calculated as the average of the combined parameters over 10 cm. A boundary of soil development was placed at the transition from below a value of 1.

8.3.6 Soil development based on well-log responses

Not all wells have cored intervals, and to estimate and extrapolate the level of pedogenic intensity in non-cored wells, the soil development index was estimated using a combination of V_{shale} and the sonic log. There is no direct relationship between the occurrence of the documented pedogenic features and

Class	Munsell colour code					Parameter	Scoring
1	10R4/6	7.5R4/6	2.5YR4/6	10R4/8		grain size	0-5
2	5YR4/4	10R4/4	10R4/3			mottling intensity	0-3
3	10R3/6	2.5YR3/6	5R3/6	7.5R3/6	2.5YR3/6	pedogenic carbonate intensity	0-3
4	10R3/4	2.5YR3/4	5YR3/4			pedogenic carbonate size	0-3
5	10R5/6	2.5YR5/6	5YR5/6	7.5R5/6		slickensides intensity	0-3
6	5YR5/4	10R5/4	2.5YR5/4			rhyzolite intensity	0-3
7	5YR6/4	10R6/6	7.5YR4/2			preserved lamination (negative scoring)	0-1
						colour scoring	0-7

TABLE 8.1 (left) and **8.2** (right) Left: The Munsell colour codes of the matrix found in the cores of the upper Lunde formation. The grouping of sediment matrix colour in terms of pedogenic intensity was done by correlating the colours with the intensity of pedogenic features such as slickensides and pedogenic carbonate content. Right: The scoring of the different sedimentary characteristics as input parameters for the high-resolution method of calculating a soil development index curve.

the top of soil development identified from core material (for more information, see: Supplementary Data Ch8S3). However, true overbank deposits characterised by the highest pedogenic alteration are generally the finest-grained sediments (e.g. Kraus et al., 1999; Varela et al., 2021). Thus, the V_{shale} forms a reasonable estimate of pedogenic development. The V_{shale} has been calculated using a combination of neutron and density readings as the gamma-ray measurements are prone to the leaching of potassium-bearing minerals such as K-feldspars, leading to low gamma-ray readings in fine-grained sediments (Nystuen and Saigal, 1993). Secondly, sonic well-log readings are generally narrow but spike near the top of palaeosol deposits. This spike is interpreted to be related to the maturity of a palaeosol as it can correspond to slickensides or pedogenic carbonate horizons (Cook et al., 2013).

Based on the V_{shale} and sonic, the top of a palaeosol is defined where a spike in sonic decreases in combination with the transition from a shaley to a sandy interval. This estimation is not as accurate as core-based identification and different confidence levels are applied to identifying boundaries. Three arbitrary confidence levels were assigned (high, medium, and low). High confidence is defined as a clear boundary in both V_{shale} and sonic logs, medium as only one of both logs is clear, and low confidence scores were given when a channelised body is (vertically) proximal or a boundary is not well identifiable in both records.

8.3.7 Well correlation

A floodplain-based correlation was constructed based on identified intervals of variability in pedogenic intensity in core and well-log data. The correlation exercise started at non-cored wells close to each other (< 400 m) and expanded to a maximum of 1 km of well spacing of two neighbouring wells. Individual splay deposits and specific grain-size trends within the floodplain deposits can aid the correlation at wells close to each other. The lateral continuity of these deposits is often larger than channelised sandstone deposits and may reach up to several kilometres of lateral extent (e.g. Mjøs et al., 1993; Reynolds, 1999; Millard et al., 2017), especially perpendicular to palaeoflow and thus lithological patterns in the floodplain deposits were used as an aid for correlation.

Due to the absence of other stratigraphic tie points with sufficient resolution, such as biostratigraphy or magnetostratigraphy, the top of the reservoir zone RZ-6 was used as a tie-point for the initial alignment of the wells. This marker can be traced confidently on seismic reflectors at 1-2 km scale.

After initial alignment, the reservoir zonation was not used further for any stratigraphic constraint. The cored wells (A-C) are positioned at a larger spacing (1-2.5 km), and at such lateral distances, the seismic marker is deemed less confident. Stable isotope excursions were used to integrate these wells into the correlation panel.

The same certainty scoring was used for the correlation as for the identification of pedogenic boundary identification. The scoring was based on trends in multiple subsequent boundaries. The similarity of patterns in the wells, such as the bundling of crevasse splays, allowed a high certainty of correlation. Otherwise, medium to low confidence scores were given to the correlations. Based on the stable carbon isotope records, the cored analysed wells were included in the floodplain-based correlation panel.

8.3.8 Average stratigraphic trends

A composite stratigraphic thickness was constructed by calculating the mean thickness of each correlated pedogenic interval and adding the means cumulatively. All nine wells were placed on the new depth scale by linear interpolation between the correlated boundaries of the floodplain-based stratigraphic framework. Vertical proportion curves of lithotypes were created (e.g. Volpi et al., 1997) using this composite stratigraphic thickness scale. This allows for average stratigraphic trends to be interpreted. The V_{shale} was used for sand content estimates and divided into four fractions ($0.2 < V_{shale} < 0.4$, $0.4 < V_{shale} < 0.6$, $V_{shale} > 0.6$). Lithofacies were calculated on wireline depth increments (15.24 cm), and the percentage of each facies was calculated on a 1 m interval for each well. A weighted average was applied and calculated using average V_{shale} subdivisions of all wells due to well clustering and unequal spatial distribution of the dataset. In this way, the concentrated well cluster (wells: F, G, H, I, and J) and possible overlapping sandstones do not skew the average. Weights were derived as the sum of the Euclidean distance from a well relative to all other wells (Supplementary Data Ch8S4). After applying the weighted average, the sand content was averaged over all wells.

A second vertical proportions curve (solution 2) was calculated to compare the floodplain-based stratigraphic framework with the existing reservoir zonation. In this case, a total of twenty-one wells were used. This calculation used the confident reservoir zones (the tops of RZ 1,4, 6, and 9) as tie points for constructing a composite stratigraphic thickness scale. Subsequently, the vertical proportion curve was calculated similarly as for solution 1.

8.3.9 Two-dimensional sandstone distribution

A two-dimensional spatial distribution of the sandstone occurrence was calculated using the reservoir zones-based composite stratigraphic thickness scale. The panel is projected onto a plane perpendicular to the average palaeoflow resulting in a west-northwest east-southeast oriented transect ($067^\circ - 247^\circ$). Channel belt width was calculated based on the thickness of the continuous sandstone intervals defined by the V_{shale} below 40% and is derived from the relationship derived by Fielding and Crane (1984):

$$W_{sst} = 49.5 * H_{sst}^{1.43}$$

Where H_{sst} is the measured sandstone thickness, and W_{sst} is the channel belt width. Because V_{shale} data does not differentiate between amalgamated or single-story sandstones, a splitting of the sandstone bodies was applied. In analysed cored wells, single-story sandstone bodies have a maximum

thickness of 11.5 m and, assuming a maximum of single-story thickness of 15 m thickness (Mjøs et al., 2005), channels above this thickness were split equally in half before individual sandstone width was calculated. A minimum thickness cut-off of 3 m (based on own observations and those by Mjøs et al., 2005) was applied to exclude thinner channelised deposits such as crevasse splay deltas.

It must be noted that the Upper Lunde Formation has a fluvial style that can be typified as high-sinuuous to meandering. This results in variable flow orientations of meandering channels, and plotting of sandstone bodies perpendicular to the average palaeoflow may lead to an overrepresentation of the width on the projection.

8.4 Floodplain sedimentology

Based on detailed observation and description of grain size, lithology, and sedimentary and pedogenic structures, a total of 640 m cored interval has been analysed. A general description and interpretation of the documented pedogenic and sedimentological features of the floodplain and channelised deposits are provided in the following sections. An overview is given in Figure. 8.2

8.4.1 Pedogenic structures

Root structures

Description:

Root structures are common to abundant in the upper Lunde Formation, and two different types of root structures are observed: tap roots and rhizoliths. Tap roots are presented as relatively large (1-5 cm width) vertically stacked carbonate nodules that fill the tap root outline and can be traced downwards from 10 to 80 cm (Fig. 8.3c). They are dominantly found in coarse-grained silt and very-fine sand deposit. The smaller rhizoliths represent a network of fine root traces, and abundant small carbonate nodules, commonly with dark-grey nodules from the root itself, filled with clay, are observed (Fig. 8.3d). The rhizoliths are dominantly found in clay to fine-grained silt deposits.

Interpretation:

The tap roots are interpreted to be formed by larger plants needing a relatively large amount of water to sustain the plant. Therefore, they likely grew at times of higher water tables or more proximal to channelised deposits (e.g. Zamian et al., 2016). Rhizoliths are interpreted to be formed by smaller shrub-like plants that need less water to sustain themselves compared to tap-root-type plants. The absence of a combination of the two structures suggests that smaller shrubs covered the distal floodplains while more proximal larger plants occupied the overbank. This is also reflected in tap root structures occurring more frequently in coarse-grained silt and very-fine sand.

Soil cracks

Description:

Besides bioturbation by roots, evidence of cracks in the soil are observed. Two forms are differentiated: larger fissures and smaller desiccation cracks. Fissures reach up to 70 cm in thickness and have a larger aperture (< 2 cm), while desiccation cracks are less thick (< 20 cm) and have a smaller aperture (< 2 mm). The fissures are usually filled with coarse-grained material than that of the surrounding matrix and have millimetre scale laminae running parallel to the walls (Fig. 8.3e). Desiccation cracks are often outlined by a grey mottling filled with a thin string of pedogenic carbonate (Fig. 8.3f). Furthermore,

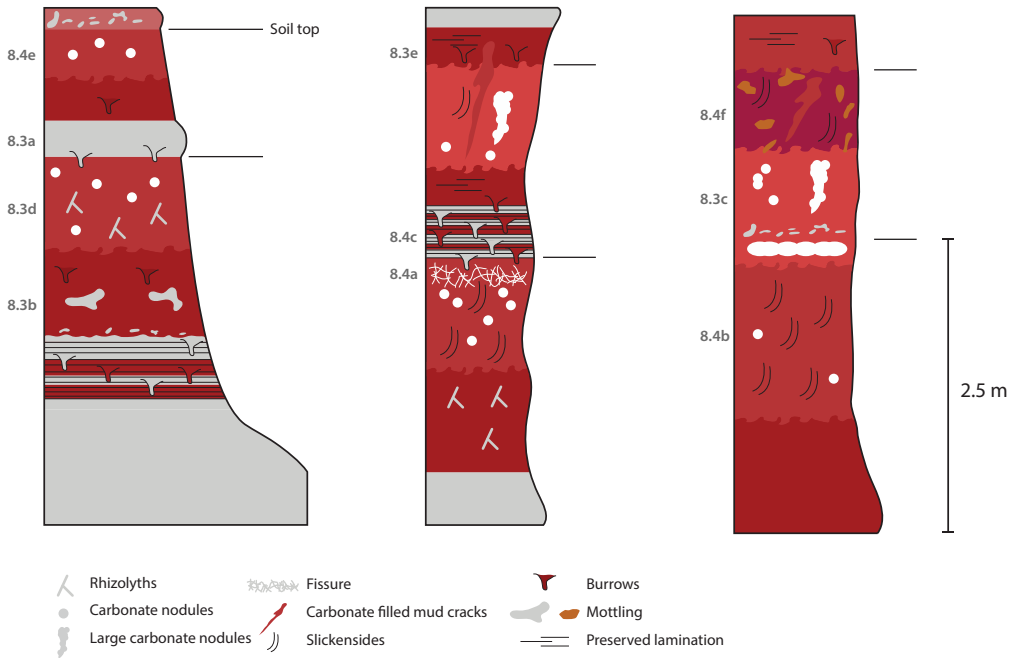


FIGURE 8.2 An overview of different palaeosol profiles and horizons found in examined cores. Figure numbers on the left of the columns refer to core photos in Figures 8.3 and 8.4.

boxwork textures are documented, forming a network of irregular fine fractures and veins extending up to 20 cm thick (Fig. 8.4a).

Interpretation:

All cracks are interpreted to be related to repeated wetting and drying of the soil. The coarse-grained infill of the fissures suggests that they gradually opened during several periods of wetting and drying, while the desiccation cracks are interpreted to have existed over a smaller period. The boxwork textures likely form during prolonged periods of subaerial exposure due to repeated wet and dry periods and are often filled with pedogenic carbonate (Müller et al., 2004).

Slickensides

Description:

Slickensides are observed as smoothly polished surfaces and can best be observed on fresh broken core material. An abundance of slickensides is found in finer grain-sized clay to fine silt deposits where the core is often finely broken.

Interpretation:

Slickensides are interpreted as frictional movement surfaces caused by seasonal changes. This can occur over several wetter seasons when the swelling pressure of the rocks exceeds the shear strength. Well-developed slickensides are often an important indicator of maturity in palaeosol as it takes more seasons to form well-developed slickensides (Kraus, 1996).

Clay aggregates

Description:

Several occurrences of soil pebbles which form lumps of densely aggregated clays are recognised. They have a spherical to semi-angular shape, range from mm-scale up to 5 cm and are surrounded by films of more loose clay (Fig. 8.4b). They occur both in intervals with abundant pedogenic features and with fewer to none. In intervals with abundant pedogenic features, the shape of these pebbles is spherical; in intervals with low pedogenic features, the shape is predominantly semi-angular. In the resin-poured slabbed core, these features are often hard to recognise while they are well identifiably on the non-resin and non-slabbed core.

Interpretation:

Müller et al. (2004) examined several cores of the upper Lunde Formation (among which wells A and B) and also documented this phenomenon, naming these pedogenic mud aggregates. While the formation of such aggregates is still unclear, it is hypothesised that they form due to the binding by organic compounds sourced by organisms. The spherical shape is believed to be formed in-situ, while the semi-angular soil pebbles are interpreted as reworked floodplain material (Müller et al., 2004). When reworked and compacted, intervals with semi-angular soil pebbles can be confused with more developed palaeosol intervals. Therefore, it is essential to recognise this 'pseudo-pedogenesis' as it can lead to erroneous determination of the level of pedogenic alternation. Massive structureless fine-grained intervals without other pedogenic features such as slickensides, mottling or root structures are interpreted to have seen a low amount of pedogenesis. An examination of the core slab and the untreated sample half is necessary to detect this properly.

Bioturbation

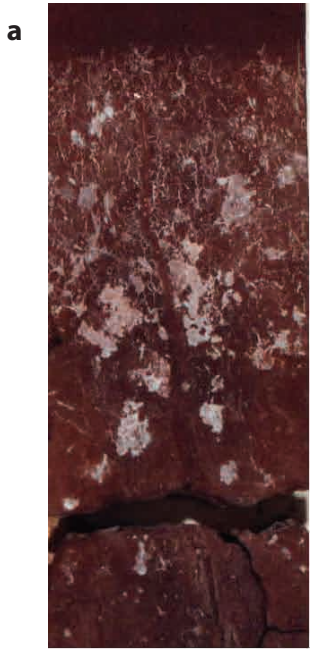
Description:

Burrows are commonly found in the core (Fig. 8.3b). They have a cylindrical shape and are non-branching with a vertical orientation, and the fill of the burrows is meniscate or featureless. They vary in length from 1 to 6 cm and range from 2 to 10 mm in diameter. They are best visible in relatively immature palaeosol deposits or in grey-bleached intervals where the burrows move in and out of the grey horizon.

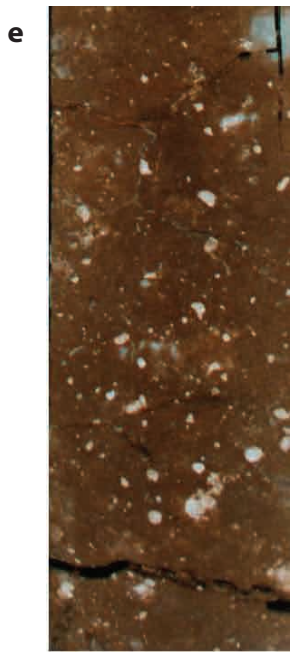
Interpretation:

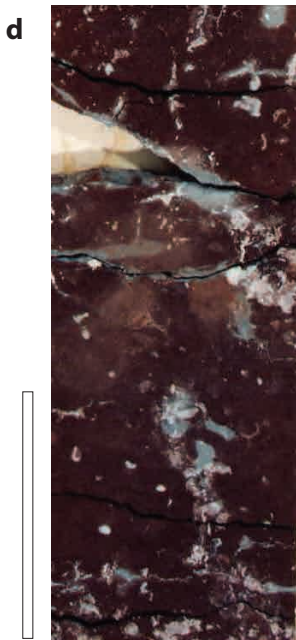
Based on their size and structure Nystuen and Sagal (1993) suggest they belong to the *Scoyenia* ichnofacies and are produced by fresh-water arthropods. The observation of burrows moving in and out of the grey bleaching horizons suggests that these bleaching horizons were formed during the

→ **FIGURE 8.3** An overview of several palaeosol and overbank characteristics. a) a boxwork texture associated with abundant calcite precipitation when the soil has subaerial exposure causing small cracks. b) Spherical soil pebbles formed of lumps of aggregated clays which are surrounded by films of loose clay. c) Laminated fine-grained shallow water deposited modified by an early stage of pedogenesis and rubification. e) Floating pedogenic carbonate nodules in a red matrix. Note how some carbonate nodules have an angular shape, suggesting a reworked origin. f) A purple soil matrix with distinct and abundant yellow mottling.

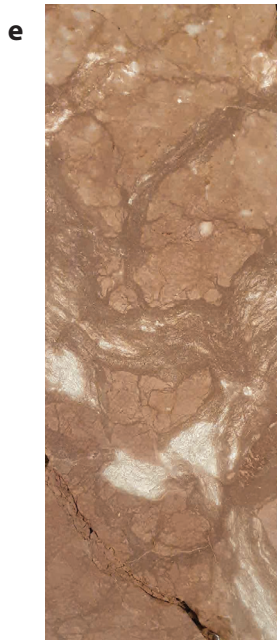


8 cm





8 cm



← **FIGURE 8.4** An overview of some palaeosol characteristics of the upper Lunde formation: a) a bleaching horizon in grey displaying small carbonate nodules at its top. Note the sharp transition from red to grey. b) Preserved original lithologic colours in light greenish-grey and starting rubification of the palaeosol with brownish colours. The unmodified, light greenish-grey sediments show preservation of slightly bioturbated lamination structures, c) Thick, vertically-stacked pedogenic carbonate structures interpreted as tap root structures filled with carbonate, d) whisp grey structures nodules interpreted as rhizocretions that are related to fossil traces of plant roots here also small pedogenic carbonate nodules are present. e) A larger fissure crack through a palaeosol matrix. Note the distinctive laminae running parallel to the walls of the crack, indicating infill after cracking. f) A small desiccation crack filled with calcite and bleached in grey due to preferred water movement alongside the crack, likely during diagenesis.

pedogenic stages and, not afterwards, during burial. Combined with the suggestion of freshwater arthropods, it could be that a groundwater table level forms these bleaching horizons.

8.4.2 Coarse-grained overbank deposits

Splay and levee deposits

Description:

Splay and levee deposits are medium- to very fine-grained to silty with moderate to poor sorting, and often have pedogenic alternation. Such deposits vary from individual sandstones with 10 cm to 1.5 m vertical thickness up to a stacking of 2-3 m vertical thickness and commonly have horizontal, planar lamination with occasional observations of current ripples in medium-grained sandstones. They are often bedded at a decimetre scale, and the thicker units (> 50 cm) have a coarsening-upwards grain-size profile.

Interpretation:

Decimetre-scale individual beds are interpreted as single events of non-channelised flooding distal from the source channel and show the highest level of pedogenesis. This can be up to full rubification and pedogenic alternation of the sediments with only grain size indicating a flooding event. The thicker (>1m) and coarse-grained sandstone units are likely deposited as crevasse channels and splays. However, some of these profiles may also represent (distal) levee deposits.

Flooding-related deposits

Description:

Flooding-related deposits are finer-grained than the splay and levee deposits and are fine to very-fine grained, with millimetre scale, parallel lamination and they can reach up to 1.5 m in thickness (Fig. 8.4c). Often, the original textures are partly removed by pedogenic alteration and bioturbation and several bleaching and rubification horizons are present.

Interpretation:

These intervals are interpreted as representing the distal and wetter part of splay deposits. They most likely represent confined wetter areas, possibly small ponds or waterholes, on the overbank, which can be caused due to micro-relief (also known as gilgai; Paton, 1974) on the floodplain and are not interpreted to be laterally extensive.

8.4.3 Sediment colour

Description:

The colours of the palaeosol in the Lunde Formation can be generally described as red. Dark red to red colours (Munsell 10R4/6, 5R5/6) occur more often in intervals with a higher pedogenic development (slickensides, soil cracks), while intervals with lesser pedogenic development usually have a duskier red to red-brown colour (Munsell 5YR-5/6, 10R3/4). Bright red intervals (Munsell 10R-4/4) are often found when large or abundant pedogenic carbonate structures are present. Besides the brown to red colour spectrum, dark red intervals with distinct purple mottles up to a purple matrix colour (Munsell 5R-4/4) have been documented in core C (Fig. 8.4c). In such intervals, the carbonate content is relatively low.

Several different types of mottling patterns are documented in the upper Lunde Formation. Most of these mottles are formed by iron depletion due to the removal of the red hematite pigment resulting in grey-greenish mottles on a centimetre to decimetre scale. These can be observed along sedimentary structures such as root traces, cracks and carbonate nodules and are linked to a preferential water flow and dissolution around these structures. Furthermore, red to brown (Munsell 10R-4/4, 5YR-6/4) mottling can be observed on a centimetre scale in the matrix of the palaeosols.

In addition to the red colour spectrum, grey-greenish colours are also documented. These grey-greenish colours (Munsell 10GY-6/1, 7.5YR-7/2) occur more frequently in the more permeable silty-sandy layers (Fig. 8.3a). A lighter greenish grey (Munsell 10Y-8/2) colour can be observed when there is no or minor pedogenic alteration. Occasionally in these zones, red mottles are documented with upwards increasing intensity.

Interpretation:

The fast occurrence of rubification after channelised or coarse-grained deposits, where often relict bedding is still present, suggests that the process of rubification acts rapidly and before other pedogenic features occur. There is a good correlation between pedogenic intensity and brightness of the rubification, indicating an effect of pedogenic processes on the early rubification. The purple colour indicates wetter conditions or increased seasonality compared to a red palaeosol and is caused by goethite instead of hematite deposition (Kraus, 1996).

The light greenish grey is interpreted as the original lithological as no pedogenic alternation is observed, and the red mottling is increased upwards and forms a transitional stage of pedogenesis. In combination with the documentation of bioturbation, the darker grey-greenish colours are likely bleaching zones and groundwater-related.

8.4.4 Sandstone sedimentology

The approach taken in this chapter focuses on using the various types of floodplain sediments and their stratigraphy as a framework to characterise reservoir properties. Only a simple characterisation of the channelised sandstone bodies in the examined cores is provided here.

Description:

Most single-story sandstone bodies have a thickness between 5 and 12 m (mean: 6.8 m; SD: 2.4; n=81; Fig. 8.5). Sandstone bodies predominantly occur as single-story bodies displaying fining-upward grain size trends. Multi-story bodies more often do not show grain-size trends within individual stories.

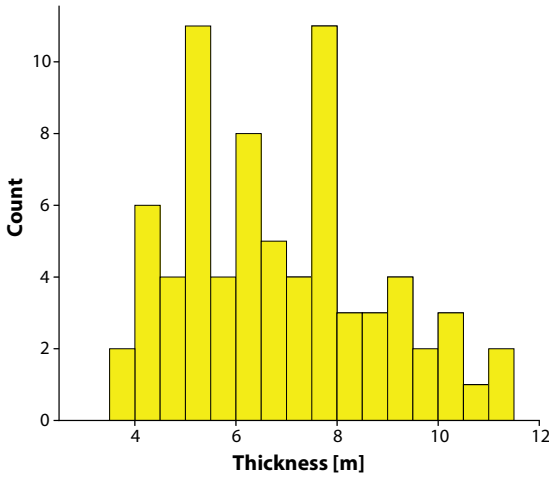


FIGURE 8.5 The thickness distribution of single-story sandstone bodies from core and well-log data of the transect. A minimal cut-off of 3 m is used, and differentiation between splay and channelised deposits has been made on the V_{shale} log-shape.

The base of the channels commonly consists of coarse-grained sandstones, including reworked pedogenic carbonate nodules (Fig. 8.3d). Calcite cementation is often observed near reworked pedogenic carbonate nodules. Above the base of the channels, fine- to medium-grained, decimetre-scale through-cross-stratified beds and/or very-fine to fine parallel laminated and structureless beds occur. Coalified plant debris and rip-up clasts of dark, organic-rich mudstones are found in one channel sandstone body. The uppermost part of a sandstone body typically consists of fine- to very fine-grained sandstones alternating with thin beds of bioturbated silt and mudstone. These tops do often display rubification in the form of individual, cm-size round mottles. Bioturbation can be found in the top of the sandstones forming up to 2 cm thick burrows in a vertical direction. Gamma-ray and V_{shale} log responses of the single-story sandstone bodies are bell-shaped, while multi-story bodies have and block-shaped pattern.

Interpretation:

The dominant occurrence of single-story channel sandbodies with fining-upward grain-size trends is interpreted as related to isolated, sinuous channels occurring within mud-dominated floodplain strata of the upper Lunde formation (Nystuen et al., 2014). The multi-story sandbodies that lack grain size trends could point to more braided-like river planform styles that contain more mid- or side-channel barforms indicating higher bed load transport possibly related to times of more flashy discharge, increased discharge and/or increased sediment delivery (e.g. Wang et al., 2022). The occurrence of pedogenic nodules in channel lag deposits indicates the reworking of the overbank fines by the channels scouring in adjacent floodplain strata. The coalified plant debris and rip-up clasts of dark, organic-rich mudstones can point towards periodically high groundwater levels in depressions and abandoned channel segments (Nystuen et al., 2014).

8.5 Floodplain stratigraphy

8.5.1 Soil profiles

Identifying individual palaeosol profiles in the Upper Lunde Formation has shown to be challenging as there are often relatively thick, cumulative palaeosol intervals without distinct, visible 'breaks' in pedogenesis. Crevasse splay sediments are often incorporated into the palaeosol profile and are only identifiable by grain size change. Nonetheless, subtle changes in pedogenesis can be observed and used to identify breaks in pedogenesis. Changes within the floodplain successions are characterised by a combination of soil colour, the intensity of pedogenic structures and grain size (Supplementary Data Ch8S5). Soil profile tops are positioned at the change from many pedogenic intervals with bright colours and mottling (10R-4/6) to intervals with less pedogenic structures and lower brightness (10R-4/2). Soil profile tops are identified macroscopically and pinpointed in the lithological columns (Fig. 8.6 and 8.7). In total, 258 individual soil profiles have been identified in 387 metres of floodplain sediments with an average soil profile thickness of 1.5 m.

8.5.2 Pedogenic intensity variability

The macroscopic, visual description of the overbank fines allows the floodplain sediments to be grouped based on pedogenic intensity. One group displays intense pedogenesis, and another group shows weak to moderate pedogenesis. Intervals with intense pedogenesis are characterised by a high-brightness red colour and a relatively fine grain size of clay to fine silt. They have abundant slickensides or larger and abundant pedogenic carbonate structures, such as thick tap roots or fissures and boxwork textures. Intervals showing low to moderate pedogenic overprints display a low brightness, red to red-brown or greenish-grey matrix colour, a clay to fine-sand grain size, and often sedimentary structures like lamination and small-scale cross-bedding. Overall, these deposits are more heterolithic than the intensely pedogenized intervals with multiple, usually thin, pulses of relatively coarse (silt to fine-sand) sediment present. They regularly display animal burrows, grey mottling and/or bleaching horizons. Typically, splay deposits are found here, and other flooding-related deposits, such as small waterholes, are identified.

These two groups alternate stratigraphically on a relatively regular basis in the thicker (>10-15 m) floodplain intervals, and, in total, thirty-four of these alternations are identified by visual inspection in the studies cores (Fig. 8.5 and 8.6). The recognition of the floodplain cyclicity becomes challenging in stratigraphic intervals with thicker and more frequent channelised sandstone bodies. Strong and weak pedogenesis alternation can differ if vertically near a channelised sandstone deposit. The proximity of a fluvial channel can cause a higher, more frequent input of sediment to the floodplain and interfere with the continuation of pedogenic processes (Kraus and Aslan, 2009). This can also cause the pedogenic intensity difference between the phases to be less pronounced or overprinted. Floodplain cycles are not recognisable in thinner floodplain intervals of less than 10 m between channelised sandstones.

Using the soil development index method, similar alternations in pedogenic intensity as the macroscopic visual description are identified, and for both methods applied, the soil top and high-resolution position of the highest point of pedogenic intensity are comparable (Fig. 8.6). The soil profile SDI record allows more easy recognition of changes from high to low pedogenic alteration as the transitions are better pronounced. The high-resolution SDI method suggests a relative continuity of sedimentation which is unlikely in fluvial floodplain records. Therefore, the soil profile SDI method was used to define floodplain alternation boundaries in the cores.

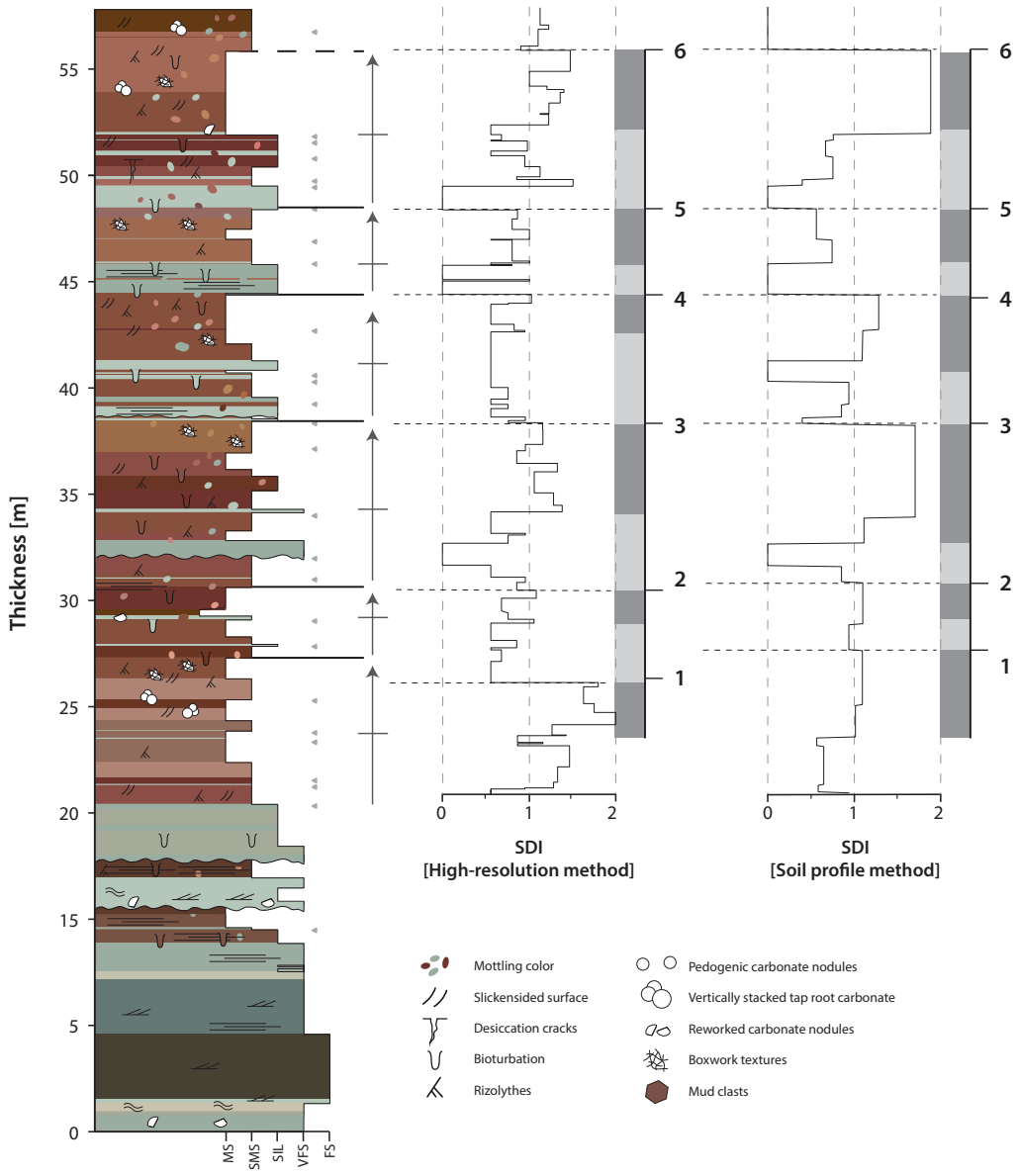


FIGURE 8.6 The lithology of well A with the observed floodplain sequences, soil profile tops and the two methods (soil profile and high-resolution) for calculating a soil development index. Note the minor differences between the two methods in floodplain sequence boundary definition and soil thickness.

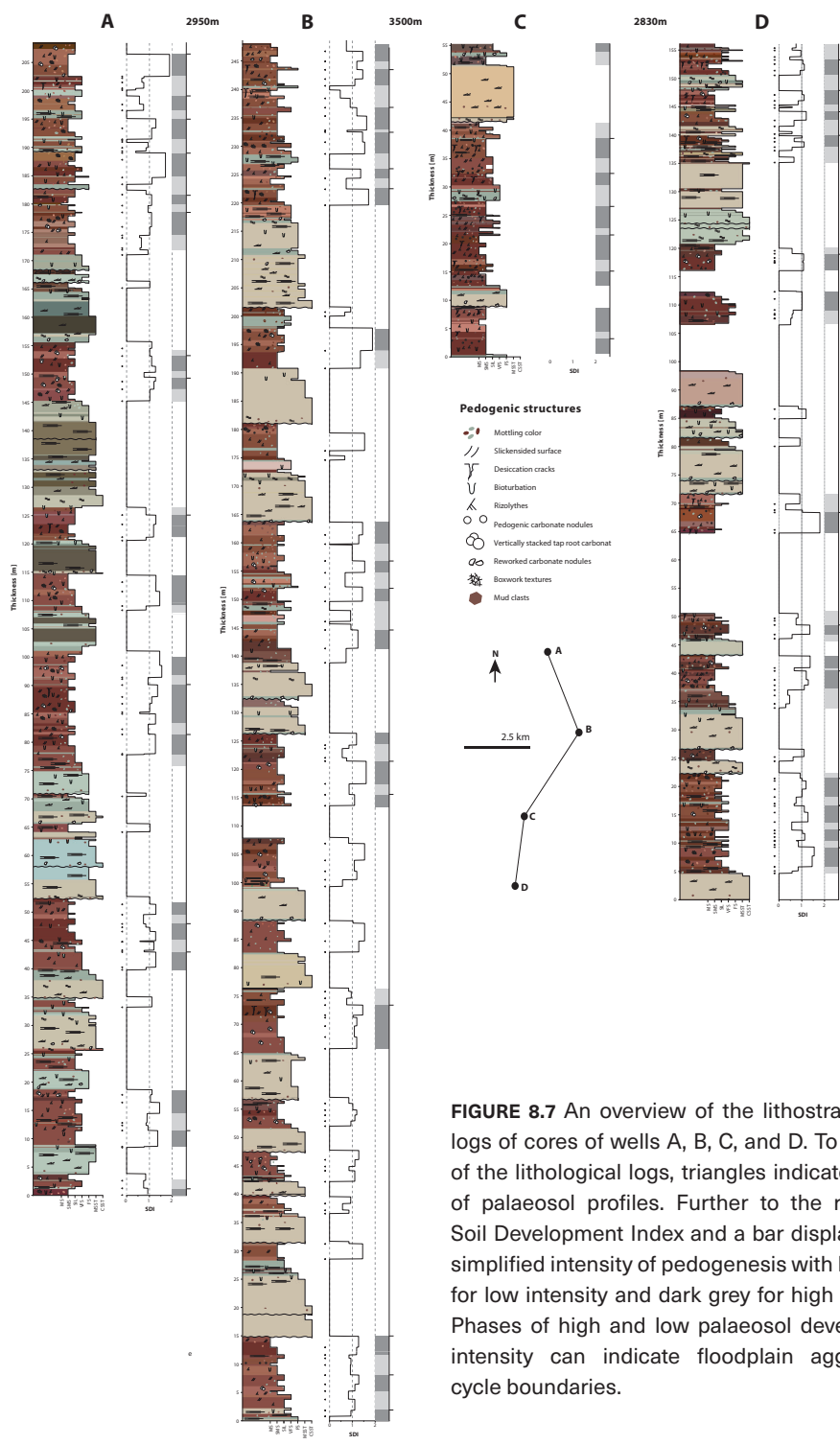


FIGURE 8.7 An overview of the lithostratigraphic logs of cores of wells A, B, C, and D. To the right of the lithological logs, triangles indicate the top of palaeosol profiles. Further to the right, the Soil Development Index and a bar displaying the simplified intensity of pedogenesis with light grey for low intensity and dark grey for high intensity. Phases of high and low palaeosol development intensity can indicate floodplain aggradation cycle boundaries.

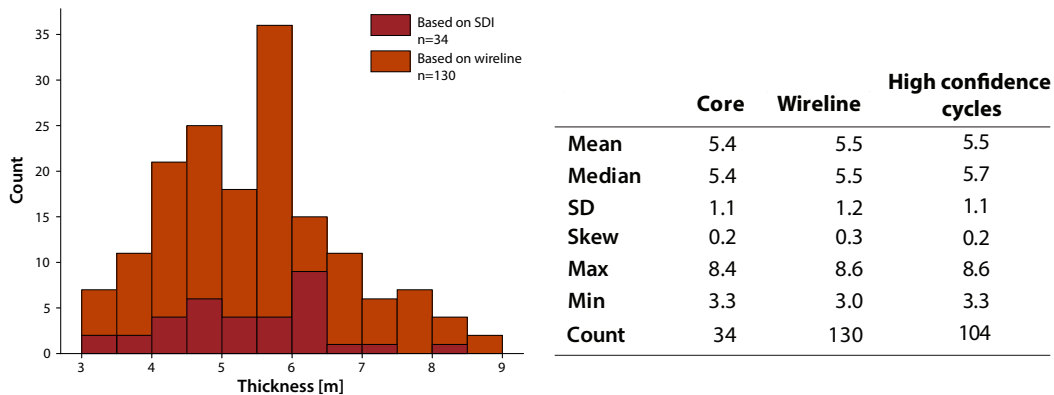


FIGURE 8.8 and **TABLE 8.3** The thickness distribution of floodplain aggradation cycles in cored and non-cored wells and for cycles which have given a high confidence score of recognition. Note the significant spread in thickness ranging from 3 up to 9 meters.

8.5.3 Floodplain alternations in 1D

Thirty-four complete floodplain alternations are recognised in the four cored wells based on the SDI curve (Fig. 8.7). Cycle transitions were positioned at the change from a value above to a value below one. The alternations range from 3.3 to 8.4 m with an average of 5.4 m (SD. 1.1, skewness: 0.2; Fig. 8.8; Table 8.3). Parallel results were found in the six non-cored wells, distinguishing 130 floodplain alternations (Fig. 8.12). These have similar thickness characteristics as cycles identified from the core. Cycles range from 3.3 to 8.4 m in thickness and average 5.5 m (SD: 1.2, skewness: 0.3; Fig. 8.8, Table 8.3).

For the non-cored wells, pedogenic intensity is estimated based on the assumption of response to V_{shale} and sonic well-logs. Here, the proposed confidence levels of boundary identification help increase robustness. 142 of the defined cycles have a medium (n=72) to high (n=70) confidence level for both the top and base of the alternation, while only 22 alternations have either a top or base defined with low confidence. A smaller channelised sandstone often truncates these cycles. Alternations with a relatively high thickness (> 6.5m) often (74%) have a large proportion of coarse-grained material ($V_{\text{shale}} < 0.40$) in the base of the cycle. Combined, the confidence non-cored identified cycles and the core-defined cycles have an average thickness of 5.5 m (SD: 1.1; skewness: 0.2; Table 6)

8.6 Stable isotope stratigraphy

In total, 2483 samples of pedogenic carbonate were taken and divided over the four cored wells (A-D). The Upper Lunde is characterised by average values of $\delta^{13}\text{C}$ -6.0‰ (SD: 2.0) and $\delta^{18}\text{O}$ -6.0‰ (SD: 1.28) and a wide range in values ($\delta^{13}\text{C}$: -3.1 to -11.5‰; $\delta^{18}\text{O}$ -2.8 to -11.1‰; Table 8.4, Fig. 8.10). Small scale stratigraphical variability is present as 87% of all the samples within a 10 cm vertical distance of each other have a spread up to 2.0‰. The internal variation within large carbonate nodules (>1 cm) has a standard deviation lower than 1.0‰ (Supplementary Data Ch8S6). Comparison between the $\delta^{13}\text{C}$ and $\delta^{18}\text{O}$ isotopes allows to assess the variability of the different groups of calcite structure sampled. The different classified pedogenic structures show no apparent clustering except for samples

	All cores	A	B	C	D
$\delta^{13}\text{C}$ [‰]	-5.96	-6.17	-5.29	-5.38	-6.75
SD	2.02	1.84	2.10	1.67	1.46
$\delta^{18}\text{O}$ [‰]	-6.89	-6.79	-7.24	-6.76	-6.68
SD	1.28	1.30	1.20	1.28	1.35

TABLE 8.4 Average $\delta^{13}\text{C}$ and $\delta^{18}\text{O}$ results and variation for all samples and per individual well.

	Core	Depth	Magnitude	Standard Error	Excursion	Type
A	187	4.44	0.37	5	onset	
A	155	4.31	0.35	4	onset	
A	115	2.25	0.42	3	recovery	
A	85	2.29	0.13	2	recovery	
B	217	5.60	0.39	4	onset	
B	180	2.70	0.18	3	recovery	
B	146	2.20	0.38	2	recovery	
B	115	4.05	0.31	1	recovery	
C	8	3.89	0.34	4	onset	
D	145	2.96	0.31	5	onset	
D	119	4.24	0.11	4	onset	
D	71	2.26	0.48	3	recovery	
D	37	2.14	0.12	2	recovery	
D	10	4.21	0.11	1	recovery	

TABLE 8.5 All observed carbon isotope excursions (Fig. 8.9) and their mean magnitude, standard error, correlation number, and correlation point.

taken from channelised sandstone bodies. Such samples show a more negative value ($\delta^{13}\text{C}$: -8‰, $\delta^{18}\text{O}$: -9‰; n=7; Supplementary Data Ch8S6). A complete sensitivity analysis is provided in supplementary data Ch8S6

A baseline of -4.5 ‰ (SD: 0.9) is defined (Fig. 8.9). No large-scale trends (> 50 m) are identifiable based on this baseline. However, fourteen carbon isotope fluctuations between 2 and 4.5‰ (Table 8.5) are identified. Due to the fragmented floodplain record, not all excursions are fully documented, and either onset or recovery is identified. There is no evident relationship between documented sedimentological and lithological characteristics of the floodplain and the excursions.

8.7 Floodplain-isotope-based well correlation

8.7.1 Floodplain correlation

The documented floodplain alternations identified in core and well-logs are used to correlate wells and generate a floodplain-based stratigraphic framework. The correlation starts on a cluster of wells proximal to cored well D with wells H, I, and J. The spacing between these wells is 330, 380 and 620 m, respectively. The floodplain alternations are already identified per well, and the wells are correlated using the top RZ-6 as the initial loose tie-point (Fig. 8.10). Furthermore, similarities in coarse-overbank deposits are used. Subsequently, the correlation is extended to wells D, E, F, and G. The

extension to these more distant wells is done using the same method of initial, loose alignment of the top of RZ-6, and the lithological patterns (Fig. 8.11).

8.7.2 Isotope correlation

The documented negative carbon isotope excursions were used as an independent basis for well-to-well correlation to include the cored wells (A-C) in the floodplain-based stratigraphic framework. Five negative carbon isotope excursions were correlated across the wells (Fig. 8.9). Since the carbon isotope record in individual wells is fragmented because sandstone intervals are devoid of data and cause gaps in the floodplain record, the excursions can be correlated with different options with individual wells shifted up and/or down. The possibilities were referenced against seismic reflectors and the reservoir zonation, resulting in one most-likely solution of isotope excursion correlation (Fig. 8.12). Other correlations between the isotope excursions produced discrepancies in seismic markers between wells above 30 m and thus above seismic resolution. Three of the correlations have high confidence as the magnitude of the excursion is large (excursions 1,4 and 5; Table 8.5), while two have lower confidence due to a lower magnitude of the excursion (excursions 2 and 3; Table 8.5). Based on the isotope excursion alignment, the identified floodplain alternations were correlated and integrated into the correlation panel.

8.7.3 Resulting stratigraphy

Thirty-seven consecutive floodplain alternations are correlated over 200 m stratigraphy (Fig. 8.11). The lower 80 m of the correlation panel up to cycle 15, in reservoir zones RZ-3 and RZ-4, has a relatively low number of correlatable floodplain alternations. A higher net-to-gross ratio characterises this interval, and longer stratigraphic intervals of floodplain fines are scarce, making a complete floodplain-based correlation more difficult as the identified alternations in adjacent wells are often not overlapping. In wells B, C and E, there is a floodplain-rich interval in cycles 2 to 5, allowing a correlation of more than two consecutive floodplain cycles and so increasing confidence. Upwards, from 80 to 100 m straddling alternations 16 to 20, the net-to-gross ratio decreases and the floodplain-based correlation gains confidence and stratigraphic resolution. In seven of the nine wells (C, D, E, F, G, H, and I), a floodplain-rich interval can be correlated continuously. In the other two wells (A and B), a large and amalgamated sandstone body is positioned in this interval.

Further upwards, from 110 to 150 m and alternations 20 to 27, an interval with increased net-to-gross levels is correlated between wells D, E, F, H, G, and I, all in close proximity of each other. This depth interval roughly covers RZ-6 and the seismic solid marker of the top of RZ-6. Using the isotope stratigraphy, floodplain cycles and patterns found in the floodplain fines, the floodplain-isotope-based correlation panel correlates this zone similarly to the interpreted seismic correlation. The amalgamated sandstone interval is not observed in wells A, B and C, and floodplain alternations are correlated. Finally, from 150 to 200 m and alternation 28 to 37, there is a relatively low sandstone content. Here, the floodplain correlation again has high confidence.

8.7.4 Comparison with reservoir zonation

The offset between the existing reservoir zonation and the floodplain-isotope correlation framework reaches a maximum of 24 m (Fig. 8.11; excursion 4, wells: A and B, reservoir zone top RZ-6). The maximum and minimum offset of each reservoir zone is given in Table 8.6. In all cases, the maximum

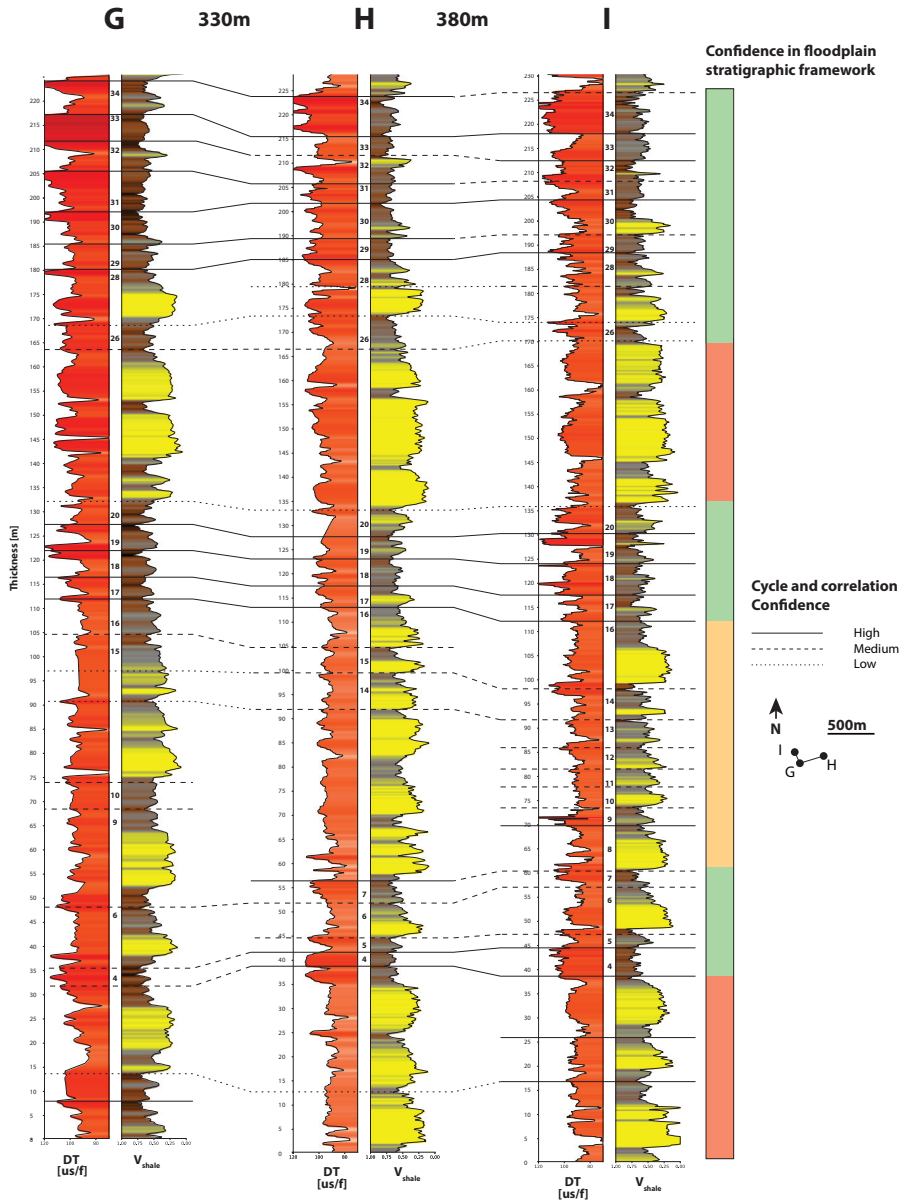


FIGURE 8.10 A zoom-in on the correlation of Wells H, I and G. These wells are relatively close by located towards each other with a 330 and 380 m spacing between them. Due to this proximity, the correlation exercise started here, where lateral variation is expected to be the smallest. The wells are correlated based on the defined floodplain alternations and matching V_{shale} and sonic patterns. Confidence in correlation scores are given with high, medium and low and the floodplain-based stratigraphic framework's relative vertical resolution is shown in green, yellow and red. The colour fill of the V_{shale} is based on a continuous fill between 0 and 1.

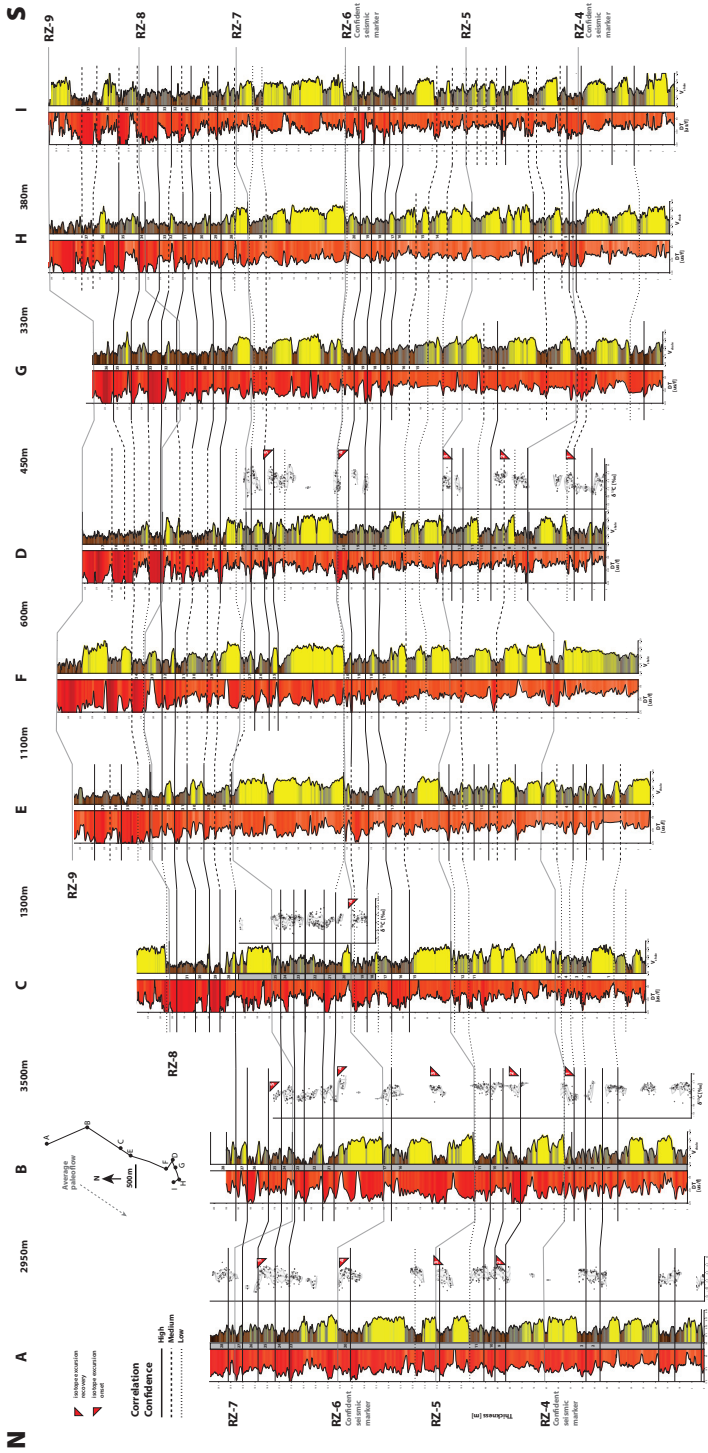
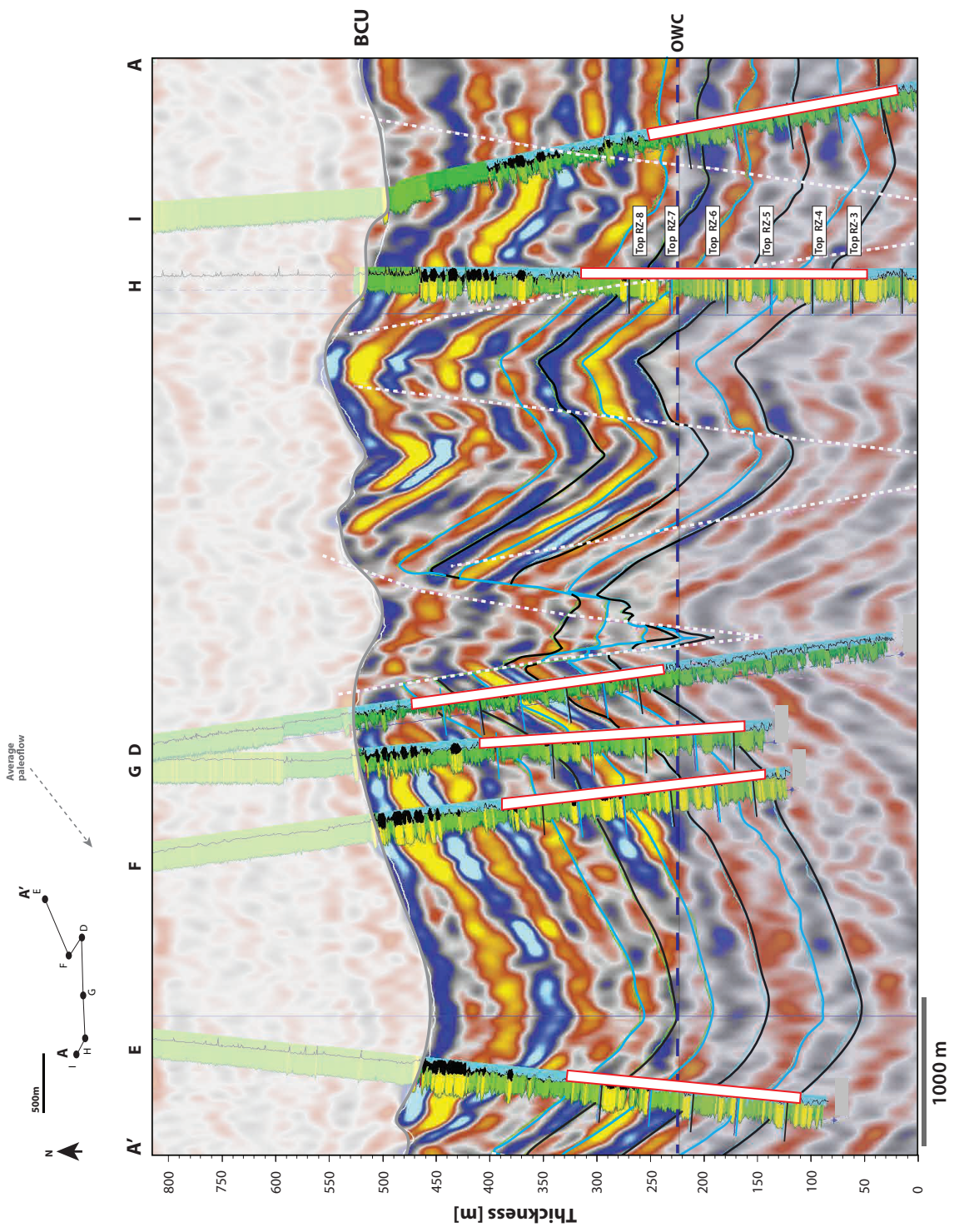


FIGURE 8.11 An overview of the cored and non-cored wells correlated based on floodplain alternations and isotope excursion. Given is the sonic log, V_{shale}, and stable carbon isotope stratigraphy. The transect follows the average palaeoflow from northeast to southwest. Red numbered triangles mark the correlated excursions and if the onset or recovery was used (see Fig. 8.9). The cored sections of wells A-D are highlighted in grey, and floodplain alternations are numbered. The confidence of correlation is shown with full, dashed, and dotted lines. The tops of the reservoir zones (RZ-4 to RZ-8) are shown as dark grey lines. The colour fill of the V_{shale} is based on a continuous fill between 0 and 1.



← **FIGURE 8.12** A seismic profile (far stack) between wells E, F, G, D, I, and J. In back and light blue lines, the isochroned reservoir zones are displayed. The V_{shale} log of the wells is displayed, and the studied intervals are marked white. The oil-water contact (OWC) reduced the impedance of the seismic reflectors as they mainly react of the oil-filled sandstones. BPU: Base Permian Unconformity.

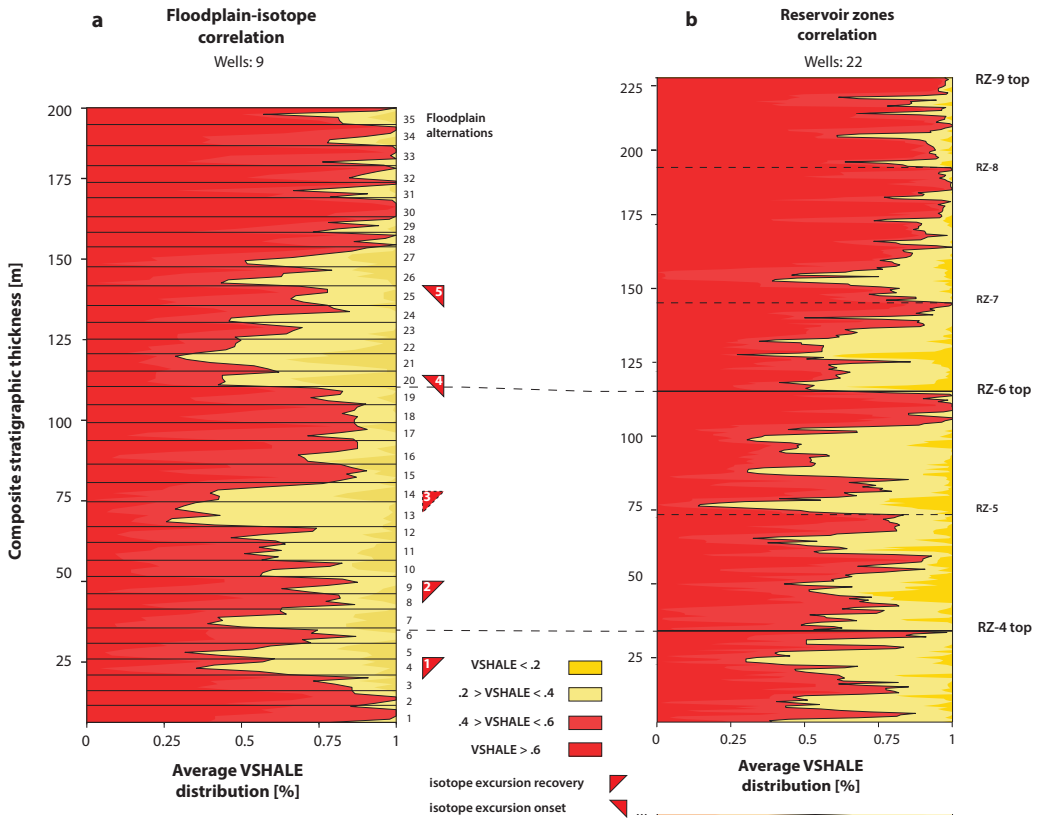
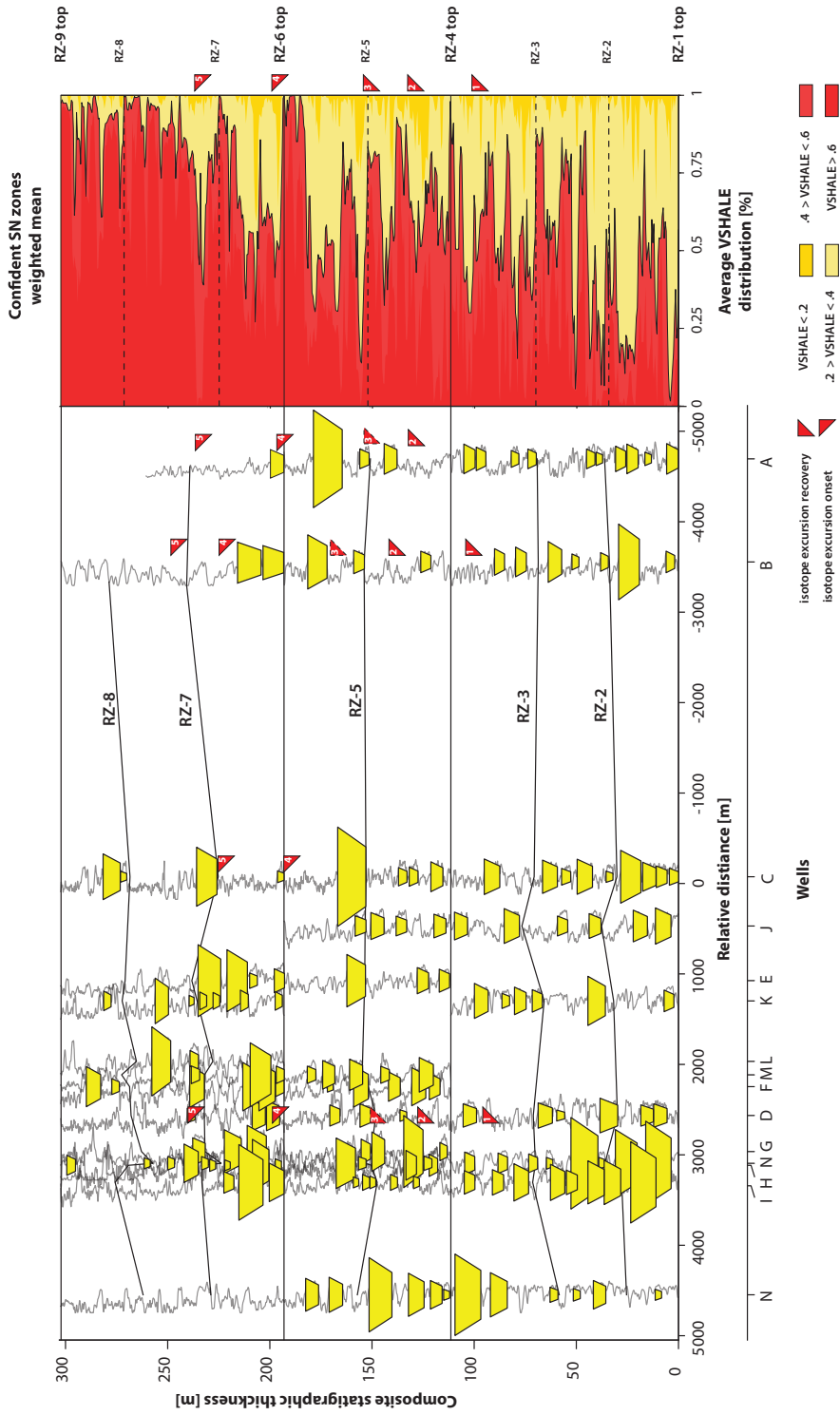


FIGURE 8.13 a) Vertical proportions curves calculated based on the nine wells correlated in the floodplain-isotope framework. On the right, the floodplain alternations and carbon isotope excursions are displayed. b) Vertical proportions curve calculated based on the strong seismic markers of the tops of RZ-1, -4, -6, and -9. The other reservoir zones have been interpreted based on the thickness and trends in sandstone occurrence.



Reservoir zone	Thickness difference [m]	Wells with largest difference
Top RZ-4	max 22	D - I
	min 3	
Top RZ-5	max 16	A - B
	min 3	
Top RZ-6	max 19	A - B
	min 1	
Top RZ-7	max 24	I - B
	min 1	
Top RZ-8	max 19	I - G
	min 2	
Top RZ-8	max 18	I - G
	min 6	

TABLE 8.6 The maximal and minimal offset of reservoir zones between wells based on the floodplain-isotope correlation.

offset from the reservoir zone boundaries is more than half of the SN subzone thickness.

The top of reservoir zone RZ-4, also marked as one of the more confident seismic markers, is traced as the transition of a well-developed floodplain into multi-lateral stacked channel fill deposits. In all studied wells, this pattern can be followed, however, based on the floodplain-isotopic framework, this marker could be further refined in a stratigraphic time context. For well D, the top of RZ-4 is positioned at the transition of a pedogenic-carbonate-rich, well-developed palaeosol, which is interpreted based on the spike in the sonic log data, into a coarse-grained floodplain interval that forms the base of alternation 7 (33 m). Compared to the other transect wells, the top of RZ-4 corresponds to a floodplain-rich interval between alternations 2 and 5 and isotope excursion 1. The sandstones (25 m) below top RZ-4 in well D, but above isotope excursion 1 and alternation 4, could be stratigraphically higher related to the other sandstones defined by the top of RZ-4. Part of this different correlation in well D is caused by the higher contrast of lithological change and the strong spike in sonic speed recognised by the seismic data. A high pedogenic carbonate content likely causes this. However, here the question is how the pedogenic carbonate-rich intervals are laterally extensive. The floodplain alternations use the pedogenic carbonate-rich intervals top as boundaries. However, it also acknowledged that it is not the only form of well-developed palaeosol intervals, and these features are not necessarily time equivalent, potentially resulting in the alternative correlation.

In wells A and B the top of RZ-5 is positioned at the base of two sandstones (111 and 87 m respectively). Based on isotope excursions 2 and 3 the lower sandstone (97 m) in well A should have a similar stratigraphic level as the top of RZ-4 in B.

Correlation of a prominent negative carbon isotope excursion between wells A, B and C (Fig. 8.11; excursion 4) suggests that the placement of the confident seismic marker top RZ-6 is possibly not equal in a stratigraphic time context. In well B, the floodplain-isotope-based correlation places the sandstone (125 m) three alternations lower (alternation 17 compared to alternation 20). The top

← **FIGURE 8.14** A projection of sandstone bodies on a composite stratigraphic thickness. The projection is perpendicular to the average palaeoflow. Sandstones were determined with a V_{shale} value above 40% and thicker than 3 m. On the right, the vertical proportion curve based on the confident seismic reservoir zones is displayed (Fig. 8.14b). The correlated carbon isotope excursions are shown in triangles.

of zone RZ-6 forms a strong seismic marker and correlates well for the cluster of wells (D, E, F, G, H, and I). However, this trend cannot be continued and maintained further away (3.5 and 3.8 km, respectively). Reviewing seismic top-view amplitude maps of the top RZ-6 marker suggests that the concentrated sandstone above the top RZ-6 marker is likely a larger channel belt complex (personal communication, Sigrid Pillen 2022; Fig. 8.14). Wells A and B are positioned on the side of this channel belt. In well A, there is a sandstone positioned above alternation 20. However, the character is different to that of the well cluster mentioned above and does not display an amalgamated character or block-pattern shape. In well B, there are only floodplain deposits in this stratigraphic interval. Cross-reference with seismic reflectors is impossible for this interval as the area has poor seismic signal and is highly faulted, causing uncertainty in the stratigraphic interpretation.

In wells C and E, the top of RZ-7 divides two sandstone bodies (located at 160 and 165 m, respectively) positioned below alternation 28. These sandstone bodies could be located in the same stratigraphic interval and closer related than assumed by the reservoir zonation based on the floodplain framework. However, observations from the Willwood Formation, Bighorn Basin, USA, (Chapters 3 and 5) suggest that the correlation of such intervals, even within one floodplain aggradation cycle, can be challenging. Similarly, the floodplain-isotope framework suggested the correlation of a sandstone body near the top of RZ-7 in wells H (175 m) and I (175 m). Both sandstone bodies are bounded between alternations 26 and 28. Similarities in the above-lying splay suggest, combined with the proximity of the wells, suggest higher stratigraphic relation between the two sandstone bodies than now assumed. All these observations are below seismic resolution (Fig. 8.12 and 8.13).

8.8 Stratigraphic lithofacies trends

The average stratigraphic trends based on the floodplain-isotope correlation (stratigraphic solution 1) and reservoir zonation (stratigraphic solution 2) are shown as vertical proportions curves in Figure 8.13. The individual floodplain alternations are visible as characterised by lower V_{shale} levels (towards 25%) at their bases in the floodplain-based correlation. Similar spikes in the reservoir zonation-based lithofacies record can be seen at this scale, spaced at an average of 7 m. The overall lithofacies trends in both stratigraphies are relatively similar, and a comparable long-term trend is visible. The reservoir zonation stratigraphic solution suggested more pulses of low V_{shale} and increased net-to-gross intervals in the basal parts of every reservoir zone, such as RZ-3, -6, -7, and -8. These net-to-gross trends are also visible in the floodplain-isotope stratigraphic framework but are less pronounced. In particular, the RZ-3, -6, and -7 sand phases also seem evident from the floodplain-isotope stratigraphy.

This similar spacing also is apparent when comparing the carbon isotope excursions with the two-dimensional display of sandstone body distribution (Fig. 8.14), as the thickness of the carbon isotope excursions is in the range of the thickness of the reservoir zonation. Furthermore, In the two-dimensional sandstone distribution plot, an apparent clustering of sandstone bodies can be seen for wells H-J above the top RZ-6 zone. Laterally, sandstone bodies are dominantly absent in other wells.

8.9 Discussion

8.9.1 Floodplain environmental interpretation

The cumulative character of the soils that developed in the floodplain sediments of the upper Lunde Formation suggests that conditions for soil development were good. This could relate to steady but relatively low aggradation rates leading to fairly continuous palaeosol development, which each new

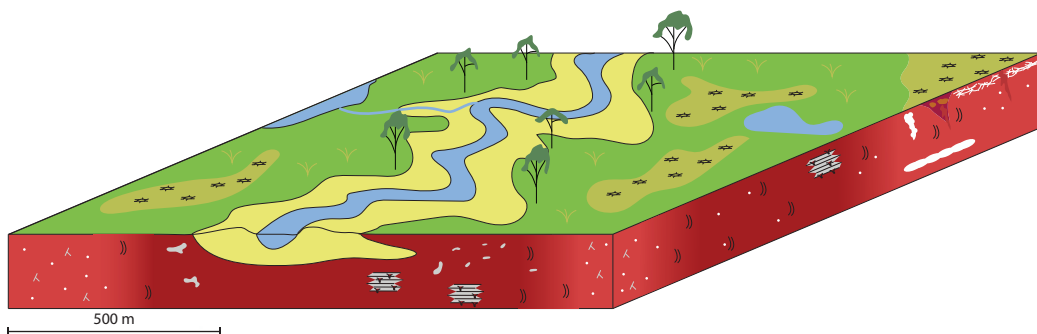


FIGURE 8.15 A schematic overview of the interpreted palaeoenvironment with different soil types correlated to the palaeoenvironment. For the legend, see Figure 8.4

package of sediment incorporated into the already existing soil profile (Kraus, 1999). At the same time, suitable climates and vegetation types may also cause rapid pedogenesis resulting in a more cumulative character of soil development while the development is also dependent on the parent material (Kraus, 1999). Comparison of the palaeosols of the New Red Sandstone in northwest Scotland, which were deposited under similar conditions and during the same time, the Upper Lunde Formation palaeosols have a less cumulative character (Müller et al., 2003), while compared to Early Eocene palaeosols red beds found in the Willwood Formation, the cumulative character is much stronger for the upper Lunde Formation (averaged 1.5 m versus 0.65 m respectively; Kraus and Bown, 1993; Abels et al., 2013; Chapter 5).

Several authors have interpreted the climate during Upper Lunde deposition as arid to semi-arid (e.g. Müller et al., 2004; Nystuen et al., 2014). In this chapter, observations are partly consistent with these previous interpretations. Detailed analysis of the floodplain sediments, however, indicates that the ‘red’ floodplain of the Upper Lunde Formation display subtle differences and saw wet and dry periods. Bright, red-coloured intervals correspond with well-drained floodplain sediments that display slickensides, root traces and a relatively high pedogenic carbonate content. The increased amount of pedogenic carbonate nodules, their large size and different shapes indicate that the upper Lunde climates underwent seasonally dry periods. This dry period was sufficiently long for dissolved calcite in groundwater to precipitate and grow pedogenic carbonate (Zamanian et al., 2016). However, compared to the Scottish New Red Sandstone, these pedogenic carbonate horizons are still relatively underdeveloped and do not form thick (> 1 m), laterally consistent beds (Müller et al., 2003). The documentation of desiccation cracks strengthens the interpretation of drought periods, with slickensides and fissures indicating subaerial soil exposure. However, the interpretation of small ponds or waterholes and purple to yellow mottling also suggest that there must have been significant wetter periods on the floodplain. Therefore, given the dry and wet indicators, the upper Lunde Formation is interpreted as a seasonally dry climate with significant wet periods (Fig. 8.15).

Compared to modern-day environments, the Australian or South African dryland systems can potentially serve as an analogue case for the Upper Lunde Formation. These systems are predominantly arid throughout the year, while they are also characterised by substantial periods of wetness, resulting

in the development of (minor) wetlands depending on the water regime of the rivers (Bunn et al., 2006; Tooth et al., 2007; Dunkerley 2011). For example, Cooper Creek, an Australian dryland river, is characterised by extreme flow variability with occasional massive flooding inundating thousands of hectares of land (Kingsford et al., 1999; Balcombe and Arthington, 2009), resulting in temporary wetlands. Small areas can stay flooded for prolonged periods due to a microtopographic relief of the so-called Gilgai landscape (Paton, 1974). Vegetation on these landscapes consists predominantly of sedges with localised larger trees (Roberts and Marston, 2011). Channels in these areas display a range of alluvial styles ranging from sinuous single channels to multiple-channel braided-like river forms (Larkin, 2019). These climatic interpretations could impact the interpretation of the fluvial styles of the Upper Lunde Formation. For example, when conducting forward processed-based modelling, the variable discharge regimes must be considered, and even ephemeral streams can be present. Observations of the major channelised sandstones in the core do not suggest an ephemeral fluvial character within the main channels of the system. However, minor distributary channels could display such characteristics.

8.9.2 Floodplain aggradation cycles

Alternations in floodplain pedogenic development patterns form a stable property of the floodplain sedimentation record of the Upper Lunde Formation. Intervals with high pedogenic development and weak to moderate pedogenic development alternate regularly and can consistently be found in core and well-log data. The vertical consistency and the lateral correlation at a 1-4 km scale suggest that the documented floodplain alternations are a persistent property of the floodplain build-up in the Upper Lunde Formation. Additionally, in the vertical proportions curve based on the existing reservoir zonation (Fig. 8.13b), pulses of sediment input are documented, which have a similar thickness as the floodplain alternations. The reservoir zonation is not based on the alternations' lateral consistency assumption.

The level of pedogenic development depends on several factors, such as groundwater, climate, source material, and time (Kraus et al., 1999; Rattelack, 2008). Grain size variation is identifiable in the floodplain alternations of the Upper Lunde Formation, both in cores and V_{shale} well-logs. This variation suggests that variability in aggradation rates on the floodplain forms a strong component on the level of pedogenic development. High pedogenic intensity is correlated with a relatively low sediment input, while low pedogenic intensity is correlated to relatively higher aggradation rates. Similar dependency on aggradation rates in palaeosol development is observed in the Willwood Formation in the USA (Abels et al., 2013) and Chinji Formation in Pakistan (Willis and Behrensmeyer, 1993).

The level of floodplain aggradation depends on the amount of sediment received from a fluvial channel and the effect of dynamic channel behaviour results in variability of the aggradation rate (e.g. Kraus 1999; Varela et al., 2021). High pedogenic intervals could be interpreted as the result of true overbank deposition. These deposits result from regular flooding of the floodplain without breaking of levees or with minor, local breakage of levees resulting in local crevasse splays. Also, these deposits relate more often to distal areas with respect to the river channels (Kraus, 1993). Weak to moderate, heterolithic deposits are interpreted to be crevasse-splay delta deposits during levee break-through, as evidenced by thicker splay and waterlogged deposits in the Upper Lunde Formation. When these deposits occur consistently at a larger regional scale (at least 1-5 km based on the correlation panel), these crevasse deltas may relate to river avulsion (Kraus, 2002; Abels et al., 2013).

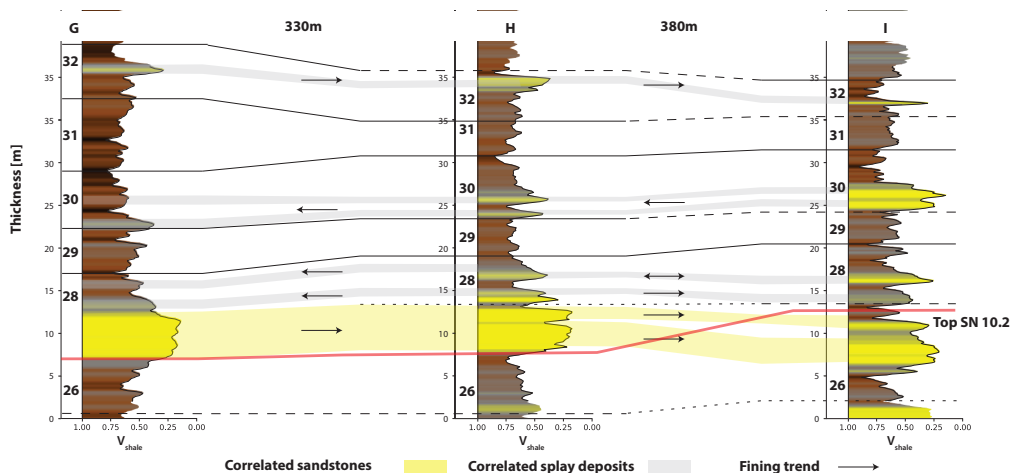


FIGURE 8.16 A possible correlation of sandstone confined by the floodplain-isotope-based framework and trend in coarse floodplain deposits. In red, the reservoir zonation top RZ-7 is given, which crosses the proposed correlation.

In the Willwood Formation, similar patterns of alternation of well-developed and weak to moderate pedogenesis are attributed to phases of channel stability and avulsion (Abels et al., 2013). Such a model could also be proposed for the Upper Lunde Formation. If these patterns hold true, the ‘avulsion belt deposits’ described for the Willwood Formation would be less developed in the Upper Lunde Formation. This is likely caused by the higher overall pedogenic overprint and lower accommodation rate.

Ultimately, the floodplain aggradation cycle model depends on channel movement and stability. Several factors could have controlled channel stability such as, for example, climatic changes. These can affect vegetation on channel banks and influence bank stability (Millar et al., 2000) but also affect changes in the rainfall regime (Jones and Schumm, 1999). Another factor is the A/S ratio (rate of accommodation space generation versus sediment input) that could lead to the relocation of channels (Wang et al., 2020). This chapter shows that the pedogenic carbonate-rich intervals often correlate with the top of a well-developed cycle, while flooding-related deposits correlate to weaker development and an increased heterolithic floodplain character. For the Upper Lunde Formation, this could suggest changes in the hydrological regime, especially peak discharge, driving channels’ stability or avulsion. Unfortunately, conclusive evidence is unavailable.

8.9.3 Floodplain-isotope stratigraphic framework

Wells can be correlated in a high resolution (5-10 m) and provide additional (chrono-) stratigraphic control below seismic resolution in sufficiently thick floodplain intervals due to the average 5.5 m thickness of the floodplain aggradation cycles. Individual splay deposits and specific grain-size trends within the floodplain aggradation cycles aid the correlation but also can be used to interpret lateral coarsening trends in the floodplain-rich intervals. These deposits can be highly variable in lithology, and the character of the deposits can laterally change rapidly when more distal to the source.

Observations from the analysed cores suggest that the pedogenic overprint of these deposits (such as removal of lamination and original colour) is significant. However, the relatively coarser grain size compared to the surrounding sediment can be used to potentially estimate sediment sources in close-by-spaced wells and help well planning (Fig. 8.16).

There are also intervals with a higher net-to-gross ratio and single- to multi-story sandstone occurrences. In these higher net-to-gross intervals, the surrounding floodplain sediments reduce the correlation uncertainty to a 20-40 m stratigraphic thickness. The incision depth of channel sandbodies defines the uncertainty within these intervals. This depth is deduced from the maximal thickness of single-story sandstone bodies measured from the correlation panel. This depth value is 11.5 m (Fig. 8.4), and combined with a potential small fine-grained infill of the top of the channel, the uncertainty of the floodplain-isotope-based floodplain stratigraphic framework is estimated to be 12 m.

8.9.4 Implications for reservoir zonation

Comparison between the floodplain correlation and the existing reservoir zonation displays an offset of 10-20 m. The leading cause for these offsets seems to be that seismic reflectors are used for the reservoir zonation. Reflectors occur where there is a strong lithological change and such strong reflectors are formed by oil-filled sandstones and by carbonate-rich palaeosols (Barclay et al., 2008). Combined with a assumption of equal lateral thicknesses, this forms a good first-order zonation. However, using the isochroned reservoir zones and the cropping of these lines to sandstones does not imply that these correlated zones are timelines.

The placement of the reservoir zone boundaries to the bases of the sandstone bodies (Fig. 8.15) and the interpolation of reservoir zones based on equal thickness theory leads to a strong assumption of laterally coeval sandstone occurrence. This is also visible in the vertical proportion curve of both stratigraphic zonations with smaller stratigraphic overlap of sandstone bodies in the existing reservoir zonation (Fig. 8.13). Multiple sandstone bodies may occur stratigraphically close to each other, resulting in correlated seismic reflections, such as at the top of RZ-6 (Fig. 8.12). However, for the Upper Lunde Formation, Mjøs et al. (2005) suggest that the maximum sandstone body width is 2.5 km with an average width of 450 m perpendicular to palaeoflow, making it unlikely that correlated sandstones are stratigraphically connected, even in close-by wells. Downflow, individual sandstone bodies may be very continuous, however, their limited lateral extent and tendency to flow in variable directions with respect to average palaeoflow results in highly uncertain correlation potential between wells. This becomes clearly visible with the alternative correlations based on the stable isotope record over larger well spacing. Both the floodplain alternations and stable isotope records can help further evaluate and refine the reservoir zonation as this concept is independent of sandstone correlation.

8.9.5 Impact on reservoir modelling

The proposition that the floodplain aggradation cycles in the upper Lunde Formation could be interpreted as alternations in depositional style resulting from river stability and regional-scale river avulsion phases suggests that the stratigraphic thickness of the floodplain alternations would relate to the thickness of the coeval sandstone bodies. Channels would avulse at a similar pace and as channel superelevation is expected before avulsion (Mohrig et al., 2000; Jerolmack and Paola, 2007), a slightly thicker channel sandbody would be expected for the Upper Lunde Formation. This is also observed in the correlation panel as the average single-story sandstone body thickness is slightly

thicker than the average floodplain aggradation cycle; 6.9 m versus 5.5 m, respectively. The ratio of 1.25 (Z_{sst}/Z_{fac}) enables estimation of average sandstone body thickness (non-amalgamated) based from floodplain intervals for the Upper Lunde Formation and could be used in detailed reservoir modelling. In the Willwood Formation in the Bighorn Basin, a similar relationship is observed with floodplain aggradation cycles of 6.9 m thick and sandstone bodies of 8.9 m (Chapter 5). However, these thicknesses are compacted thicknesses, so comparing their absolute values remains uncertain, and the Upper Lunde study did not include detailed differentiation into fluvial styles, as sandstone bodies may have different geometric properties.

Furthermore, the lateral consistency of the floodplain alternations in the Upper Lunde Formation implies a stratigraphic line up of sandstones, and the Low V_{shale} spikes in both correlations (floodplain-based: Fig. 8.14a, and reservoir-zone-based: Fig. 8.14b) could relate to these phases. In that case, the low values relate to the avulsion-belt heterolithic deposits observed in the floodplain alternations and to coeval sandstone bodies. The individual sandstone bodies have limited lateral extent but may be connected via the lateral persistent avulsion-belt sandstones. The stratigraphic organisation of channel sandstones with avulsion-belt sandstones may thus result in increased connectivity between individual bodies. However, this depends on the porosity and permeability for flow in such deposits, which has not been studied.

8.9.6 Floodplain aggradation cycle pacing

The vertical persistency and lateral correlatability of floodplain aggradation cycles in the Upper Lunde Formation could point to an allogenic driver behind the cyclicity. The similar ranged, 7-8 m thick, floodplain aggradation cycles in the Willwood Formation have been related to a 19- to 22-kyr period and linked to precession-driven orbital climate change (Abdul Aziz et al., 2008; Abels et al., 2013; van der Meulen et al., 2020).

Precession is a dominant cyclic forcing on palaeoclimate changes, as proven for many marine, lacustrine and continental records (e.g. Herbert et al., 1990; Olsen et al., 1996; Prokopenko et al., 2006). In the upper Triassic, the duration of the orbital and climatic precession cycle has components between 19.1-kyr and 21.5 kyr (Laskar et al., 2004). In Triassic times, the Upper Lunde Formation was located at 33–35 degree N latitude (Torsvik et al., 2002). These latitudes are expected to be dominated by summer monsoonal climates and suggest seasonal wetting and drying in an overall dry, clay-rich environment (e.g. Bosmans et al., 2012). This aligns with the wet-dry seasonal climate as interpreted from palaeosol character. At these latitudes, precession cyclicity strongly influences hydroclimate related to monsoon activity (Rossignol-Strick et al. 1983, Hilgen et al. 1995). Therefore, precession forcing of climate cycles could have significantly impacted Upper Lunde floodplain deposition.

Independent time control in the Lunde formation is hard to obtain due to the absence of microfossils in this terrestrial series. The presence of stable carbon isotope records may strengthen the precession suggestion. Marine sediment records show that the eccentricity cycle can drive stable carbon isotope excursions, with dominant cycles of 100 kyr and 400 kyr eccentricity, respectively (Cramer et al., 2003; Zachos et al., 2010; Boilila et al., 2014; Lauretano et al., 2018). In the Upper Lunde Formation, the thickness ratio of isotope excursions and floodplain aggradation cycles seems constant. The recoveries of excursions 1 and 2 are spaced by four cycles, and the onset of excursions 4 and 5 by five (Fig. 8.13a). For excursion 3 there is not enough stratigraphic constraint to correlate in detail to floodplain aggradation cycles as it is embedded between thick sandstones. Thickness patterns

relate the position of isotope excursion 3 to cycle 14. The fragmented isotope record makes analysis of multiple subsequent excursions impossible as excursion onset and recovery cannot be compared. Nonetheless, the approximately 5:1 of isotope excursion and floodplain aggradation cycles is similar to the 100 kyr short-eccentricity to 21 kyr precession ratio. Furthermore it is expected that not each short-eccentricity fluctuation is equally expressed in the carbon isotope record. There is a strong modulation of the 400 kyr but also the 2.4 myr long-eccentricity on short-eccentricity as evidenced from the marine realm (Cramer et al., 2003; Zachos et al., 2010). This potentially can also be seen in the magnitude of the documented excursions as excursions 1,4 and 5 are larger than 2 and 3 (Table 8.5).

Extrapolation of the precession forcing of floodplain aggradation cyclicity results in a sedimentation rate of ± 280 m/Myr. A similar rate is observed for the Willwood Formation with 320 m/Myr (Chapter 5). This estimate would align with more cumulative palaeosols in Upper Lunde Formation compared to Willwood Formation, as a lower sedimentation rate gives more time to develop continuous palaeosols horizons. The constant thickness of the floodplain aggradation cycles over the entire studied interval suggests that the 280 m/Myr sedimentation rate would be relatively stable for the whole studied interval.

8.9.7 Large-scale climate forcing of sandstone occurrence

The suggestion can be made that the short and possibly long eccentricity cycle correlate to seismic markers and sand occurrence as the thickness of the carbon isotopes excursions have a similar thickness range as the reservoir zonation and they align moderately well with the isotope excursions (Fig. 8.13 and 8.14). If astronomically paced, short, 100 kyr eccentricity would be expected at 30 m cycle thickness and long, 400 kyr eccentricity is expected to occur at a cycle thickness of circa 110-115 m. On a 30 m interval, individual pulses of more sand at alternations 3-5, alternation 7, alternations 13-14, alternations 20-22, and alternations 26-27 are observed and could represent a short-eccentricity forcing component. Furthermore, the confident seismic markers (the tops of RZ-1, Top RZ-4, Top RZ-6 and Top RZ-9) are spaced 110, 80, and 105 m from each other (Fig. 8.14) and could align with the long-eccentricity curve. Both vertical proportion curves show variability at these, on average, 100 m thickness intervals as two significant sand-rich phases from alternations 3 to 14, and from alternations 20 to 27, and higher net-to-gross levels are present above the confident seismic markers (Fig. 8.13). The discrepancy between the isotope excursions and the seismic markers can be explained by the different signals measured and the non-linear response of orbital forcing.

Similar observations in net-to-gross variability are made in other basins. The Willwood Formation in the Bighorn Basin reveals net-to-gross changes at the long eccentricity scale (Chapter 6), where variability is related to changes in fluvial style from dominantly sinuous fluvial styles in low net-to-gross intervals towards more braided-like systems in high net-to-gross intervals. In the Carboniferous Westoe and Cleaver Formations, similar high and low net-to-gross intervals were also found to be paced by long eccentricity (Chapter 7). Furthermore, Smith et al. (2014) suggest that in the Green River Formation in Wyoming (USA) there is an alternation of alluvial with lacustrine modes within the depositional system, impacting the net-to-gross levels. Similarly, Valero et al. (2017) find patterns of changes in channel density in the Almazán Basin (Spain), while Olsen et al. (1995) suggest possible forcing in the Mesaverde group in Utah (USA), and Olsen (1990) shows changing fluvial styles driven by eccentricity cycles in Devonian terrestrial series of Greenland.

The observations with fitting thickness ratios between floodplain aggradation cycles, stable carbon isotope excursions, and the phases of low and high net-to-gross stratigraphy strongly suggest orbital forcing of the Upper Lunde alluvial stratigraphy. However, the evidence for short and long eccentricity forcing of the Upper Lunde Formation is inconclusive as better age constrain is needed. Nevertheless, the proposition of such a model impacts interpreted reservoir architecture at a 30-100 m scale. Changes in fluvial styles and properties over eccentricity cyclicity as found in other basins, could also have impacted the net-to-gross levels in the Upper Lunde Formation. Planform style changes are not directly observed for Upper Lunde Formation, but an increased sand discharge could also cause avulsion-belt deposits to be more sand-rich in high net-to-gross intervals, increasing the impact of avulsion-belts connecting sandbodies. The high net-to-gross phases at around alternations 3-5, 13-14, 21-22, and 26-27 could thus represent relatively well-connected sand-prone intervals.

8.10 Conclusions

Detailed analysis of the floodplain fines shows that the apparent 'red' intervals display subtle differences and can be used to gather valuable information for reservoir characterisation that cannot be derived from their coarser-grained sandstone counterparts. The overbank sediments of the Upper Lunde Formation were deposited under semi-arid conditions and underwent significant periods of wetness. Rhythmic alternations of strong and weak to moderate pedogenic intensity form a stable factor in the low net-to-gross interval and can be identified both in core and well-logs. These alternations are interpreted to be formed by variability in aggradation rates driven by channel mobility and stability phases and can be used to construct a floodplain-based stratigraphic framework at 1-5 km lateral scale. Using high-resolution stable isotope records, the floodplain-based stratigraphic framework can be further refined. Correlation of floodplain alternations can be made over greater distance as multiple carbon isotope excursions are documented and used as tie points for correlation. The average thickness of these floodplain aggradation cycles implies a resolution which cannot be achieved by seismic data and, in the absence of other stratigraphic control, forms a good additional constraint for stratigraphic correlation, on the basis of which the existing reservoir zonation can be further refined. In this way, combining traditional reservoir zonation and the proposed cyclostratigraphic approach should further complement each other to achieve a higher-resolution correlation. A precession pacing is proposed for the floodplain alternations. The observations with fitting thickness ratios between floodplain aggradation cycles, stable carbon isotope excursions, and low and high net-to-gross stratigraphy phases suggest orbital forcing as a controlling allogenic component on the Upper Lunde alluvial stratigraphy. However, without sufficient age control, there is no conclusive evidence. Nonetheless, integrating orbital forcing in the analysis of floodplain sediments and the definition of stratigraphic patterns for reservoir characterisation is powerful, It provides additional and more refined input to reservoir modelling and can be used to improve model scenarios which can be further tested and used for well planning purposes. This can be done on a small scale (5-10 m), at which the average thickness and stratigraphic occurrence of sandstone bodies can be estimated, and at large scale (10-100 m).



9

A cyclostratigraphic reservoir correlation and characterisation methodology

A cyclostratigraphic reservoir correlation and characterisation methodology

Based on the previous chapters and learnings from the case studies, a general workflow is proposed for the application of cyclostratigraphic reservoir correlation and characterisation in low net-to-gross fluvial stratigraphy. The steps of the workflow are visualised in Figure 9.1 and described below.

9.1 Requirements

Before implementation of the workflow, it needs to be assessed whether the target reservoir interval is suitable for successful application. For this, there are multiple factors which need to be considered:

- First and foremost is the net-to-gross ratio. When the number of channelised sandstone bodies is too large, this results in a fragmented dataset with low correlation potential and resolution. The proposed cyclostratigraphic methodology is particularly suitable for low net-to-gross successions.
- A fluvial succession with a relatively high-aggradation rate is preferred. With increasing aggradation rates, the vertical scales of the stratigraphic impact of internal and external processes become increasingly different and the preservation chances of the expression of external, cyclic forcing increases.
- A powerful syn-tectonic imprint makes a target series less suitable. In both case studies and the field case of this dissertation, it was assumed that the basins were subject to steady tectonic activity, not strongly variably impacting different areas of the basins. Sedimentation rates that are different between segments of a basin are not a problem for the methodology if these differences remain within range. A case where tectonic activity is powerful and likely irregular through a basin seems not the best case for the proposed methodology.
- The target interval has a thickness of at least 100 m or ten floodplain aggradation cycles during which background circumstances remained relatively stable, such as to document the floodplain cyclicality. Longer-term variability can be expected starting from five floodplain aggradation cycles, so a longer series is needed.
- The series has a well-data that allows to identify the sedimentary facies changes. A large well-log suite will help the identification of sedimentary variability. Starting a study using (long) cores is preferred.
- The methodology will be more feasible in a target series of closely spaced wells and a target series with a high number of wells. This is because fluvial stratigraphy shows lateral variation and nearby wells can reveal this variability as lithological patterns can be aligned more accurately. A larger number of wells allows more easily uncovering the average stratigraphic patterns.
- First-order correlation tie points are needed. This can be any other stratigraphic control such as magnetostratigraphic, isotope stratigraphy, biostratigraphy, or seismic correlations, or a combination of those. This does not have to be at a high resolution or confidence; it may have a relatively large error, but the cyclostratigraphic methodology will not work if no rough control is available.

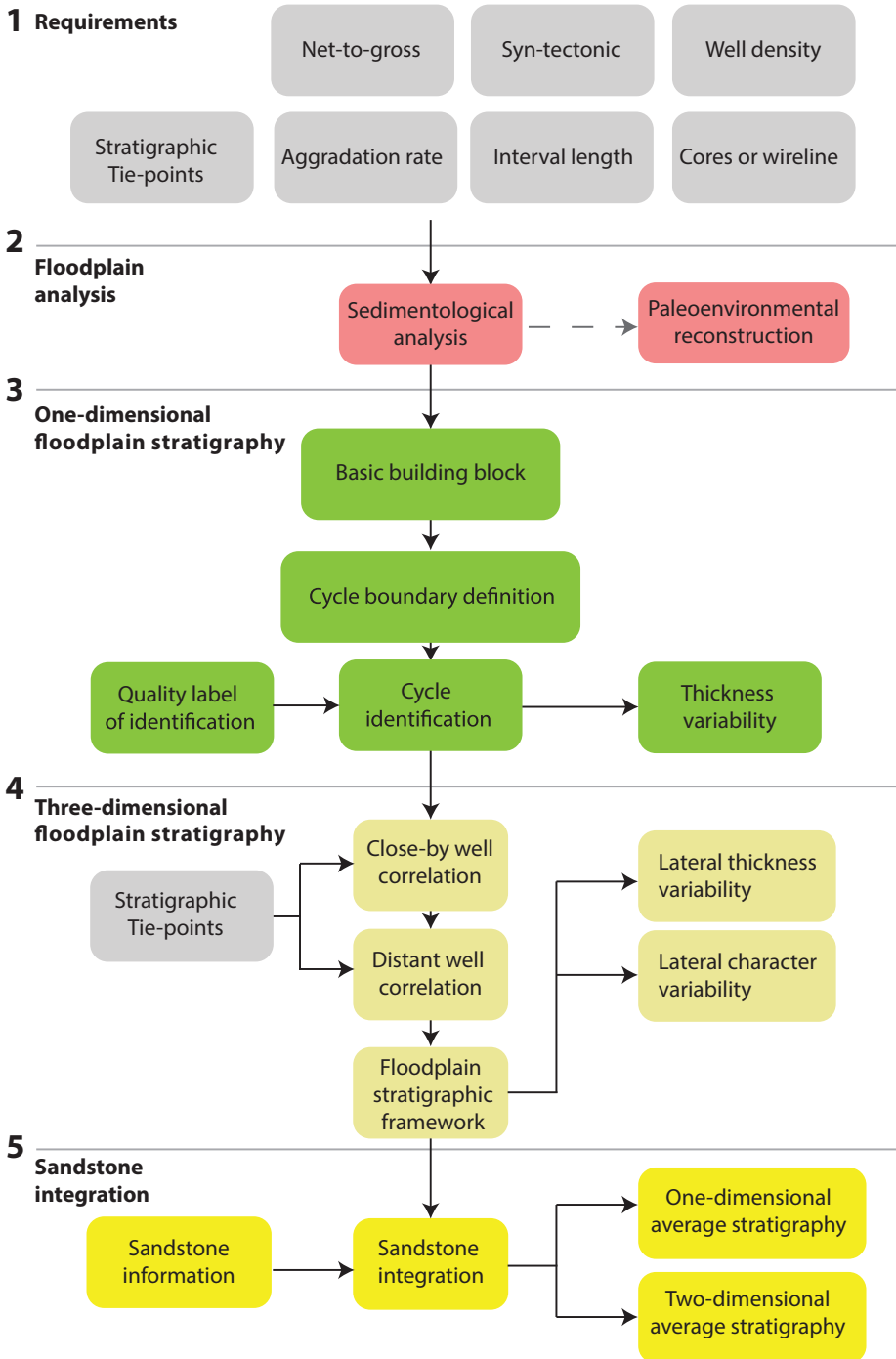


FIGURE 9.1 A flow diagram for the general workflow applied in this thesis.

9.2 Floodplain analysis

After the feasibility evaluation, the first part of the workflow consists of a general analysis of the floodplain sediments. Here, the aim is to assess the stratigraphic facies variability and potential cyclicity in the floodplain fines. These can be visible readily in lithological changes in core or wireline log. Detailed sedimentary descriptions and analysis should be done or consulted to evaluate what the facies variability means in terms of changing sedimentary environments and what the controls may have been. This is often already performed for well-studied reservoirs, and sedimentary alternations are often described. In some descriptions, floodplain cycles will be labelled as the basic sedimentary cycle or alternation, although it may well be that the focus has not been placed on the floodplain fines at all, and these were hardly described. Observations and their palaeoenvironmental and potential palaeoclimatological changes could be placed into a depositional model (See Chapter 8).

9.3 One-dimensional floodplain stratigraphy

The subsequent step is to identify the “basic building block” of the floodplain series or the meter-scale repetitive facies variability that can be identified. This can be done for several wells; no spatial dependency is needed. Several techniques, including the Deviation Curve or other spectral analysis methods, such as wavelet, power spectra, and bandpass filtering, can detect cyclicity in floodplain sediments (see Chapters 3, 5, 7, and 8). A cyclic depositional model may be produced.

Once the floodplain sedimentary alternations are identified, a cycle boundary needs to be defined that should be easy to identify in the data available. This can be done using the Soil Development Index or a lithofacies depth rank, facies descriptions, or well logs. It is handy to define the boundary between two successive cycles at a sudden decrease, such as from high to low pedogenesis (see Chapters 3, 5, and 8), because then it may be straightforward to identify the cycles in the successions.

Now that the cycle boundary is identified, all cycles should be identified in each well. In the subsurface, there are only one-dimensional records from boreholes and sedimentary variability, in association with the occurrence of channelised deposits, can make it challenging to identify cyclic repetitions. Defining a quality label for the identification and noting these with each boundary is helpful. A simple three-partite classification of confident, less confident, and unconfident allows uncertainty analysis.

Followed by identification across the wells, the variability of the cycles can be defined in different ‘cycle types’ and the cyclic depositional model may be refined. For example, splitting a coal seam can lead to a single or double coal seam within one cycle, or variation in thickness of an avulsion belt deposit depending on the proximity towards a channelised deposit produces different cycles. It is expected that the vertical variation documented in 1D wells is also present in the lateral domain.

The thicknesses of cycles identified in the different wells should be analysed statistically as a last step. The average thickness indicates the expected cyclicity in the wells. This can differ between study areas because of tectonics’ different rates of accommodation space creation (Chapter 7). The range of cycle thicknesses indicates lateral thickness variability of individual cycles, which is an additional constraint for the later well correlation exercise.

9.4 Three-dimensional floodplain stratigraphy

A well-to-well correlation can be made based on the identification of the cyclicity in the one-dimensional domain. First, wells should be roughly aligned based on the predefined stratigraphic tie

points. Depending on the used stratigraphic marker, there is an error margin which potentially can be large, and it should be allowed in the methodology to go even beyond the error margins if indications for that are strong. Correlations may start from a single correlation marker, and tests can be made by making different correlations starting with different markers every time and comparing the results. To make the approach as independent as possible, the markers should be removed from the correlation after the initial alignment of the wells.

Well correlation should start between the most proximal wells available. Here, it is assumed that the lateral variation between cycles is minimal and confidence in correlation highest. Depending on the available data this can be done for multiple clusters of wells proximal to each other. This exercise also provides additional information about the lateral character variation and the rate and of lateral change. Subsequently, the correlation distance between wells can be extrapolated to more distant wells. Similar to the cycle boundary identification, a quality label should be attributed to each correlation line to provide additional robustness.

Sand-rich intervals are encapsulated from below and above by correlating 'known' correlation lines and gradually moving towards sand-rich intervals that are uncorrelateable.

9.5 Sandstone statistics

The following step is the integration of the channel sandstone bodies and the sand percentage into the framework. First, general data is gathered about the sandstone bodies as character, aggradation or incision style, planform type, and thickness (single and or multi-story). This is often performed and described in previous studies and can be integrated within the floodplain-based stratigraphic correlation framework.

To do so, all wells can be projected on a composite stratigraphic depth scale. This is done by taking the cumulative average thickness of the floodplain aggradation cycle. By averaging multiple wells, the local autogenic variation is suppressed, and allogenic, reservoir-wide trends become better visible. With the wells placed on a similar depth scale, the one-dimensional reservoir trends can be calculated using the average of all wells to generate vertical proportion curves. As wells have an unequal spatial distribution, the average must be calculated by a weighted mean. Depending on the user, the gamma-ray or V_{shale} can be used as input, and a cut-off value needs to be defined.

The same composite depth scale can be used in two-dimensional space to visualise the sandstone bodies perpendicular to the palaeoflow. Depending on the reservoir scale and constructed correlation, this can provide additional information about the architecture and patterns observed, such as channel belts and the spatial movement of clustered sandstone bodies. A width estimate can be calculated based on the sandstone thickness and planform style and using literature-based empirical relationships. Wells can be projected on a two-dimensional plane, and the widths can be plotted with or without lateral scaling.



10

Synthesis

10.1 Brief summary

This dissertation investigated the role of regular-paced orbital forced control of climate variability on low net-to-gross alluvial stratigraphy and the utilisation of cyclic patterns for improved correlation and characterisation in the subsurface. As this thesis has shown, such forcing is best documented in the floodplain fines of the alluvial system. The results of an extensive outcrop study of the Willwood Formation in the Bighorn Basin, Wyoming, USA, showed that repetitions in the floodplain record are relatively regular and continuous and have a high potential to serve as regional markers for correlation. Sedimentological analysis of channelised sandstone bodies in the Willwood Formation in terms of processes and products revealed different river planform styles. Because floodplain sediments derive from processes associated with channels, both have an intrinsic relationship. This relationship has been studied, conceptual depositional models were proposed, and observations regarding the spatial distribution of sandstone bodies in the stratigraphy (including spacing and connectivity) were derived. A floodplain-based stratigraphic framework was constructed using repetitive patterns in palaeosols developed in the floodplain. The documented sandstone bodies were populated within this framework, revealing a vertical change in river planform style. A predictive link between orbital climate forcing and alluvial architecture is suggested using available age constraints.

The acquired outcrop-based knowledge has been successfully applied to two subsurface case studies in the North Sea. Floodplain sedimentary alternations were detected in both cases and used to correlate between wells resulting in further uncertainty reduction of existing correlations. The constructed floodplain-based stratigraphic frameworks were used to analyse basin-wide trends revealing potential links between reservoir architecture and orbital forcing on a large scale. Based on the outcrop and subsurface studies, a general workflow for applying cyclostratigraphic, floodplain-based reservoir modelling is suggested.

A total of seven main implications of this thesis are given below and illustrated in Figure 10.1. In the following paragraphs, these main conclusions are divided into two main components of this study: correlation and characterisation. Both parts will be further elaborated, and uncertainties and future needs will be discussed.

1. Floodplain aggradation cycles of 5-15 m thickness, consisting of overbank fines alternating with avulsion sands, are a dominant factor of alluvial stratigraphy and can be recognised in cores and in wireline logs.
2. Floodplain aggradation cycles allow improved stratigraphic correlations between nearby wells (1-2 km) at high certainty at 5-15 m vertical resolution and distant wells (2-30 km) at medium certainty at 5-30 m vertical resolution in low net-to-gross alluvial stratigraphy resulting in a floodplain-based stratigraphic framework.
3. Sandstone bodies are 0.8 to 1.3 times as thick as the floodplain aggradation cycles in the studied low net-to-gross upstream-dominated alluvial stratigraphies and 0.6 times as thick in the base-level controlled case study.
4. Floodplain sedimentary cyclicity indicates sandstone-body cyclicity, causing relatively even stratigraphic spreading of sandstone bodies reducing stochastic reservoir connectivity.

5. Sandstone bodies occur preferentially with their bases and tops in the laterally extensive avulsion and splay sands, potentially improving reservoir connectivity.
6. Long-term climatic variability significantly influences alluvial architecture at 100-200 m scales with phases in which sandstone abundances and body properties, such as planform style and geometry, change.
7. Long-term floodplain sedimentary changes are coeval with sandstone body changes and could be a strong indicator for locating these high net-to-gross intervals in the subsurface.

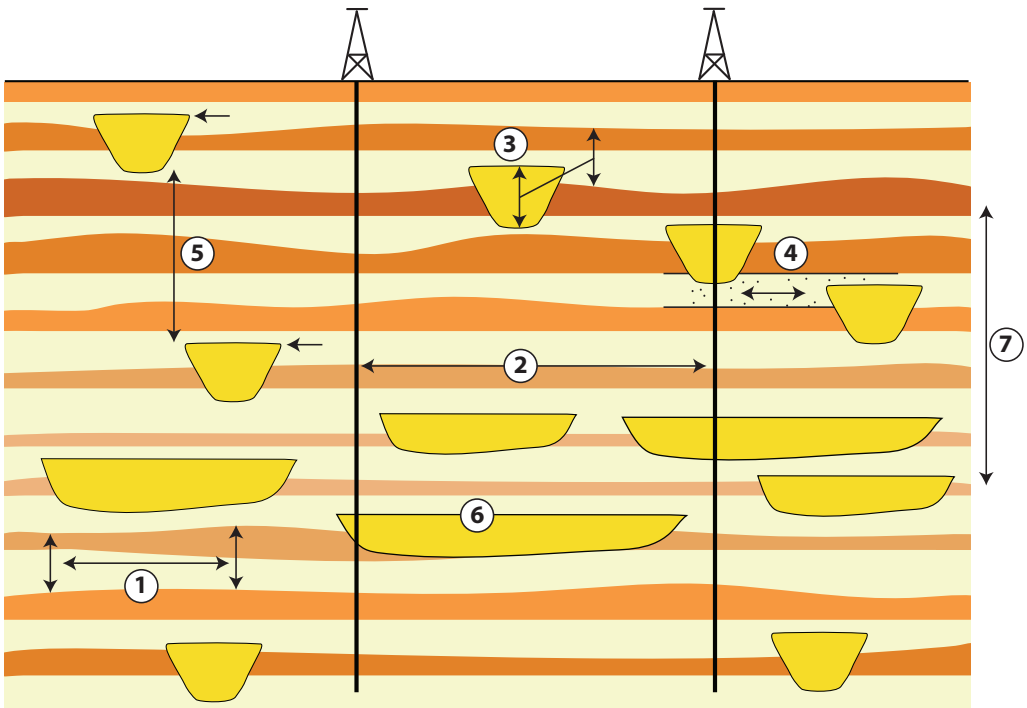


FIGURE 10.1 An illustration of the main outcomes of this dissertation. The orange and pale brown alternations represent the floodplain aggradation cycles. The numbers refer to the numbering of the main conclusions discussed in this chapter.

10.2 Alluvial stratigraphic correlation

10.2.1 Floodplain aggradation cycles

The analysis done in this thesis has demonstrated that repetitive sediment aggradation phases are a stable factor in the studied floodplain sediment records. As they are interpreted to represent variability in the aggradation rate on the floodplain, they are named floodplain aggradation cycles, and in each examined case, rapidly deposited coarse-grained sedimentation alternates with slower-deposited fine-grained sediment.

The ability to recognise these alternations in the Bighorn Basin outcrop is good and done by assessment of the level of pedogenic development. While initially and best done in a trench (Abels et al., 2013), these alternations can be reliably estimated from photographs and digital outcrop models (Chapter 3 and 5; Fig. 3.1). Similarly, floodplain aggradation cycles in the Upper Triassic Lunde Formation look relatively similar to the repetitions found in the Bighorn Basin (Chapter 8). They are also documented by assessing the level of pedogenic development. However, this assessment had to be modified for the specific situation. This adjustment suggests that a certain amount of “tailoring” is required for each basin the approach is applied to. While the forcing conditions may be similar, the expression of cyclic control is governed by regional conditions, such as source material, climate, and basin geometry. This variability in expression also becomes apparent in the studied Upper Carboniferous Westoe and Cleaver formations (Chapter 7). The cycles differ significantly from the upstream alluvial sediments studied in the Wilwood and Lunde formations as this setting has a dominant base-level controlled component, and the fines represent the basinal sediments deposited under subaqueous conditions.

The floodplain aggradation cycles documented in this thesis are between 5 and 15 m thick. This thickness range is the smallest repetition found and seems to be the stratigraphy’s fundamental or basic building block. A comparison of other fluvial basins outside this study also indicates a similar range in thickness. For example, in the Late Silurian to Early Devonian Moor Cliff Formation cyclic behaviour of floodplain maturity occurs at a 10 m scale (Love et al., 2000), and the Late Triassic Chinle Formation in New Mexico has floodplain cyclicity at a 5 to 10 m scale (Atchley et al., 2014). Based on the available dating, similar sedimentation rate is estimated in all three studied basins (Willwood Formation: 320 m/Myr; Lunde Formation 280 m/Myr; Westoe and Cleaver formations: 270 m/Myr). As low net-to-gross intervals are often typified by relatively high aggradation rates and fast generation of accommodation space, there seems to be a correlation between the floodplain aggradation cycles thickness and their occurrence in low net-to-gross reservoirs. Correspondingly, the Moor Cliff Formation and Chinle formations can be defined as low net-to-gross.

Because the Willwood Formation is only one (well-studied) outcrop example, the concept of floodplain aggradation cycles and allogenic forcing in alluvial strata needs further investigation using other basins and examples. Three potential sites are suggested here. The Chinji Formation in Northern Pakistan and Afghanistan show good potential (Willis and Behrensmeier, 1994; Behrensmeier et al., 2007). Like the Willwood Formation, the Middle Miocene Chinji Formation displays well-developed palaeosols deposits traceable for multiple kilometres. However, due to the political situation, the area is currently inaccessible. This area will form a good target for further study if future changes allow. Another site of interest could be the Late Cretaceous through Early Tertiary deposits in the Tornillo Basin, Texas, USA. Here also, palaeosol-bearing alluvial strata are exposed over long distances laterally,

and fluvial aggradation cycles are documented and correlated to a strong base-level component (Atchley et al., 2004). Lastly, with a combined control of upstream and downstream forcing, the Lourinhã Formation in Portugal (Taylor et al., 2014) may offer an interesting prospect. The Lourinhã Formation could allow investigation of the interaction between upstream and downstream allogenic control.

10.2.2 Subsurface recognition

The variability in the expression of floodplain aggradation cycles per basin has implications for the successful recognition in the subsurface. In two of the three studied basins the pedogenic development form the main identification factor (Chapters 3 and 8), and core material plays an essential role. When core is absent, wireline data must be used to trace floodplain cyclicity. This remains challenging as the degree of soil development on floodplain sediments is difficult, if not impossible, to trace in traditional wireline log responses. For the Upper Triassic case study, it was found that soil development imprint, as documented in the cores, was not one-on-one translated to wireline log responses. A combination of the V_{shale} and sonic logs was used the best available proxy. This was used to correlate non-cored wells; however, recognition and correlation of the cycles were with less confidence than in cored material, especially over larger (>500 m) distances (Chapter 8).

While recognising palaeosol (or shale) in well-logs is common, more detailed study is needed to differentiate between pedogenic maturity and palaeosols features reliably. Here, newer wireline tools may help. As observed in the core and outcrop analysis, the soil's rubification level provides a good pedogenic intensity estimate. In the digital outcrop models, this is the main indicator for the position of floodplain aggradation cycle boundaries (Chapters 3 and 5, Fig. 3.1). The level of rubification is linked to the iron content levels in the sediment as oxidation causes the formation of goethite and red colour. For this reason, cores from the Bighorn Basin Coring Project (Clyde et al., 2013) also show a good correlation between soil colour and measured iron content (Westerhold et al., 2018). Similarly, using spectroscopy element scanning of the iron content, Cook et al. (2014) demonstrate the ability to recognise palaeosols in the Lunde Formation and Early Jurassic Statford Group. It is suggested that element spectroscopy could be used to create a more detailed wireline-based soil development index. However, these data must be produced for wells, as this is not common practice and unavailable for older (non-scientific) wells.

Furthermore, in non-cored wells, cuttings and, in particular, side-wall cores could potentially help to bridge the gap between cored and non-cored wells. Because of drilling conditions, cutting samples often form a mix from different stratigraphic positions. However, they could still provide an estimate of the level of pedogenesis through stratigraphy. To do so, cutting samples need to be taken at a high enough resolution to potentially trace the floodplain aggradation cyclicity.

10.2.3 Subsurface correlation

Both subsurface case studies show that detailed well correlations are possible based on floodplain characteristics. Correlation can be found starting from closely spaced wells and a few basic correlation tie points from biostratigraphy or seismic correlations. Floodplain aggradation cycle property analysis and the well correlations are deemed more certain if a few wells are in close range laterally (<2 km) and some wells very closely spaced (<500m). The closely spaced wells allow correlation of lithological

patterns to qualify and quantify the floodplain aggradation cycle consistency and variability (Chapters 7 and 8).

Learnings from the outcrop and Westoe and Cleaver formation studies indicate that large variability can exist in floodplain cycle thickness and lithological character. This variability is interpreted as caused by geomorphological differences and autogenic influences within the system (Chapters 3 and 7; Fig. 7.4). It is suggested that the spatial continuity of the floodplain aggradation cycles is best developed parallel to palaeoflow due to morphological elements oriented in the direction of palaeoflow causing higher consistency of sedimentary features (Chapter 3).

Nevertheless, lateral consistency of the cyclothem may occur at scales of up to tens of kilometres, such as in the Upper Carboniferous case study. It is implied that this large distance consistency could be caused by the presence of a significant downstream controlled base-level component and would indicate that the recognition of floodplain methodology in such systems can be applied at large scales. This large-scale consistency also is illustrated from other Upper Carboniferous studies, where (climate-based) correlations are made over large distances (e.g. De Jong et al., 2007, Smith and Joeckel, 2020; Opluštil et al., 2022); however, on a lower vertical resolution as done in this thesis.

As with each approach of correlation in the subsurface, there remains a level of uncertainty. To address this, a confidence score was given for the identification of individual floodplain aggradation cycles in wells and the correlation of the cycles between wells (Chapters 7 and 8). This scoring allows for semi-quantifying the produced correlations' uncertainty range. Stratigraphic intervals that contain more sand mostly could not be correlated at a 5 to 15 m scale resolution (Chapter 8). However, by correlation of floodplain aggradation cycles below and on top of these sandy intervals, a stratigraphic correlation uncertainty was obtained of around 20-40 m for such intervals. For the proposed cyclostratigraphic methodology, this implies that, in the floodplain-based stratigraphic framework, sandstone bodies remain 'floating' to some extent as these may be incising, aggradational, or amalgamated. In both case studies and the Willwood Formation outcrop study, the stratigraphic thickness of these processes is between 5 to 20 m. From a well-log response, appointing one of these processes and excluding the others is impossible. Consequently, the highest correlation resolution in intervals with a higher sandstone body content (or higher net-to-gross level) will be above 20 m using subsurface data.

10.2.4 Autogenic or allogenic origin

This study proposes further evidence for the allogenic forcing of floodplain aggradation cycles, although an autogenic-driven model, or a combination, can still not be entirely ruled out. It has been shown that autogenic forcing can cause similar patterns via random avulsion and compensational stacking (Staub et al., 2009; Hajek and Straub, 2017). However, either assuming an autogenic or allogenic driving mechanism controlling sedimentary cyclicity, part of the value of the cyclostratigraphic methodology presented here is similar. A lateral consistency of the cyclicity at a 2–5-kilometre scale in outcrop as detected by physic-tracing of beds (Chapters 3 and 5) suggests stability of sedimentary alternations at this scale and is suitable for correlation.

To further constrain the lateral extent of the floodplain aggradation cycles in the Willwood Formation, the two studied sites of this thesis, the Deer Creek and Gillmore Hill areas, could be correlated with each other. While this has been done on one-dimensional sections (Westerhold et al., 2018), the outcrop quality in between these sites allows for continuous tracing of the floodplain

aggradation cycles over the approximately 17 km between the two areas (Fig. 2.2). Furthermore, it allows the occurrence of the ETM2 event for accurate stratigraphic control over this tracing. If the floodplain cycles are allogenic, a continuity would be expected at this scale, while if they are autogenic forced likely there will be a diachroneity of strata. The practical realisation of this suggestion would require digital outcrop models over the entire distance between the two areas and will take a significant effort.

10.2.5 Non-specialist correlation approach

The workflow applied to both case studies requires expert knowledge and experience. Cyclostratigraphy is a discipline on its own, like any stratigraphic discipline, but cyclostratigraphy is not a commonly applied discipline as it is relatively new. For this reason, a non-specialist workflow was developed and tested in the Upper Carboniferous case study. The semi-automated floodplain aggradation cycle recognition was applied to the well-log data using a combination of statistical methodologies (Chapter 7). The correlation between wells resulted in fairly similar results as the ‘specialist’ correlation, however, the correlation of individual floodplain aggradation cycles is less accurate, occasionally resulting in a 20-40 m vertical uncertainty. Once averaged over a stratigraphic interval, this semi-automated method shows similar patterns in net-to-gross trends. This is believed to be due to the compensational stacking patterns within the system. In both the Willwood Formation and the Upper Carboniferous, a similar 85% of the vertical variability is reduced after 2 to 3 cycles (Chapter 3 and 7). Although less accurate, with limited knowledge needed, integration of the non-specialist workflow, would be easy and relatively fast way to implement in a cyclostratigraphic approach and provide an additional and potentially different view of reservoir trends.

Currently, the methodology used here is still robust and simplistic, and the workflow could be further refined. The identification of the floodplain cycle is now based on the deviation curve (Chapter 7), which forms a good estimate but is not always entirely accurate as the position of a boundary can lag, and the method is also sensitive to thicker (>10 m) sandstone bodies (Fig. 7.3). The integration of machine learning could improve the detection of these cycle boundaries when learned from manual interpretation (e.g. Tokpanov et al., 2020). Furthermore, other correlations could be generated and compared based on different methods. Currently, this is based on subsequent peak matching, but techniques such as dynamic time-warping algorithms (Edwards et al., 2016, Baville et al., 2022) could also be helpful.

10.3 Alluvial stratigraphic characterisation

10.3.1 Floodplain aggradation cycle models

Two sedimentary models for depositing floodplain aggradation cycles are developed based on the Bighorn Basin (Chapter 5). The floodplain cycles could be controlled by super-elevation and channel avulsion, which ends the aggradation of the existing sandstone body and starts a new sandstone body at another location. An alternative model with increased and decreased siliciclastic input and/or water discharge phases is proposed. However, the precise internal dynamics of floodplain aggradation cycles are still not fully understood. In this thesis, this topic is only briefly discussed with the correlation of crevasse splays and individual palaeosols (Fig. 5.4), and questions are still open. For example, how much time is represented by palaeosol build-up or the overbank and avulsion phases. Accurately dating

at high-resolution (< 10 m) remains challenging due to the limited temporal resolution of current methods and the degree of homogenisation in palaeosols. Here, younger deposits such as the Miocene Chinji Formation (Willis and Behrensmeyer, 1994; Behrensmeyer et al., 2007) could potentially be a better target to resolve such timing-related questions as dating uncertainties are smaller.

Furthermore, the relationship between orbital forcing via insolation variability and the palaeoclimatic response remains enigmatic. Here, the carbon isotope record might help. In marine records of the ETM2 hypothermal event, a clear imprint of precession in the carbon isotope record is found (Stap et al., 2009). Potentially, this imprint can be seen in the Bighorn Basin carbon isotope record of van der Meulen et al. (2020), where fluctuations and a stepwise decrease in $\delta^{13}\text{C}$ values align with the floodplain aggradation cycles (Head of Big Sand Coulee record, 100-130 m). Detection of a correlation between stable carbon isotope and floodplain aggradation cycles could lead to the deduction of the phase relationship of precession and the overbank and avulsion phases. However, the natural variability within the pedogenic carbonate is around 1 to 2 ‰ (Abels et al., 2016); thus, a very high (more than two samples per 25 cm, as done in this thesis) is needed. Ultimately, better knowledge of internal variability and the sequence of sedimentological events within a floodplain aggradation cycle may help develop more accurate models for the Willwood Formation.

10.3.2 Small-scale alluvial architecture

The above-discussed questions are fundamentally interesting; however, this sub-floodplain aggradation cycle resolution is less necessary for subsurface application. Both models for the Willwood Formation suggest that major channelised sandstone bodies occur with every floodplain aggradation cycle. This indicates that recognising floodplain aggradation cycles has a predictive value for channel sandstone stratigraphy and dimensions. Furthermore, in the Upper Triassic case study, similar patterns in sandstone content on a 5-10 m scale are found, as evidenced by the vertical proportions curves of the floodplain-based stratigraphic framework (Fig. 8.13). A fully upstream-controlled environment is assumed in both the Willwood and Lunde formations. However, in the dominantly downstream controlled Upper Carboniferous case study, these models do not fit, and a different model is proposed (Chapter 7). This different model implies different consequences on sandstone stratigraphy and dimensions. Nevertheless, as discussed below, predictive relationships on alluvial architectural elements can still be suggested.

Floodplain to Sandstone thickness ratio

This study suggests that floodplain sedimentary cyclicity can be used to predict the thickness of coeval sandstone bodies. A reasonably stable ratio between the thickness of both is found in the Willwood Formation and the Upper Triassic case study. In the Bighorn Basin, sandstone bodies are, on average, 1.1 times thicker than floodplain aggradation cycles. Braided-style sandstone bodies are 0.8 times, and sinuous-like sandstone bodies are 1.3 times the thickness of floodplain aggradation cycles. In the Lunde, the sandstone bodies are also 1.3 times the thickness of the floodplain cycles. The positive number further strengthens the idea that channels start and end within avulsion-belt deposits. In the Upper Carboniferous case study, sandstone bodies are 0.6 times thinner than the related cyclothem. The difference between the Carboniferous study and the Lunde and Willwood formations is believed to be related to the fact that the Carboniferous case relates to lacustrine sedimentation in most of the floodplain cycle. Only a minor part relates to delta top facies, so the sedimentary process of regional-

scale avulsions controls the Carboniferous strata.

Future studies may find that average sandstone body thickness can be predicted solely based on the thickness of a floodplain aggradation cycle via a ratio. More study is needed to differentiate between planform style and aggradational or incision character to unravel under what conditions such a thickness ratio can be applied and when it cannot be applied.

Sandstone cyclicity

The presence of floodplain cyclicity can also point to vertical sandstone body cyclicity at the scale of the floodplain aggradation cycles. Based on the proposed models, it is anticipated that the occurrence of separate channel sandstone bodies in stratigraphy with every floodplain sedimentary alternation. Such a stratigraphic distribution could reduce sandstone body connectivity by a vertical, equally spaced stratigraphic architecture (Chapter 5, Fig. 5.7). For the Willwood and Lunde formations this is predominantly at the base of the floodplain aggradation cycle. In the Upper Carboniferous case study, the sandstones are primarily positioned at the top of a cycle. As mentioned, the depositional system and mechanism differ in both cases. However, there is still a preferential position of sandstone bodies in the alternation. Generally, this vertical sandstone body spacing is interpreted to produce less stochastic connectivity due to floodplain fines separating sandstone bodies. In the Willwood Formation, crevasse splays and relatively coarser-grained sediments form the avulsion-belt deposits and connect the isolated sandstone bodies, which might counterbalance the 'layer-cake' stratigraphic architecture (e.g. Colombera and Mountney, 2021).

10.3.3 Large-scale alluvial architecture

Net-to-gross variability

It is suggested that significant changes in sandstone architecture at a stratigraphic scale of 100-200 m are related to climate change caused by the 400 kyr long-eccentricity cycle in both the Willwood Formation and the Upper Carboniferous case study. In response to this climate change, the abundance of sandstone bodies and their properties, such as planform style, geometry and grain size variations, change. In the Triassic case study, suggestions are made about net-to-gross clustering on a similar eccentricity pace; however, the evidence is inconclusive, as there is no sufficient age control. The long-eccentricity cycle is a dominant cycle controlling Earth's palaeoclimate and is well documented in the marine and lacustrine realm (e.g. Zachos et al., 2010; Hilgen et al., 2015; Vervoort et al., 2021); thus, detecting it in the alluvial sedimentary record is not surprising. Besides results in this thesis, the idea of long-eccentricity control on alluvial architecture is gaining more traction, and more studies document the imprint (e.g. Smith et al., 2014; Noorbergen et al., 2020; Sharma et al., 2023).

In the subsurface, long-term, temporary increases in sand content and change in planform style can increase reservoir potential in otherwise overall low net-to-gross stratigraphy. The developed new floodplain-based stratigraphic frameworks allow for the analysis of long-term net-to-gross-level trends with a relatively low degree of uncertainty in both case studies (Fig. 7.8 and Fig. 8.13). Convincing indications for external control on the formation of stratigraphic zones with either relatively high or low net-to-gross also increases the confidence level to include these trends in reservoir zonation schemes and geomodels.

Palaeosol as variability indicators

At eccentricity-scale, stratigraphic net-to-gross patterns and planform style changes are coeval with long-term floodplain sedimentary changes (Chapters 6 and 7). The floodplains are sensitive to palaeoclimate change (Kraus et al., 2000), so it seems logical that they similarly register this long-term climatic variability. Intervals formed by poorly developed floodplain aggradation cycles in the Willwood Formation that are sandier and include less pronounced palaeosol colours are an indication of such eccentricity control. These alternate with intervals typified by well-developed floodplain aggradation cycles that are thinner, less sandy, and show more pronounced palaeosol colours. In the Carboniferous, a variability in coal seams characteristics are documented as the coal seams show intervals of thicker and laterally more consistent occurrence alternating with thinner and less laterally consistent occurrence.

Careful study of the long-term changes in the floodplain sedimentary record could reveal long-term sandstone stratigraphy changes. A predictive indicator may emerge when consistent changes between sand occurrence and floodplain change are found. Particularly when a conceptual depositional model can be made, the uncertainty of such a predictive indicator for reservoir modelling will decrease. At these larger scales (100-200 m), the resolution of dating may be sufficient to help provide a further constraint. Comprehensive understanding of the sedimentary systems and how these, through time and space, produce the fluvial stratigraphic record is of high value for subsurface prediction.

10.3.4 Palaeosol characteristics as distance indicators

As palaeosols are partly dependent on the distance of their source material (e.g. Kraus 1999), the character of palaeosol will change with respect to the distance from the channel. In essence, this would suggest that a detailed analysis of a palaeosol's characteristics and level of pedogenesis could be used as an indicator of channel proximity in the subsurface. For example, the decrease in the drainage conditions within palaeosols moving away from the main channel bodies could be used to indicate channel proximity (e.g. Varela et al., 2021). Part of this predictive value is apparent from the Upper Triassic case study (Chapter 8), where individual sediment pulses could be traced over a kilometre scale within palaeosols and estimate the direction of the sediment source (i.e. channel; Fig. 8.16). However, multiple factors complicate the proposal. For example, the pedogenic change and characteristics change over relatively short distances of 250 - 500 m from proximal to distal palaeosols relative to channel deposits (Kraus et al., 1999; Love et al., 2000; Varela et al., 2021), multiple channels could be feeding the same position on the floodplain (Ghosh and Sarkar et al., 2011), and characteristic of pedogenesis differ per environmental setting. Therefore, estimating the proximity of a channel based on core data, although having potential, warrants further study.

10.3.5 Digital outcrop models

Over the last two decades, the use of digital outcrop models for the reconstruction of alluvial architecture has become more common (e.g. Pringle et al., 2006; Enge et al., 2007; Jones et al., 2009). Likewise, the digital outcrop models constructed in this thesis provide a good opportunity to reconstruct alluvial architecture as they are used for expanding the field-collected dataset and analysing facies' spatial distribution (Chapters 3 to 6). Still, more information can be extracted from these models. In Chapter 6, the first efforts are shown of systematic two-dimensional slicing of the digital outcrop model to create snapshots of vertical and lateral distributions of sandstone bodies

(Fig. 6.3). Expanding on this, the models could be used to generate training images for numerical models and multiple-point statistics (Pickel et al., 2015). Such exercises have been done before in vertical and lateral domains. However, commonly, this is based on steep two-dimensional cliff faces (e.g. Villamizar et al., 2015; Jackson et al., 2019) or relatively small outcrops portraying only a single channel belt (e.g. Yeste et al., 2021).

The size (~10 and ~2.5 km²), outcrop shape, and presence of floodplain markers in the Deer Creek but especially the Gillmore Hill area (Chapter 5) would allow for a detailed reconstruction of the alluvial architecture in three dimensions. As shown in Chapter 4, channel belts can be traced in the outcrop (Fig. 4.8), and by mapping the stratigraphic position of sandstone bodies to their corresponding floodplain aggradation cycle, top-view maps with channel distribution can be created for successive floodplain aggradation cycles. However, such an exercise would require extensive and detailed effort. One step further would be to populate the generated and fill a three-dimensional cube with petrophysical properties. Nevertheless, filling in the unknown, non-model remains stays challenging.

10.4 Final remarks

This study has attempted to utilise the sedimentary archive of floodplain deposits and the climatic imprint in these to improve the correlation and characterisation of low net-to-gross alluvial stratigraphy. As discussed above, this cyclostratigraphic approach has significant potential, and it provides a different, new, perspective. Still, the most complete or accurate view of alluvial stratigraphy will always require an integrated approach. The learnings from this thesis need to be combined with other disciplines, such as geomorphology and numerical modelling. For application to the subsurface, the ideas presented here should be further integrated with seismic data, pressure data and other stratigraphic methods. Cyclostratigraphy and orbital-paced climate forcing can play an important part in subsurface correlation and characterisation and should not be overlooked.

Author contributions

The chapters were authored by the people listed below. Author contributions are listed via the Contributor Role Taxonomy (CRediT) after Brand et al. (2015). Funding acquisition for all chapters was done by A.W. Martinius and H.A. Abels

Chapter 3: Lateral and vertical characteristics of floodplain aggradation cycles in the lower Eocene Willwood Formation, Bighorn Basin, Wyoming, USA

T.F. Baars: Conceptualisation, Investigation, Methodology, Data curation, Writing Original Draft, Formal Analysis, Visualisation,

Y. Wang: Conceptualisation, Investigation, Methodology, Data curation, Writing Original Draft, Formal Analysis, Software

J.E.A. Storms: Investigation, Writing - Review and Editing

A.W. Martinius: Investigation, Writing - Review and Editing, Supervision

P.D. Gingerich: Investigation, Writing - Review and Editing

M. Chmielewska: Data curation, Resources

S.J. Buckley: Data curation, Resources

H.A. Abels: Conceptualisation, Investigation, Writing - Review and Editing, Supervision

Chapter 3 has been submitted to the Geological Society of America Bulletin

Chapter 4: Sandstone body character and river planform styles of the lower Eocene Willwood Formation, Bighorn Basin, Wyoming, USA

Y. Wang: Conceptualisation, Investigation, Methodology, Data curation, Writing Original Draft, Formal Analysis, Software

T.F. Baars: Conceptualisation, Methodology, Writing Original Draft, Formal Analysis, Visualisation

H. Sahoo: Investigation

J.E.A. Storms: Investigation, Writing - Review and Editing

A.W. Martinius: Conceptualisation, Investigation, Methodology, Writing - Review and Editing, Supervision

P.D. Gingerich: Formal Analysis, Writing - Review and Editing

H.A. Abels: Conceptualisation, Investigation, Writing - Review and Editing, Supervision

Chapter 4 is based upon: Wang, Y., Baars, T.F., Sahoo, H., Storms, J.E., Martinius, A.W., Gingerich, P. and Abels, H.A., 2022. Sandstone body character and river planform styles of the lower Eocene Willwood Formation, Bighorn Basin, Wyoming, USA. *Sedimentology*, 69(7), pp.2897-2924. <https://doi.org/10/grb6x5>

Chapter 5: Stratigraphic relation between river channels and channel sandstone bodies with floodplain sedimentary environments and stratigraphy in the Willwood Formation of the Bighorn Basin, Wyoming, USA

T.F. Baars: Conceptualisation, Methodology, Investigation, Writing Original Draft, Formal Analysis, Visualisation

A.W. Martinius: Conceptualisation, Investigation, Writing - Review and Editing, Supervision

H.A. Abels: Conceptualisation, Investigation, Writing - Review and Editing, Supervision

Chapter 6: Long-term alluvial changes driven by orbital eccentricity in the lower Eocene Bighorn Basin, Wyoming

T.F. Baars: Conceptualisation, Methodology, Investigation, Writing Original Draft, Formal Analysis, Visualisation

Y. Wang: Conceptualisation, Methodology, Investigation, Data curation, Formal Analysis

A.W. Martinius: Conceptualisation, Investigation, Writing - Review and Editing, Supervision

H.A. Abels: Conceptualisation, Investigation, Writing - Review and Editing, Supervision

Chapter 7: A cyclostratigraphic framework of the Upper Carboniferous Westoe and Cleaver formations in the southern North Sea Basin as a methodology for stratigraphic reservoir characterisation

T.F. Baars: Conceptualisation, Methodology, Investigation, Writing Original Draft, Formal Analysis, Visualisation, Software

R. Huis in 't Veld: Conceptualisation, Investigation, Writing - Review and Editing, Resources

L. Zhang: Investigation, Formal Analysis

M. Koopmans: Resources, Writing - Review and Editing

D. McLean: Formal Analysis, Writing - Review and Editing, Resources

A.W. Martinius: Writing - Review and Editing, Supervision

H.A. Abels: Conceptualisation, Investigation, Writing - Review and Editing, Supervision

Chapter 7 is based upon: Baars, T.F., Huis in 't Veld, R., Zhang, L., Koopmans, M., McLean, D., Martinius, A.W., Abels, H.A., 2023, A cyclostratigraphic framework of the Upper Carboniferous Westoe and Cleaver formations in the southern North Sea Basin as a methodology for stratigraphic reservoir characterization, *Netherlands Journal of Geosciences*, 102, p. e9. <https://doi:10.1017/njg.2023.8>

Chapter 8: Implementation of cyclostratigraphic concepts and methodology in the Upper Triassic Lunde Formation to improve stratigraphic reservoir characterisation.

T.F. Baars: Conceptualisation, Methodology, Investigation, Writing Original Draft, Formal Analysis, Visualisation, Software

A.W. Martinius: Conceptualisation, Investigation, Writing - Review and Editing, Supervision

H.A. Abels: Conceptualisation, Investigation, Writing - Review and Editing, Supervision

Supplementary material

Chapter 3: Lateral and vertical characteristics of floodplain aggradation cycles in the lower Eocene Willwood Formation, Bighorn Basin, Wyoming, USA

Ch3S1 - Calculation of the Coefficient of Variation

For a stratigraphic interval that has three floodplain aggradation cycles, there are three types of assemblages, including assemblages containing only one floodplain aggradation cycle (i.e. floodplain aggradation cycle 1, floodplain aggradation cycle 2, and floodplain aggradation cycle 3), assemblages containing two cycles (i.e. floodplain aggradation cycle 1 + floodplain aggradation cycle two and floodplain aggradation cycle 2 + floodplain aggradation cycle 3), and an assemblage containing three cycles (i.e. floodplain aggradation cycle 1 + floodplain aggradation cycle 2 + floodplain aggradation cycle 3). Before calculating the CV, the thicknesses of all assemblages are rescaled by dividing the thickness over the regionally averaged mean of each assemblage. For example, when calculating the CV of the assemblages containing two floodplain aggradation cycles, we use the following equations:

$$AB_{\text{rescaled}} = \left\{ \frac{a1+b1}{a+b} \quad \frac{a2+b2}{a+b} \right\}$$
$$BC_{\text{rescaled}} = \left\{ \frac{b1+c1}{b+c} \quad \frac{b2+c2}{b+c} \right\}$$
$$\text{Assemblage_2} = \{ AB_{\text{rescaled}}, BC_{\text{rescaled}} \}$$
$$CV_{\text{assemblage_2}} = \frac{\text{std}(\text{assemblage_2})}{1}$$

Where Assemblage_2 has two components, namely floodplain aggradation cycle 1 + floodplain aggradation cycle2 and floodplain aggradation cycle 2 + floodplain aggradation cycle 3; AB_{rescaled} and BC_{rescaled} refer to the sets of rescaled thicknesses of floodplain aggradation cycle1 + floodplain aggradation cycle 2 and floodplain aggradation cycle 2 + floodplain aggradation cycle 3, respectively.

In this context, as the number of floodplain aggradation cycles that comprise an assemblage grows, it is expected that the thickness variation over the study area should become smaller. By some point, we define that the assemblage is fully compensated when the CV value stops decreasing and stabilises.

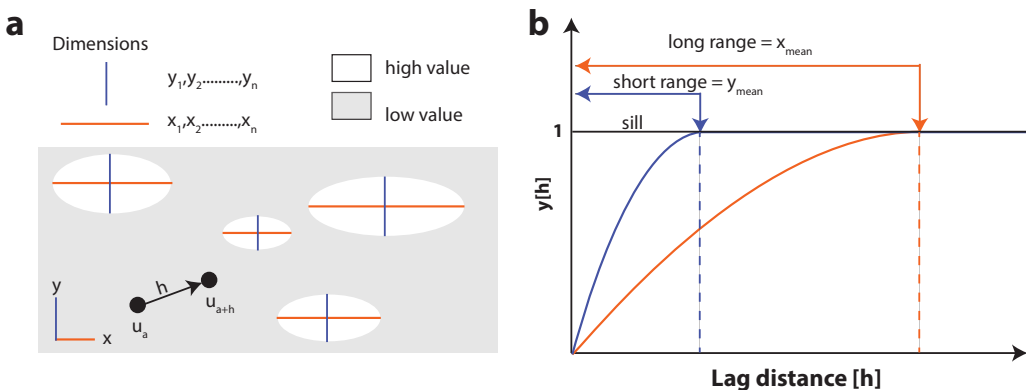
Ch3S2 - Calculation compensational stacking index.

To practically identify T_c based on 1-D data, the following workflow can be implemented:

1. draw a line with a slope of -1 (i.e. $k = 1$).
2. move this line over the data points to best fit the larger-value parts of the dataset.
3. identify the knickpoint where the leftmost data point can't be fit by this line with a slope of -1 (i.e. $k=1$).
4. observe the data points on the left of this knickpoint and get the slope of a new line that best fits the data points (this line has a slope of $-k'$).
5. compare the value of $-k'$ with values in Figure 2 by Straub and Wang (2013) to see how large autogenics influence the stratigraphy.

Ch3S4 – Variogram analysis explained

Schematic illustration of variogram components (modified from Pyrcz and Deutsch, 2003). a) There are lenses with high values in the low-value background, with various long axes (orange horizontal lines with lengths of x_1, x_2, \dots, x_n , averaging x_{mean}) and short axes (blue vertical lines with lengths of y_1, y_2, \dots, y_n , averaging y_{mean}); b) The long and short ranges corresponding to x_{mean} and y_{mean} of the high-value lens in Figure S1A, indicating the maximum distance of confident correlation and thus reflecting the spatial continuity of these lenses. Observations appear independent (i.e. variance no longer increases) when the lag distance is beyond the range, indicating non-correlation between a pair of two points when the distance between them is larger than the range.



Ch3S5 – Variogram analysis results

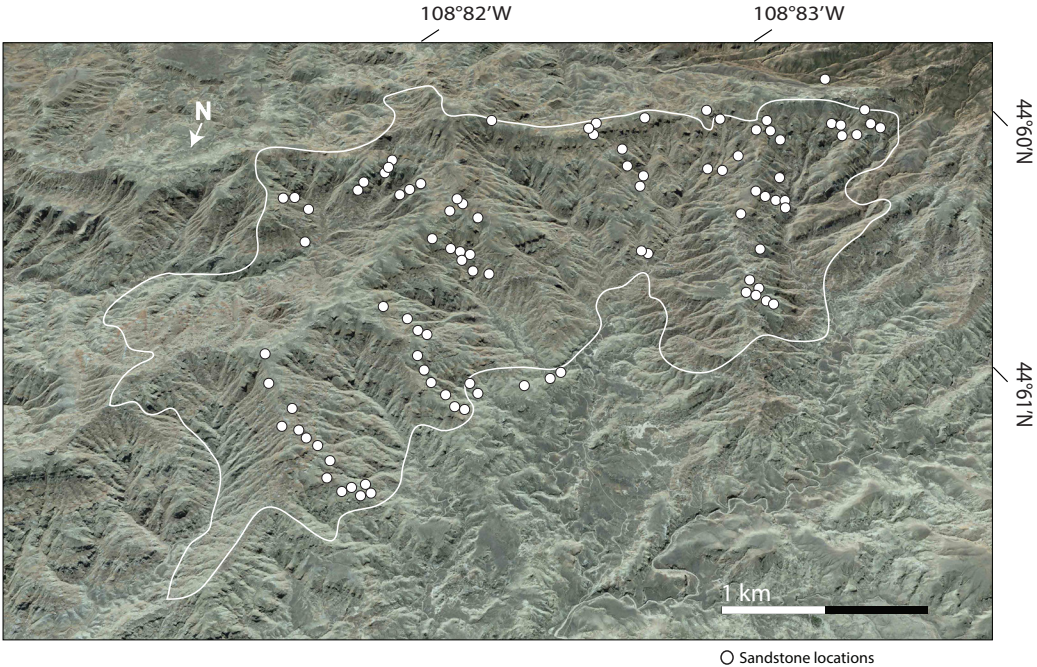
Geostatistical features of thicknesses of different floodplain aggradation cycles.

FAC ID	Short range [km]	Long range [km]	Aspect ratio	Long range azimuth
N	0.6	1.6	2.7	15°
M	0.5	1.3	2.6	350°
L	0.8	1.1	1.4	5°
K	0.7	1.4	2	80°
J	0.7	1.2	1.7	320°
I	0.4	1.2	3	310°
H	0.3	1.6	5.3	5°
Average	0.6	1.3	2.2	1°

Chapter 4: Sandstone body character and river planform styles of the lower Eocene Willwood Formation, Bighorn Basin, Wyoming, USA

Ch4S1 – Sandstone Locations

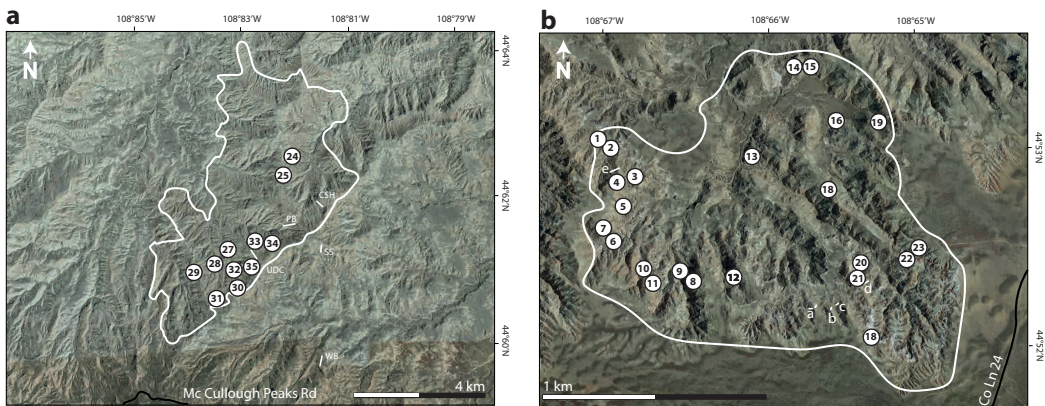
A Bird's eye view showing unmanned aerial vehicle (UAV)-based photogrammetric model coverage and field-documented sandstone bodies in the McCullough Peaks area. For further detail about the digital outcrop model see Chapter 2. Abbreviations: DCA, Deer Creek Amphitheatre section (Abels et al., 2013); UDC, Upper Deer Creek section (Abels et al., 2012); CSH, Creek Star Hill section (Abels et al., 2016); and PB, Purple Butte section. Satellite imagery from Google Earth Pro (version 7.3.6.; Eye altitude 44 km)



Chapter 5: Stratigraphic relation between river channels and channel sandstone bodies with floodplain sedimentary environments and stratigraphy in the Willwood Formation of the Bighorn Basin, Wyoming, USA

Ch5S1 – Sandstone locations

a) the Deer Creek photogrammetry model outline (for more information see Chapter 2) with locations of the sandstone bodies used in this chapter. b) the Gillmore Hill photogrammetry panel outline with locations of the sandstone bodies used in this study. In with the trench sections are indicated labelled from a to e. Satellite imagery from Google Earth Pro (version 7.3.6.; Eye altitude 44 km)



○ Sandstone locations

Ch5S2 – Gillmore Hill Isotope Data

The raw isotope data is provided as separate excel file at 4TU.Center for Research Data, with DOI: 10.4121/0c547a41-9633-4b8e-bf24-3d2f61a204db

Ch5S3 – Channel Margins

All channel margins studied in this chapter. This is provided as a separate file at 4TU.Center for Research Data, with DOI: 10.4121/0c547a41-9633-4b8e-bf24-3d2f61a204db

Chapter 7: A cyclostratigraphic framework of the Upper Carboniferous Westoe and Cleaver formations in the southern North Sea Basin as a methodology for stratigraphic reservoir characterisation

Ch7S1 – Biozones

Biozones and corresponding species picks for the wells of the study area. Biozonation is after McLean et al. (2005). Sample uncertainty is the range between the sample above and below the picked sample. The lithology of the sample is provided as this might influence the species range. Furthermore, the corresponding cycle number for the manual cyclostratigraphic framework is given.

Well	Biozone	Palynostratigraphic event	Sample lithology	Depth [md]	Sample uncertainty [m]	Corresponding cycle
44/21-3						
	Top W5a	L.O. - <i>T. sculptilis</i> ,	Mudstone	4240	30	22
44/21-4						
	Top W5a	L.O. - <i>T. sculptilis</i> ,	Mudstone	3944	21	24
	Top W4c	F.O. - <i>V. magna</i> ; L.O. - <i>T. sculptilis</i> ,	Mudstone	3992	8	21
	-	L.O. - <i>L. noctuina noctuina</i>	Mudstone	4023	12	18
	Top W4b	L.O. - <i>L. noctuina noctuina</i> ●	Mudstone	4050	21	16
	Top W4a	L.O. - <i>cingulicamerata</i> spp.	Coal	4148	18	-
44/22-8st						
	Top W5a	L.O. - <i>D. duriti</i> , <i>T. sculptilis</i> , L.O. - <i>V. magna</i> ,	Mudstone	3904	16	24
	Top W4c	F.O. - <i>V. magna</i>	Mudstone	3947	21	21
	-	L.O. - <i>L. noctuina noctuina</i>	Mudstone	3984	46	17
	Top W4b	L.O. - <i>L. noctuina noctuina</i> ●	Coal	4025	79	14
	Top W4a	L.O. - <i>cingulicamerata</i> spp.	Mudstone	4121	34	6
44/23g-14						
	Top W4b	L.O. - <i>L. noctuina noctuina</i> ●	Coal	4175	27	10
	Top W4a	L.O. - <i>Ahrensiporites</i> spp.	Mudstone	4226	9	6
44/23b-11						
	Top W4c	L.O. - "coal measures palynofacies"	Mudstone	3932	21	21
	-	L.O. - <i>L. noctuina noctuina</i>	Coal	3980	15	16
	Top W4b	L.O. - <i>L. noctuina noctuina</i> ●	Coal	4026	24	12
44/23b-13						
	Top W4c	L.O. - "coal measures palynofacies"	Mudstone	3941	30	21
	Top W4b	L.O. - <i>L. noctuina noctuina</i>	Mudstone	3986	15	16
	-	L.O. - <i>L. noctuina noctuina</i> ●	Mudstone	4038	15	11
	Top W4a	L.O. - <i>S. Infans</i>	Mudstone	4112	3	6
44/23g-15						
	Top W5a	L.O. - <i>T. tribullatus</i> , F.O. <i>Po. Granifer</i>	Mudstone	5036	48	22
	-	L.O. - <i>L. noctuina noctuina</i>	Coal	5114	33	18
	Top W4b	L.O. - <i>L. noctuina noctuina</i> ●	Coal	5138	48	10
	Top W4a	L.O. - Common <i>cingulicamerates</i>	Coal	5303	66	6

Chapter 8: Implementation of cyclostratigraphic concepts and methodology in the Upper Triassic Lunde Formation to improve stratigraphic reservoir characterisation

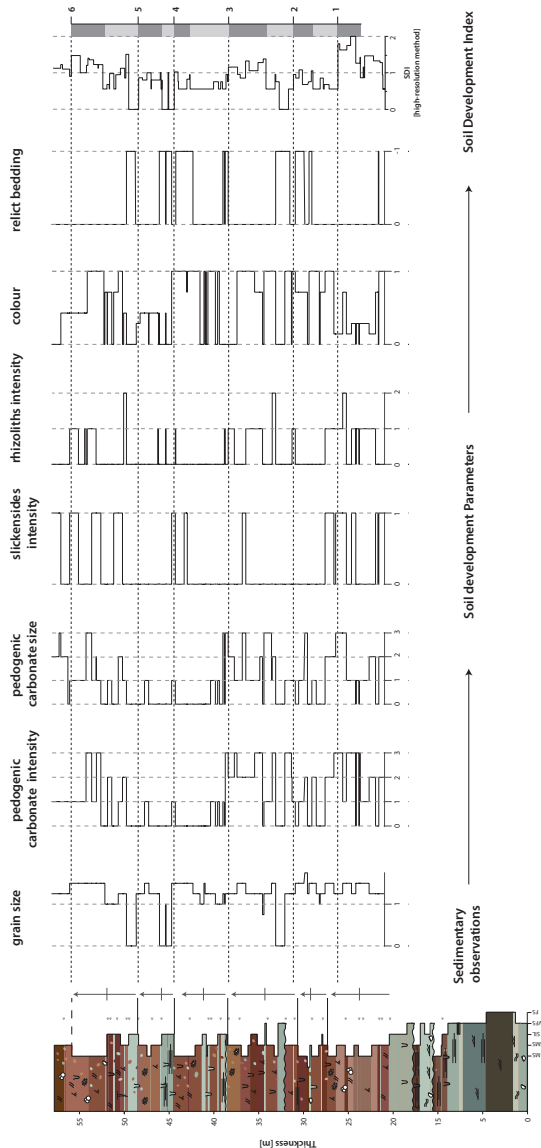
Ch8S1 – Pedogenic structures

The different groups of pedogenic carbonate structures which have been sampled and documented. All samples have been classified in at least one class but can have multiple classes based on their features.

Pedogenic carbonate group					
1	Prefered nodule	5	White nodule	9	In a channel-base
2	Angular nodule	6	In a grey matrix	10	Rhyzolith
3	Large nodule (> 1cm)	7	Fractured nodule	11	Crystalaria
4	Brown nodule	8	In a sandstone	12	Fissure
				13	Burrow

Ch8S2 – High resolution method soil development index

The input parameters for the soil development index using the ‘high-resolution method’ in cores of well. To the right of the lithological log, arrows indicate the top of palaeosol and hand interpreted floodplain aggradation cycles. Then from left to right the different, lithological-log based, parameters are displayed. These are grain size, pedogenic carbonate intensity, pedogenic carbonate size, slickensides intensity, rhizoliths intensity, colour, relict bedding and the Soil Development Index. All these individual parameters are standardized and combined into a single curve which indicates the level of pedogenic intensity of the log, the soil development index.

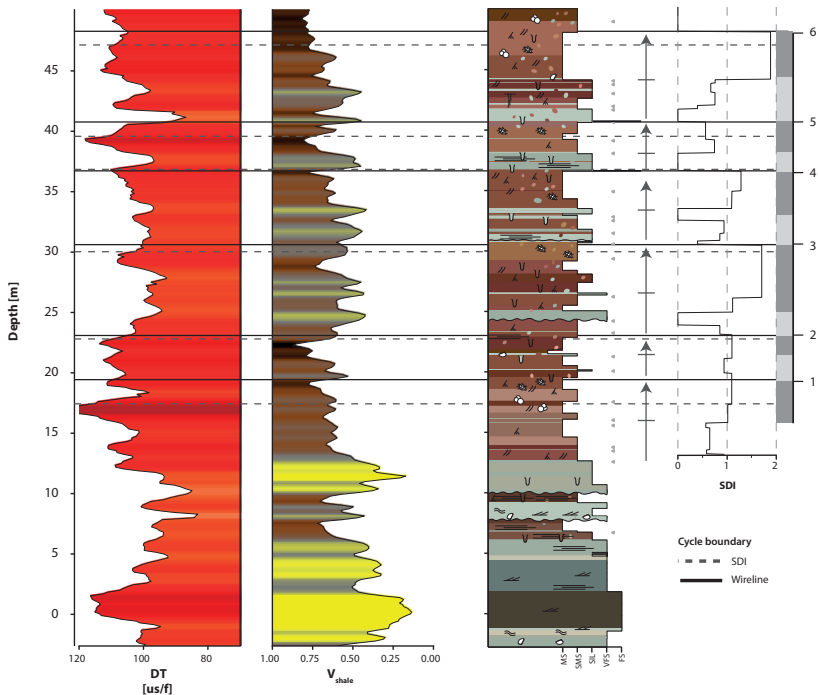


Ch8S3 – Soil development based on well-log responses

The true overbank deposits characterised by highest pedogenic alteration are generally the finest and most clay-rich sediments. These are expected to produce consistent, higher gamma-ray counts reflected as a near-vertical curve. Gamma-ray curves of the Snorre palaeosols, however, occasionally also show a gradual upwards decrease in radiation intensity. This generally implies upwards coarsening sequences or shales becoming sandier upwards. However, Nystuen and Saigal (1993) suggest that the leaching of potassium-bearing minerals such as K-feldspars and mica during pedogenic processes could also cause this effect. For this reason, further analysis of grain size was done on the V_{shale} record calculated from density and neutron porosity separation.

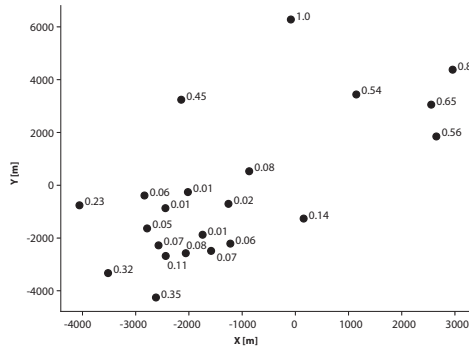
Assessment of the well-log responses was done using the SDI in core intervals. The palaeosol signature of the bulk density (RHOB) does not show significant variations and is generally quite narrow (2.4- 2.5 g/cm³), while the neutron porosity (NPHI) is marked by a broad signature (0.20-0.45 apparent limestone porosity). Sonic measurements are also generally narrow (90-110 μ s/ft) (Fig. 13). However, the sonic log could potentially be used for palaeosol identification as a spike in sonic velocity occurs near the top of a palaeosol profile. This spike could be related to the maturity and corresponding better development of slickensides in the palaeosols or a significant pedogenic carbonate horizon. Both alter the physical properties of the coherence of the palaeosol. However, there is no direct relationship between the occurrence of these features and the top of soil development.

Below: an overview of the petrophysical parameter, V_{shale} and sonic, and the correlation to the litholog, the soil development index, and the floodplain aggradation cycles. Horizontal lines mark the tops of floodplain aggradation cycles based on the SDI, while dashed lines are based on the well-responses.



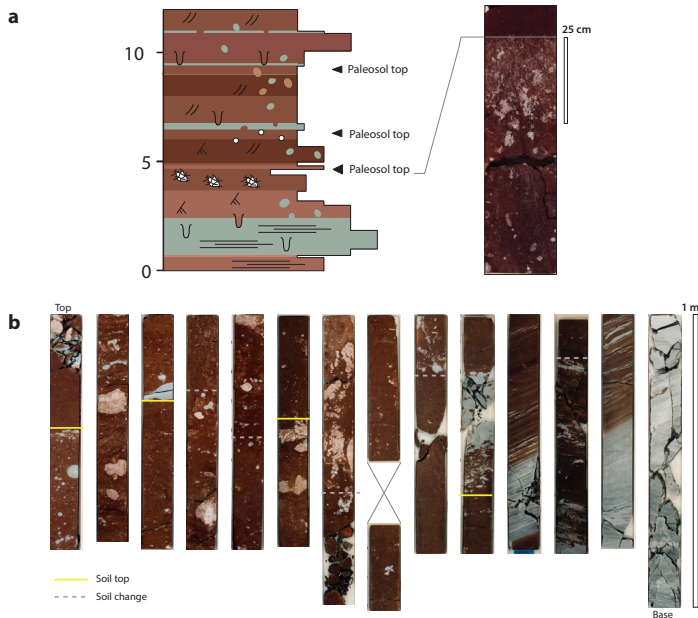
Ch8S4 – Weighted average wells

The weights used for the remove biases of well grouping when constructing vertical proportions curves. Weights were derived as the sum of the Euclidean distance from a well relative to all other wells.



Ch8S5 - Soil profiles

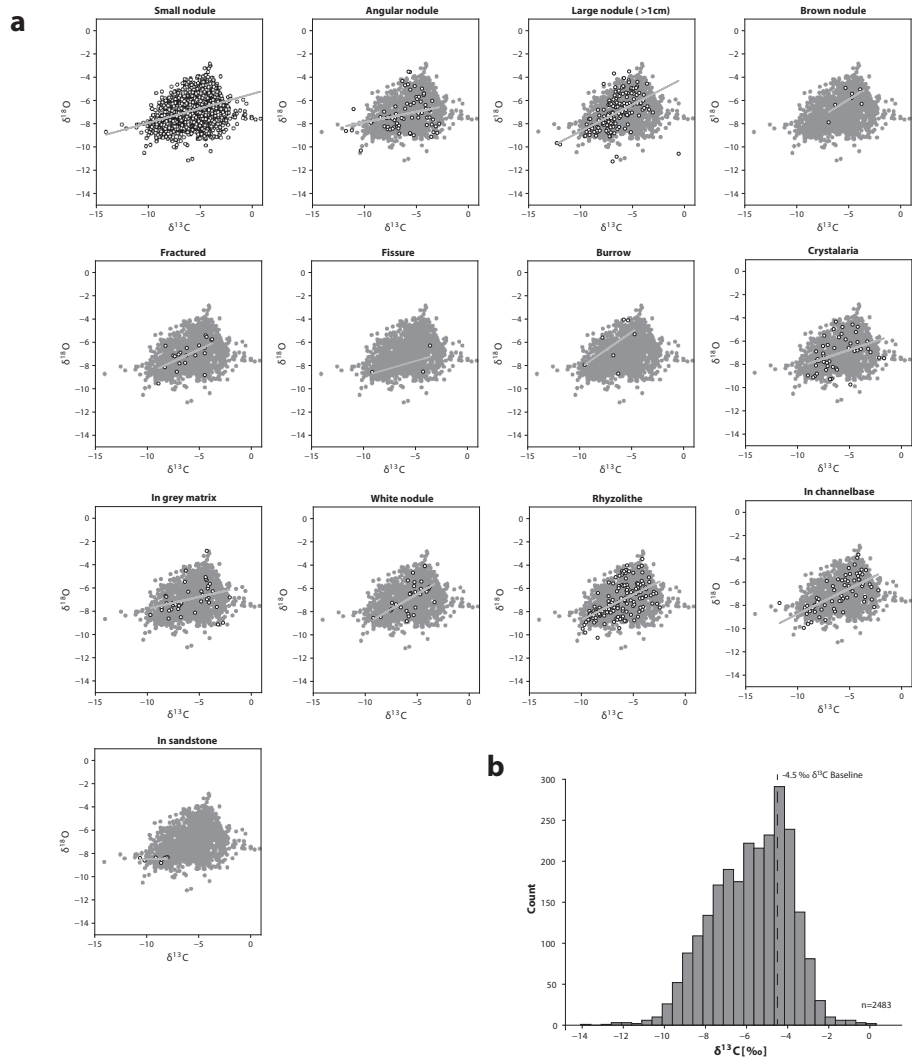
a) An overview of a succession of palaeosol development in core of well A with transitions in soil characteristics (dotted lines) and proposed soil profile tops (grey lines) indicated. Note how the soil maturity increases from right to left with several intervals of bright red (high chroma), pedogenic carbonate rich soils and darker red (low chroma) homogenous intervals. In this seemingly continuous palaeosol interval such breaks in soil maturity are used as to identify soil profile tops. b) The lower soil profile is shown in the core-photograph to the right. In this soil, a mudcracked, pedogenic carbonate-filled and interval where also carbonate nodules are present underlies a featureless coarser-grained and darker, muddy siltstone.



CH8S6 - Stable isotope variability and sensitivity

The measurements are comparable to previously measured ($n=27$) samples of the upper Lunde Formation from Nystuen and Saigal (1993), and other palaeosols records of the Late Triassic show similar ranges (Tanner, 2000; Cleveland et al., 2009). The mean $\delta^{13}\text{C}$ in this study is 0.8 ‰ lower than compared to Nystuen and Saigal (1993; -6.0 ‰ and -6.8‰ respectively), and the variability is slightly larger (-1.5 to -11.4‰ and -3 to -11‰ respectively; Fig. Ch8S6a). Using different sources of calcite for constructing the carbon isotope record might cause differences in isotopic signal as different pathways could lead to other diffraction of the stable isotope ratios (e.g. O'Leary, 1993). However, the various structures do not suggest apparent preferential clustering and specific isotopic ratios, indicating that all the sources can be used for the isotope records (Fig. Ch8S6b). Only samples within channelised sandstone deposits show more negative values ($\delta^{13}\text{C}$: -8‰, $\delta^{18}\text{O}$: -9‰). This might relate to preferential fluid flow through the more porous sandstones. However, samples from the channel base of sandstone, which is often cemented, do not display this trend. As these pedogenic carbonates are not formed at this stratigraphic position but are reworked material, samples taken from within the sandstone and the channel base are excluded. Carbonate nodule samples from channel bases have similar isotopic values as the floodplain, confirming that the nodules in the channels lag are derived from the palaeosols during erosion of the overbank sediments by channels. The raw isotope data is provided as separate excel file at 4TU.Center for Research Data, with DOI: 10.4121/0c547a41-9633-4b8e-bf24-3d2f61a204db

FIG. CH8S6 a) Several big carbonate structures were sampled in a transect to see if there is a significant internal variation within these carbonates (Table C). Nystuen and Saigal (1993) suggest that these carbonate structures formed in different growth stages, evidenced by internal carbonate cracks. Variations with these structures are within a 1‰ range similar to other documented palaeosols (e.g. in the Willwood Formation; Abels et al., 2016), suggesting there was no sizeable internal alteration or diagenesis of the calcite structures. The large variability in a small (< 10 cm) stratigraphic interval illustrates the need for a high-resolution record for stable isotopes in alluvial deposits. a) The Internal variation of $\delta^{13}\text{C}$ and $\delta^{18}\text{O}$ in the samples showing the variability over a small vertical interval or in one pedogenic carbonate structure in the different cores. b) Cross plot of the correlation of $\delta^{13}\text{C}$ and $\delta^{18}\text{O}$ isotopes for different groups of pedogenic carbonate structures (See Supplementary Data Ch8S1 for the classes). In the top left, the preferred small carbonate nodule group is plotted. This is used as a grey backdrop in other plots. Here, the different documented structures are shown. Note how there is no preferential clustering in the different groups expect for pedogenic carbonate sampled in channelized sandstone intervals. The grey line is a linear regression line indicating the average trend. c) The distribution of the $\delta^{13}\text{C}$ measurements with a proposed baseline of -4.5‰. Note the skewed distribution towards more negative values.



c

Core	Samples	$\delta^{13}\text{C}$	SD	$\delta^{18}\text{O}$	SD	note
D	5	-7.02	0.97	-6.85	0.92	3 cm nodule
D	5	-7.73	0.97	-8.18	0.31	5 cm nodule
D	6	-6.02	0.19	-8.42	0.13	4 cm nodule
B	10	-6.15	1.27	-5.85	1.49	3 cm concentrated nodule interval
A	9	-8.62	0.36	-8.60	0.43	10 cm tap root

Literature

- Abdul Aziz, H., Hilgen, F.J., van Luijk, G.M., Sluijs, A., Kraus, M.J., Pares, J.M. and Gingerich, P.D., 2008. Astronomical climate control on paleosol stacking patterns in the upper Paleocene–lower Eocene Willwood Formation, Bighorn Basin, Wyoming. *Geology*, 36(7), pp.531-534. <https://doi.org/10.1130/G24734A.1>
- Abels, H.A., Simaey, S.V., Hilgen, F.J., Man, E.D. and Vandenberghe, N., 2007. Obliquity-dominated glacio-eustatic sea level change in the early Oligocene: evidence from the shallow marine siliciclastic Rupelian stratotype (Boom Formation, Belgium). *Terra Nova*, 19(1), pp.65-73. <https://doi.org/10.1111/j.1365-3121.2006.00716.x>
- Abels, H.A., Clyde, W.C., Gingerich, P.D., Hilgen, F.J., Fricke, H.C., Bowen, G.J. and Lourens, L.J., 2012. Terrestrial carbon isotope excursions and biotic change during Palaeogene hyperthermals. *Nature Geoscience*, 5(5), pp.326-329. <https://doi.org/10/f3xn2h>
- Abels, H.A., Kraus, M.J. and Gingerich, P.D., 2013. Precession-scale cyclicity in the fluvial lower Eocene Willwood Formation of the Bighorn Basin, Wyoming (USA). *Sedimentology*, 60(6), pp.1467-1483. <https://doi.org/10/gfkwtm>
- Abels, H.A., Lauretano, V., Van Yperen, A.E., Hopman, T., Zachos, J.C., Lourens, L.J., Gingerich, P.D. and Bowen, G.J., 2016. Environmental impact and magnitude of paleosol carbonate carbon isotope excursions marking five early Eocene hyperthermals in the Bighorn Basin, Wyoming. *Climate of the Past*, 12(5), pp.1151-1163. <https://doi.org/10.5194/cp-12-1151-2016>
- Allen, J.R.L., 1974. Studies in fluvial sedimentation: Implications of pedogenic carbonate units. Lower Old Red Sandstone, Anglo-Welsh outcrop. *Geological Journal*, 9(2), pp.181-208. <https://doi.org/10/dwf995>
- Allen, J.R.L., 1978. Studies in fluvial sedimentation: an exploratory quantitative model for the architecture of avulsion-controlled alluvial suites. *Sedimentary Geology*, 21(2), pp.129-147. <https://doi.org/10/crr26h>
- Allen, P.A., 2008. Time scales of tectonic landscapes and their sediment routing systems. *Geological Society, London, Special Publications*, 296(1), pp.7-28. <https://doi.org/10/cgw4zb>
- Allen, P.A., Armitage, J.J., Carter, A., Duller, R.A., Michael, N.A., Sinclair, H.D., Whitchurch, A.L. and Whittaker, A.C., 2013. The Qs problem: Sediment volumetric balance of proximal foreland basin systems. *Sedimentology*, 60(1), pp.102-130. <https://doi.org/10/gjtch4>
- Archer, S.G., McKie, T., Andrews, S.D., Wilkins, A.D., Hutchison, M., Young-Ziolkowski, N., Osunde, C., Matheson, J., Thackrey, S., Lang, M. and Sola, B., 2022. Triassic mudstones of the Central North Sea: cross-border characterization, correlation and their palaeoclimatic significance. *Geological Society, London, Special Publications*, 494(1), pp.333-378. <https://doi.org/10/grwbmw>
- Armitage, J.J., Whittaker, A.C., Zakari, M. and Campforts, B., 2018. Numerical modelling of landscape and sediment flux response to precipitation rate change. *Earth Surface Dynamics*, 6(1), pp.77-99. <https://doi.org/10/gc4czn>
- Ashmore, P.E., 1988. Bed load transport in braided gravel-bed stream models. *Earth Surface*

- Processes and Landforms*, 13(8), pp.677-695. <https://doi.org/10/dcwrnj>
- Aslan, A., 2013. Fluvial environments | sediments. In S. A. Elias & C. J. Mock (Eds.), *Encyclopedia of quaternary science* (2nd ed.), pp.663–675. Elsevier. <https://doi.org/10.1016/B978-0-444-53643-3.00111-4>
- Atchley, S.C., Nordt, L.C. and Dworkin, S.I., 2004. Eustatic control on alluvial sequence stratigraphy: a possible example from the Cretaceous-Tertiary transition of the Tornillo Basin, Big Bend National Park, West Texas, USA. *Journal of Sedimentary Research*, 74(3), pp.391-404. <https://doi.org/10/drtd5d>
- Atchley, S.C., Nordt, L.C., Dworkin, S.I., Cleveland, D.M., Mintz, J.S. and Harlow, R.H., 2013. Alluvial stacking pattern analysis and sequence stratigraphy: concepts and case studies. <https://doi.org/10.2110/sepmsp.104.13>
- Badley, M.E., Price, J.D., Rambech Dahl, C. and Agdestein, T., 1988. The structural evolution of the northern Viking Graben and its bearing upon extensional modes of basin formation. *Journal of the Geological Society*, 145(3), pp.455-472. <https://doi.org/10/crqb77>
- Balcombe, S.R. and Arthington, A.H., 2009. Temporal changes in fish abundance in response to hydrological variability in a dryland floodplain river. *Marine and Freshwater Research*, 60(2), pp.146-159. <https://doi.org/10/bq2chm>
- Barclay, F., Bruun, A., Rasmussen, K.B., Alfaro, J.C., Cooke, A., Cooke, D., Salter, D., Godfrey, R., Lowden, D., McHugo, S. and Özdemir, H., 2008. Seismic inversion: Reading between the lines. *Oilfield Review*, 20(1), pp.42-63.
- Baville, P., Apel, M., Hoth, S., Knaust, D., Antoine, C., Carpentier, C. and Caumon, G., 2022. Computer-assisted stochastic multi-well correlation: Sedimentary facies versus well distality. *Marine and Petroleum Geology*, 135, p.105371. <https://doi.org/10/grwbk5>
- Beerbower, J.R., 1964. Cyclothems and cyclic depositional mechanisms in alluvial plain sedimentation. *Kansas Geological Survey Bulletin*, 169(1), pp.31-32. <http://www.kgs.ku.edu/Publications/Bulletins/169/Beerbower/>
- Van den Berg, J.H., Martinius, A.W. and Houthuys, R., 2017. Breaching-related turbidites in fluvial and estuarine channels: Examples from outcrop and core and implications to reservoir models. *Marine and Petroleum Geology*, 82, pp.178-205. <https://doi.org/10/f94z4v>
- Berger, A., 1988. Milankovitch theory and climate. *Reviews of geophysics*, 26(4), pp.624-657. <https://doi.org/10/fpdq8f>
- Berger, A.L., 1977. Support for the astronomical theory of climatic change. *Nature*, 269, pp.44-45. <https://doi.org/10/c7hmf4>
- Berger, A., Loutre, M.F. and Laskar, J., 1992. Stability of the astronomical frequencies over the Earth's history for paleoclimate studies. *Science*, 255(5044), pp.560-566. <https://doi.org/10/fwwtz5>
- Birgenheier, L.P., Berg, M.V., Plink-Björklund, P., Gall, R.D., Rosencrans, E., Rosenberg, M.J., Toms, L.C. and Morris, J., 2020. Climate impact on fluvial-lake system evolution, Eocene Green River Formation, Uinta Basin, Utah, USA. *GSA Bulletin*, 132(3-4), pp.562-587. <https://doi.org/10.1130/B31808.1>

- Blum, M.D. and Aslan, A., 2006. Signatures of climate vs. sea-level change within incised valley-fill successions: Quaternary examples from the Texas Gulf Coast. *Sedimentary Geology*, 190(1-4), pp.177-211. <https://doi.org/10/czpx8m>
- Blum, M.D. and Törnqvist, T.E., 2000. Fluvial responses to climate and sea-level change: a review and look forward. *Sedimentology*, 47, pp.2-48. <https://doi.org/10/dh7bcv>
- de Boer, P.L. and Smith, D.G., 1994. Orbital forcing and cyclic sequences. *Orbital forcing and cyclic sequences*, pp.1-14. <https://doi.org/10.1002/9781444304039.ch1>
- Bosmans, J.H.C., Drijfhout, S.S., Tuenter, E., Lourens, L.J., Hilgen, F.J. and Weber, S.L., 2012. Monsoonal response to mid-holocene orbital forcing in a high resolution GCM. *Climate of the Past*, 8(2), pp.723-740. <https://doi.org/10/gb9bwc>
- Bowen, G.J., Maibauer, B.J., Kraus, M.J., Röhl, U., Westerhold, T., Steimke, A., Gingerich, P.D., Wing, S.L. and Clyde, W.C., 2015. Two massive, rapid releases of carbon during the onset of the Palaeocene–Eocene thermal maximum. *Nature Geoscience*, 8(1), pp.44-47. <https://doi.org/10/gfb5ms>
- Bown, T.M. and Kraus, M.J., 1981. Lower Eocene alluvial paleosols (Willwood Formation, northwest Wyoming, USA) and their significance for paleoecology, paleoclimatology, and basin analysis. *Palaeogeography, Palaeoclimatology, Palaeoecology*, 34, pp.1-30. <https://doi.org/10/b3wthn>
- Bown, T.M. and Kraus, M.J., 1987. Integration of channel and floodplain suites; I, Developmental sequence and lateral relations of alluvial Paleosols. *Journal of Sedimentary Research*, 57(4), pp.587-601. <https://doi.org/10/dgvzf9>
- Brand, A., Allen, L., Altman, M., Hlava, M. and Scott, J., 2015. Beyond authorship: attribution, contribution, collaboration, and credit. *Learned Publishing*, 28(2), pp.151-155. <https://doi.org/10/gc6v3m>
- Braudrick, C.A., Dietrich, W.E., Leverich, G.T. and Sklar, L.S., 2009. Experimental evidence for the conditions necessary to sustain meandering in coarse-bedded rivers. *Proceedings of the National Academy of Sciences*, 106(40), pp.16936-16941. <https://doi.org/10/frvv5r>
- Bridge, J.S., 1993. The interaction between channel geometry, water flow, sediment transport and deposition in braided rivers. *Geological Society, London, Special Publications*, 75(1), pp.13-71. <https://doi.org/10/fq5476>
- Bridge, J.S. and Leeder, M.R., 1979. A simulation model of alluvial stratigraphy. *Sedimentology*, 26(5), pp.617-644. <https://doi.org/10/czbf2s>
- Bridge, J.S. and Tye, R.S., 2000. Interpreting the dimensions of ancient fluvial channel bars, channels, and channel belts from wireline-logs and cores. *AAPG bulletin*, 84(8), pp.1205-1228. <https://doi.org/10.1306/A9673C84-1738-11D7-8645000102C1865D>
- Bryant, M., Falk, P. and Paola, C., 1995. Experimental study of avulsion frequency and rate of deposition. *Geology*, 23(4), pp.365-368. <https://doi.org/10/bzs73v>
- Buckley, S.J., Ringdal, K., Naumann, N., Dolva, B., Kurz, T.H., Howell, J.A. and Dewez, T.J., 2019. LIME: Software for 3-D visualization, interpretation, and communication of virtual geoscience models. *Geosphere*, 15(1), pp.222-235. <https://doi.org/10.1130/GES02002.1>

- Burg, J.P., 1975. *Maximum entropy spectral analysis*. Stanford university.
- Carlson, C.A., Bates, N.R., Hansell, D.A. and Steinberg, D. K., 2001. Carbon cycle. In J.H. Steele (Ed.), *Encyclopedia of ocean sciences* (2nd ed.), pp.477–486. Academic Press. <https://doi.org/10.1016/B978-012374473-9.00272-1>
- Carson, M.A., 1986. Characteristics of high-energy “meandering” rivers: the Canterbury Plains, New Zealand. *Geological Society of America Bulletin*, 97(7), pp.886-895. [https://doi.org/10.1130/0016-7606\(1986\)97<886:COHMRT>2.0.CO;2](https://doi.org/10.1130/0016-7606(1986)97<886:COHMRT>2.0.CO;2)
- Castelltort, S. and Van Den Driessche, J., 2003. How plausible are high-frequency sediment supply-driven cycles in the stratigraphic record?. *Sedimentary geology*, 157(1-2), pp.3-13. <https://doi.org/10/fwpm5>
- Cazenave, A. and Nerem, R.S., 2004. Present-day sea level change: Observations and causes. *Reviews of Geophysics*, 42(3). <https://doi.org/10/dpq6mv>
- Cecil, C.B., Dulong, F.T., Cobb, J.C. and Supardi, X.X., 1993. Allogenic and autogenic controls on sedimentation in the Central Sumatra Basin as an analogue for Pennsylvanian coal-bearing strata in the Appalachian Basin. *Special Papers-Geological Society Of America*, pp.3-3. <https://doi.org/10.1130/SPE286-p3>
- Church, M., 1992. Channel morphology and typology. In C. Callow & G. Petts (Eds.), *The rivers handbook: Hydrological and ecological principles*, pp.126-143.
- Church, M., 2006. Bed material transport and the morphology of alluvial river channels. *Annu. Rev. Earth Planet. Sci.*, 34, pp.325-354. <https://doi.org/10/ftcf3z>
- Cleveland, D.M., Atchley, S.C. and Nordt, L.C., 2007. Continental sequence stratigraphy of the Upper Triassic (Norian–Rhaetian) Chinle strata, northern New Mexico, USA: allocyclic and autocyclic origins of paleosol-bearing alluvial successions. *Journal of Sedimentary Research*, 77(11), pp.909-924. <https://doi.org/10.2110/jsr.2007.082>
- Cleveland, D.M., Nordt, L.C., Dworkin, S.I. and Atchley, S.C., 2008. Pedogenic carbonate isotopes as evidence for extreme climatic events preceding the Triassic-Jurassic boundary: Implications for the biotic crisis?. *Geological Society of America Bulletin*, 120(11-12), pp.1408-1415. <https://doi.org/10/cm7pdv>
- Clyde, W.C. and Christensen, K.E., 2003. Testing the relationship between pedofacies and avulsion using Markov analysis. *American Journal of Science*, 303(1), pp.60-71. <https://doi.org/10.2475/ajs.303.1.60>
- Clyde, W.C., Gingerich, P.D., Wing, S.L., Röhl, U., Westerhold, T., Bowen, G., Johnson, K., Baczynski, A.A., Diefendorf, A., McInerney, F. and Schnurrenberger, D., 2013. Bighorn Basin Coring Project (BBCP): a continental perspective on early Paleogene hyperthermals. *Scientific Drilling*, 16, pp.21-31. <https://doi.org/10/gb9pfw>
- Clyde, W.C., Stamatakos, J. and Gingerich, P.D., 1994. Chronology of the Wasatchian land-mammal age (early Eocene): Magnetostratigraphic results from the McCullough Peaks section, northern Bighorn Basin, Wyoming. *The Journal of Geology*, 102(4), pp.367-377. <https://doi.org/10/chmtwk>
- Colombera, L., Arévalo, O.J. and Mountney, N.P., 2017. Fluvial-system response to climate change: the Paleocene-Eocene Tresp group, Pyrenees, Spain. *Global and Planetary Change*, 157, pp.1-17.

<https://doi.org/10/gcgtm6>

- Cook, M., Horstmann, M., Irondelle, M. and Hugall, J., 2014, April. Integration of Real-time LWD Spectroscopy Data to Optimize Drilling Through Paleosols Supports Low Energy Drilling Operations. In *SPE Bergen One Day Seminar*. OnePetro. <https://doi.org/10.2118/169193-ms>
- Coulthard, T.J. and Van de Wiel, M.J., 2013. Climate, tectonics or morphology: what signals can we see in drainage basin sediment yields?. *Earth Surface Dynamics*, 1(1), pp.13-27. <https://doi.org/10.5194/esurf-1-13-2013>
- Cross, T.A., 2000. Stratigraphic controls on reservoir attributes in continental strata. *Earth Science Frontiers*, 7(4), pp.322-350.
- Dalman, R.A. and Weltje, G.J., 2008. Sub-grid parameterisation of fluvio-deltaic processes and architecture in a basin-scale stratigraphic model. *Computers & Geosciences*, 34(10), pp.1370-1380. <https://doi.org/10/dsgfxj>
- Dalrymple, M., 2001. Fluvial reservoir architecture in the Statfjord Formation (northern North Sea) augmented by outcrop analogue statistics. *Petroleum Geoscience*, 7(2), pp.115-122. <https://doi.org/10/cb7sk9>
- D'Ambrosia, A.R., Clyde, W.C., Fricke, H.C., Gingerich, P.D. and Abels, H.A., 2017. Repetitive mammalian dwarfing during ancient greenhouse warming events. *Science Advances*, 3(3), p.e1601430. <https://doi.org/10/f9vxdz>
- Deegan, C.T. and BJ, S., 1977. A standard lithostratigraphic nomenclature for the Central and Northern North Sea.
- Demko, T.M., Currie, B.S. and Nicoll, K.A., 2004. Regional paleoclimatic and stratigraphic implications of paleosols and fluvial/overbank architecture in the Morrison Formation (Upper Jurassic), Western Interior, USA. *Sedimentary Geology*, 167(3-4), pp.115-135. <https://doi.org/10/bnqzcd>
- Dickens, G.R., O'Neil, J.R., Rea, D.K. and Owen, R.M., 1995. Dissociation of oceanic methane hydrate as a cause of the carbon isotope excursion at the end of the Paleocene. *Paleoceanography*, 10(6), pp.965-971. <https://doi.org/10/c2vxfx>
- Donselaar, M.E., Bhatt, A.G. and Ghosh, A.K., 2017. On the relation between fluvio-deltaic flood basin geomorphology and the wide-spread occurrence of arsenic pollution in shallow aquifers. *Science of the total environment*, 574, pp.901-913. <https://doi.org/10/gr9cc8>
- Donselaar, M.E., Overeem, I., Reichwein, J.H. and Visser, C.A., 2011. Mapping of fluvial fairways in the Ten Boer Member, southern Permian Basin. <https://doi.org/10.2110/pec.11.98.0105>
- Duchaufour, P., 1976. Dynamics of organic matter in soils of temperate regions: its action on pedogenesis. *Geoderma*, 15(1), pp.31-40. <https://doi.org/10/bksx6t>
- Edmonds, D.A., Hajek, E.A., Downton, N. and Bryk, A.B., 2016. Avulsion flow-path selection on rivers in foreland basins. *Geology*, 44(9), pp.695-698. <https://doi.org/10/f827sp>
- Edwards, J., Lallier, F., Caumon, G. and Carpentier, C., 2018. Uncertainty management in stratigraphic well correlation and stratigraphic architectures: A training-based method. *Computers & Geosciences*, 111, pp.1-17. <https://doi.org/10/gcw2ww>
- Eiler, J.M., 2011. Paleoclimate reconstruction using carbonate clumped isotope

- thermometry. *Quaternary Science Reviews*, 30(25-26), pp.3575-3588. <https://doi.org/10/b4qg39>
- Enge, H.D., Buckley, S.J., Rotevatn, A. and Howell, J.A., 2007. From outcrop to reservoir simulation model: Workflow and procedures. *Geosphere*, 3(6), pp.469-490. <https://doi.org/10/ccjg2n>
- Fagan, S.D. and Nanson, G.C., 2004. The morphology and formation of floodplain-surface channels, Cooper Creek, Australia. *Geomorphology*, 60(1-2), pp.107-126. <https://doi.org/10/dmdcx8>
- Fielding, C.R., 1986. Fluvial channel and overbank deposits from the Westphalian of the Durham coalfield, NE England. *Sedimentology*, 33(1), pp.119-140. <https://doi.org/10/cmxc8k>
- Fielding, C.R., Alexander, J. and Allen, J.P., 2018. The role of discharge variability in the formation and preservation of alluvial sediment bodies. *Sedimentary Geology*, 365, pp.1-20. <https://doi.org/10/gc8hb7>
- Fielding, C.R. and Crane, R.C., 1987. An application of statistical modelling to the prediction of hydrocarbon recovery factors in fluvial reservoir sequences. <https://doi.org/10.2110/pec.87.39.0321>
- Fielding, C.R. and Webb, J.A., 1996. Facies and cyclicity of the Late Permian Bainmedart Coal Measures in the Northern Prince Charles Mountains, MacRobertson Land, Antarctica. *Sedimentology*, 43(2), pp.295-322. <https://doi.org/10/bqc97s>
- Finn, T.M., Kirschbaum, M.A., Roberts, S.B., Condon, S.M., Roberts, L.N.R. and Johnson, R.C., 2010. Cretaceous–Tertiary composite total petroleum system (503402), Bighorn basin, Wyoming and Montana. *US Geological Survey Digital Data Series DDS–69–V*, p.157.
- Foreman, B.Z., 2014. Climate-driven generation of a fluvial sheet sand body at the Paleocene–Eocene boundary in north-west Wyoming (USA). *Basin Research*, 26(2), pp.225-241. <https://doi.org/10/gfkwjtj>
- Foreman, B.Z., Heller, P.L. and Clementz, M.T., 2012. Fluvial response to abrupt global warming at the Palaeocene/Eocene boundary. *Nature*, 491(7422), pp.92-95. <https://doi.org/10/f4chsqq>
- Foreman, B.Z., Lai, S.Y., Komatsu, Y. and Paola, C., 2015. Braiding of submarine channels controlled by aspect ratio similar to rivers. *Nature Geoscience*, 8(9), pp.700-703. <https://doi.org/10/gr9cdb>
- Foreman, B.Z. and Straub, K.M., 2017. Autogenic geomorphic processes determine the resolution and fidelity of terrestrial paleoclimate records. *Science advances*, 3(9), p.e1700683. <https://doi.org/10/gbxnn4>
- Ghosh, P. and Sarkar, S., 2011. Pedogenic and sedimentologic criteria for recognition of overbank sub-environments in a Triassic anabranching-river deposit. <https://doi.org/10.2110/sepmsp.097.125>
- Gibling, M.R., 2006. Width and thickness of fluvial channel bodies and valley fills in the geological record: a literature compilation and classification. *Journal of sedimentary Research*, 76(5), pp.731-770. <https://doi.org/10.2110/jsr.2006.060>
- Gibling, M.R., Bashforth, A.R., Falcon-Lang, H.J., Allen, J.P. and Fielding, C.R., 2010. Log jams and flood sediment buildup caused channel abandonment and avulsion in the Pennsylvanian of Atlantic Canada. *Journal of Sedimentary Research*, 80(3), pp.268-287. <https://doi.org/20100420125341>
- Gibling, M.R. and Davies, N.S., 2012. Palaeozoic landscapes shaped by plant evolution. *Nature*

- Geoscience*, 5(2), pp.99-105. <https://doi.org/10/gdj36t>
- Giles, P.T., Whitehouse, B.M. and Karymbalis, E., 2018. Interactions between alluvial fans and axial rivers in Yukon, Canada and Alaska, USA. *Geological Society, London, Special Publications*, 440(1), pp.23-43. <https://doi.org/10.1144/SP440.3>
- Gingerich, P.D., 1983. Paleocene-Eocene faunal zones and a preliminary analysis of Laramide structural deformation in the Clark's Fork Basin, Wyoming.
- Gingerich, P.D., 2010. Mammalian faunal succession through the Paleocene–Eocene thermal maximum (PETM) in western North America. *Vertebrata PalAsiatica*, 48(4), p.308-327. <http://www.vertpala.ac.cn/EN/Y2010/V48/I4/308>
- Godard, V., Tucker, G.E., Burch Fisher, G., Burbank, D.W. and Bookhagen, B., 2013. Frequency-dependent landscape response to climatic forcing. *Geophysical Research Letters*, 40(5), pp.859-863. <https://doi.org/10/gjq4jc>
- Gradstein, F.M., Ogg, J.G., Schmitz, M. and Ogg, G. eds., 2012. *The geologic time scale 2012*. Elsevier.
- Gries, R., 1983. North-south compression of Rocky Mountain foreland structures. In J.D. Lowell (Ed.), *Rocky Mountain foreland basins and uplifts: Denver, Colorado*, pp.9–32. Rocky Mountain Association of Geologists.
- Hajek, E.A., Heller, P.L. and Schur, E.L., 2012. Field test of autogenic control on alluvial stratigraphy (Ferris Formation, Upper Cretaceous–Paleogene, Wyoming). *Bulletin*, 124(11-12), pp.1898-1912. <https://doi.org/10/f4fdgc>
- Hajek, E.A., Heller, P.L. and Sheets, B.A., 2010. Significance of channel-belt clustering in alluvial basins. *Geology*, 38(6), pp.535-538. <https://doi.org/10/dp8gnm>
- Hajek, E.A. and Straub, K.M., 2017. Autogenic sedimentation in clastic stratigraphy. *Annual Review of Earth and Planetary Sciences*, 45, pp.681-709. <https://doi.org/10/gft259>
- Hajek, E.A. and Wolinsky, M.A., 2012. Simplified process modeling of river avulsion and alluvial architecture: Connecting models and field data. *Sedimentary Geology*, 257, pp.1-30. <https://doi.org/10/fv8j2p>
- Hampson, G.J., Jewell, T.O., Irfan, N., Gani, M.R. and Bracken, B., 2013. Modest change in fluvial style with varying accommodation in regressive alluvial-to-coastal-plain wedge: Upper Cretaceous Blackhawk Formation. *Journal of Sedimentary Research*, 83(2), pp.145-169. <https://doi.org/10.2110/jsr.2013.8>
- Hartley, A.J., Weissmann, G.S., Nichols, G.J. and Warwick, G.L., 2010. Large distributive fluvial systems: characteristics, distribution, and controls on development. *Journal of Sedimentary Research*, 80(2), pp.167-183. <https://doi.org/10.2110/jsr.2010.016>
- Hartley, A.J., Owen, A., Weissmann, G.S. and Scuderi, L., 2018. Modern and ancient amalgamated sandy meander-belt deposits: recognition and controls on development. *Fluvial Meanders and Their Sedimentary Products in the Rock Record*, pp.349-383. <https://doi.org/10.1002/9781119424437.ch14>
- Henkes, G.A., Passey, B.H., Grossman, E.L., Shenton, B.J., Yancey, T.E. and Pérez-Huerta, A., 2018. Temperature evolution and the oxygen isotope composition of Phanerozoic oceans from carbonate clumped isotope thermometry. *Earth and Planetary Science Letters*, 490, pp.40-50.

<https://doi.org/10/gdf6jf>

- Hilgen, F.J., Hinnov, L.A., Abdul Aziz, H., Abels, H.A., Batenburg, S., Bosmans, J.H.C., de Boer, B., Hüsing, S.K., Kuiper, K.F., Lourens, L.J., Rivera, T., Tuenter, E., Wal, R.S.W., Wotzlaw, J.F. and Zeeden, C., 2015. Stratigraphic continuity and fragmentary sedimentation: the success of cyclostratigraphy as part of integrated stratigraphy, *404*, pp.157-197. The Geological Society of London. <https://doi.org/10/gdj4bm>
- Hilgen, F.J., Krijgsman, W., Langereis, C.G., Lourens, L.J., Santarelli, A. and Zachariasse, W.J., 1995. Extending the astronomical (polarity) time scale into the Miocene. *Earth and Planetary Science Letters*, *136*(3-4), pp.495-510. <https://doi.org/10/bbvdq2>
- Hinnov, L.A., 2000. New perspectives on orbitally forced stratigraphy. *Annual Review of Earth and Planetary Sciences*, *28*(1), pp.419-475. <https://doi.org/10/cjb2dg>
- Holbrook, J.M. and Allen, S.D., 2021. The case of the braided river that meandered: Bar assemblages as a mechanism for meandering along the pervasively braided Missouri River, USA. *Bulletin*, *133*(7-8), pp.1505-1530. <https://doi.org/10/gmjxw4>
- Holbrook, J., Scott, R.W. and Oboh-Ikuenobe, F.E., 2006. Base-level buffers and buttresses: a model for upstream versus downstream control on fluvial geometry and architecture within sequences. *Journal of Sedimentary Research*, *76*(1), pp.162-174. <https://doi.org/10.2110/jsr.2005.10>
- de Hoop, S. and Voskov, D., 2021, October. Fast and robust scheme for uncertainty quantification in naturally fractured reservoirs. In *SPE reservoir simulation conference*. OnePetro. <https://doi.org/10.2118/203968-MS>
- Howell, J.A., Martinius, A.W. and Good, T.R., 2014. The application of outcrop analogues in geological modelling: a review, present status and future outlook. *Geological Society, London, Special Publications*, *387*(1), pp.1-25. <https://doi.org/10.1144/SP387.12>
- Hoy, R.G. and Ridgway, K.D., 1997. Structural and sedimentological development of footwall growth synclines along an intraforeland uplift, east-central Bighorn Mountains, Wyoming. *Geological Society of America Bulletin*, *109*(8), pp.915-935. [https://doi.org/10.1130/0016-7606\(1997\)109%3C0915:SASDOF%3E2.3.CO;2](https://doi.org/10.1130/0016-7606(1997)109%3C0915:SASDOF%3E2.3.CO;2)
- Ielpi, A. and Ghinassi, M., 2014. Planform architecture, stratigraphic signature and morphodynamics of an exhumed Jurassic meander plain (Scalby Formation, Yorkshire, UK). *Sedimentology*, *61*(7), pp.1923-1960. <https://doi.org/10.1111/sed.12122>
- Jensen, M.A. and Pedersen, G.K., 2010. Architecture of vertically stacked fluvial deposits, Atane formation, cretaceous, Nuussuaq, central West Greenland. *Sedimentology*, *57*(5), pp.1280-1314. <https://doi.org/10/dcvj7g>
- Jerolmack, D.J. and Paola, C., 2007. Complexity in a cellular model of river avulsion. *Geomorphology*, *91*(3-4), pp.259-270. <https://doi.org/10/dcq8sr>
- Jerolmack, D.J. and Paola, C., 2010. Shredding of environmental signals by sediment transport. *Geophysical Research Letters*, *37*(19). <https://doi.org/10/cxwbmm>
- Jirásek, J., Opluštil, S., Sivek, M., Schmitz, M.D. and Abels, H.A., 2018. Astronomical forcing of Carboniferous paralic sedimentary cycles in the Upper Silesian Basin, Czech Republic

- (Serpukhovian, latest Mississippian): New radiometric ages afford an astronomical age model for European biozonations and substages. *Earth-Science Reviews*, 177, pp.715-741. <https://doi.org/10/gc6npk>
- Jones, H.L. and Hajek, E.A., 2007. Characterizing avulsion stratigraphy in ancient alluvial deposits. *Sedimentary Geology*, 202(1-2), pp.124-137. <https://doi.org/10/cgpkjf>
- Jones, L.S. and Schumm, S.A., 1999. Causes of avulsion: an overview. *Fluvial sedimentology VI*, pp.169-178. <https://doi.org/10/bktxrs>
- Jones, R.R., McCaffrey, K.J.W., Clegg, P., Wilson, R.W., Holliman, N.S., Holdsworth, R.E., Imber, J. and Waggott, S., 2009. Integration of regional to outcrop digital data: 3D visualisation of multi-scale geological models. *Computers & Geosciences*, 35(1), pp.4-18. <https://doi.org/10/bkfn3n>
- de Jong, M., Nio, S.D., Smith, D. and Böhm, A.R., 2007. Subsurface correlation in the Upper Carboniferous (Westphalian) of the Anglo-Dutch Basin using the climate stratigraphic approach. *first break*, 25(12).<https://doi.org/10/bsgk4s>
- Jordan, D.W. and Pryor, W.A., 1992. Hierarchical levels of heterogeneity in a Mississippi River meander belt and application to reservoir systems. *AAPG bulletin*, 76(10), pp.1601-1624. <https://doi.org/10.1306/BDF8A6A-1718-11D7-8645000102C1865D>
- Kasse, C., Vandenberghe, J., Van Huissteden, J., Bohncke, S.J.P. and Bos, J.A.A., 2003. Sensitivity of Weichselian fluvial systems to climate change (Nochten mine, eastern Germany). *Quaternary Science Reviews*, 22(20), pp.2141-2156. <https://doi.org/10/cdph4m>
- Kennedy, J.F., 1969. The formation of sediment ripples, dunes, and antidunes. *Annual review of fluid mechanics*, 1(1), pp.147-168. <https://doi.org/10/bfmccx>
- Kim, W., Connell, S.D., Steel, E., Smith, G.A. and Paola, C., 2011. Mass-balance control on the interaction of axial and transverse channel systems. *Geology*, 39(7), pp.611-614. <https://doi.org/10/b99h2v>
- Kingsford, R.T., Curtin, A.L. and Porter, J., 1999. Water flows on Cooper Creek in arid Australia determine 'boom' and 'bust' periods for waterbirds. *Biological Conservation*, 88(2), pp.231-248. <https://doi.org/10/c7r9dh>
- Koch, P.L., Zachos, J.C. and Gingerich, P.D., 1992. Correlation between isotope records in marine and continental carbon reservoirs near the Palaeocene/Eocene boundary. *Nature*, 358(6384), pp.319-322. <https://doi.org/10/dp6zwx>
- Kovalevskiy, E.V., Gogonenkov, G.N. and Perepechkin, M.V., 2007, June. Automatic well-to-well correlation based on consecutive uncertainty elimination. In *69th EAGE Conference and Exhibition incorporating SPE EUROPEC 2007* (pp. cp-27). European Association of Geoscientists & Engineers. <https://doi.org/10.3997/2214-4609.201401693>
- Kraus, M.J. and Gingerich, P.D., 1980. Genesis of a fluvial sheet sandstone, Willwood Formation, northwest Wyoming. *Early Cenozoic Paleontology and Stratigraphy of the Bighorn Basin, Wyoming. University of Michigan Papers on Paleontology*, 24, pp.87-94.
- Kraus, M.J., 1982. Genesis of Early Tertiary Exotic Metaquartzite Conglomerates in the Absaroka-Bighorn Region, NW Wyoming.
- Kraus, M.J., 1984. Sedimentology and tectonic setting of early Tertiary quartzite conglomerates,

northwest Wyoming.

- Kraus, M.J., 1985. Early Tertiary quartzite conglomerates of the Bighorn Basin and their significance for paleogeographic reconstruction of northwest Wyoming. *Rocky Mountain Section (SEPM)*.
- Kraus, M.J., 1987. Integration of channel and floodplain suites; II, Vertical relations of alluvial Paleosols. *Journal of Sedimentary Research*, 57(4), pp.602-612. <https://doi.org/10.1306/212F8BB6-2B24-11D7-8648000102C1865D>
- Kraus, M.J., 1997. Lower Eocene alluvial paleosols: pedogenic development, stratigraphic relationships, and paleosol/landscape associations. *Palaeogeography, Palaeoclimatology, Palaeoecology*, 129(3-4), pp.387-406. <https://doi.org/10/b8mngj>
- Kraus, M.J., 1999. Paleosols in clastic sedimentary rocks: their geologic applications. *Earth-Science Reviews*, 47(1-2), pp.41-70. <https://doi.org/10/d456kx>
- Kraus, M.J., 2002. Basin-scale changes in floodplain paleosols: implications for interpreting alluvial architecture. *Journal of Sedimentary Research*, 72(4), pp.500-509. <https://doi.org/10/djrqsr>
- Kraus, M.J. and Aslan, A., 1993. Eocene hydromorphic Paleosols; significance for interpreting ancient floodplain processes. *Journal of Sedimentary Research*, 63(3), pp.453-463. <https://doi.org/10/bpvh5c>
- Kraus, M.J. and Aslan, A., 1995. Palaeosol sequences in floodplain environments: a hierarchical approach. *Palaeoweathering, palaeosurfaces and related continental deposits*, pp.303-321. <https://doi.org/10/drh854>
- Kraus, M.J. and Davies-Vollum, K.S., 2004. Mudrock-dominated fills formed in avulsion splay channels: examples from the Willwood Formation, Wyoming. *Sedimentology*, 51(5), pp.1127-1144. <https://doi.org/10/cdmj7p>
- Kraus, M.J. and Gwinn, B., 1997. Facies and facies architecture of Paleogene floodplain deposits, Willwood Formation, Bighorn basin, Wyoming, USA. *Sedimentary Geology*, 114(1-4), pp.33-54. <https://doi.org/10/fbdj67>
- Kraus, M.J. and Hasiotis, S.T., 2006. Significance of different modes of rhizolith preservation to interpreting paleoenvironmental and paleohydrologic settings: examples from Paleogene paleosols, Bighorn Basin, Wyoming, USA. *Journal of Sedimentary Research*, 76(4), pp.633-646. <https://doi.org/20121219164834>
- Kraus, M.J. and Middleton, L.T., 1987. Contrasting architecture of two alluvial suites in different structural settings.
- Van de Lageweg, W.I., Schuurman, F., Cohen, K.M., Van Dijk, W.M., Shimizu, Y. and Kleinhans, M.G., 2016. Preservation of meandering river channels in uniformly aggrading channel belts. *Sedimentology*, 63(3), pp.586-608. <https://doi.org/10/f8d7vs>
- Lanci, L., Galeotti, S., Ratcliffe, K., Tohver, E., Wilson, A. and Flint, S., 2022. Astronomically forced cycles in Middle Permian fluvial sediments from Karoo Basin (South Africa). *Palaeogeography, Palaeoclimatology, Palaeoecology*, 596, p.110973. <https://doi.org/10/gqvjdj5>
- Larue, D.K. and Hovadik, J., 2006. Connectivity of channelized reservoirs: a modelling approach. *Petroleum Geoscience*, 12(4), pp.291-308. <https://doi.org/10/d8m8j4>
- Larue, D.K. and Hovadik, J., 2008. Why is reservoir architecture an insignificant uncertainty in

- many appraisal and development studies of clastic channelized reservoirs?. *Journal of Petroleum Geology*, 31(4), pp.337-366. <https://doi.org/10/dtfm2r>
- Laskar, J., Fienga, A., Gastineau, M. and Manche, H., 2011. La2010: a new orbital solution for the long-term motion of the Earth. *Astronomy & Astrophysics*, 532, p.A89. <https://doi.org/10.1051/0004-6361/201116836>
- Laskar, J., Robutel, P., Joutel, F., Gastineau, M., Correia, A.C. and Levrard, B., 2004. A long-term numerical solution for the insolation quantities of the Earth. *Astronomy & Astrophysics*, 428(1), pp.261-285. <https://doi.org/10/bj3pbv>
- Lecce, S.A., 1997. Spatial patterns of historical overbank sedimentation and floodplain evolution, Blue River, Wisconsin. *Geomorphology*, 18(3-4), pp.265-277. <https://doi.org/10/bncfdt>
- Leclair, S.F. and Bridge, J.S., 2001. Quantitative interpretation of sedimentary structures formed by river dunes. *Journal of Sedimentary Research*, 71(5), pp.713-716. <https://doi.org/10/dxnrg4>
- Leeder, M.R., 1977. A quantitative stratigraphic model for alluvium, with special reference to channel deposit density and interconnectedness.
- Leopold, L.B. and Wolman, M.G., 1957. *River channel patterns: braided, meandering, and straight*. US Government Printing Office. <https://doi.org/10/ghvf3d>
- Lillegraven, J.A. and Albright, L.B., 2009. Where was the western margin of northwestern Wyoming's Bighorn Basin late in the early Eocene?. *Museum of Northern Arizona Bulletin*, 65, pp.37-81.
- Lillegraven, J.A. and Ostresh, L.M., 1988. Evolution of Wyoming early Cenozoic topography and drainage
- Lorenz, J.C. and Nadon, G.C., 2002. Braided-river deposits in a muddy depositional setting: the Molina Member of the Wasatch Formation (Paleogene), west-central Colorado, USA. *Journal of Sedimentary Research*, 72(3), pp.376-385. <https://doi.org/10/bx5kc3>
- Lourens, L.J., Sluijs, A., Kroon, D., Zachos, J.C., Thomas, E., Röhl, U., Bowles, J. and Raffi, I., 2005. Astronomical pacing of late Palaeocene to early Eocene global warming events. *Nature*, 435(7045), pp.1083-1087. <https://doi.org/10/cpzpbc>
- Love, S.E. and Williams, B.P., 2000. Sedimentology, cyclicity and floodplain architecture in the Lower Old Red Sandstone of SW Wales. *Geological Society, London, Special Publications*, 180(1), pp.371-388. <https://doi-org/10.1144/GSL.SP.2000.180.01.19>
- Lyster, S.J., Whittaker, A.C. and Hajek, E.A., 2022. The problem of paleo-planforms. *Geology*, 50(7), pp.822-826. <https://doi.org/10/gr9cc5>
- Machlus, M.L., Olsen, P.E., Christie-Blick, N. and Hemming, S.R., 2008. Spectral analysis of the lower Eocene Wilkins Peak Member, Green River Formation, Wyoming: Support for Milankovitch cyclicity. *Earth and Planetary Science Letters*, 268(1-2), pp.64-75. <https://doi.org/10/ct5dc3>
- Mackey, S.D. and Bridge, J.S., 1995. Three-dimensional model of alluvial stratigraphy; theory and applications. *Journal of Sedimentary Research*, 65(1b), pp.7-31. <https://doi.org/10/dwt67>
- Mahon, E.M. and Wallace, M.W., 2022. Sedimentology and seismic geomorphology of Paleocene coastal peatlands from the offshore Gippsland Basin, SE Australia. *Sedimentary Geology*, 434,

p.106145. <https://doi.org/10/grwbkw>

- Malatesta, L.C., Prancevic, J.P. and Avouac, J.P., 2017. Autogenic entrenchment patterns and terraces due to coupling with lateral erosion in incising alluvial channels. *Journal of Geophysical Research: Earth Surface*, 122(1), pp.335-355. <https://doi.org/10/f9r4d2>
- Malone, D.H., Craddock, J.P., Link, P.K., Foreman, B.Z., Scroggins, M.A. and Rappe, J., 2017. Detrital zircon geochronology of quartzite clasts, northwest Wyoming: Implications for Cordilleran Neoproterozoic stratigraphy and depositional patterns. *Precambrian Research*, 289, pp.116-128. <https://doi.org/10/f9qw2c>
- Martinius, A.W., 2000. Labyrinthine facies architecture of the Tortola fluvial system and controls on deposition (Late Oligocene-Early Miocene, Loranca Basin, Spain). *Journal of Sedimentary Research*, 70(4), pp.850-867. <https://doi.org/10/bv7qqc>
- Martinius, A.W., Geel, C.R. and Arribas, J., 2002. Lithofacies characterization of fluvial sandstones from outcrop gamma-ray logs (Loranca Basin, Spain): the influence of provenance. *Petroleum Geoscience*, 8(1), pp.51-62. <https://doi.org/10/c3rf4z>
- Maynard, J.R., 2006. Fluvial response to active extension: evidence from 3D seismic data from the Frio Formation (Oligo-Miocene) of the Texas Gulf of Mexico Coast, USA. *Sedimentology*, 53(3), pp.515-536. <https://doi.org/10/fgm66b>
- McBride, E.F., 1963. A classification of common sandstones. *Journal of Sedimentary Research*, 33(3), pp.664-669. <https://doi.org/10.1306/74D70EE8-2B21-11D7-8648000102C1865D>
- McInerney, F.A. and Wing, S.L., 2011. The Paleocene-Eocene Thermal Maximum: A perturbation of carbon cycle, climate, and biosphere with implications for the future. *Annual Review of Earth and Planetary Sciences*, 39, pp.489-516. <https://doi.org/10/b2dw9w>
- McKie, T. and Williams, B., 2009. Triassic palaeogeography and fluvial dispersal across the northwest European Basins. *Geological Journal*, 44(6), pp.711-741. <https://doi.org/10/btf6qk>
- Mearns, E.W., Knarud, R., Raestad, N., STANLEY, K.T. and Stockbridge, C.P., 1989. Samarium-neodymium isotope stratigraphy of the Lunde and Statfjord formations of Snorre oil field, northern North Sea. *Journal of the Geological Society*, 146(2), pp.217-228. <https://doi.org/10/fm3z4f>
- van der Meulen, B., Gingerich, P.D., Lourens, L.J., Meijer, N., van Broekhuizen, S., van Ginneken, S. and Abels, H.A., 2020. Carbon isotope and mammal recovery from extreme greenhouse warming at the Paleocene–Eocene boundary in astronomically-calibrated fluvial strata, Bighorn Basin, Wyoming, USA. *Earth and Planetary Science Letters*, 534, p.116044. <https://doi.org/10/ggjq5>
- Meyers, S.R., 2015. The evaluation of eccentricity-related amplitude modulation and bundling in paleoclimate data: An inverse approach for astrochronologic testing and time scale optimization. *Paleoceanography*, 30(12), pp.1625-1640. <https://doi.org/10/gfxq2r>
- Miall, A.D., 1985. Architectural-element analysis: a new method of facies analysis applied to fluvial deposits. *Earth-Science Reviews*, 22(4), pp.261-308. <https://doi.org/10/drtc98>
- Miall, A.D., 1994. Reconstructing fluvial macroform architecture from two-dimensional outcrops; examples from the Castlegate Sandstone, Book Cliffs, Utah. *Journal of Sedimentary Research*, 64(2b), pp.146-158. <https://doi.org/10.1306/D4267F78-2B26-11D7->

- Miall, A.D., 2013. *The geology of fluvial deposits: sedimentary facies, basin analysis, and petroleum geology*. Springer.
- Milankovitch, M.M., 1941. Canon of insolation and the iceage problem. *Koniglich Serbische Akademice Beograd Special Publication*, 132.
- Millard, C., Hajek, E. and Edmonds, D.A., 2017. Evaluating controls on crevasse-splay size: Implications for floodplain-basin filling. *Journal of Sedimentary Research*, 87(7), pp.722-739. <https://doi.org/10.2110/jsr.2017.40>
- Mjøs, R., 2005. Evaluation report, stratigraphy, and sedimentology of the Snorre field. Internal report, Statoil ASA
- Mohrig, D., Heller, P.L., Paola, C. and Lyons, W.J., 2000. Interpreting avulsion process from ancient alluvial sequences: Guadalupe-Matarranya system (northern Spain) and Wasatch Formation (western Colorado). *Geological Society of America Bulletin*, 112(12), pp.1787-1803. [https://doi.org/10.1130/0016-7606\(2000\)112%3C1787:IAPFAA%3E2.0.CO;2](https://doi.org/10.1130/0016-7606(2000)112%3C1787:IAPFAA%3E2.0.CO;2)
- Montgomery, D.R., 2001. Slope distributions, threshold hillslopes, and steady-state topography. *American Journal of science*, 301(4-5), pp.432-454. <https://doi.org/10/fhxcsw>
- Müller, R., Ngstuen, J.P., Eide, F. and Lie, H., 2005. Late Permian to Triassic basin infill history and palaeogeography of the Mid-Norwegian shelf—East Greenland region. In *Norwegian Petroleum Society Special Publications* (Vol. 12, pp. 165-189). Elsevier. <https://doi.org/10/b395g7>
- Muller, R., Nystuen, J.P. and Wright, V.P., 2004. Pedogenic mud aggregates and paleosol development in ancient dryland river systems: criteria for interpreting alluvial mudrock origin and floodplain dynamics. *Journal of Sedimentary Research*, 74(4), pp.537-551. <https://doi.org/10/dwk6zf>
- Murray, A.B. and Paola, C., 2003. Modelling the effect of vegetation on channel pattern in bedload rivers. *Earth Surface Processes and Landforms: The Journal of the British Geomorphological Research Group*, 28(2), pp.131-143. <https://doi.org/10/bgr5hg>
- Muto, T., Steel, R.J. and Swenson, J.B., 2007. Autostratigraphy: a framework norm for genetic stratigraphy. *Journal of Sedimentary Research*, 77(1), pp.2-12. <https://doi.org/10.2110/jsr.2007.005>
- Neasham, J., 1967. *The stratigraphy of the Willwood Formation in the vicinity of Sheep Mountain, southwestern Big Horn County, Wyoming* (Doctoral dissertation).
- Neasham, J.W., 1970. *Sedimentology of the Willwood Formation (Lower Eocene): an alluvial molasse facies in northwestern Wyoming, USA*. Iowa State University.
- Neasham, J.W. and Vondra, C.F., 1972. Stratigraphy and petrology of the lower Eocene Willwood formation, Bighorn Basin, Wyoming. *Geological Society of America Bulletin*, 83(7), pp.2167-2180. [https://doi.org/10.1130/0016-7606\(1972\)83](https://doi.org/10.1130/0016-7606(1972)83)
- Nicholas, A.P., Aalto, R.E., Smith, G.S. and Schwendel, A.C., 2018. Hydrodynamic controls on alluvial ridge construction and avulsion likelihood in meandering river floodplains. *Geology*, 46(7), pp.639-642. <https://doi.org/10/gdvhfg>
- Nie, J., Garzione, C., Su, Q., Liu, Q., Zhang, R., Heslop, D., Necula, C., Zhang, S., Song, Y. and Luo,

- Z., 2017. Dominant 100,000-year precipitation cyclicity in a late Miocene lake from northeast Tibet. *Science advances*, 3(3), p.e1600762. <https://doi.org/10/gr5wmt>
- Noorbergen, L.J., Abels, H.A., Hilgen, F.J., Robson, B.E., de Jong, E., Dekkers, M.J., Krijgsman, W., Smit, J., Collinson, M.E. and Kuiper, K.F., 2018. Conceptual models for short-eccentricity-scale climate control on peat formation in a lower Palaeocene fluvial system, north-eastern Montana (USA). *Sedimentology*, 65(3), pp.775-808. <https://doi.org/10/gc65cq>
- Noorbergen, L.J., Turtu, A., Kuiper, K.F., Kasse, C., van Ginneken, S., Dekkers, M.J., Krijgsman, W., Abels, H.A. and Hilgen, F.J., 2020. Long-eccentricity regulated climate control on fluvial incision and aggradation in the Palaeocene of north-eastern Montana (USA). *Sedimentology*, 67(5), pp.2529-2560. <https://doi-org/10.1111/sed.12710>
- Saigal, G. and Nystuen, J.P., 1999. Paleosol Development and Alluvial Processes in the Upper Triassic and Lower Jurassic Lunde and Statfjord Formations, Snorre Field, Northern North Sea. <https://www.osti.gov/etdeweb/biblio/20008101>
- Nystuen, J.P. and Fält, L.M., 1995. Upper Triassic-Lower Jurassic reservoir rocks in the Tampen Spur area, Norwegian North Sea. In *Norwegian petroleum society special publications* (Vol. 4, pp. 135-179). Elsevier. [https://doi.org/10.1016/S0928-8937\(06\)80041-X](https://doi.org/10.1016/S0928-8937(06)80041-X)
- Nystuen, J.P., Kjemperud, A.V., Müller, R., Adestål, V. And Schomacker, E.R., 2014. Late Triassic to Early Jurassic climatic change, northern North Sea region: impact on alluvial architecture, palaeosols and clay mineralogy. *From depositional systems to sedimentary successions on the Norwegian continental margin*, pp.59-99. <https://doi.org/10.1002/9781118920435.ch3>
- Nystuen, J.P., Knarud, R., Jorde, K. and Stanley, K.O., 1989. Correlation of Triassic to Lower Jurassic sequences, Snorre field and adjacent areas, northern North Sea. In *Correlation in Hydrocarbon Exploration: Proceedings of the conference Correlation in Hydrocarbon Exploration organized by the Norwegian Petroleum Society and held in Bergen, Norway, 3-5 October 1988* (pp. 273-289). Springer Netherlands. https://doi.org/10.1007/978-94-009-1149-9_21
- Van Ojik, K., Böhm, A.R., Cremer, H., Geluk, M.C., De Jong, M.G., Mijndieff, H.F. and Nio, S.D., 2011. The rationale for an integrated stratigraphic framework of the Upper Rotliegend II depositional system in The Netherlands. <https://doi.org/10.2110/pec.11.98.0037>
- O'Leary, M.A., 1993. Biochemical basis of carbon isotope fractionation. In 'Stable isotopes and plant carbon-water relations'. (Eds JR Ehleringer, AE Hall, GD Farquhar) pp. 19-28. <https://doi.org/10.1016/B978-0-08-091801-3.50009-X>
- Olsen, H. (1990). Astronomical forcing of meandering river behaviour: Milankovitch cycles in Devonian of East Greenland. *Palaeogeography, Palaeoclimatology, Palaeoecology*, 79(1), 99-115. <https://doi.org/10/bqsr4>
- Olsen, H., 1994. Orbital forcing on continental depositional system-lacustrine and fluvial cyclicity in the Devonian of East Greenland. *Orbital forcing and cyclic sequences*, pp.429-438. <https://doi-org/10.1002/9781444304039.ch26>
- Olsen, T., Steel, R., Hogseth, K., Skar, T. and Roe, S.L., 1995. Sequential architecture in a fluvial succession; sequence stratigraphy in the Upper Cretaceous Mesaverde Group, Prince Canyon, Utah. *Journal of Sedimentary Research*, 65(2b), pp.265-280. <https://doi.org/10/bk5g2w>

- Opluštil, S., Laurin, J., Hýlová, L., Jirásek, J., Schmitz, M. and Sivek, M., 2022. Coal-bearing fluvial cycles of the late Paleozoic tropics; astronomical control on sediment supply constrained by high-precision radioisotopic ages, Upper Silesian Basin. *Earth-Science Reviews*, 228, p.103998. <https://doi.org/10/grwbkv>
- Owen, A., Ebinghaus, A., Hartley, A.J., Santos, M.G. and Weissmann, G.S., 2017. Multi-scale classification of fluvial architecture: An example from the Palaeocene–Eocene Bighorn Basin, Wyoming. *Sedimentology*, 64(6), pp.1572-1596. <https://doi.org/10/gbw2rr>
- Owen, A., Hartley, A.J., Ebinghaus, A., Weissmann, G.S. and Santos, M.G., 2019. Basin-scale predictive models of alluvial architecture: Constraints from the Palaeocene–Eocene, Bighorn Basin, Wyoming, USA. *Sedimentology*, 66(2), pp.736-763. <https://doi-org/10.1111/sed.12515>
- Oyama, M., & Takehara, H., 1970. Revised standard soil color charts. *Research Council for Agriculture, Forestry*.
- Paola, C., Straub, K., Mohrig, D. and Reinhardt, L., 2009. The “unreasonable effectiveness” of stratigraphic and geomorphic experiments. *Earth-Science Reviews*, 97(1-4), pp.1-43. <https://doi.org/10/dz8cgt>
- Paredes, J.M., Foix, N. and Allard, J.O., 2016. Sedimentology and alluvial architecture of the Bajo Barreal Formation (Upper Cretaceous) in the Golfo San Jorge Basin: Outcrop analogues of the richest oil-bearing fluvial succession in Argentina. *Marine and Petroleum Geology*, 72, pp.317-335. <https://doi.org/10/gkmz48>
- Parker, G., 1976. On the cause and characteristic scales of meandering and braiding in rivers. *Journal of fluid mechanics*, 76(3), pp.457-480. <https://doi.org/10/fdtk62>
- Pickel, A., Frechette, J.D., Comunian, A. and Weissmann, G.S., 2015. Building a training image with Digital Outcrop Models. *Journal of Hydrology*, 531, pp.53-61. <https://doi.org/10/f74bpw>
- Plink-Björklund, P., 2015. Morphodynamics of rivers strongly affected by monsoon precipitation: Review of depositional style and forcing factors. *Sedimentary Geology*, 323, pp.110-147. <https://doi.org/10/f7gn7v>
- Posamentier, H.W., Davies, R.J., Cartwright, J.A. and Wood, L., 2007. Seismic geomorphology-an overview. *Special Publication-Geological Society of London*, 277, p.1. <https://doi.org/10/d5rvg2>
- Powell, E.J., Kim, W. and Muto, T., 2012. Varying discharge controls on timescales of autogenic storage and release processes in fluvio-deltaic environments: Tank experiments. *Journal of Geophysical Research: Earth Surface*, 117(F2). <https://doi.org/10/gmv8xm>
- Pranter, M.J., Cole, R.D., Panjaitan, H. and Sommer, N.K., 2009. Sandstone-body dimensions in a lower coastal-plain depositional setting: lower Williams Fork Formation, Coal Canyon, Piceance Basin, Colorado. *AAPG bulletin*, 93(10), pp.1379-1401. <https://doi.org/10/cnt4pc>
- Pringle, J.K., Howell, J.A., Hodgetts, D., Westerman, A.R. and Hodgson, D.M., 2006. Virtual outcrop models of petroleum reservoir analogues: a review of the current state-of-the-art. *First break*, 24(1093). <https://doi.org/10.3997/1365-2397.2006005>
- Project, C. I., 2023. 'Teaching materials'. <https://www.cyclostratigraphy.org/teaching-materials>
- Pryor, W.A., 1960. Cretaceous sedimentation in upper Mississippi Embayment. *AAPG Bulletin*, 44(9), pp.1473-1504. <https://doi.org/10.1306/0BDA61C4-16BD-11D7->

- Pyrzcz, M. (2020). <https://github.com/GeostatsGuy/>
- Pyrzcz, M.J. and Deutsch, C.V., 2003. The whole story on the hole effect. *Geostatistical Association of Australasia, Newsletter*, 18, pp.3-5.
- Pyrzcz, M.J. and Deutsch, C.V., 2014. *Geostatistical reservoir modeling*. Oxford university press.
- Reinhardt, J. and Sigleo, W.R. eds., 1988. *Paleosols and weathering through geologic time: principles and applications* (Vol. 216). Geological Society of America.
- Retallack, G.J., 2008. *Soils of the past: an introduction to paleopedology*. John Wiley & Sons.
- Rohling, E.J. and Hilgen, F.J., 2007. The eastern Mediterranean climate at times of sapropel formation: a review. *Netherlands Journal of Geosciences/Geologie en Mijnbouw*, (Classic Papers).
- Romans, B.W., Castellort, S., Covault, J.A., Fildani, A. and Walsh, J.P., 2016. Environmental signal propagation in sedimentary systems across timescales. *Earth-Science Reviews*, 153, pp.7-29. <https://doi.org/10/f8gq8k>
- Rossignol-Strick, M., 1983. African monsoons, an immediate climate response to orbital insolation. *Nature*, 304(5921), pp.46-49. <https://doi.org/10/d7gb6q>
- Ruddiman, W.F., 2006. Orbital changes and climate. *Quaternary Science Reviews*, 25(23-24), pp.3092-3112. <https://doi.org/10/cf3tnz>
- Sahoo, H., Gani, M.R., Gani, N.D., Hampson, G.J., Howell, J.A., Storms, J.E., Martinius, A.W. and Buckley, S.J., 2020. Predictable patterns in stacking and distribution of channelized fluvial sand bodies linked to channel mobility and avulsion processes. *Geology*, 48(9), pp.903-907. <https://doi.org/10/ghp3xx>
- Sambrook Smith, G.H., Ashworth, P.J., Best, J.L., Woodward, J. and Simpson, C.J., 2006. The sedimentology and alluvial architecture of the sandy braided South Saskatchewan River, Canada. *Sedimentology*, 53(2), pp.413-434. <https://doi.org/10/bctmcw>
- Santos, M.G., Mountney, N.P. and Peakall, J., 2017. Tectonic and environmental controls on Palaeozoic fluvial environments: reassessing the impacts of early land plants on sedimentation. *Journal of the Geological Society*, 174(3), pp.393-404. <https://doi.org/10/f98nz8>
- Savitzky, A. and Golay, M.J., 1964. Smoothing and differentiation of data by simplified least squares procedures. *Analytical chemistry*, 36(8), pp.1627-1639. <https://doi.org/10/dktbw4>
- Schumm, S.A., 1985. Patterns of alluvial rivers. *Annual Review of Earth and Planetary Sciences*, 13(1), pp.5-27. <https://doi.org/10/fvstcc>
- Scotese, C.R., Song, H., Mills, B.J. and van der Meer, D.G., 2021. Phanerozoic paleotemperatures: The earth's changing climate during the last 540 million years. *Earth-Science Reviews*, 215, p.103503. <https://doi.org/10/ghtg89>
- Secord, R., Wing, S.L. and Chew, A., 2008. Stable isotopes in early Eocene mammals as indicators of forest canopy structure and resource partitioning. *Paleobiology*, 34(2), pp.282-300. <https://doi.org/10/b33s98>
- Seeland, D., 1998. Late Cretaceous, Paleocene, and early Eocene paleogeography of the Bighorn Basin and northwestern Wyoming.

- Shanley, K.W. and McCabe, P.J., 1994. Perspectives on the sequence stratigraphy of continental strata. *AAPG bulletin*, 78(4), pp.544-568. <https://doi.org/10.1306/BDF9258-1718-11D7-8645000102C1865D>
- Sharma, N., Whittaker, A.C., Watkins, S.E., Valero, L., V´erit´e, J., Puigdefabregas, C., Adatte, T., Garc´es, M., Guillocheau, F. and Castellort, S., 2023. Water discharge variations control fluvial stratigraphic architecture in the Middle Eocene Escanilla formation, Spain. *Scientific Reports*, 13(1), p.6834. <https://doi.org/10/gr9cc4>
- Shepherd, M., 2009. The reservoir framework.
- Simpson, G. and Castellort, S., 2012. Model shows that rivers transmit high-frequency climate cycles to the sedimentary record. *Geology*, 40(12), pp.1131-1134. <https://doi.org/10/f4hb5h>
- Slater, C., Preston, T. and Weaver, L.T., 2001. Stable isotopes and the international system of units. *Rapid Communications in Mass Spectrometry*, 15(15), pp.1270-1273. <https://doi.org/10/dvd5pj>
- Slingerland, R. and Smith, N.D., 2004. River avulsions and their deposits. *Annu. Rev. Earth Planet. Sci.*, 32, pp.257-285. <https://doi.org/10/fnnmp7>
- Smedes, H.W. and Prostka, H.J., 1972. *Stratigraphic framework of the Absaroka volcanic supergroup in the Yellowstone National Park region* (No. 729-C). <https://doi.org/10/gr9cdd>
- Smith, M.E., Carroll, A.R., Scott, J.J. and Singer, B.S., 2014. Early Eocene carbon isotope excursions and landscape destabilization at eccentricity minima: Green River Formation of Wyoming. *Earth and Planetary Science Letters*, 403, pp.393-406. <https://doi.org/10/f6jjtb>
- Smith, N.D., Cross, T.A., Dufficy, J.P. and Clough, S.R., 1989. Anatomy of an avulsion. *Sedimentology*, 36(1), pp.1-23. <https://doi.org/10/fm8djf>
- Ditzler, C., Scheffe, K. and Monger, H.C., 2017. Soil science division staff. *Soil survey manual. USDA Handbook, 18*, p.603. Staff, S. S. D. (1993). Soil survey manual. In *Soil conservation service, U.S. department of agriculture* (Vol. 18).
- Stap, L., Sluijs, A., Thomas, E., & Lourens, L. (2009). Patterns and magnitude of deep sea carbonate dissolution during Eocene Thermal Maximum 2 and H2, Walvis Ridge, southeastern Atlantic Ocean. *Paleoceanography*, 24(1). <https://doi.org/10.1029/2008PA001655>
- Steel, R.J., 1993. Triassic–Jurassic megasequence stratigraphy in the Northern North Sea: rift to post-rift evolution. In *Geological Society, London, Petroleum Geology Conference series* (Vol. 4, No. 1, pp. 299-315). The Geological Society of London. <https://doi-org.tudelft.idm.oclc.org/10.1144/0040299>
- Steel, R. and Ryseth, A., 1990. The Triassic–Early Jurassic succession in the northern North Sea: megasequence stratigraphy and intra-Triassic tectonics. *Geological Society, London, Special Publications*, 55(1), pp.139-168.
- Stolper, D.A. and Eiler, J.M., 2015. The kinetics of solid-state isotope-exchange reactions for clumped isotopes: A study of inorganic calcites and apatites from natural and experimental samples. *American Journal of Science*, 315(5), pp.363-411. <https://doi.org/10/f77htv>
- Stouthamer, E. and Berendsen, H.J., 2001. Avulsion frequency, avulsion duration, and interavulsion period of Holocene channel belts in the Rhine-Meuse delta, the Netherlands. *Journal of*

- Sedimentary Research*, 71(4), pp.589-598. <https://doi.org/10/dvvnqb>
- Stouthamer, E. and Berendsen, H.J., 2007. Avulsion: the relative roles of autogenic and allogenic processes. *Sedimentary Geology*, 198(3-4), pp.309-325. <https://doi.org/10/fqh2g8>
- Straub, K.M., Duller, R.A., Foreman, B.Z. and Hajek, E.A., 2020. Buffered, incomplete, and shredded: The challenges of reading an imperfect stratigraphic record. *Journal of Geophysical Research: Earth Surface*, 125(3), p.e2019JF005079. <https://doi.org/10/ggnbq2>
- Straub, K.M. and Foreman, B.Z., 2018. Geomorphic stasis and spatiotemporal scales of stratigraphic completeness. *Geology*, 46(4), pp.311-314. <https://doi.org/10/gc9xkx>
- Straub, K.M., Paola, C., Mohrig, D., Wolinsky, M.A. and George, T., 2009. Compensational stacking of channelized sedimentary deposits. *Journal of Sedimentary Research*, 79(9), pp.673-688. <https://doi.org/10.2110/jsr.2009.070>
- Straub, K.M. and Pyles, D.R., 2012. Quantifying the hierarchical organization of compensation in submarine fans using surface statistics. *Journal of Sedimentary Research*, 82(11), pp.889-898. <https://doi.org/10.2110/jsr.2012.73>
- Straub, K.M. and Wang, Y., 2013. Influence of water and sediment supply on the long-term evolution of alluvial fans and deltas: Statistical characterization of basin-filling sedimentation patterns. *Journal of Geophysical Research: Earth Surface*, 118(3), pp.1602-1616. <https://doi.org/10/gr9cdc>
- Sundell, K.A., 1990. Sedimentation and tectonics of the Absaroka Basin of northwestern Wyoming.
- Tal, M. and Paola, C., 2010. Effects of vegetation on channel morphodynamics: results and insights from laboratory experiments. *Earth Surface Processes and Landforms*, 35(9), pp.1014-1028. <https://doi.org/10/b4wh4r>
- Tanner, L.H., 2000. Palustrine-lacustrine and alluvial facies of the (Norian) Owl Rock Formation (Chinle Group), Four Corners Region, southwestern USA: implications for late Triassic paleoclimate. *Journal of Sedimentary Research*, 70(6), pp.1280-1289. <https://doi.org/10/dc4xps>
- Taylor, A.M., Gowland, S., Leary, S., Keogh, K.J. and Martinius, A.W., 2014. Stratigraphical correlation of the Late Jurassic Lourinhã Formation in the Consolação Sub-basin (Lusitanian Basin), Portugal. *Geological Journal*, 49(2), pp.143-162. <https://doi.org/10/f54sx2>
- Thonon, I., Middelkoop, H. and Van der Perk, M., 2007. The influence of floodplain morphology and river works on spatial patterns of overbank deposition. *Netherlands Journal of Geosciences*, 86(1), pp.63-75. <https://doi.org/10/grwbnf>
- Tokpanov, Y., Smith, J., Ma, Z., Deng, L., Benhallam, W., Salehi, A., Zhai, X., Darabi, H. and Castineira, D., 2020, October. Deep-learning-based automated stratigraphic correlation. In *SPE Annual Technical Conference and Exhibition*. OnePetro. <https://doi.org/10.2118/201459-MS>
- Van Toorenburg, K.A., Donselaar, M.E., Noordijk, N.A. and Weltje, G.J., 2016. On the origin of crevasse-splay amalgamation in the Huesca fluvial fan (Ebro Basin, Spain): Implications for connectivity in low net-to-gross fluvial deposits. *Sedimentary Geology*, 343, pp.156-164. <https://doi.org/10/gr9cc9>
- Törnqvist, T.E. and Bridge, J.S., 2002. Spatial variation of overbank aggradation rate and its influence on avulsion frequency. *Sedimentology*, 49(5), pp.891-905. <https://doi.org/10/d7xjdd>

- Torsvik, T.H., Carlos, D., Mosar, J., Cocks, L.R.M. and Malme, T., 2002. Global reconstructions and North Atlantic paleogeography 440 Ma to recent. *BATLAS–Mid Norway plate reconstruction atlas with global and Atlantic perspectives. Geological Survey of Norway, Trondheim, 18*, p.39.
- Tucker, G.E. and Slingerland, R., 1997. Drainage basin responses to climate change. *Water Resources Research*, 33(8), pp.2031-2047. <https://doi.org/10/cnx8v5>
- Valenza, J.M., Edmonds, D.A., Hwang, T. and Roy, S., 2020. Downstream changes in river avulsion style are related to channel morphology. *Nature Communications*, 11(1), p.2116. <https://doi.org/10/ggk93>
- Valenza, J.M., Edmonds, D.A. and Weissmann, G.S., 2022. Quantifying river avulsion activity from satellite remote sensing: Implications for how avulsions contribute to floodplain stratigraphy in foreland basins. *Journal of Sedimentary Research*, 92(6), pp.487-502. <https://doi.org/2022071314071317100>
- Valero, L., Huerta, P., Garcés, M., Armenteros, I., Beamud, E. and Gómez-Paccard, M., 2017. Linking sedimentation rates and large-scale architecture for facies prediction in nonmarine basins (Paleogene, Almazán Basin, Spain). *Basin Research*, 29, pp.213-232. <https://doi.org/10/f9rzq4>
- Valero, L., Peris, S., Sharma, N., Watkins, S., Beamud, E., Garces, M., Vinyoles, A., Tremblin, M., Zaki, A., Guillocheau, F. and Whittaker, A.C., 2020, December. Source to Sink Upstream or Downstream Propagation of Climate Cycles and Events: Insights from the South Pyrenean Foreland Basin. In *AGU Fall Meeting Abstracts* (Vol. 2020, pp. PP037-0011).
- Vandenberghe, J., 1995. Timescales, climate and river development. *Quaternary Science Reviews*, 14(6), pp.631-638. <https://doi.org/10/fr8jjq>
- Vandenberghe, J., 2003. Climate forcing of fluvial system development: an evolution of ideas. *Quaternary Science Reviews*, 22(20), pp.2053-2060. <https://doi.org/10/fbfpnj>
- Vandenberghe, N., Hilgen, F.J., Speijer, R., 2012. The paleogene period. In Gradstein, F.M., Ogg, J.G., Schmitz, M. and Ogg, G. eds., 2012. *The geologic time scale 2012*. elsevier.
- Varela, A.N., 2015. Tectonic control of accommodation space and sediment supply within the Mata Amarilla Formation (lower Upper Cretaceous) Patagonia, Argentina. *Sedimentology*, 62(3), pp.867-896. <https://doi.org/10/f68sgq>
- Varela, A.N., 2015. Tectonic control of accommodation space and sediment supply within the Mata Amarilla Formation (lower Upper Cretaceous) Patagonia, Argentina. *Sedimentology*, 62(3), pp.867-896. <https://doi.org/10/gbbnmX>
- Varela, A.N., Yeste, L.M., Viseras, C., García-García, F. and Paz, D.M., 2021. Implications of palaeosols in low net-to-gross fluvial architecture reconstruction: Reservoir analogues from Patagonia and Spain. *Palaeogeography, Palaeoclimatology, Palaeoecology*, 577, p.110553. <https://doi.org/10/grwbk8>
- Vaughan, A., Hansen, T., Cardon, H. and Radcliffe, N., 1999. Litho-flow facies prediction in an alluvial fan/fluvial system, central North Sea. *Petroleum Geoscience*, 5(4), pp.409-419. <https://doi.org/10/cgxtc5>
- Vaughan, S., Bailey, R.J. and Smith, D.G., 2011. Detecting cycles in stratigraphic data: Spectral analysis in the presence of red noise. *Paleoceanography*, 26(4). <https://doi.org/10/dz2pmd>

- Villamizar, C.A., Hampson, G.J., Flood, Y.S. and Fitch, P.J., 2015. Object-based modelling of avulsion-generated sandbody distributions and connectivity in a fluvial reservoir analogue of low to moderate net-to-gross ratio. <https://doi.org/10.1144/petgeo2015-004>
- Visconti, F., Camporeale, C. and Ridolfi, L., 2010. Role of discharge variability on pseudomeandering channel morphodynamics: Results from laboratory experiments. *Journal of Geophysical Research: Earth Surface*, 115(F4). <https://doi.org/10/b3gxgz>
- Wainman, C.C. and McCabe, P.J., 2020. Correlation of fluvial strata in the subsurface—A review. *Marine and Petroleum Geology*, 122, p.104611. <https://doi.org/10/ghp3zc>
- Walling, D.E. and He, Q., 1998. The spatial variability of overbank sedimentation on river floodplains. *Geomorphology*, 24(2-3), pp.209-223. <https://doi.org/10/fdjqmh>
- Wang, C., Adriaens, R., Hong, H., Elsen, J., Vandenberghe, N., Lourens, L.J., Gingerich, P.D. and Abels, H.A., 2017. Clay mineralogical constraints on weathering in response to early Eocene hyperthermal events in the Bighorn Basin, Wyoming (Western Interior, USA). *GSA Bulletin*, 129(7-8), pp.997-1011. <https://doi.org/10.1130/B31515.1>
- Wang, Y., 2021. Alluvial Stratigraphic Response to Astronomical Climate Change: Numerical modelling and outcrop study in the Bighorn Basin, Wyoming, USA.
- Wang, Y., Baars, T.F., Sahoo, H., Storms, J.E., Martinius, A.W., Gingerich, P. and Abels, H.A., 2022. Sandstone body character and river planform styles of the lower Eocene Willwood Formation, Bighorn Basin, Wyoming, USA. *Sedimentology*, 69(7), pp.2897-2924. <https://doi.org/10.1111/sed.13027>
- Wang, Y., Storms, J.E., Martinius, A.W., Karssenbergh, D. and Abels, H.A., 2021. Evaluating alluvial stratigraphic response to cyclic and non-cyclic upstream forcing through process-based alluvial architecture modelling. *Basin Research*, 33(1), pp.48-65. <https://doi.org/10/ghp3xn>
- Wang, Y., Straub, K.M. and Hajek, E.A., 2011. Scale-dependent compensational stacking: An estimate of autogenic time scales in channelized sedimentary deposits. *Geology*, 39(9), pp.811-814. <https://doi.org/10/dvbwwh>
- Weissmann, G.S., Hartley, A.J., Scuderi, L.A., Nichols, G.J., Owen, A., Wright, S., Felicia, A.L., Holland, F. and Anaya, F.M.L., 2015. Fluvial geomorphic elements in modern sedimentary basins and their potential preservation in the rock record: a review. *Geomorphology*, 250, pp.187-219. <https://doi.org/10/ghs3wf>
- Wells, N.A. and Dorr Jr, J.A., 1987. Shifting of the Kosi river, northern India. *Geology*, 15(3), pp.204-207. <https://doi.org/10/bd4td8>
- Went, D.J. and McMahan, W.J., 2018. Fluvial products and processes before the evolution of land plants: evidence from the lower Cambrian Series Rouge, English Channel region. *Sedimentology*, 65(7), pp.2559-2594.
- Westerhold, T., Marwan, N., Drury, A.J., Liebrand, D., Agnini, C., Anagnostou, E., Barnet, J.S., Bohaty, S.M., De Vleeschouwer, D., Florindo, F. and Frederichs, T., 2020. An astronomically dated record of Earth's climate and its predictability over the last 66 million years. *Science*, 369(6509), pp.1383-1387. <https://doi.org/10/gg994r>
- Westerhold, T., Röhl, U., Donner, B., McCarren, H.K. and Zachos, J.C., 2011. A complete

- high-resolution Paleocene benthic stable isotope record for the central Pacific (ODP Site 1209). *Paleoceanography*, 26(2). <https://doi.org/10/cm6p92>
- Westerhold, T., Röhl, U., Laskar, J., Raffi, I., Bowles, J., Lourens, L.J. and Zachos, J.C., 2007. On the duration of magnetochrons C24r and C25n and the timing of early Eocene global warming events: Implications from the Ocean Drilling Program Leg 208 Walvis Ridge depth transect. *Paleoceanography*, 22(2). <https://doi.org/10.1029/2006PA001322>
- Willis, B.J. and Behrensmeyer, A.K., 1994. Architecture of Miocene overbank deposits in northern Pakistan. *Journal of Sedimentary Research*, 64(1b), pp.60-67. <https://doi.org/10.1306/D4267F46-2B26-11D7-8648000102C1865D>
- Willis, B.J. and Behrensmeyer, A.K., 1995. Fluvial systems in the Siwalik Miocene and Wyoming paleogene. *Palaeogeography, Palaeoclimatology, Palaeoecology*, 115(1-4), pp.13-35. [https://doi.org/10.1016/0031-0182\(94\)00105-H](https://doi.org/10.1016/0031-0182(94)00105-H)
- Winy, S.L. and Bown, T.M., 1985. Fine scale reconstruction of late Paleocene-early Eocene paleogeography in the Bighorn Basin of northern Wyoming. Rocky Mountain Section (SEPM).
- Wise, D.U., 2000. Laramide structures in basement and cover of the Beartooth uplift near Red Lodge, Montana. *AAPG bulletin*, 84(3), pp.360-375.
- Yang, C.S. and Baumfalk, Y.A., 1994. Milankovitch cyclicity in the Upper Rotliegend Group of the Netherlands offshore. *Orbital forcing and cyclic sequences*, pp.47-61. <https://doi.org/10.1002/9781444304039.ch5>
- Yonkee, W.A. and Weil, A.B., 2015. Tectonic evolution of the Sevier and Laramide belts within the North American Cordillera orogenic system. *Earth-Science Reviews*, 150, pp.531-593. <https://doi.org/10/gg2vjg>
- Yuretich, R.F., Hickey, L.J., Gregson, B.P. and Hsia, Y.L., 1984. Lacustrine deposits in the Paleocene fort union formation, northern Bighorn Basin, Montana. *Journal of Sedimentary Research*, 54(3), pp.836-852. <https://doi.org/10.1306/212F8512-2B24-11D7-8648000102C1865D>
- Zachos, J.C., McCarren, H., Murphy, B., Röhl, U. and Westerhold, T., 2010. Tempo and scale of late Paleocene and early Eocene carbon isotope cycles: Implications for the origin of hyperthermals. *Earth and Planetary Science Letters*, 299(1-2), pp.242-249. <https://doi.org/10/fm8n2s>
- Zachos, J., Pagani, M., Sloan, L., Thomas, E. and Billups, K., 2001. Trends, rhythms, and aberrations in global climate 65 Ma to present. *science*, 292(5517), pp.686-693. <https://doi.org/10/ckdj6v>
- Zamanian, K., Pustovoytov, K. and Kuzyakov, Y., 2016. Pedogenic carbonates: Forms and formation processes. *Earth-Science Reviews*, 157, pp.1-17. <https://doi.org/10/f8s68w>
- Zeeden, C., Meyers, S.R., Lourens, L.J. and Hilgen, F.J., 2015. Testing astronomically tuned age models. *Paleoceanography*, 30(4), pp.369-383. <https://doi.org/10/f7cbx4>
- Zhang, J., Burgess, P.M., Granjeon, D. and Steel, R., 2019. Can sediment supply variations create sequences? Insights from stratigraphic forward modelling. *Basin Research*, 31(2), pp.274-289. <https://doi.org/10.1111/bre.12320>
- Zhang, Y., Person, M., Paola, C., Gable, C.W., Wen, X.H. and Davis, J.M., 2005. Geostatistical analysis of an experimental stratigraphy. *Water resources research*, 41(11).

Chapter cover images

Chapter 1: Top view drone photo of a splay depositing on top of a red paleosol bed. Photo taken during the 2019 field campaign by T.F. Baars

Chapter 2: Satellite image of the Bighorn Basin. Satellite imagery from Google Earth Pro (version 7.3.6.; Eye altitude 525 km)

Chapter 3: Drone photo of the red beds of the Willwood Formation at the Polecat Bench section in the Bighorn Basin. Taken during the 2019 field campaign by T.F. Baars

Chapter 4: A trunk classified sandstone body with water escape convolution structures. Photo taken by A. Martinius

Chapter 5: Drone photo of a sandstone body interfingering with floodplain fines in the Willwood Formation in the Deer Creek Area of the Bighorn Basin. Photo taken during the 2018 field campaign by M. Chmielewska

Chapter 6: Drone photo a braided style sandstone body and red beds at the Polecat Bench section in the Bighorn Basin. Photo taken during the 2019 field campaign by T.F. Baars

Chapter 7: Core photographs of core 44/21-4 with finely laminated clay and siltstones of the Westoe Formation. Photo taken from the British Geology Survey repository.

Chapter 8: Core sections of the Upper Lunde Formation which have been described and sampled for pedogenic carbonate. Photo taken during a 2021 sampling campaign in Stavanger, Norway by T.F. Baars.

Chapter 9: A photograph of a drone (Phantom 4) used for gathering areal imagery for digital outcrop models. Photo taken during the 2018 field campaign by H.A. Abels

Chapter 10: The highest part of the Gillmore Hill area with a thunderstorm in the background. Photo taken during the 2019 field campaign by T.F. Baars

Acknowledgements

Looking back to my time as a PhD candidate, I am grateful for all the help and support I have gotten throughout these years. It is impossible to mention all of you here, so please accept my sincere gratitude to you, especially.

First, I would like to thank my promotor, Allard Martinius, who has shown me the pragmatism and industry approach to doing science and helped me translate my ‘science for science’ into applying and integrating methods for practical use. Your relaxed attitude and helicopter view have helped me put everything into perspective.

I especially want to thank my copromotor and daily supervisor, Hemmo Abels, for all our meetings, discussions, fieldwork, and core viewings. Running after an almost 2-meter-tall curious and always enthusiastic guy in the field can be more challenging than it seems! Hemmo, I hugely appreciate your mentorship, companionship, and, above all, trust.

I would also like to thank Joep Storms. You have always been there to discuss my work but also stretch the importance of my personal life and that there is more than pursuing a PhD.

I wish to thank Philip Gingerich for welcoming me to the Bighorn Basin and sharing your 50 plus years experience of the basin with me, showing me around, and especially listening to your stories while having dinner or sitting on the porch with a beer after a long day in the field.

Stephan ‘Barry’ de Hoop, thank you for being a fantastic colleague. From my first day as a PhD, we hit it off. You have helped me tremendously with math and programming, and I appreciated our digital working together sessions. Thanks to you, I discovered some great music, and over the last five years, you have become a true friend.

Emilio Cecchetti, thank you for all the help and fun in the office and field. I enjoyed our camping, and your flying skills (both tent and drone), in the Bighorn Basin and the numerous coffee breaks, lunches, and discussions about work and music, in the office.

Youwei Wang, thank you for all our shared work, fun in the field, and the outstanding (authentic) Chinese cuisine you let me discover. Without you and your ideas, this book would be half the size.

Akeel ‘Yalla’ Alharbi, you always came by to check in how I was doing which I highly appreciated. Thank you for the shared field trips and fun time in office.

Rémi Charton, thank you for all the advice, welcoming me as a young PhD student, and organising the Think and Drink and other social activities. Your attitude really makes our world a better place.

This study was funded by TKI Nieuw Gas from the Topsector Energie programme, Wintershall Noordzee B.V., and Equinor ASA. From Wintershall, I thank Richard Huis in 't Veld, Maaïke Koopmans and Fred Kluin for sharing their knowledge and expertise for the Upper Carboniferous case study. From Equinor, I would like to thank Vincent Wagner and Sigrid Pillen for their enthusiasm and active discussions and Michal Warchol, Cathrine Pedersen and Harry Brandsen for their expertise and help in the Upper Triassic Case study. Furthermore, I would like to thank the Snorre geologists and geophysicists for their help with sampling.

I also want to thank everyone from the Applied Geology section for sharing the office and having a joyfull time! Thank you, Giovanni Bertotti, Jan Kees Blom, Pierre-Olivier Bruna, Andrea Cuesta Cano, Sebastian Geiger, Jasper Hupkes, Parvin Kolah-Kaj, Santosh Kumar, Jasper Maars, Nazif Onaral, Guillaume Rongier, Eli Kamel Targhi, and Aulia Valencia.

Furthermore, I want to thank the Bachelor and Master students I guided, Deema Albeesh , Harold Jolly, Hein Lafeber, Shlahga Tapa, Rutger Treur, and Linzhi Zhang.

I would also like to thank Jeroen van der Lubbe and Suzan Warmerdam-Verdegaal from the Vrije Universiteit Amsterdam stable isotope laboratory for their help in the lab and doing stable isotope analysis.

Thank you, Sven and Peter, for your support, the endless board game and magic nights, cycling trips, and for coping with my non-responsive moments of drifting off and thinking about my PhD.

I want to thank my father and dog Acca for their support, always welcoming me home, and for helping out where they can.

Nienke, thank you for cooping with me, always supporting and encouraging me, and sometimes holding me back. Because of you, I feel confident and know everything will be alright. You bring me joy.

Last, I want to thank my mother. Mama, dankjewel, zonder jou had ik dit niet gekund en dit boekje is voor jou.

Curriculum Vitae

About the author

Timothy Baars was born on February 25, 1994, in Hoevelaken. From an early age on he was interested in geology and history as his parents were teachers in geography and history while his granddad worked as a geologist at the Dutch engineering company Grontmij. After graduating from the Vathorst College in Amersfoort in 2012, he started the Geology curriculum with a Bachelor's at the Vrije Universiteit Amsterdam and continued with his Master's at Utrecht University. Here he got interested in climate reconstruction, sedimentology, integrated stratigraphy, and drilling cores while working under the supervision of dr. B. van der Schootbrugge, dr. M. Ziegler and dr. H.J.L. van der Lubbe. He worked on the Early Jurassic Toarcian ocean anoxic event and the Pleistocene Indo-Pacific Walker cell circulation using core material. His PhD thesis project, under the supervision of Prof. dr. A.W. Martinius and dr. H.A. Abels allowed him to further develop expertise in integrated stratigraphic research and sedimentology on alluvial stratigraphy while also working closely together with industry and the application of research for subsurface characterisation. The interplay between sedimentology, cyclostratigraphy and subsurface data is his favourite topic.



Spotify code: some recommendations while reading this thesis.



Publications

- Baars, T.F.**, Huis in 't Veld, R., Zhang, L., Koopmans, M., McLean, D., Martinius, A.W., Abels, H.A., 2023, A cyclostratigraphic framework of the Upper Carboniferous Westoe and Cleaver formations in the southern North Sea Basin as a methodology for stratigraphic reservoir characterization, *Netherlands Journal of Geosciences*, 102, p. e9. [hppts://doi:10.1017/njg.2023.8](https://doi.org/10.1017/njg.2023.8)
- Wang, Y., **Baars, T.F.**, Sahoo, H., Storms, J.E., Martinius, A.W., Gingerich, P. and Abels, H.A., 2022. Sandstone body character and river planform styles of the lower Eocene Willwood Formation, Bighorn Basin, Wyoming, USA. *Sedimentology*, 69(7), pp.2897-2924. <https://doi.org/10/grb6x5>
- Van der Lubbe, H.J.L., Hall, I.R., Barker, S., Hemming, S.R., **Baars, T.F.**, Starr, A., Just, J., Backeberg, B.C. and Joordens, J.C.A., 2021. Indo-Pacific Walker circulation drove Pleistocene African aridification. *Nature*, 598(7882), pp.618-623. <https://doi.org/10/gnhq3z>
- Zhang, J., Jiang, Z., Liang, C., **Baars, T.F.**, Wang, Y. and Abels, H.A., 2022. Astronomical forcing of meter-scale organic-rich mudstone–limestone cyclicity in the Eocene Dongying sag, China: Implications for shale reservoir exploration. *AAPG Bulletin*, 106(8), pp.1557-1579. <https://doi.org/10.1306/02072220103>

Samenvatting

Alluviale afzettingen in de ondergrond zijn essentieel voor geo-energieproductie en -opslag in veel regio's wereldwijd. Een nauwkeurige correlatie en karakterisering van alluviale stratigrafie vereist inzicht in hoe rivierguelen ruimtelijk zijn afgezet en welke geomorfologische processen hierop invloed hadden. Dit geldt vooral voor alluviale stratigrafie met een relatief laag zandsteen gehalte. Zo genoemde 'low nett-to-gross' stratigrafie bestaat uit een relatief lage gehalte reservoirs van zandsteen en veel klei en silt afzettingen die geen reservoir vormen. Hier zijn de zandstenengeulen vaak van elkaar geïsoleerd en vertonen ze een zwakke driedimensionale connectiviteit met elkaar. Hierdoor is de zowel correlatie als de karakterisering in alluviale systemen met een lage netto-brutoverhoudingen een uitdaging.

Regionaal doorlopende oppervlakken, zoals paleosolen of steenkoollagen, kunnen helpen bij het correleren van dergelijke afzettingen omdat ze een grote laterale omvang van tientallen kilometers kunnen hebben. De vorming van zulke paleosolen of steenkoollagen wordt vaak bepaald door factoren die onafhankelijk van het riviersysteem zijn en gedreven worden op een bekkenwijde schaal, zogenaamde allogene factoren. Een van de belangrijkste allogene invloeden in riviersystemen aan het begin van het systeem (het bronnengebied) is klimaatvariabiliteit. Deze treedt op in verschillende tijdschalen. Deze klimaatbeheersing is vaak cyclisch van aard. In die gevallen waar dit cyclische signaal bewaard is gebleven, kan er een sterke verticale herhaling van ruimte tussen paleosolen of steenkoollagen zijn, wat nuttig kan zijn bij het voorspellen van alluviale architectuur. Door deze afzettingen te identificeren en te correleren, kan het dus mogelijk zijn om stratigrafische correlatie en karakterisering van zandsteenverdeling in alluviale stratigrafie met een lage netto-brutoverhouding te verbeteren.

Deze scriptie onderzoekt het potentieel van cyclische klimaatbeheersing door orbitale forcing in fluviale systemen en de toepassing ervan op reservoirkarakterisering en ondergrondse correlatie. Hiervoor worden zes studies gepresenteerd. Vier van deze studies zijn gericht op een analoge locatie in de Bighorn Basin, Wyoming, VS, waar goed blootgestelde rood gekleurde afzettingen van de vroege Eoceen in de overstromingsvlakte worden bestudeerd. Deze rode afzettingen vormen een ritmische afwisseling met afzettingen van lichtbruine kleur en worden verondersteld te worden aangedreven door precessie-gestuurde orbitale forcing. De bevindingen van deze studies worden vervolgens toegepast in twee casusstudies in de ondergrond van de Noordzee.

Hoofdstuk 3 maakt gebruik van een driedimensionaal digitaal model van de analoge locatie om de laterale en verticale variabiliteit van de cycli in de overstromingsvlakte in het Bighorn Basin te bestuderen. De meeste afwisselingen zijn consequent te traceren in het model, maar er is aanzienlijke laterale en verticale diktevariatie. Er bestaat een sterke relatie tussen de diktevariatie en de gemiddelde paleostroomrichting in laterale richting, waarbij de variatie in dikte groter is loodrecht op de paleostroomrichting dan langs de paleostroomrichting. Deze variabiliteit wordt geïnterpreteerd als het gevolg van morfologische elementen die georiënteerd zijn in de paleostroomrichting, waardoor er meer consistentie is in sedimentaire kenmerken. In de verticale richting zijn er aanzienlijke diktevariëaties tussen opeenvolgende sedimentaire afwisselingen; dünnere cycli volgen dükkere dan gemiddelde cycli in de overstromingsvlakte. Deze variabiliteit wordt verklaard door interne paleotopografische verschillen en wordt verondersteld te worden gecompenseerd door stapelgedrag.

Hoofdstuk 4 onderzoekt de zandsteenlichamen in het Bighorn Basin. Er worden in totaal vier lithofaciesassociaties van kanalen erkend, die worden geïnterpreteerd als afzettingen van vier rivierpatroonstijlen: scheurkanaal, hoofdkanaal, gevlochten kanaal en sinusoidaal kanaal, waarbij de laatste twee stijlen dominant zijn. De afwisselende aanwezigheid van sinusoidale en gevlochten rivierstijlen biedt inzicht in een nieuwe reconstructie van een paleogeografisch model voor het Bighorn Basin. In het geschematiseerde model komen verschillende dwarse systemen samen met een axiaal systeem dat min of meer de richting van het bekken volgt, in overeenstemming met eerdere reconstructies.

Hoofdstuk 5 combineert de waarnemingen uit de vorige twee hoofdstukken en onderzoekt de relatie tussen de cyclische afwisselingen in de overstromingsvlakte en de gekanaliseerde zandsteenlichamen. Het blijkt dat zandsteenlichamen een voorkeurspositie hebben aan de basis van de cycli in de overstromingsvlakte en dat er een dikteverhouding tussen beide bestaat. Op basis van de waarnemingen worden twee afzettingsmodellen besproken voor de cycli in de overstromingsvlakte. Een model dat wordt aangedreven door kanaalaggradatie, superverheffing en afsnijding, en een model dat wordt aangedreven door fasen van fluviale activiteit en inactiviteit. Beide modellen geven aan dat de detectie van cyclische afwisselingen in de overstromingsvlakte kan wijzen op cyclische zandsteenlichamen en invloed kan hebben op de verticale verdeling ervan.

Hoofdstuk 6 documenteert grootschalige (100-200 m) veranderingen in alluviale stratigrafie. Op basis van een stratigrafisch kader van de overstromingsvlakte worden twee onderscheidende intervallen gedocumenteerd. Een interval gedomineerd door sinusoidale afzettingen met sterk uitgesproken kleuren van paleosolen en een interval gedomineerd door gevlochten afzettingen met minder goed uitgesproken kleuren van paleosolen. Op basis van een stabiel koolstofisotooprecord wordt de stratigrafie gecorreleerd met het mariene domein. Dit maakte een correlatie mogelijk tussen de gedefinieerde intervallen met lange-excentriciteit. Gevlochten fluviale architectuur domineerde tijdens perioden van minimale excentriciteit, terwijl sinusoidale fluviale architectuur dominant was tijdens perioden van maximale excentriciteit. Deze correlatie suggereert dat de link tussen orbitale excentriciteit als klimaatforcering en rivierpatroonstijlen en overstromingsvlaktekenmerken een instrument kan bieden voor toekomstige analyses van alluviale stratigrafie en dat vergelijkbare patronen in de ondergrond kunnen worden gevonden.

Hoofdstuk 7, de eerste ondergrondse casusstudie, onderzoekt de Upper Carboniferous Westoe en Cleaver formaties in de zuidelijke Noordzee. Sequenties met groffer wordende korrelgrotte, ook wel cyclothememen genoemd, worden gebruikt om putten op een hoge resolutie en over grote afstanden te correleren. Cyclothememen vertonen variabele diktes en lithologische kenmerken, en verschillende typen worden gedefinieerd. Deze variabiliteit wordt geïnterpreteerd als interne fluviale dynamiek. Er worden twee putcorrelaties gemaakt - één handmatige correlatie en één semi-geautomatiseerde correlatie op basis van de automatische detectie van cyclothememen. De handmatige aanpak wordt als nauwkeuriger beschouwd voor de correlatie van afzonderlijke putten. Gemiddelde stratigrafische trends van de correlaties worden vergeleken, en vergelijkbare resultaten in zandsteeninhoud worden gevonden met twee intervallen waarin de zandsteeninhoud toeneemt. Deze intervallen worden in verband gebracht met controle door lang-excentriciteit via fluctuaties in het basisniveau en kunnen de exploratie in de overigens lage netto-bruto instelling sturen.

Hoofdstuk 8, de tweede ondergrondse casusstudie, onderzoekt de Upper Triassic Lunde formatie in de noordelijke Noordzee. Er worden stabiele afwisselingen van sterke en zwakke tot matige

bodemvorming gevonden in het record van de overstromingsvlakte en deze worden gebruikt om putten over een afstand van 1-5 km te correleren. Aanvullende putten over grotere afstanden worden toegevoegd met behulp van een gegenereerd stabiel koolstofisotooprecord als referentiepunten. De resulterende op de overstromingsvlakte gebaseerde stratigrafische zonering wordt vergeleken met de bestaande reservoirzonering en er worden verbeteringen voorgesteld. Gemiddelde stratigrafische trends tonen variabiliteit in de niveaus van zandsteeninhoud, en in combinatie met het stabiele koolstofisotooprecord wordt een koppeling gemaakt met precessie-gestuurde orbitale forcing. Deze bevindingen kunnen de exploratie en productie van de Lunde formatie in de noordelijke Noordzee beïnvloeden.

Deze scriptie benadrukt het potentieel van het gebruik van cyclische klimaatbeheersing door orbitale forcing als een hulpmiddel bij de correlatie en karakterisering van alluviale stratigrafie met een lage netto-brutoverhouding. Het onderstreept het belang van regionaal continue oppervlakken, zoals paleosolen of steenkoollagen, bij het identificeren en correleren van afzettingen in alluviale systemen. De bevindingen van de studies in het Bighorn Basin worden toegepast op ondergrondse casusstudies in de Noordzee, waarbij vergelijkbare patronen worden gevonden. Deze benadering kan waardevolle inzichten bieden voor de exploratie en productie van geo-energie uit alluviale afzettingen met een lage netto-brutoverhouding.